A Novel therapeutic strategy targeting TIRAP-mediated signaling in sepsis

Ph.D. Thesis

By

SAJJAN RAJPOOT

DEPARTMENT OF BIOSCIENCES AND BIOMEDICAL ENGINEERING

INDIAN INSTITUTE OF TECHNOLOGY INDORE

OCTOBER 2022

A Novel therapeutic strategy targeting TIRAP-mediated signaling in sepsis

A THESIS

Submitted in partial fulfillment of the
requirements for the award of the degree
of
DOCTOR OF PHILOSOPHY

by

SAJJAN RAJPOOT

DEPARTMENT OF BIOSCIENCES AND BIOMEDICAL ENGINEERING
INDIAN INSTITUTE OF TECHNOLOGY INDORE
OCTOBER 2022

INDIAN INSTITUTE OF TECHNOLOGY INDORE

I hereby certify that the work which is being presented in the thesis entitled **A Novel therapeutic strategy targeting TIRAP-mediated signaling in sepsis** in the partial fulfillment of the requirements for the award of the degree of **DOCTOR OF PHILOSOPHY** and submitted in the **DEPARTMENT OF BIOSCIENCES AND BIOMEDICAL ENGINEERING, INDIAN INSTITUTE OF TECHNOLOGY INDORE**, is an authentic record of my own work carried out during the time period from **October 2017 to October 2022** under the supervision of **Dr MIRZA SAQIB BAIG, Associate Professor, BSBE, IIT Indore**.

The matter presented in this thesis has not been submitted by me for the award of any other degree of this or any other institute.

25.01.2023.

Signature of the student with date

(SAJJAN RAJPOOT)

This is to certify that the above statement made by the candidate is correct to the best of my/our knowledge.

25-1-23

Signature of Thesis Supervisor with date

(Dr MIRZA SAQIB BAIG)

SAJJAN RAJPOOT has successfully given his Ph.D. Oral Examination held on **25/01/2023**.

25-1-23

Signature of Thesis Supervisor with date

(Dr MIRZA SAQIB BAIG)

ACKNOWLEDGEMENT

Whatever has been started will come to closure at some point and here is the time for me to complete the long journey as a PhD scholar and to embark the new beginning as a more learned and responsible researcher. However, before that it is most imperative to express my sincere gratitude to all those who are the part of this unforgettable journey. For me this journey is the best part of my life till now both professionally and personally.

At first and foremost, I must begin to express my sincere gratitude and respect to my supervisor, ***Dr. Mirza Saqib Baig****. I belief that expressing just thanks and gratitude is never justifiable for a person like Dr Baig, who leaves no stone unturned for my scientific discoveries and achievements. I take proud to say that no such word can define his guidance, support, teaching, knowledge, encouragement, motivation he gave to me throughout the journey of my Ph.D. I have been privileged to be his Ph.D student. I still remember my first day in his lab that how naïve I was in this filed and proud say that he has now shaped in all way to take any challenges in future endeavour. He has taught me professionally about science, research, experiments, writing to personally to be positive, motivated, inspired and ready for challenges. I learnt from him that if determined, no hurdle can stop our scientific progress. My Ph.D journey faced the once in a century, the viral pandemic (COVID-19) and was the toughest phase of my journey. It was Dr Baig's support, motivation, understanding, encouragement and enthusiasm to science which help me to make most out of that period and to keep progressing in my research work. I can't stop sharing my overall experience with Dr Baig's in his lab but at the end I am significantly obligated for his support, motivation, and always understanding nature.*

Further, I would like to extend my sincere thanks to my PSPC members, ***Dr. Hem Chandra Jha, Dr Kiran Bala, Dr. Munir A. Nayak*** *and* ***Dr. Sushabhan Sadhukhan****, for their guidance and valuable suggestions throughout the progress of my work. I am grateful to* ***Dr. Hem Chandra Jha and Dr Kiran Bala*** *for their continuous suggestions me insightful ideas during my research and for future directions as well.*

*I wish to express my sincere thanks to the **Director**, IIT Indore, for providing the infrastructural support and necessary amenities involved in the research. I would like to thank **IIT Indore** for providing the laboratory, computational facilities, and financial support during the doctoral work.*

*I am grateful to the **DPGC convener, Head of the Department,** and all the **faculty members** of Department of Biosciences and Biomedical Engineering (**BSBE)** for directly or indirectly contributing to my research work. I would also like to thank BSBE office staff, **Mr. Amit Mishra, Mr. Arif Patel**, **Mr. Gaurav Kumar, and Mr. Murphy Ganveer** for providing all facilities and support in the department. I also acknowledge the sincere efforts of all the academic staff, library staff, and other technical and non-technical staff of IIT Indore for their constant support and help.*

*Further, I am grateful for the **confocal microscopy facility** at **Sophisticated instrument center (SIC), IIT Indore** and would like to extend my gratitude and thanks to **Dr Ravindra Kumar**, for providing me the technical and analytical support.*

*After the supervisor, the Ph.D journey is never complete without the lab members and friends who are family members away from home. I extend my deepest appreciation and thanks to all my lab members. My special thanks go to **Dr Mansi Srivastava**, first graduated student of Dr. Baig's Lab, who was not just a lab member but she is sister to me. In one sentence, she is available all rund clock, day and night, through the year for any support. The time we spent together in lab the best time of my whole Ph.D. She is not only good at her research work professionally, but an outstanding person personally. In our life we make some friendship and relationship which last forever, Dr. Mansi is one such sister and friend to me. Next to her, my special thanks go to **Dr Adnan Naim**. He taught me a lot. He is very focused and composed person and taught me well about time management and to think beyond. I would also like to thank deep from my heart to other lab members my juniors **Mr Shiva, Mr Ajay**, **Mr. Kundan**, **Mr. Pramod**, **Mr. Khandu, Mr Rajat** and master students **Mr Rahul and Ms Neha for their support and help**. In every aspect of the journey, their involvement in problem-solving and discussions are appreciable. At last, but not least, this journey was never easy without the support from our lab technician, **Mr Lateefur Rahman Khan.** Thanks to all my lab members for their generous help, co-operation, and enjoyable moments we had experienced in this journey of Ph.D.*

*Also, I would like to acknowledge and thanks to the friends and seniors **Vishal Kaushik, Swati Rajput, Dharmendra, Umashankar, Ankit, Chanchal, Charu, Navpreet, Nisha, Saumya, Rinki, Prashant, Ritu, Eshan, Arun, Vishal** for their motivation, support and scientific discussions. I take pardon if I have missed anyone's name.*

*Finally, I would like to express my deep gratitude towards **my parents, in-laws and family members**. They are my constant inspirational source. Words are not enough to define their sacrifice and to expresses and show my gratitude towards my father **Santosh Singh,** mother **Tara Devi Singh,** father-in-law **Late Amber B Rai, and** mother-in-law **Chandra Kala Rai.** I express my sincere gratitude to my elder sister **Tanuja** and my elder brother **Dr Sanjio Singh** and sister-in-law **Abha Kumari**, who are next to father and mother and taught the most about the life and troubleshooting. I also thanks to my niece and nephew **Sanvi and Shaarav** to make me smiling. Without their support, it would have been difficult to complete this journey. Their blessings and love helped me to accomplish this journey.*

*It is a special thanks to my beloved wife, **Roja Bell Rai.** She is my pillar who is always beside me. In each of my achievements, she has equal contribution backstage. She is one stop for me to reach-out in any situation. And finally, much and much love to my cute daughter, **Shaambhavi (Sia)**. She arrived at the end of my Ph.D and changed our life completely. She is the biggest inspiration and motivation for me to do more and more for science and I feel proud to be her father.*

At last but not least, I would like to extend my deep respect to God for showering me with blessings throughout my research work to complete it successfully.

-SAJJAN RAJPOOT

Dedicated to

My parents, in-laws,

my wife (Roja Bell Rai)

and

my daughter (Shaambhavi)

SYNOPSIS

Introduction

Sepsis syndrome, its epidemiology, and causes: Sepsis is a critical clinical syndrome with life-threatening organ dysfunction induced by a dysregulated host response to infection. It is a life-threatening and expensive disease burden worldwide [1, 2]. Although sepsis has long been recognized, it was not clinically defined until the late 20th century due to the lack of sepsis patients surviving long enough to be studied or develop organ dysfunction sequelae. In the past 50 years, sepsis was being defined as the development of host systemic inflammatory response syndrome (SIRS) against microbial infection [3]. However, according to the Third International Consensus Definitions for Sepsis and Septic Shock (Sepsis-3) held in 2016, sepsis is defined as "a life-threatening organ dysfunction originating due to the dysregulated host immune response to the infection" and septic shock as its subset, where the exaggerated and abnormal response in circulatory, cellular, and metabolic system are major factors for a greater risk of mortality among patients as compared to sepsis alone [1-3]. Sepsis is considered a major cause of health loss, but data for the global burden of sepsis are limited as the estimated figures are based upon data mainly collected from high-income countries, while data are scarce on its incidence in low- and middle-income countries. A recently compiled report on the global burden of sepsis (from 1990 to 2017) estimated about 48·9 million (95% uncertainty interval [UI] 38·9–62·9) incident cases of sepsis worldwide and 11·0 million (10·1–12·0) sepsis-related deaths representing 19·7% (18·2–21·4) of all global deaths in the year 2017 only [4-6]. As per the report, the 282 underlying causes of sepsis are broadly categorized into infections, injuries, and non-communicable diseases (NCDs) which account for the total sepsis in both sexes as depicted in **Figure 1** [4].

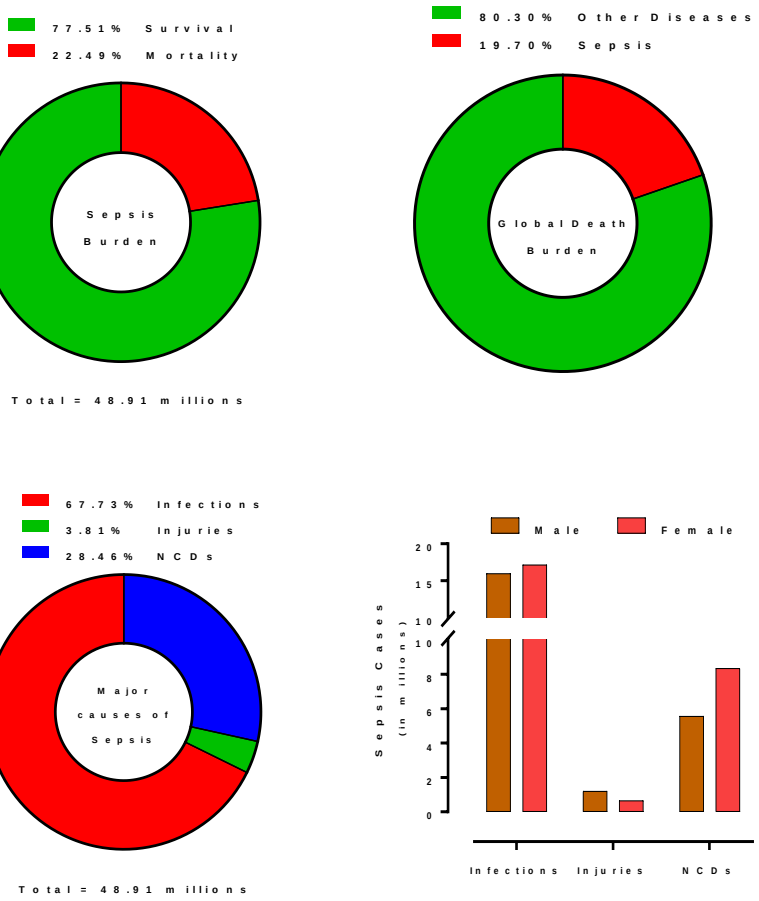

Figure 1. Epidemiology of Sepsis, 2017. *Non-communicable diseases (NCDs)*

Innate immunity, Inflammation, and toll-like receptor (TLR) signalling in Sepsis: Innate immune system is the primary defense mechanism of the host to protect against invading pathogens. In humans, the innate immune system mainly comprises innate immune cells (i.e. monocytes/macrophages, neutrophils, dendritic cells (DCS), natural killer (NK) cells, mast cells (MCs), eosinophils, basophils, innate lymphoid cells (ILCs) and mucosa-associated invariant T (MAIT) cells, etc. It also includes innate humoral components such as complement system, cytokines, chemokines, and antimicrobial peptides (AMPs; LL37 and bactericidal/permeability-increasing protein (BPI), etc.) secreted by the innate immune cells. These innate immune cells express various pattern recognition receptors (PRRs) such as toll-like receptors (TLRs), nod-

like receptors (NLRs), RIG-like helicases (RLH) such as melanoma differentiation-associated protein 5 (MDA-5), C-type lectin receptors (CLRs) [Dectin 1 or C-type lectin domain containing 7A (CLEC7A), dectin 2 or CLEC6A, DC-specific ICAM3-grabbing non-integrin (DC-SIGN)], complement receptor 3 (CR3), Triggering receptors expressed on myeloid cells (TREM-1), and myeloid DNAX activating protein of 12 kDa (DAP-12) associated lectin (MDL-1) [2, 7].

The involvement of intricate inflammatory signaling pathways and dysregulated host response makes sepsis a life-threatening heterogeneous syndrome different from a mild infection **(Figure 2)**. As a clinical syndrome, sepsis occurs when an infection is associated with the systemic inflammatory response. In sepsis, the expected and appropriate inflammatory response to an infectious process becomes amplified leading to organ dysfunction or risk for secondary infection **(Figure 2)**. The inflammatory response, an essential part of innate immunity first-line defense, is a complex physiological mechanism of the host immune system against infectious stimuli and a prerequisite for eliminating pathogens, followed by affected tissue repair and regeneration. Acute inflammation's primary goal is to eliminate these infectious agents. The key objective of acute inflammation is to respond and clear the infectious agents in the early stage and resolve the inflammation. But in several conditions, the inflammation persists for an extended period, leading to a chronic inflammatory situation. In the late stage, chronic inflammation eventually leads to sepsis including other numerous pathological conditions such as pulmonary disorder, cardiac dysfunction, kidney dysfunction, metabolic disorder, neurological disorder, cancer, etc. It breaches the localized inflammation leading to the cause of sepsis which results in exaggerated innate immune response and cytokines storm imparting a crucial role in multi-organ dysfunction and mortality in many cases. Taken together, in contrast to an uncomplicated and localized infection, sepsis is a multifaceted disruption of the finely tuned immunological balance of pro-inflammation and anti-inflammation [2, 8].

Toll-like receptors belong to the most studied family of PRRs, due to their central role in host defenses and involvement in several pathological processes that include sepsis.

The initiating event of effective innate immune responses against pathogens and induction of sepsis is host recognition of microbial-derived pathogen-associated molecular patterns (PAMPs) or endogenous damage-associated molecular patterns (DAMPs) by a series of PRRs located either at the cell membrane (TLR1, TLR2, TLR4, and TLR6) or intracellular space in the organelles including lysosomes, endosomes, phagosomes, phagolysosomes, and endolysosomes (TLR3, TLR7, TLR8, and TLR9). One of the best examples in recent times of host-pathogen interaction leading to infection and severe immune response can be well understood from the interaction between the angiotensin-converting enzyme 2 (ACE2) receptor of human host and spike (S) protein of severe acute respiratory syndrome coronavirus-2 (SARS-CoV-2). In immune cells, expressed at the cell surface, TLR4 detects LPS from Gram-negative bacteria and also shuttles to late endosomes to induce alternative signaling following LPS sensing. TLR2 as heterodimers in association with either TLR1 or TLR6 (and possibly TLR10) senses a variety of microbial products, such as lipopeptides, lipoproteins, peptidoglycan, porins, β-glucan, glycosylphosphatidylinositol (GPI) anchors, and glycoproteins from Gram-positive bacteria, Gram-negative bacteria, mycoplasma, mycobacteria, fungi, parasites, and viruses. TLR5 senses flagellin of bacterial flagella. TLR3, TLR7, TLR8, and TLR9 are strategically expressed in endosomal compartments to recognize microbial nucleic acids: double-stranded RNA (dsRNA) by TLR3, single-stranded RNA (ssRNA) by TLR7 and TLR8, and unmethylated CpG motif-containing DNA by TLR9 [7, 9, 10].

Macrophage role in sepsis- The majority of patients diagnosed with severe forms of sepsis are infected with gram-negative or gram-positive bacteria. This fact points out to TLR 2 and 4, predominantly expressed by macrophages, as major mediators of septic injury, due to their ability to recognize structures present in these classes of bacteria and trigger the inflammatory response leading to cytokines storm [11]. Macrophages are sentinel cells of the innate immune system; their location varies from peripheral blood to various organs including lungs, liver, brain, kidneys, skin, testes, and vascular endothelium. Consequently, dysregulated activation of macrophages

impacts the outcome of diverse organ systems in a multitude of diseases. Of the signaling pathways that modulate macrophage function, Toll-like receptors (TLRs) constitute a key signaling system **(Figure 2)**. Therefore, macrophages are recognized to play essential roles throughout all phases of sepsis and affect both immune homeostasis and inflammatory processes, and macrophage dysfunction is considered to be one of the major causes of sepsis. In the early stage of sepsis, macrophages undergo M1 differentiation and promote host defense by eliminating invading pathogens or damaged tissues and releasing massive amounts of pro-inflammatory cytokines such as tumor necrosis factor-alpha (TNF-α), interleukin-1 beta (IL-1β), interleukin-6 (IL-6) and interleukin-8 (IL-8), interleukin-12 (IL-12), interleukin-23 (IL-23), etc. However, macrophages may be excessively activated during the early phase and produce excessive pro-inflammatory cytokines, cytokine storm, which have been identified as one of the major causes for the high mortality rate in the early stage of sepsis [12-15].

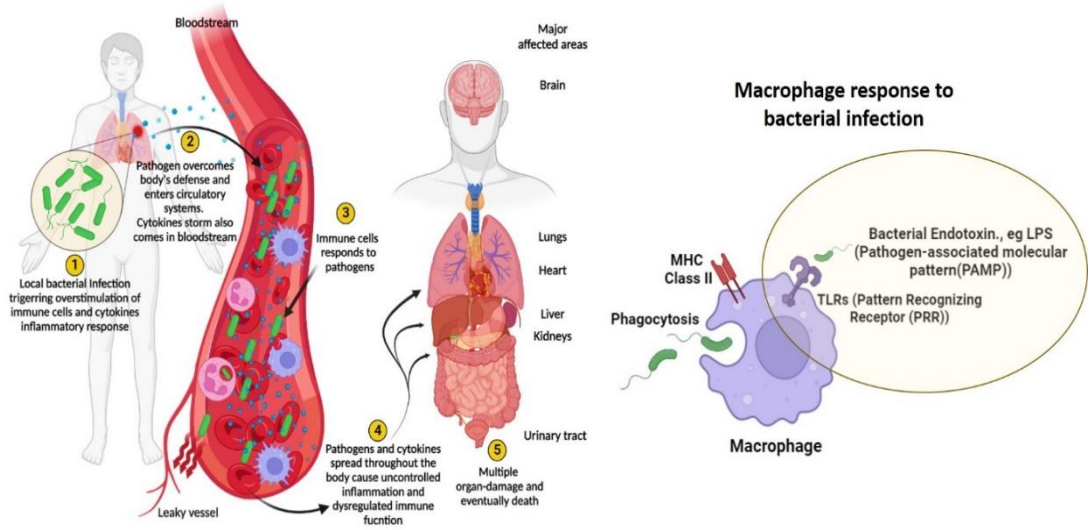

Figure 2: Illustration of sepsis pathogenesis and the diverse response of macrophage in events of sepsis.

Background and Significance of the study

Toll-like receptors (TLRs) are of interest to immunologists because of their front-line role in the initiation of innate immunity against invading pathogens. The key signalling domain, which is unique to the TLR system, is the Toll/interleukin-1 (IL-1) receptor (TIR) domain, which is located in the cytosolic face of each TLR, and also in the adaptors. TIR domain-containing adaptors have been found to have crucial roles in TLR-signalling pathways because they provide specificity to the response generated by signalling through each TLR. Similar to the TLRs, the adaptors are conserved across many species. Signalling by TLRs involves five adaptor proteins that are recruited by TIR/TIR domain interactions. These adaptors (as per the sequence of their discovery) are: myeloid differentiation primary response gene (MyD88), TIR domain-containing adaptor protein (TIRAP, also known as MyD88-adaptor-like (MAL)), TIR-domain-containing adaptor protein inducing IFNβ (TRIF; also known as TICAM1), TRIF-related adaptor molecule (TRAM; also known as TICAM2) and sterile α- and armadillo-motif containing protein (SARM) [9, 16].

Briefly, MyD88 is essential for signaling through all TLRs except TLR3 and is involved in early nuclear factor-κB (NFκB) and mitogen-activated protein kinases (MAPKs) activation and pro-inflammatory gene expression. TIRAP serves as a bridge to recruit MyD88 to TLR2 and TLR4. TRIF initiates MyD88-independent IFN regulatory factor 3 (IRF3) and late NF-κB activation involved in the production of type I IFNs and IFN-inducible genes. TRIF is recruited to the cytoplasmic domain of TLR3 and, in late endosome, through TRAM that bridges TRIF to TLR4. A fifth TIR domain-containing adaptor, sterile α-, and armadillo-motif-containing protein (SARM) acts as a negative regulator of TLR3 and TLR4 signaling. SARM interacts with TRIF and inhibits the induction of TRIF-dependent genes [9, 16].

The second adaptor in the TIR-domain-containing adaptor family TIRAP was discovered as the adaptor required for signalling by TLR2 and TLR4, serving as a bridge to recruit MyD88. Accumulating evidence suggests the specific role of TIRAP was confirmed in TIRAP-deficient mice, which were shown to be defective in TLR4

and TLR2 signalling in terms of cytokine induction. This led to the conclusion that MAL is required for signalling only by TLR2 and TLR4. For TLR4 signalling, the phenotype in MAL-deficient cells was the same as that for MyD88-deficient cells — involving a delay in NF-κB and p38 MAPK activation while no role in the activation of IRF3 and so the conclusion was drawn that MAL is an essential component of the inflammatory pathway [17].

Besides, many other features of TIRAP have also been uncovered that distinguish it from other adaptors mainly MyD88, for example, TIRAP has a TRAF6-binding domain and it also undergoes tyrosine phosphorylation for activation, which has a role in both TLR4 and TLR2 signalling, and in turn leads to the increased activity of NF-κB, which is required for cytokines gene expression **(Figure 3).** Since the discovery of TIRAP in 2001, initial studies were mainly focused on its role as an adaptor protein that couples MyD88 with TLR4/2, to activate MyD88-dependent TLRs signalling. Subsequent studies highlighted and delineated TIRAP's role as a transducer of signalling events through its interactions with several non-TLR signalling mediators. Indeed, the ability of TIRAP to interact with an array of intracellular signalling mediators suggests its central role in various immune responses. Therefore, continued studies that elucidate the molecular basis of various TIRAP-protein interactions and how they affect the signalling magnitude, should provide key information on the inflammatory disease mechanisms.

TIRAP-deficient mice have not been tested in as many disease models as MyD88-deficient mice. However, TIRAP has been shown to be crucial for early immune responses to *Escherichia coli* and LPS in the lung, and also in the induction of antimicrobial peptides in the lung in response to *Klebsiella pneumoniae*, but not to *Pseudomonas aeruginosa*. LPS-induced airway hyper-reactivity has also been shown to involve TIRAP [17]. Therefore, the TIRAP holds a huge potential for further study in disease conditions where it may make differential interactions to regulate the signalling. Hence understanding TIRAP structure and its function in signalling could be therapeutically significant and novel in chronic inflammatory diseases. Human

TIRAP consists of 221 amino acids, constituting two main domains; a phosphatidylinositol 4,5-bisphosphate (PIP2) binding domain (PBD), which is responsible for targeting TIRAP to discrete regions of the plasma membrane upon Phosphatidylinositol 4-Phosphate 5-Kinase (PIP5Ka)-mediated production of PIP2 (11, 12) and a TIR domain, which is mainly involved in protein-protein interactions with numerous inflammatory-related proteins.

For TIRAP to impart its function in the TLR4/2 pathway, it mainly requires aligning at the cell surface and undergoing the tyrosine phosphorylation in the TIR domain for its activation subsequently after its interaction with ligand-bound receptor TLR4/2. Six conserved tyrosine (Y86, Y106, Y159, Y187, Y195, and Y196) residues in then TIR domain of human TIRAP are the potential phosphor-acceptor site. The first four residues Y86, Y106, Y159, and Y187 in TIRAP are experimentally identified as the phospo-sites mainly responsible for TIRAP activity. Meanwhile, the mutation of these four tyrosine residues only and not the Y195 and Y196, either with alanine or phenylalanine describes them as the crucial sites, as after stimulation, the mutation impaired the TIRAP to interact with upstream kinase, similar to the previously reported P125H variant of TIRAP and play a dominant negative role and impair NF-kB activation. One of the well-studied upstream kinases bruton's tyrosine kinase (BTK) is a prerequisite for TIRAP phosphorylation to initiate the TLR4-TIRAP-MyD88 axis mediated downstream signalling and activation of NF-kB and MAPK (mitogen-activated protein kinase) leading to proinflammatory responses. However, further studies, including ours, delineated that TIRAP activity is also regulated by another kinase protein kinase C delta (PKCδ). Previous studies, however, are limited to revealing the downstream signalling via TIRAP and PKCδ axis and its significance for therapeutic purposes. The interacting interface in the TIR domain of TIRAP with PKCδ could be potential for therapeutic targeting. It would be, therefore, highly interesting and significant to reveal the novel downstream signalling events and to dissect the protein-protein interaction of TIRAP with kinases and other downstream proteins to harness the therapeutic angel for inflammatory diseases.

Due to its potential to involve in several signalling events **(Figure 3)**, the novel target TIRAP may emerge as the key molecule to counter the uncontrolled inflammation in different pathophysiological conditions. In sepsis, we proposed to study the novel TIRAP-PKCδ mediated signalling and identify a potential drug candidate targeting host-specific molecule TIRAP in sepsis conditions. Drug identification is a tedious and time-consuming process. However, advancements in various biological, chemical and mainly computational technologies have paved the drug discovery process faster and more economical. In the same process is drug repurposing. The urgency of an effective drug for sepsis may be answered through drug repurposing which will hugely cut down the time and cost. We, therefore, proposed to include the identification of approved small molecules to repurpose as a potential anti-inflammatory agent to tackle sepsis conditions. Collectively, we propose to study the importance of the TIR domain in TIRAP as a key interface involved in protein interactions which could hence serve as a therapeutic target to dampen the extent of acute and chronic inflammatory conditions.

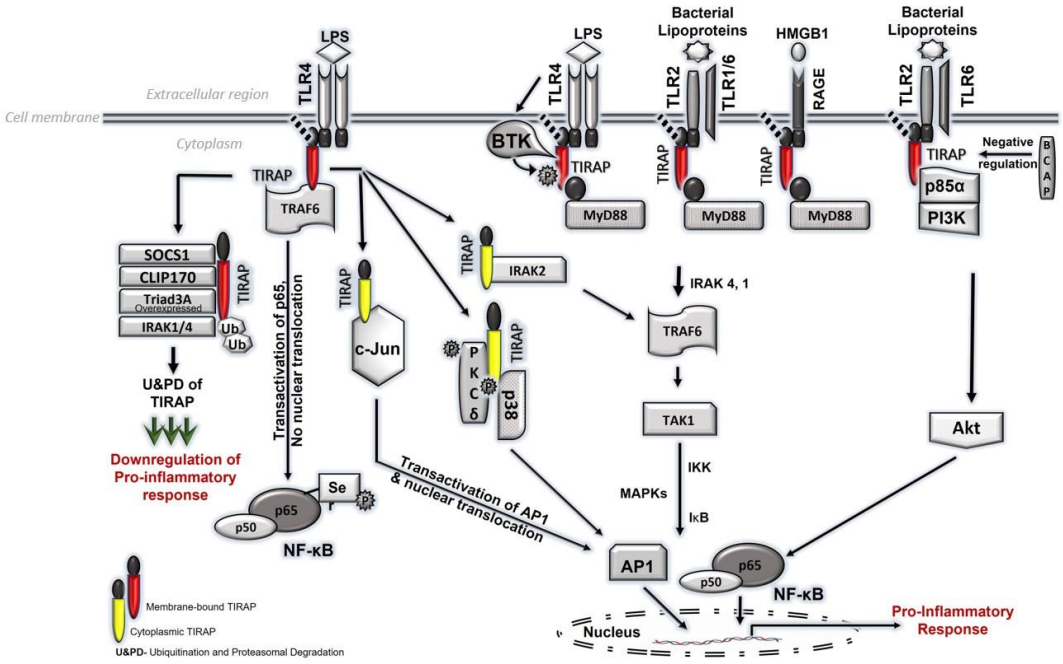

Figure 3: TIRAP in the mechanism of inflammation

Scope and Objectives of the Study

The study proposes to understand the significance of TIRAP-mediated signaling in the TLR4 pathway of macrophages to develop a novel therapeutic strategy for sepsis. The TIRAP shows huge therapeutic potential due to its key involvement in several inflammatory pathways and hence could be a novel target in pathophysiological conditions. Besides, the regulation of pathogenic agents, the host-specific target is crucial to curb the uncontrolled inflammation in response to infections which play a central role in initiating the sepsis condition. Therefore, it would be therapeutically beneficial to pursue the TIRAP-mediated signalling in response to various infectious stimulants and identify the candidate molecules targeting TIRAP to dampen the exaggerated response.

Henceforth, the study's main objective is focused on exploring the TIRAP-mediated inflammatory signaling in macrophages. The following major aims are therefore proposed for it:-

- **Aim 1:-** To understand the TIRAP protein interaction with PKCδ in LPS/TLR4 pathway to regulate the chronic inflammatory signaling and identification of small molecules through in-silico study for validation as an anti-sepsis agent through in-vitro and in-vivo model study.
- **Aim 2:-** To understand the tyrosine phosphorylation in the TIRAP TIR domain in relation to p38 MAPK interaction and its activation using in silico approaches.
- **Aim 3:-** To understand the non-phosphorylated and phosphorylated state of upstream kinases BTK and PKCδ interaction with TIRAP for identification of consensus interface on TIRAP and drug targeting for simultaneous inhibition of kinase interactions.

Structure of Chapters

Chapter 01- Introduction and literature review on Sepsis, its pathophysiology, TLR-mediated macrophage inflammatory signaling in sepsis and the urgency of drug identification for sepsis.

The first chapter describes several aspects of sepsis including the epidemiology, and an overview of signalling in sepsis mainly through macrophages. The chapter presents the recently concluded new definition of sepsis, its global burden data and its major causes. Also, it discusses the innate immunity, inflammation and signalling in chronic inflammatory conditions with emphasis on the role of macrophage TLR adaptor proteins in mediating the downstream signalling. The chapter further deals with the urgency of host-target-specific drug discovery for sepsis.

Chapter 02- The background and significance of the study with emphasis on TIRAP-mediated signaling.

This chapter discusses the TIR domain-containing adaptor proteins in TLR4/2 pathways and the significance of TIRAP in signalling. We have also elaborated on the several signalling being mediated by TIRAP since its discovery and its significance in inflammation. Besides, this chapter emphasizes the upstream kinases BTK and PKCδ involved in the regulation of TIRAP activity as well as the downstream key kinase p38MAPK which is centrally involved in the activation of transcription factors. Further, the chapter describes the significance of identifying the novel target TIRAP for a therapeutic purpose to counter the uncontrolled inflammation and hence the initiation of sepsis as well as the identification of candidate molecules against the TIRAP interface site to dampen its crucial interaction in signalling. Based on these concepts, this chapter presents the major objectives of this study.

Chapter 03- Dorzolamide (DZD) attenuates the inflammatory response through PKCδ -TIRAP-p38 MAPK signaling axis.

In this study, we determine how TIRAP's interaction with protein kinase C delta (PKCδ) shapes the inflammatory response via the activation of NF-κB and AP-1. Our

in-vitro and in-silico studies suggest TIRAP and PKCδ interaction as the driver of LPS-induced inflammatory signaling. We show that this interaction facilitates p38 MAPK phosphorylation and activation to further activate NF-κB and AP-1. The significance of this study holds the promise to disrupt TIRAP and PKCδ interaction to dampen macrophage inflammatory signaling, pushing the response toward resolution and repair would be the significant importance of this study.

In TLR4 signaling, stimulation with LPS leads to the activation of numerous kinases, such as syk, srk lyn, src, BTK, PKCδ, etc., which act on phosphorylation of the TIR domain (51, 43). The tyrosine phosphorylation of the TIRAP TIR domain is crucial for its activation and function (42). Earlier, most of the studies focused on BTK for TIRAP tyrosine phosphorylation and this kinase is well-studied in the regulation of TIRAP activation (52, 15). However, the role of another tyrosine-protein kinase, abundantly present in macrophages, PKCδ, in phosphorylation and activation of TIRAP in TLR4 signaling is not studied much, whereas limited information is available on the PKCδ-TIRAP mediated signaling axis.

In the current study, we found that the interaction of TIRAP with PKCδ in response to LPS is accentuated, which eventually leads to activation of downstream p38 MAPK and increased expression of pro-inflammatory cytokines through AP-1 and NF-κB transcription factors, whereas virtually screened dorzolamide (DZD) significantly attenuated the underlying signaling via inhibition of TIRAP interaction with PKCδ **(Figure 4)**. We confirmed the interaction of TIRAP with PKCδ through immunoblotting of co-immunoprecipitated and co-localization by immunofluorescence techniques in LPS-stimulated mouse macrophage cells (Figure 1A-F). Further, we performed molecular docking of TIRAP and PKCδ structures in pyDockWEB and identified the protein-protein interface and interacting residues through Chimera and PDBePISA for therapeutic targeting. Therefore, we used a library of approved small molecules from the ZINC15 database for virtual screening against the TIRAP interface with PKCδ. We advanced the best molecule DZD to testing in macrophages. The expression of cytokines is an end-point marker of an

inflammatory pathway and modulates the microenvironment in the host. Interestingly, we observed that DZD could significantly attenuate the cytokines expression in LPS-stimulated mouse BMDM and RAW 264.7 cells, respectively. Further, the molecular dynamics simulation of the complex of DZD with TIRAP and in the TIRAP-PKCδ complex was extensively performed for 500ns, which demonstrated that the DZD binding is energetically stable (ΔG_{bind} = -64.33) and DZD diminishes the hydrogen bonds and salt bridges between TIRAP and PKCδ. Tyrosine phosphorylation of TIRAP is crucial for its activity and PKCδ is reported to phosphorylate TIRAP mainly at Y86. Interestingly, phosphorylation of TIRAP increases with time in response to LPS and is significantly downregulated at 30 min in presence of DZD, while no major change was observed at the earlier time point of 5 and 15 min with DZD. To further confirm this, we performed co-immunoprecipitation at 30 min time point and observed that the interaction of TIRAP with PKCδ was significantly reduced in presence of DZD.

DZD treatment of LPS-stimulated macrophages reduced expression of pro-inflammatory cytokines via decreasing TIRAP interaction with PKCδ and its tyrosine phosphorylation. To reveal the downstream signaling and transcription factors responsible for gene expression, we investigated MAPK activity. Notably, we found that the DZD-treated RAW 264.7 macrophages display a significant decrease in p38 MAPK in comparison to LPS-stimulated macrophages, while the other two MAPKs ERK and JNK remained unchanged. Activated p38 MAPK leads to the activation of transcription

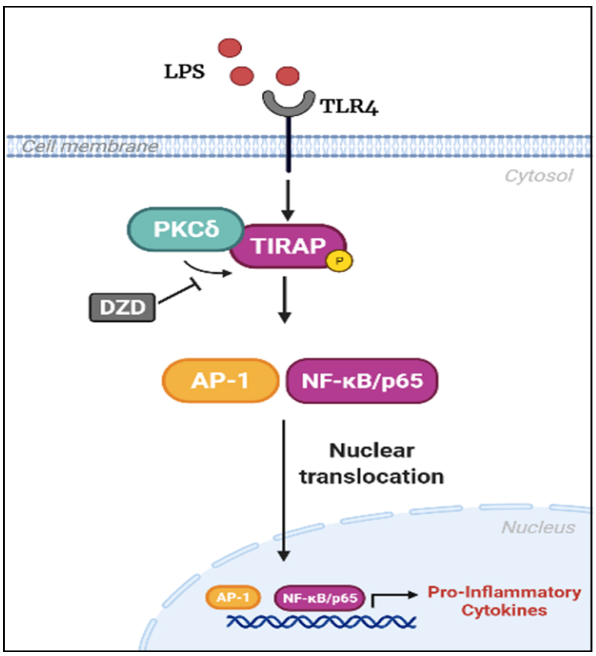

Figure 4: Illustration of TIRAP-PKCδ mediated signalling in LPS stimulated macrophage.

factors, primarily AP-1 and NF-κB. The negative regulator IκB degradation leads to the nuclear translocation of NF-κB and cytokine response. We observed that IκB was protected and protein expression mainly recovered at 1h upon DZD treatment. Subsequently, we checked for phosphorylation and nuclear translocation of NF-κB/p65 through immunoblotting and immunofluorescence and observed that its phosphorylation, as well as nuclear translocation, are significantly inhibited in DZD-treated RAW 264.7 macrophages. Further, this was also confirmed through the immunoblot analysis of cytoplasmic and nuclear protein fraction of phosphorylated NF-κB/p65. Overall, our in-vitro investigation indicates that the TIRAP-PKCδ mediated signaling axis in the LPS-stimulated TLR4 pathway regulates p38 MAPK activation and NF-κB activity for pro-inflammatory gene expression. Moreover, the in-vivo study of the protective role of DZD in septic mice indicates the significance of TIRAP- PKCδ signaling. Importantly, inhibition of this signaling by DZD in LPS-induced septic mice significantly reduced the mortality rate as well as alleviated the LPS-induced lung injury and inflammation. Our study further highlights the central role of TIRAP and PKCδ mediated responses in different pathophysiological conditions associated with inflammation and proposes harnessing the inhibitory effect of TIRAP in the regulation of inflammation. Besides, more studies on DZD at the biophysical level with TIRAP and in-vivo level will pave the way for repurposing this as a potential anti-inflammatory agent.

Chapter 04- TIRAP-mediated activation of p38 MAPK in inflammatory signaling.

Overall, signaling events are tightly controlled in cellular settings and are highly regulated by several mechanisms which govern the normal functioning and maintenance of the body's homeostasis. The major event in signaling is the transduction of messenger signals to downstream molecules which mainly involves the communication between signaling mediators. protein-protein interaction which can either be a kinase-kinase or kinase-non-kinase protein interaction is one of the major events which play a crucial role between the start and the end of the signaling process.

The dynamic regulations are achieved through post-translational modifications. Phosphorylation is one of the crucial post-translational modifications where the phospho-residues serine, threonine, and tyrosine regulate the function of the proteins. The importance of phospho-tyrosine residues is associated with protein-protein interaction in signaling events. Meanwhile, the presence of tyrosine residues at the binding interface has been shown to enhance the binding stability and energy of the protein complex.

Similarly, tyrosine phosphorylation in the TIR domain of TIRAP is very critical for its function. In toll-like receptor (TLR) 4/2 signaling, Bruton's tyrosine kinase (BTK) and Protein kinase C delta (PKCδ) are known to phosphorylate the Y86, Y106, Y159, and Y187 of TIRAP which is crucial for the downstream function of MAPKs (mitogen-activated protein kinases) activation. The objective of this study is to understand the interaction of TIRAP with p38 MAPK through molecular docking and identify the importance of TIRAP tyrosine phosphorylation in p38 MAPK interaction. We have performed the structural analysis of TIRAP and p38 MAPK interaction through multiple molecular docking studies in HADDOCK 2.4, pyDockWEB, ClusPro 2.0, and ZDOCK 3.0.2, and the same has also been validated at the cellular level through in-vitro immunostaining study to colocalize both the proteins in murine macrophages RAW 264.7 cells **(Figure 5)**. We further sought to understand the effect of TIRAP tyrosine phosphorylation on p38 MAPK interaction and created the in-silico site-specific phosphorylated structures of TIRAP through the discovery studio platform to study the conformational changes in protein docking and their binding affinities with p38 MAPK in comparison to non-phosphorylated state. Our in-silico data suggest that the phosphorylated Y86 of TIRAP is crucial in maintaining the structural stability of the complex since its dephosphorylation negatively impacts the binding affinity with p38 MAPK. Interestingly, phosphorylation of all four tyrosine sites jointly enhances TIRAP binding when compared to the non-phosphorylated TIRAP which is also mainly through the pY86. The phosphorylated Y86 shows to pull the TIRAP closer to the active site region in the kinase domain of p38 MAPK (T180 and Y182) while the

docking of phosphorylated Y187 conformation keeps it away from the active region of p38 MAPK. Notably, the molecular docking and further molecular simulation study of 500 ns also define the highest stable hydrogen bonds in the complex with the phosphorylated Y86 TIRAP. The structural evaluation provides an insight into the importance of tyrosine phosphorylation of TIRAP mainly at Y86 for p38 MAPK interaction. Additionally, it provides a platform for their therapeutic interventions by targeting these hydrogen bonds such as the strongest between Y86 in TIRAP and K118 in p38 MAPK for the regulation of downstream signaling and prolonged inflammatory responses responsible for several inflammatory-associated diseases.

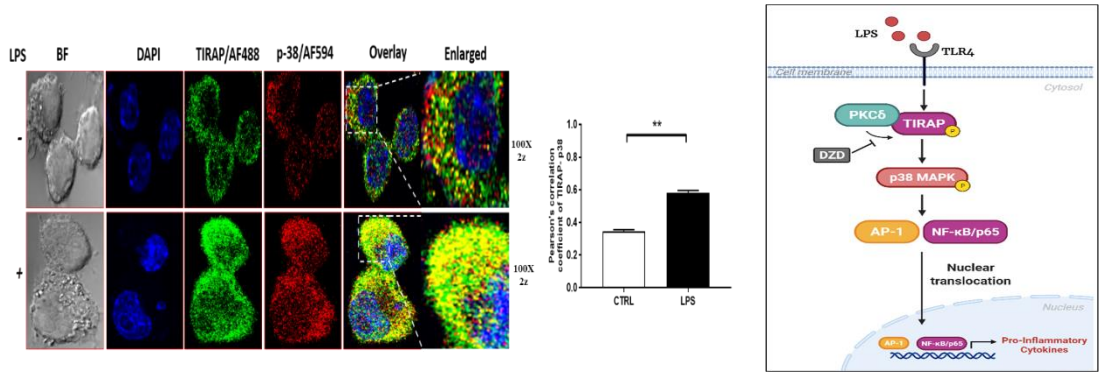

Figure 5: Co-localization of TIRAP and p38MAPK in LPS stimulated macrophages and illustration of p38 MAPK activation downstream of TIRAP.

Chapter 05- Identification of novel inhibitors targeting TIRAP interactions with BTK and PKCδ in inflammation through an in-silico approach.

In TLR4/2 signaling, the transduction of signals mainly initiates the interaction of the TIR domains of receptor and adaptor proteins. However, besides this TIR–TIR interaction, the upstream kinases BTK, as well as PKCδ, plays a crucial role in regulating downstream signalling via the adaptor protein TIRAP. The activation of TLR4 by ligands, such as its classical ligand lipopolysaccharide (LPS), leads to the activation of a series of kinases such as Lck, Src, BTK, and PKC, which eventually phosphorylates the TLR4 as well as the TIRAP TIR domain. In LPS-stimulated macrophages, both BTK and PKCδ are activated and regulate TIRAP function through tyrosine phosphorylation. Therefore, the understanding of TIRAP and tyrosine kinases

BTK as well as PKCδ protein-protein interaction could be significant in regulating the inflammatory responses and may consider an effective therapeutic target **(Figure 6)**. The precise molecular interaction of TIRAP with BTK and PKCδ, required to generate a selective therapeutic target, has not been previously described. A critical step in defining therapeutic sites is the structural analysis of interacting proteins and their binding complex. To obtain this, the prerequisite material is a suitable structure for these proteins. Unfortunately, the required crystal structure of BTK with SH3, SH,2, and kinase domains and PKCδ with the kinase domain is not available in the protein database, and no such model structures with these domains are modelled previously. Hence, we focused to create high-quality homology-based 3D structure models of both the structures and completing the loop modelling of the TIRAP crystal structure missing important loops from residue positions 110 to 127 in the TIR structure.

To mimic the native conditions, the protein-protein docking complexes of TIRAP with inactive non-phosphorylated and active tyrosine-phosphorylated BTK and PKCδ were crucial in determining potential therapeutic sites. We used three different docking platforms (HADDOCK 2.4, pyDockWEB, and ClusPro 2.0) to cross-check the docking results of the complexes. Importantly, the structural analysis from all docking platforms confirms the TIRAP TIR domain interaction with the kinase domain of BTK and PKCδ. Therefore, for a therapeutic molecule to abolish both of these interactions, we determined closely interacting residues within the 4 Å region of TIRAP-BTK and TIRAP-PKCδ complex interfaces. Finally, the comparative analysis between their interacting residues was conducted to determine the common residues of the

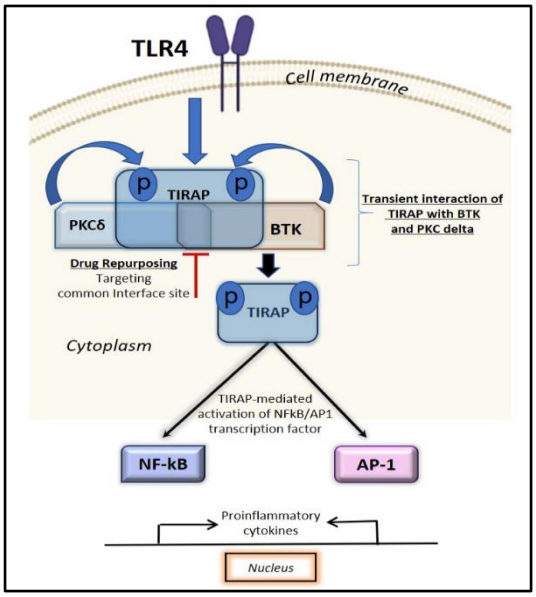

Figure 6: Schematic representation of TIRAP common innterface targeted for inhibition of its interaction with upstream kinases BTK and PKCδ.

TIRAP TIR domain P169, F193, M194, and Y195 from the C-terminal region significantly interacted with both the kinase domains from BTK and PKCδ. Hence, they were determined to serve as the best target site for drug repurposing. Structure-based drug screening against TIRAP was performed in the Discovery studio LibDock module. The proposed set of six virtually screened FDA-approved drugs with repurposing potential, block the interface site in the TIR domain of TIRAP which accommodates the key interacting residues involved in the interaction with both BTK and PKCδ. Moreover, these six drug candidates were re-confirmed with another docking platform AutoDock Vina, suggesting their specificity towards the determined target site on TIRAP. Further, the MD simulation study suggested the four drugs lomitapide, crizotinib, rolapitant, and montelukast as promising compounds in terms of their highly stable binding with TIRAP which remained bound to TIRAP throughout the simulation study with no deviations. The ponatinib and fosaprepitant simulations were not comparable with these four compounds in complex with TIRAP due to their deviations and fluctuations from the binding site. Interestingly, all six compounds, though, show to attenuate the key pro-inflammatory cytokines expression in macrophages and may be further studied in detail.

Chapter 06- Conclusions and the future prospects of the study

The report that TIRAP acts as a second adaptor protein after MyD88 in the year 2001 was marked as a major discovery in the mechanism of TLR4-dependent inflammatory signaling. More recent studies show that TIRAP not only acts as a bridging protein between TLR4/2 and MyD88 but also propagates the transduction of downstream signaling events through other protein interactions.

Being central to innate immune response and canonically known for participation in inflammatory signaling mainly in macrophages, the TIRAP serves as a suitable and potential therapeutic target for the resolution of inflammation and its associated diseases. Recent reports indicate that there is no such drug that passed the clinical trials and is approved for sepsis that can work on host targets. Mostly, the treatment regimen includes the administration of antibiotics against foreign pathogens. However, to cease

the provoked and prolonged inflammation in response to such pathogens can not only resolute by anti-microbial antibiotics rather we need host-target-specific drugs. Therefore, there is an urgent need to identify suitable targets in inflammation pathways and to develop target-specific drugs. TIRAP can serve as one and hence it would be interesting to study the TIRAP involvement in various inflammation-associated pathophysiological conditions and profiling of its interaction in the early and late phases of inflammatory signalling to understand the pattern of its regulation. We attempted to reveal this novel pathway of the TIRAP- PKCδ signalling axis via the p38 MAPK and NF-κB which may further be studied in sepsis models and patients and could be beneficial to protect the inflammation through their disruption by DZD. However, the DZD needs more biophysical, in-vivo, and clinical studies to establish its repurposing as an anti-inflammatory agent. We also propose to study the derivatives or intermediates of DZD which could be more potential in regulating the TIRAP-PKCδ signaling axis. In continuation, we have also highlighted the importance of p38 MAPK in this signalling where the activated TIRAP interacts with p38 MAPK. We showed the significance of tyrosine phosphorylation of TIRAP mainly at Y86 in p38 MAPK binding and activation. Combinedly, the PKCδ-TIRAP-p38 MAPK axis regulates the downstream transcription factor's activity. Furthermore, the study also explores the possibility of completely blocking the TIRAP activation by inhibiting its interaction with both the known upstream kinases BTK and PKCδ. To do so, we employed a novel strategy of identifying the common interacting interface on TIRAP and identified six drugs that could be the potential to block both of the interactions of the kinase with TIRAP and hence significantly suppress the chronic inflammatory responses. Interestingly, all the predicted drugs showed a significant effect in attenuating the key pro-inflammatory cytokines in LPS-stimulated cells> However, these drugs need to be further tested through various experiments and in in-vivo models to identify the suitable one highest efficacy. We propose to use these drugs to develop a combination therapy with in-use antibiotics for sepsis.

References

1. Jarczak D, Kluge S, Nierhaus A. Sepsis—pathophysiology and therapeutic concepts. *Frontiers in Medicine* 609 (2021).
2. Kumar V. Toll-like receptors in sepsis-associated cytokine storm and their endogenous negative regulators as future immunomodulatory targets. *International immunopharmacology* 89 107087 (2020).
3. Gotts JE, Matthay MA. Sepsis: pathophysiology and clinical management. *Bmj* 353 (2016).
4. Rudd KE, Johnson SC, Agesa KM *et al*. Global, regional, and national sepsis incidence and mortality, 1990–2017: analysis for the Global Burden of Disease Study. *The Lancet* 395(10219), 200-211 (2020).
5. Chiu C, Legrand M. Epidemiology of sepsis and septic shock. *Current Opinion in Anesthesiology* 34(2), 71-76 (2021).
6. World Health O. Global report on the epidemiology and burden of sepsis: current evidence, identifying gaps and future directions. (2020).
7. Zhang Y-Y, Ning B-T. Signaling pathways and intervention therapies in sepsis. *Signal Transduction and Targeted Therapy* 6(1), 1-36 (2021).
8. Chen L, Deng H, Cui H *et al*. Inflammatory responses and inflammation-associated diseases in organs. *Oncotarget* 9(6), 7204-7218 (2018).
9. Savva A, Roger T. Targeting toll-like receptors: promising therapeutic strategies for the management of sepsis-associated pathology and infectious diseases. *Front Immunol* 4 387 (2013).
10. Tsujimoto H, Ono S, Efron PA, Scumpia PO, Moldawer LL, Mochizuki H. Role of Toll-like receptors in the development of sepsis. *Shock* 29(3), 315-321 (2008).
11. Possolo Souza H, Lima-Salgado T, Monteiro Da Cruz Neto L. Toll-like receptors in sepsis: a tale still being told. *Endocrine, Metabolic & Immune Disorders-Drug Targets (Formerly Current Drug Targets-Immune, Endocrine & Metabolic Disorders)* 10(3), 285-291 (2010).
12. Angus DC, Van Der Poll T. Severe sepsis and septic shock. *The New England journal of medicine* 369 840-851 (2013).
13. Cheng Y, Marion TN, Cao X, Wang W, Cao Y. Park 7: a novel therapeutic target for macrophages in sepsis-induced immunosuppression. *Frontiers in Immunology* 9 2632 (2018).

14. Murray PJ, Wynn TA. Protective and pathogenic functions of macrophage subsets. *Nature reviews immunology* 11(11), 723-737 (2011).

15. Fujiwara N, Kobayashi K. Macrophages in inflammation. *Current Drug Targets-Inflammation & Allergy* 4(3), 281-286 (2005).

16. Salomão R, Martins PS, Brunialti MKC *et al*. TLR signaling pathway in patients with sepsis. *Shock* 30(7), 73-77 (2008).

17. O'neill LA, Bowie AG. The family of five: TIR-domain-containing adaptors in Toll-like receptor signalling. *Nat Rev Immunol* 7(5), 353-364 (2007).

LIST OF PUBLICATIONS

(A) Publications from Ph.D. Thesis work

1. **Rajpoot, S**., Wary, K. K., Ibbott, R., Liu, D., Saqib, U., Thurston, T. L., & Baig, M. S. (2021). TIRAP in the Mechanism of Inflammation. ***Frontiers in immunology***, 12, 2722.
2. **Rajpoot, S**., Kumar, A., Zhang, K. Y., Gan, S. H., & Baig, M. S. (2022). TIRAP-mediated activation of p38 MAPK in inflammatory signaling. ***Scientific reports***, 12(1), 1-15.
3. **Rajpoot, S**., Srivastava, G., Siddiqi, M. I., Saqib, U., Parihar, S. P., Hirani, N., & Baig, M. S. (2022). Identification of novel inhibitors targeting TIRAP interactions with BTK and PKCδ in inflammation through an in-silico approach. ***SAR and QSAR in Environmental Research***, 33(3), 141-166.
4. **Rajpoot, S**[†]., Ohishi, T[†]., Kumar, A[†]., Pan, Q., Banerjee, S., Zhang, K. Y., & Baig, M. S. (2021). A novel therapeutic peptide blocks SARS-CoV-2 spike protein binding with host cell ACE2 receptor. ***Drugs in R&D***, 21(3), 273-283.
5. **Rajpoot, S**[†]., Solanki, K[†]., Kumar, A[†]., Zhang, K. Y., Pullamsetti, S. S., Savai, R., ... & Baig, M. S. (2022). In-Silico Design of a Novel Tridecapeptide Targeting Spike Protein of SARS-CoV-2 Variants of Concern. ***International Journal of Peptide Research and Therapeutics***, 28(1), 1-15.
6. **Rajpoot, S.,** Kumar, A., Gaponenko, V., Thurston, T. L., Mehta, D., Faisal, S.M., Zhang, K. Y., Jha, H.C., Darwhekar, G.N., and Baig, M.S. (2022). Dorzolamide (DZD) suppresses PKCδ -TIRAP-p38 MAPK signalling axis to dampen the inflammatory response. ***Future Medicinal Chemistry*** *(Under Review)*.

(B) Other publications during Ph.D. work

First author papers

1. **Rajpoot, S†**., Alagumuthu, M†., & Baig, M. S. (2021). Dual targeting of 3CLpro and PLpro of SARS-CoV-2: a novel structure-based design approach to treat COVID-19. ***Current research in structural biology***, 3, 9-18.
2. Solanki, K†., **Rajpoot, S†**., Bezsonov, E. E., Orekhov, A. N., Saluja, R., Wary, A., ... & Baig, M. S. (2022). The expanding roles of neuronal nitric oxide synthase (NOS1). ***PeerJ***, 10, e13651.
3. Alagumuthu, M†., **Rajpoot, S†**., & Baig, M. S. (2021). Structure-based design of novel peptidomimetics targeting the SARS-CoV-2 spike protein. ***Cellular and Molecular Bioengineering***, 14(2), 177-185.
4. Wang, Y†., **Rajpoot, S†**., Li, P†., Lavrijsen, M., Ma, Z., Hirani, N., ... & Baig, M. S. (2022). Repurposing dyphylline as a pan-coronavirus antiviral therapy. ***Future medicinal chemistry***, 14(10), 685-699.
5. Solanki, K†., **Rajpoot, S†**., Kumar, A†., J Zhang, K.Y., Ohishi, T., Hirani, N., Wadhonkar, K., Patidar, P., Pan, Q. and Baig, M.S., 2022. Structural analysis of spike proteins from SARS-CoV-2 variants of concern highlighting their functional alterations. ***Future Virology***, (0).
6. Baig, M.S†., **Rajpoot, S†**, Tomokazu Ohishi†, Rajkumar Savai, Sascha Seidel, Nina A. Kamennaya, Evgeny E. Bezsonov, Alexander S N. Orekhov, Pratik Mahajan, Kundan S Solanki, Uzma Saqib., 2022. Anti-lung cancer properties of cyanobacterial bioactive compounds. ***Archives of Microbiology,*** *204(10):603.*
7. Baig, M.S†., Roy, A†., **Rajpoot, S†**., Liu, D., Savai, R., Banerjee, S., Kawada, M., Faisal, S.M., Saluja, R., Saqib, U. and Ohishi, T. (2020). Tumor-derived exosomes in the regulation of macrophage polarization. ***Inflammation Research***, 69(5), pp.435-451.

Co-author papers

8. Wang, Y., Li, P., **Rajpoot, S**., Saqib, U., Yu, P., Li, Y., Li, Y., Ma, Z., Baig, M.S. and Pan, Q. (2021). Comparative assessment of favipiravir and remdesivir against human coronavirus NL63 in molecular docking and cell culture models. ***Scientific reports***, 11(1), pp.1-13.
9. Baig, M. S., Alagumuthu, M., **Rajpoot, S**., & Saqib, U. (2020). Identification of a potential peptide inhibitor of SARS-CoV-2 targeting its entry into the host cells. ***Drugs in R&D***, 20(3), 161-169.
10. Ohishi, T., Hishiki, T., Baig, M.S., **Rajpoot, S**., Saqib, U., Takasaki, T. and Hara, Y., 2022. Epigallocatechin gallate (EGCG) attenuates severe acute respiratory coronavirus disease 2 (SARS-CoV-2) infection by blocking the interaction of SARS-CoV-2 spike protein receptor-binding domain to human angiotensin-converting enzyme 2. ***PloS one***, 17(7), p.e0271112.
11. Baig, M.S., Roy, A., Saqib, U., **Rajpoot, S**., Srivastava, M., Naim, A., Liu, D., Saluja, R., Faisal, S.M., Pan, Q. and Turkowski, K. (2018). Repurposing Thioridazine (TDZ) as an anti-inflammatory agent. ***Scientific reports***, 8(1), pp.1-10.

Table of Contents

LIST OF FIGURES

Chapter 1

Chapter 2

Chapter 3

Chapter 4

Chapter 5

LIST OF TABLES

NOMENCLATURE

Da- Kilo Dalton

µg/ml- Microgram per millilitre

ng/ml- Nanogram per millilitre

µM- Micro molar

U/ml- Unit per millilitre

°C- Centigrade

%- Percentage

min- Minutes

h- Hour

mM- Milli molar

g- Gravitational force

µg- Microgram

ACRONMYS

SIRS-	Systemic inflammatory response syndrome
ACCP-	American College of Chest Physicians
SCCM-	Society of Critical Care Medicine
MAP-	Mean arterial pressure
PaO2-	Partial pressure of oxygen
FIO2-	Fractional inspired oxygen
SOFA-	Sequential Organ Failure Assessment
qSOFA-	quickSOFA
ICU-	Intensive care unit
NCDs-	Non-communicable diseases
DCs-	Dendritic cells
NK-	Natural killer cells
MCs-	Mast cells
ILCs-	Innate lymphoid cells
MAIT-	Mucosa-associated invariant T
AMPs-	Antimicrobial peptides
BPI-	Bactericidal/permeability-increasing protein
PRRs-	Pattern recognition receptors
TLRs-	Toll-like receptors
NLRs-	Nod-like receptors
RLH-	RIG-like helicases
MDA-5-	Melanoma differentiation-associated protein 5
CLRs-	C-type lectin receptors
CLEC7A-	Dectin 1 or C-type lectin domain containing 7A
CLEC6A-	Dectin 2 or C-type lectin domain containing 6A
DC-SIGN-	DC-specific ICAM3-grabbing non-integrin

CR3-	Complement receptor 3
TREM-1-	Triggering receptors expressed on myeloid cells
MDL-1-lectin	Myeloid DNAX activating protein of 12 kDa (DAP-12) associated
PAMP-	Pathogen-associated molecular patterns
DAMPs-	Damage-associated molecular patterns
GPI-	Glycosylphosphatidylinositol
TLR 1-	Toll like receptor 1
TLR 2-	Toll like receptor 2
TLR 3-	Toll like receptor 3
TLR 4-	Toll like receptor 4
TLR 5-	Toll like receptor 5
TLR 6-	Toll like receptor 6
TLR 7-	Toll like receptor 7
TLR 8-	Toll like receptor 8
TLR 9-	Toll like receptor 9
TLR 10-	Toll like receptor 10
LPS-	Lipopolysaccharide
dsRNA-	double-stranded RNA
ssRNA-	single-stranded RNA
TNF-α-	Tumour necrosis factor α
IL-1β-	Interleukin-1 beta
IL-6-	Interleukin-6
IL-8-	Interleukin-8
IL-12-	Interleukin-12
IL-23-	Interleukin-23
IL-10-	Interleukin 10
TGF-β-	Transforming growth factor-β

TIR-	Toll/interleukin-1 (IL-1) receptor
MyD88-	Myeloid differentiation primary response protein
TIRAP-	Toll Interleukin 1 receptor domain containing adaptor protein
MAL-	MyD88-adaptor-like
TRIF-	TIR-domain-containing adaptor protein inducing IFNβ
TICAM1-	TIR Domain Containing Adaptor Molecule 1
TRAM-	TRIF-related adaptor molecule
TICAM2-	TIR domain-containing adapter molecule 2
SARM-	Sterile α- and armadillo-motif containing protein
DD-	Death domain
IMD-	Intermediate domain
PBD-	Phosphatidylinositol 4,5-bisphosphate (PIP-2)-binding domain
PEST-	Pro, Glu, Ser, and Thr-rich domain
NTD-	N-terminal domain
ARM-	Armadillo repeats motif
SAM-	Sterile α-motif
NF-kB-	Nuclear factor kappa B
MAPK-	Mitogen-activated protein kinase
IRF3-	IFN regulatory factor 3
p38 MAPK-	p38 Mitogen-activated protein kinase
AP1-	Activator protein 1
PI3K-	Phosphoinositide 3-kinase
Akt-	Protein kinase B
CLIP170-	Cytoplasmic linker protein 170
RAGE-	Receptor for advanced glycation end-products
TRAF1-	Tumor necrosis factor receptor–associated factor1
TRAF2-	Tumor necrosis factor receptor–associated factor2
TRAF3-	Tumor necrosis factor receptor–associated factor3

TRAF4-	Tumor necrosis factor receptor–associated factor4
TRAF5-	Tumor necrosis factor receptor–associated factor5
TRAF6-	Tumor necrosis factor receptor–associated factor6
SOCS-1-	Suppressor of cytokine signaling 1
BTK-	Bruton's tyrosine kinase
PKCδ -	Protein kinase C delta
IRAK-2-	Interleukin-1 receptor-associated kinase 2
TAK-	TGF-β activating kinase
BCAP-	B-cell adaptor for phosphoinositide 3-kinase
IRAK-1-	Interleukin-1 receptor-associated kinase 1
IRAK-4-	Interleukin-1 receptor-associated kinase 4
IRAK-3-	Interleukin-1 receptor-associated kinase 3
BCR-	B cell receptor
AGE-	Advanced glycation end products
HMGB1-	High mobility group box-1
PKC-z-	Protein Kinase C-z
esRAGE-	endogenous soluble RAGE
cdc42-	cell division cycle 42
PIP3-	Phosphatidylinositol (3,4,5)-triphosphate
MALP-2-	Macrophage activating lipopeptide-2
HO-1-	Heme Oxygenase-1
DBB-	Dof/BANK1/BCAP domains
ANK-	Ankyrin repeat
DAG-	Diacylglycerol
IP3-	Inositol trisphosphate
NO-	Nitric oxide
ROS-	Reactive oxygen species
H2O2-	Hydrogen peroxide

CAPGly-	Cytoskeleton-associated protein Glycine rich
TcpB-	TIR domain-containing effector protein
JNK-	c-Jun N-terminal kinase
ERK-	Extracellular signal-regulated kinase
ICE-	IL-1beta converting enzyme
GSDMD-	Gasdermin-D
SH2-	Src homology 2
JAK-STAT-	Janus kinase/signal transducers and activators of transcription
IκB-	I kappa B kinase
NOS1-	Nitric oxide synthase 1
SNO-	SNitrosylation
PKC-	Protein kinase C
nPKCs-	novel PKCs
aPKCs-	atypical PKCs
XLA-	X-linked agammaglobulemia
Ig-	Immunoglobulins
PTK-	Protein tyrosine kinases
TCR-	T cell receptor
PH-	Pleckstrin homology
TH-	Tec homology
SH3-	Src homology 3
ATF-	Activating transcription factor
CARD-	Caspase Activation and Recruitment Domain
DZD-	Dorzolamide
FDA-	Food and drug administration
TF-	Transcription factors
NCCS-	National Centre for Cell Science
BMDM-	Bone marrow-derived macrophages

DMEM- Dulbecco’s minimal essential medium

FBS- Fetal bovine serum

PFA- Paraformaldehyde

PBS- Phosphate buffer saline

TBST- Tris-buffered saline with Tween 20

DAPI- 4',6-diamidino-2-phenylindole

EDTA- Ethylenediamine tetra acetic acid

PMSF- Phenyl methyl sulfonyl fluoride

Co-IP- Co-immunoprecipitation

NaF- Sodium fluoride

Na2VO3- Sodium orthovanadate

HRP- Horseradish peroxidase

ProTSAV- Protein structure analysis and validation

RT- Reverse transcribed

qPCR- Quantitative PCR

MD- Molecular dynamics

AMBER- Assisted Model Building with Energy Refinement

RIPA- Radioimmunoprecipitation assay

SDS-PAGE- Sodium Dodecyl Sulfate Polyacrylamide Gel Electrophoresis

RT- Room temperature

ECL- Enhanced chemiluminescence

IAEC- Institutional Animal Ethics Committee

CPCSEA- Committee for Control and Supervision of Experiments on Animals

DMSO- Dimethyl sulfoxide

H&E- Haematoxylin and eosin

PCC- Pearson’s correlation coefficient

PKC θ- Protein kinase C theta

RMSD- Root mean square deviation

p-ERK- Phospho Extracellular signal-regulated kinase

p-JNK- Phospho c-Jun N-terminal kinases

qRT-PCR- Real-Time Quantitative Reverse Transcription PCR

CA- Carbonic anhydrase

IOP- Intraocular pressure

PPIs- Protein–protein interactions

BSA- Bovine serum albumin

pYall04- All four phosphorylated tyrosine

p- Phosphorylated

dp- Dephosphorylated

PDBQT- Protein Data Bank, Partial Charge (Q), & Atom Type (T)

muTIRAP- Mutated TIRAP

all04A TIRAP- All four-alanine mutated TIRAP sites

RCSB PDB- Protein Data Bank, Partial Charge (Q), & Atom Type (T))

CASP- Critical Assessment of Techniques for Protein Structure Prediction

wtTIRAP- Wild-type TIRAP

RMSF- Root mean square fluctuation

Chapter 1

(Introduction)

Chapter 1: Introduction

1.1. Sepsis Overview:

Sepsis is a critical clinical syndrome with life-threatening organ dysfunction induced by a dysregulated host response to infection. It is a life-threatening and expensive disease burden worldwide [1-3]. The word sepsis is derived from the Greek word meaning “decomposition” or “decay,” and it was first documented about 2700 years ago in Homer’s poems. Subsequently, it was used in the works of Hippocrates and Galen in later centuries. In the 1800s, the “Germ theory” of disease was conceived and there was some recognition that sepsis originated from harmful microorganisms. However, in 1914, Hugo Schottmüller attempted to first give the modern definition of sepsis that “sepsis is present if a focus has developed from which pathogenic bacteria, constantly or periodically, invade the bloodstream in such a way that this causes subjective and objective symptoms.” Although sepsis has long been recognized, it was not clinically defined until the late 20th century due to the lack of sepsis patients surviving long enough to be studied or develop organ dysfunction sequelae. However, over the period of the 20th century, several experimental and clinical trials were able to demonstrate the importance of the host immune response to the manifestations of sepsis but due to the heterogeneity of the disease process, it posed serious difficulties in recognizing, treating, and studying sepsis [3, 4].

In the past 50 years, sepsis was being defined as the development of host systemic inflammatory response syndrome (SIRS) against microbial infection [5]. In the last two decades, our understanding of the complex pathophysiology of sepsis has improved, and so has our ability to define sepsis. This understanding has led to changes in the definition of sepsis and contributed to better management of sepsis leading to changes in the epidemiology of sepsis. In 1991 at the American College of Chest Physicians (ACCP) and the Society of Critical Care Medicine (SCCM) conference, Roger Bone and his colleagues laid the foundation for the first consensus definition of sepsis [3, 5-7].

1.1.1. Sepsis 1 (1991) Definition-

Systemic inflammatory response syndrome (SIRS): systemic inflammatory response to a variety of severe clinical insults: Temperature >38°C or <36°C; heart rate > 90 beats per min; respiratory rate > 20 breaths per min or PaCO2 < 32 mmHg; and white blood cell count > 12,000/cu mm, <4000/cu mm, or >10% immature (band) forms.

Sepsis: is a systemic response to infection, manifested by two or more of the SIRS criteria as a result of infection.

Severe sepsis: Sepsis associated with organ dysfunction, hypoperfusion, or hypotension; hypoperfusion and perfusion abnormalities may include, but not limited to, lactic acidosis, oliguria, or an acute alteration in mental status.

Septic shock: Sepsis-induced, with hypotension despite adequate fluid resuscitation along with the presence of perfusion abnormalities that may include, but not limited to, lactic acidosis, oliguria, or an acute alteration in mental status; patients who are receiving inotropic or vasopressor agents may not be hypotensive at the time that perfusion abnormalities are measured.

1.1.2. Sepsis 2 (2001) Definition-

A group of experts and opinion leaders revisited the 1992 sepsis guidelines and found that apart from expanding the list of signs and symptoms of sepsis to reflect clinical bedside experience, no evidence exists to support a change to the definitions [8]. The expanding list of signs and symptoms includes-

General parameters: Fever (core temperature > 38.3°C); hypothermia (core temperature < 36°C); heart rate > 90 beats per min or > 2 SD above the normal value for age; tachypnea: respiratory rate > 30 breaths per min; altered mental status; significant edema or positive fluid balance (>20 mL kg−1 over 24 h); Hyperglycemia (plasma glucose > 110 mg dL−1 or 7.7 mM L−1) in the absence of diabetes.

Inflammatory parameters: Leukocytosis (white blood cell count > 12,000/μL); leukopenia (white blood cell count < 4000/μL); normal white blood cell count with > 10% immature forms; plasma C-reactive protein > 2 SD above the normal value; and plasma procalcitonin > 2 SD above the normal value.

Hemodynamic parameters: Arterial hypotension (systolic blood pressure < 90 mmHg, MAP < 70 mmHg, or a systolic blood pressure decrease > 40 mmHg in adults or < 2 SD below normal for age, mixed venous oxygen saturation > 70%, cardiac index > 3.5 L min−1 m−2)

Organ dysfunction parameters: Arterial hypoxemia (PaO2/FIO2 < 300); acute oliguria (urine output < 0.5 mL kg−1 h−1 or 45 mM L−1 for at least 2 h); creatinine increase ⩾ 0.5 mg dL−1; coagulation abnormalities (international normalized ratio > 1.5 or activated partial thromboplastin time > 60 s); ileus (absent bowel sounds); thrombocytopenia (platelet count < 100,000 μL−1) Hyperbilirubinemia (plasma total bilirubin > 4 mg dL−1 or 70 mmol L−1)

Tissue perfusion parameters: Hyperlactatemia (>3 mmol L−1); decreased capillary refill or mottling

1.1.3. Sepsis 3 (2016) Definition-

Due to considerable advances in the pathobiology (changes in organ function, morphology, cell biology, biochemistry, immunology, and circulation), management, and epidemiology of sepsis, the task force suggests the need for re-examination of the sepsis definition [9]. Limitations of previous definitions included an excessive focus on inflammation, the misleading model that sepsis follows a continuum from severe sepsis to shock, and inadequate specificity and sensitivity of the systemic inflammatory response syndrome (SIRS) criteria. Multiple definitions and terminologies are currently in use for sepsis, septic shock, and organ dysfunction, leading to discrepancies in reported incidence and observed mortality. The task force concluded the term *severe sepsis* was redundant [9].

Sepsis is not a specific illness but rather a syndrome encompassing a still-uncertain pathobiology. Sepsis is a multifaceted host response to an infecting pathogen that may be significantly amplified by endogenous factors. The original conceptualization of sepsis as an infection with at least 2 of the 4 SIRS criteria focused solely on inflammatory excess. However, the validity of SIRS as a descriptor of sepsis pathobiology has been challenged. Sepsis is now recognized to involve early activation of both pro- and anti-inflammatory responses, along with major modifications in nonimmunologic pathways such as cardiovascular, neuronal, autonomic, hormonal, bioenergetic, metabolic, and coagulation, all of which have prognostic significance [9-11].

Therefore, according to the latest Third International Consensus Definitions for Sepsis and Septic Shock (Sepsis-3) held in 2016, sepsis is now defined as *"a life-threatening organ dysfunction originating due to the dysregulated host immune response to the infection"* and septic shock as its subset, where the exaggerated and abnormal response in circulatory, cellular, and metabolic system are major factors for a greater risk of mortality among patients as compared to sepsis alone [1-3, 5, 7, 9].

1.2. Key concepts of sepsis

- Sepsis is the primary cause of death from infection, especially if not recognized and treated promptly. Its recognition mandates urgent attention.
- Sepsis is a syndrome shaped by pathogen factors and host factors (eg, sex, race and other genetic determinants, age, comorbidities, environment) with characteristics that evolve over time. What differentiates sepsis from infection is an aberrant or dysregulated host response and the presence of organ dysfunction.
- Sepsis-induced organ dysfunction may be occult; therefore, its presence should be considered in any patient presenting with infection. Conversely, an unrecognized infection may be the cause of new-onset organ dysfunction. Any unexplained organ dysfunction should thus raise the possibility of underlying infection.

- The clinical and biological phenotype of sepsis can be modified by preexisting acute illness, long-standing comorbidities, medication, and interventions.
- Specific infections may result in local organ dysfunction without generating a dysregulated systemic host response.

1.3. New terms in sepsis-

- Organ dysfunction can be identified as an acute change in total Sequential [Sepsis-related] Organ Failure Assessment (SOFA) score ≥2 points consequent to the infection.
- The baseline SOFA score can be assumed to be zero in patients not known to have preexisting organ dysfunction.
- A SOFA score ≥2 reflects an overall mortality risk of approximately 10% in a general hospital population with suspected infection. Even patients presenting with modest dysfunction can deteriorate further, emphasizing the seriousness of this condition and the need for prompt and appropriate intervention, if not already being instituted.
- In lay terms, sepsis is a life-threatening condition that arises when the body's response to an infection injures its own tissues and organs.
- Patients with suspected infection who are likely to have a prolonged ICU stay or to die in the hospital can be promptly identified at the bedside with quickSOFA (qSOFA), ie, alteration in mental status, systolic blood pressure ≥100 mm Hg, or respiratory rate ≥22/min.
- Patients with septic shock can be identified with a clinical construct of sepsis with persisting hypotension requiring vasopressors to maintain MAP ≥65 mm Hg and having a serum lactate level >2 mmol/L (18mg/dL) despite adequate volume resuscitation. With these criteria, hospital mortality is in excess of 40%.

1.4. Sepsis epidemiology and causes

It is difficult to estimate the global epidemiological burden of sepsis [12, 13]. Despite significant advancements in the understanding of the pathophysiology of this clinical syndrome, advancements in hemodynamic monitoring tools, and resuscitation measures, sepsis remains one of the major causes of morbidity and mortality in critically ill patients. Sepsis is among the most common reasons for admission to intensive care units (ICUs) throughout the world [7, 14]. Sepsis is considered a major cause of health loss, but data for the global burden of sepsis are limited as the estimated figures are based upon data mainly collected from high-income countries, while data are scarce on its incidence in low- and middle-income countries. A recently compiled report on the global burden of sepsis (from 1990 to 2017) estimated about 48·9 million (95% uncertainty interval [UI] 38·9–62·9) incident cases of sepsis worldwide and 11·0 million (10·1–12·0) sepsis-related deaths representing 19·7% (18·2–21·4) of all global deaths in the year 2017 only [12, 13, 15]. As per the report, the 282 underlying causes of sepsis are broadly categorized into (i) infections, (ii) injuries, and (iii) non-communicable diseases (NCDs) which account for the total sepsis in both sexes as depicted in **Figure 1.1** [13].

In the infection category, globally, for both sexes and all age groups combined, the most common underlying cause of sepsis-related death was a lower respiratory infection every year from 1990 to 2017, with 2·8 million (95% UI 2·3–3·2) sepsis-related deaths in 1990 and 1·8 million (1·3–2·1) sepsis-related deaths in 2017 attributable to lower respiratory infections. In the injury category, the most common underlying causes of sepsis-related deaths in 2017 were road injuries were the most common injury-related cause with 145 520 (95% UI 100 480–200 090) sepsis-related deaths, and neonatal disorders were the most common NCD with 801 615 (627 191–996 840) sepsis-related deaths (appendix pp 63–68). Globally, among children younger than 5 years, the three most common causes of sepsis-related deaths in 2017 were neonatal disorders (801 615 [95% UI 627 191–996 840] deaths), lower

respiratory infections (641 682 [508 331–748 106] deaths), and diarrheal diseases (447 783 [340 224–532 225] deaths [13].

As per the reports, the global age-standardized sepsis-related mortality in 2017 was higher among males than females (164·2 [95% UI 150·1–180·1] per 100 000 vs 134·1 [123·6–146·1] per 100 000). Meanwhile, the percentage of all global deaths (from any cause) which were related to sepsis in 2017 peaked in early childhood, declined through early adulthood, and rose among older. In 2017, there were an estimated 2·9 million (95% UI 2·6–3·2) deaths related to sepsis worldwide among children younger than 5 years, 454 000 (418 000–493 000) among children and adolescents aged 5–19 years, and 7·7 million (6·9–8·5) among adults 20 years and older[13].

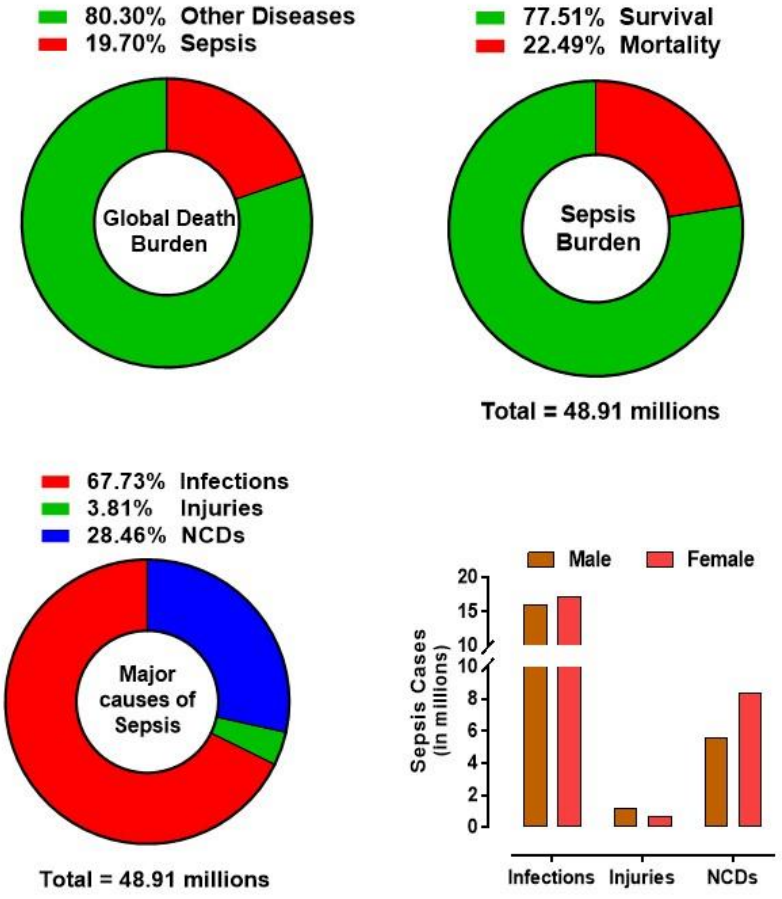

Figure 1. 1. Overview of sepsis epidemiology and causes.

1.5. Inflammatory Signalling in Sepsis

The innate immune system is the primary defense mechanism of the host to protect against invading pathogens. In humans, the innate immune system mainly comprises innate immune cells (i.e. monocytes/macrophages, neutrophils, dendritic cells (DCS), natural killer (NK) cells, mast cells (MCs), eosinophils, basophils, innate lymphoid cells (ILCs) and mucosa-associated invariant T (MAIT) cells, etc. It also includes innate humoral components such as complement system, cytokines, chemokines, and antimicrobial peptides (AMPs; LL37 and bactericidal/permeability-increasing protein (BPI), etc.) secreted by the innate immune cells. These innate immune cells express various pattern recognition receptors (PRRs) such as toll-like receptors (TLRs), nod-like receptors (NLRs), RIG-like helicases (RLH) such as melanoma differentiation-associated protein 5 (MDA-5), C-type lectin receptors (CLRs) [Dectin 1 or C-type lectin domain containing 7A (CLEC7A), dectin 2 or CLEC6A, DC-specific ICAM3-grabbing non-integrin (DC-SIGN)], complement receptor 3 (CR3), Triggering receptors expressed on myeloid cells (TREM-1), and myeloid DNAX activating protein of 12 kDa (DAP-12) associated lectin (MDL-1) [2, 11, 16, 17].

The involvement of intricate inflammatory signaling pathways and dysregulated host response makes sepsis a life-threatening heterogeneous syndrome different from a mild infection **(Figure 1.2)**. As a clinical syndrome, sepsis occurs when an infection is associated with the systemic inflammatory response. In sepsis, the expected and appropriate inflammatory response to an infectious process becomes amplified leading to organ dysfunction or risk for secondary infection **(Figure 1.2)**.

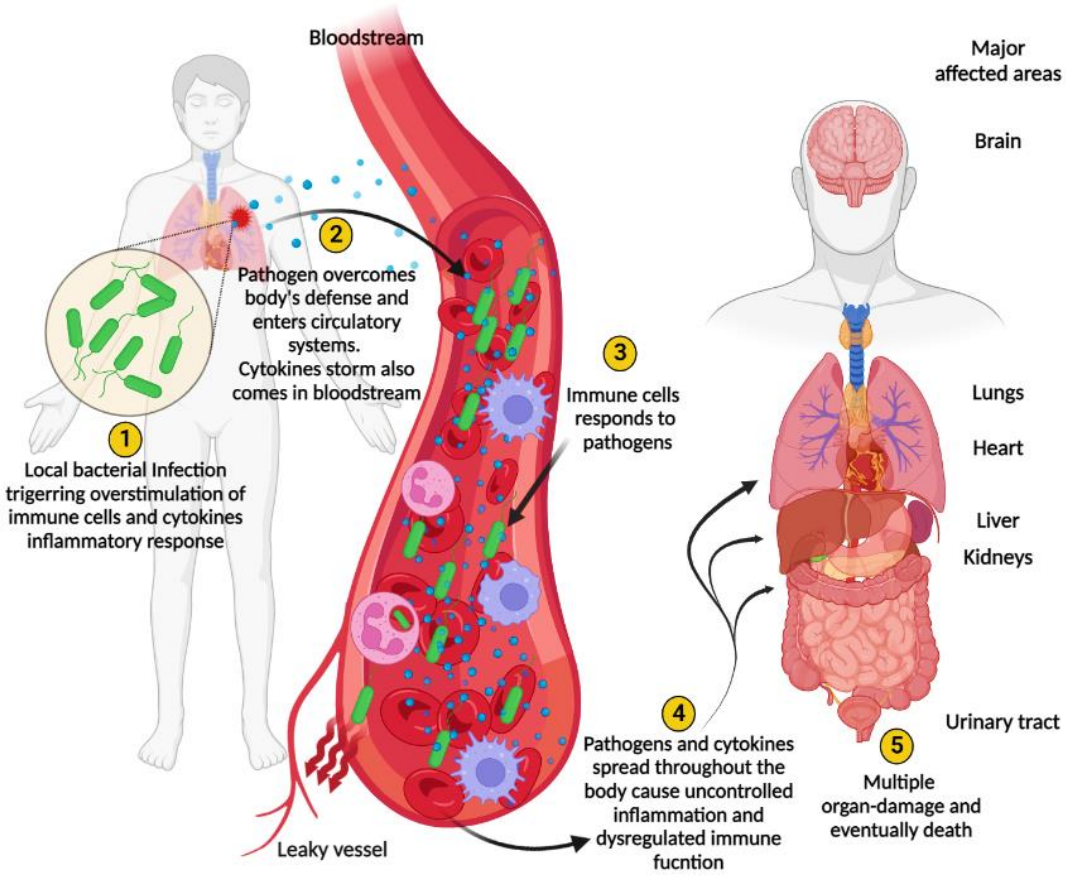

Figure 1. 2. Illustration of stages in sepsis pathogenesis.

The inflammatory response, an essential part of innate immunity first-line defense, is a complex physiological mechanism of the host immune system against infectious stimuli and a prerequisite for eliminating pathogens, followed by affected tissue repair and regeneration. Acute inflammation's primary goal is to eliminate these infectious agents. The key objective of acute inflammation is to respond and clear the infectious agents in the early stage and resolve the inflammation. But in several conditions, the inflammation persists for an extended period, leading to a chronic inflammatory situation. In the late stage, chronic inflammation eventually leads to sepsis including other numerous pathological conditions such as pulmonary disorder, cardiac dysfunction, kidney dysfunction, metabolic disorder, neurological disorder, cancer, etc. It breaches the localized inflammation leading to the cause of sepsis which results

in exaggerated innate immune response and cytokines storm imparting a crucial role in multi-organ dysfunction and mortality in many cases. Taken together, in contrast to an uncomplicated and localized infection, sepsis is a multifaceted disruption of the finely tuned immunological balance of pro-inflammation and anti-inflammation **(Figure 1.3)** [1, 2, 16, 18, 19].

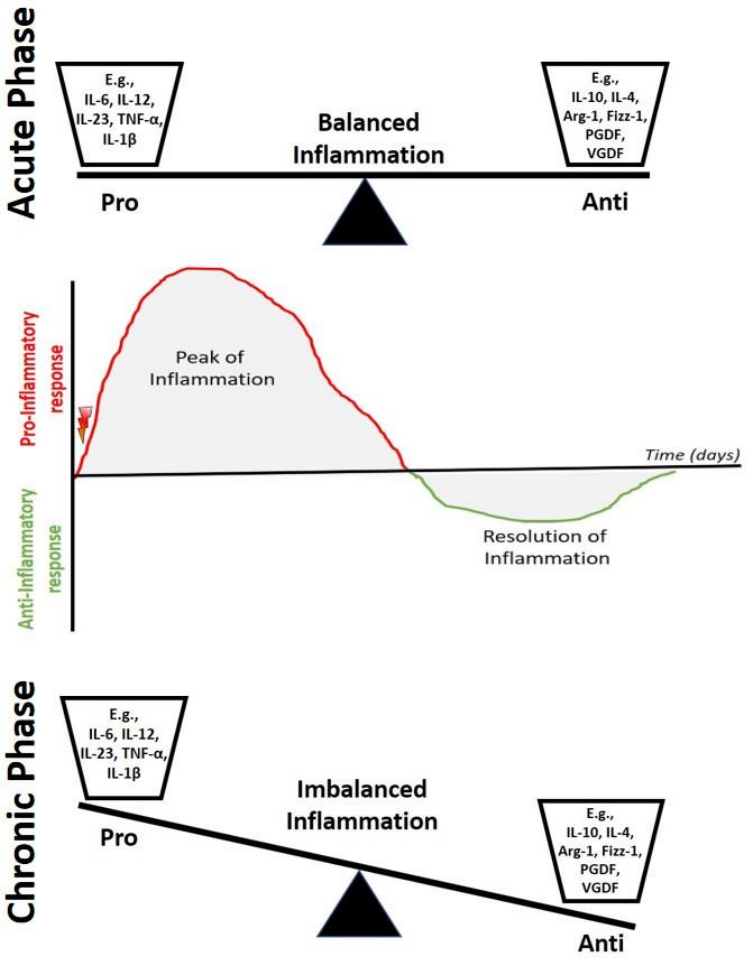

Figure 1. 3. Schematic representation of acute and chronic inflammatory phases showing the balanced and imbalanced cytokines expression, respectively. During balanced cytokines expression, the pro-inflammatory response triggered by stimulant resolute over the time followed by an anti-inflammatory response whereas an uncleared stimulant leads to overstimulation of the pro-inflammatory response causing imbalanced cytokines expression.

Toll-like receptors belong to the most studied family of PRRs, due to their central role in host defenses and involvement in several pathological processes that include sepsis. The initiating event of effective innate immune responses against pathogens and induction of sepsis is 'host-pathogen interaction' which involves the recognition of microbial-derived pathogen-associated molecular patterns (PAMPs) or endogenous damage-associated molecular patterns (DAMPs) by a series of PRRs located either at the cell membrane (TLR1, TLR2, TLR4, and TLR6) or intracellular space in the organelles including lysosomes, endosomes, phagosomes, phagolysosomes, and endolysosomes (TLR3, TLR7, TLR8, and TLR9).

One of the best examples in recent times of host-pathogen interaction leading to infection and severe immune response can be well understood from the interaction between the angiotensin-converting enzyme 2 (ACE2) receptor of human host and spike (S) protein of severe acute respiratory syndrome coronavirus-2 (SARS-CoV-2) **(Figure 1.4 A & B)** [20]. A critical step in this crosstalk between the virus and the host cell is the binding of the receptor-binding domain (RBD) of the SARS-CoV-2 spike protein to the peptidase domain of the ACE2 receptor present on the surface of host cells. The S-protein is divided into two functional parts, S1 and S2. Entry of the virus into the host cell is mediated by the combined action of both subunits, with S1 catalyzing attachment and S2 mediating fusion. The S1 subunit is further divided into two functional domains: An N-terminal domain and a C-terminal domain. A 211-amino acid region (residues 319–529) at the S1 C-terminal comprises a receptor-binding domain (RBD), mediating a pivotal role in the interaction of the virus with the host cell ACE2 receptor [20, 21]. Such interaction then leads to the internalization of pathogenic viruses and initiation of signalling causing a robust increase of inflammatory response in the host. In such conditions, the primary therapeutic approach could be the inhibition of host-pathogen interaction through the design of peptide inhibitors or the identification of small molecule inhibitors **(Figure 1.4 C)** [21].

Similarly in the case of TLR signalling, expressed at the cell surface, TLR4 detects LPS from Gram-negative bacteria and also shuttles to late endosome to induce alternative signaling following LPS sensing. TLR2 as heterodimers in association with either TLR1 or TLR6 (and possibly TLR10) senses a variety of microbial products, such as lipopeptides, lipoproteins, peptidoglycan, porins, β-glucan, glycosylphosphatidylinositol (GPI) anchors, and glycoproteins from Gram-positive bacteria, Gram-negative bacteria, mycoplasma, mycobacteria, fungi, parasites, and viruses. TLR5 senses flagellin of bacterial flagella. TLR3, TLR7, TLR8, and TLR9 are strategically expressed in endosomal compartments to recognize microbial nucleic acids: double-stranded RNA (dsRNA) by TLR3, single-stranded RNA (ssRNA) by TLR7 and TLR8, and unmethylated CpG motif-containing DNA by TLR9 [16, 22-28].

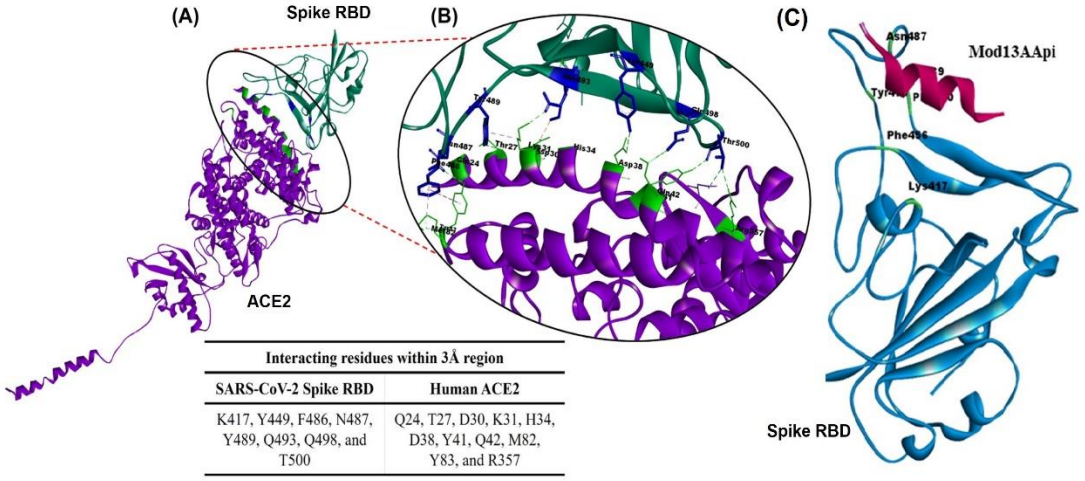

Interacting residues within 3Å region	
SARS-CoV-2 Spike RBD	Human ACE2
K417, Y449, F486, N487, Y489, Q493, Q498, and T500	Q24, T27, D30, K31, H34, D38, Y41, Q42, M82, Y83, and R357

Figure 1. 4. (A) Illustration of the host-pathogen interaction of the severe acute respiratory syndrome coronavirus-2 (SARS-CoV-2) spike receptor-binding domain [RBD] (green) and human angiotensin-converting enzyme 2 [ACE2] (purple) from the crystal structure (PDB ID 6M17) and interacting interface (encircled). **(B)** Identification of the interacting residues within the 3 Å region of the host and pathogen. The highlighted residues in the pathogen SARS-CoV-2 spike RBD (blue) interact with the human host receptor ACE2 peptidase domain residues (bright green) as demonstrated with the Discovery studio Visualizer tool. The Table shows the interacting residues within a 3 Å region that was analyzed using the Chimera tool. **(C)** Therapeutic approach to counter the SARS-CoV-2 Spike protein receptor binding domain (S-RBD) with our designed peptide inhibitor Mod13AApi. S-RBD is shown

in Blue while Mod13AApi is shown in Red. The interacting residues of S1 with peptide are shown in green along with the 3-letter code amino acid and residue number.

1.6. Macrophage role in sepsis

Macrophages are critical effector cells contributing to the altered innate immune response against infection, as they are the most efficient pathogen scavengers and the predominant source of inflammatory cytokines. Severe sepsis has been shown to be associated with progressing macrophage dysfunction [29-32]. The majority of patients diagnosed with severe forms of sepsis are infected with gram-negative or gram-positive bacteria. This fact points out to TLR 2 and 4, predominantly expressed by macrophages, as major mediators of septic injury, due to their ability to recognize structures present in these classes of bacteria and trigger the inflammatory response leading to cytokines storm [26]. Macrophages are sentinel cells of the innate immune system; their location varies from peripheral blood to various organs including lungs, liver, brain, kidneys, skin, testes, and vascular endothelium. Consequently, dysregulated activation of macrophages impacts the outcome of diverse organ systems in a multitude of diseases. Of the signaling pathways that modulate macrophage function, Toll-like receptors (TLRs) constitute a key signaling system **(Figure 1.2)**. Therefore, macrophages are recognized to play essential roles throughout all phases of sepsis and affect both immune homeostasis and inflammatory processes, and hence macrophage dysfunction is considered to be one of the major causes of sepsis. In the early stage of sepsis, macrophages undergo M1 differentiation and promote host defense by eliminating invading pathogens or damaged tissues and releasing massive amounts of pro-inflammatory cytokines such as tumor necrosis factor-alpha (TNF-α), interleukin-1 beta (IL-1β), interleukin-6 (IL-6) and interleukin-8 (IL-8), interleukin-12 (IL-12), interleukin-23 (IL-23), etc. However, macrophages may be excessively activated during the early phase and produce excessive pro-inflammatory cytokines, cytokine storm, which have been identified as one of the major causes for the high mortality rate in the early stage of sepsis [10, 33-35]. Conversely, an excessive increase

in M2-like macrophages during late-stage sepsis stimulates the release of large quantities of IL-10, transforming growth factor-β (TGF-β), and other anti-inflammatory cytokines that induce an immunosuppressive state in the host. These different polarization states are important manifestations of macrophages that are involved in regulating immune homeostasis in the host's microenvironment. Elucidating the regulatory processes and molecular mechanisms of macrophage polarization during different stages of sepsis can facilitate the maintenance of immune homeostasis within a septic microenvironment and the treatment of complications. The host's immune response is highly inflammatory in the early stage when a large number of inflammatory mediators are present that damage both tissues and immune cells; this is followed by an advanced stage of sepsis characterized by host immunosuppression [29]. Therefore, regulation of the host's immune balance is the primary goal of immunotherapy for sepsis patients [36].

1.7. Macrophages-mediated signaling in sepsis

Toll-like receptors (TLRs) are of interest to immunologists because of their front-line role in the initiation of innate immunity against invading pathogens. The key signalling domain, which is unique to the TLR system, is the Toll/interleukin-1 (IL-1) receptor (TIR) domain, which is located in the cytosolic face of each TLR, and also in the adaptors. TIR domain-containing adaptors have been found to have crucial roles in TLR-signalling pathways because they provide specificity to the response generated by signalling through each TLR [37]. Similar to the TLRs, the adaptors are conserved across many species. Signalling by TLRs involves five adaptor proteins that are recruited by TIR/TIR domain interactions. These adaptors (as per the sequence of their discovery) are: myeloid differentiation primary response gene (MyD88), TIR domain-containing adaptor protein (TIRAP, also known as MyD88-adaptor-like (MAL)), TIR-domain-containing adaptor protein inducing IFNβ (TRIF; also known as TICAM1), TRIF-related adaptor molecule (TRAM; also known as TICAM2) and sterile α- and armadillo-motif containing protein (SARM) [22, 28, 37] **(Figure 1.4)**.

Briefly, MyD88 is essential for signaling through all TLRs except TLR3 and is involved in early nuclear factor-κB (NF-κB) and mitogen-activated protein kinases (MAPKs) activation and pro-inflammatory gene expression. TIRAP serves as a bridge to recruit MyD88 to TLR2 and TLR4. TRIF initiates MyD88-independent IFN regulatory factor 3 (IRF3) and late NF-κB activation involved in the production of type I IFNs and IFN-inducible genes. TRIF is recruited to the cytoplasmic domain of TLR3 and, in late endosome, through TRAM that bridges TRIF to TLR4. A fifth TIR domain-containing adaptor, sterile α-, and armadillo-motif containing protein (SARM) acts as a negative regulator of TLR3 and TLR4 signaling. SARM interacts with TRIF and inhibits the induction of TRIF-dependent genes [22, 28].

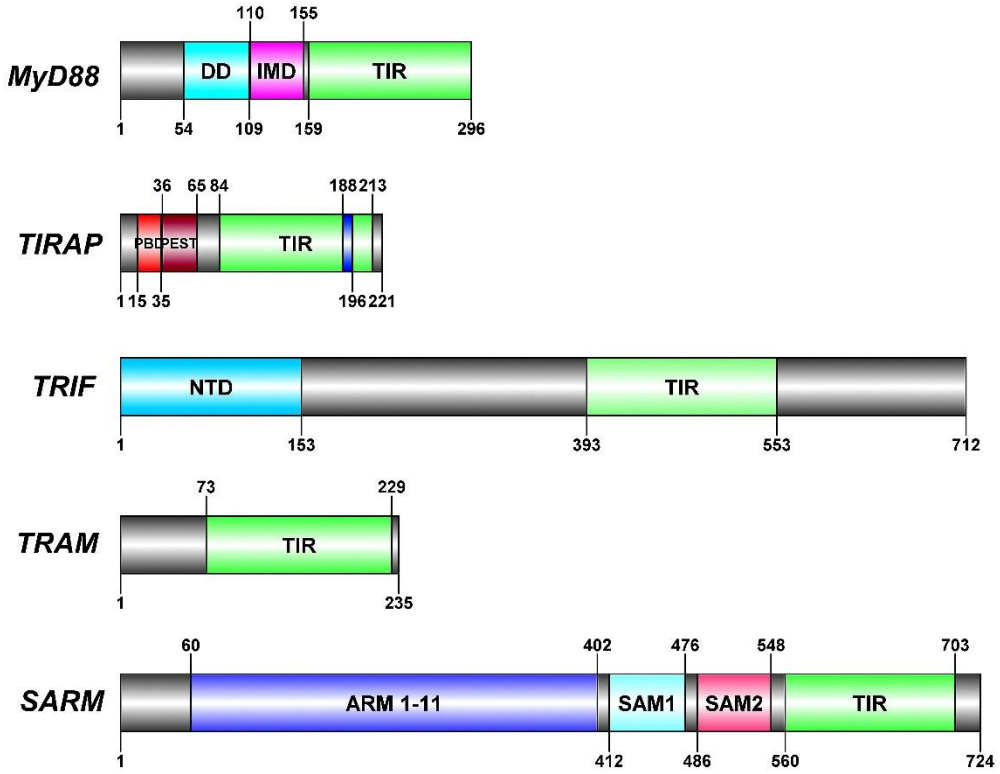

Figure 1. 5. Schematic representation of the five TIR domain-containing adaptor proteins highlighting structural and functional domains and motifs. *DD- death domain; IMD- intermediate domain; PBD- phosphatidylinositol 4,5-bisphosphate (PIP-2)-binding domain; PEST- Pro, Glu, Ser, and Thr-rich domain; TIRAP (188-196)- TRAF6 binding motif; NTD- N-terminal domain; ARM- armadillo repeats motif; SAM- sterile α-motif.*

1.8. References

1. Jarczak, D., S. Kluge, and A. Nierhaus, *Sepsis—pathophysiology and therapeutic concepts.* Frontiers in Medicine, 2021: p. 609.
2. Kumar, V., *Toll-like receptors in sepsis-associated cytokine storm and their endogenous negative regulators as future immunomodulatory targets.* International immunopharmacology, 2020. **89**: p. 107087.
3. Gyawali, B., K. Ramakrishna, and A.S. Dhamoon, *Sepsis: The evolution in definition, pathophysiology, and management.* SAGE open medicine, 2019. **7**: p. 2050312119835043.
4. Funk, D.J., J.E. Parrillo, and A. Kumar, *Sepsis and septic shock: a history.* Critical care clinics, 2009. **25**(1): p. 83-101.
5. Gotts, J.E. and M.A. Matthay, *Sepsis: pathophysiology and clinical management.* Bmj, 2016. **353**.
6. Gül, F., et al., *Changing definitions of sepsis.* Turkish journal of anaesthesiology and reanimation, 2017. **45**(3): p. 129.
7. Taeb, A.M., M.H. Hooper, and P.E. Marik, *Sepsis: current definition, pathophysiology, diagnosis, and management.* Nutrition in Clinical Practice, 2017. **32**(3): p. 296-308.
8. Levy, M.M., et al., *2001 sccm/esicm/accp/ats/sis international sepsis definitions conference.* Intensive care medicine, 2003. **29**(4): p. 530-538.
9. Singer, M., et al., *The third international consensus definitions for sepsis and septic shock (Sepsis-3).* Jama, 2016. **315**(8): p. 801-810.
10. Angus, D.C. and T. Van der Poll, *Severe sepsis and septic shock.* N Engl J Med, 2013. **369**: p. 840-851.
11. Wiersinga, W.J., et al., *Host innate immune responses to sepsis.* Virulence, 2014. **5**(1): p. 36-44.
12. Chiu, C. and M. Legrand, *Epidemiology of sepsis and septic shock.* Current Opinion in Anesthesiology, 2021. **34**(2): p. 71-76.
13. Rudd, K.E., et al., *Global, regional, and national sepsis incidence and mortality, 1990–2017: analysis for the Global Burden of Disease Study.* The Lancet, 2020. **395**(10219): p. 200-211.
14. Marik, P.E., *Early management of severe sepsis: concepts and controversies.* Chest, 2014. **145**(6): p. 1407-1418.
15. World Health, O., *Global report on the epidemiology and burden of sepsis: current evidence, identifying gaps and future directions.* 2020.
16. Zhang, Y.-y. and B.-t. Ning, *Signaling pathways and intervention therapies in sepsis.* Signal Transduction and Targeted Therapy, 2021. **6**(1): p. 1-36.
17. Cinel, I. and S.M. Opal, *Molecular biology of inflammation and sepsis: a primer.* Critical care medicine, 2009. **37**(1): p. 291-304.
18. Chen, L., et al., *Inflammatory responses and inflammation-associated diseases in organs.* Oncotarget, 2018. **9**(6): p. 7204-7218.
19. Chousterman, B.G., F.K. Swirski, and G.F. Weber. *Cytokine storm and sepsis disease pathogenesis*. Springer.
20. Rajpoot, S., et al., *A Novel Therapeutic Peptide Blocks SARS-CoV-2 Spike Protein Binding with Host Cell ACE2 Receptor.* Drugs R D, 2021.
21. Rajpoot, S., et al., *In-Silico Design of a Novel Tridecapeptide Targeting Spike Protein of SARS-CoV-2 Variants of Concern.* Int J Pept Res Ther, 2022. **28**(1): p. 28.
22. Savva, A. and T. Roger, *Targeting toll-like receptors: promising therapeutic strategies for the management of sepsis-associated pathology and infectious diseases.* Front Immunol, 2013. **4**: p. 387.

23. Tsujimoto, H., et al., *Role of Toll-like receptors in the development of sepsis.* Shock, 2008. **29**(3): p. 315-321.
24. Cristofaro, P. and S.M. Opal, *The Toll-like receptors and their role in septic shock.* Expert opinion on therapeutic targets, 2003. **7**(5): p. 603-612.
25. Weighardt, H. and B. Holzmann, *Role of Toll-like receptor responses for sepsis pathogenesis.* Immunobiology, 2008. **212**(9-10): p. 715-722.
26. Possolo Souza, H., T. Lima-Salgado, and L. Monteiro da Cruz Neto, *Toll-like receptors in sepsis: a tale still being told.* Endocrine, Metabolic & Immune Disorders-Drug Targets (Formerly Current Drug Targets-Immune, Endocrine & Metabolic Disorders), 2010. **10**(3): p. 285-291.
27. Gao, H., et al. *Severe sepsis and Toll-like receptors*. Springer.
28. Salomão, R., et al., *TLR signaling pathway in patients with sepsis.* Shock, 2008. **30**(7): p. 73-77.
29. Chen, X., et al., *The roles of macrophage polarization in the host immune response to sepsis.* 2021. **96**: p. 107791.
30. Huang, X., et al., *PD-1 expression by macrophages plays a pathologic role in altering microbial clearance and the innate inflammatory response to sepsis.* Proceedings of the National Academy of Sciences, 2009. **106**(15): p. 6303-6308.
31. Munoz, C., et al., *Dysregulation of in vitro cytokine production by monocytes during sepsis.* The Journal of clinical investigation, 1991. **88**(5): p. 1747-1754.
32. Ayala, A. and I.H. Chaudry, *Immune dysfunction in murine polymicrobial sepsis: mediators, macrophages, lymphocytes and apoptosis.* Shock (Augusta, Ga.), 1996. **6**: p. S27-38.
33. Cheng, Y., et al., *Park 7: a novel therapeutic target for macrophages in sepsis-induced immunosuppression.* Frontiers in Immunology, 2018. **9**: p. 2632.
34. Murray, P.J. and T.A. Wynn, *Protective and pathogenic functions of macrophage subsets.* Nature reviews immunology, 2011. **11**(11): p. 723-737.
35. Fujiwara, N. and K. Kobayashi, *Macrophages in inflammation.* Current Drug Targets-Inflammation & Allergy, 2005. **4**(3): p. 281-286.
36. Chen, F., et al., *Targeting toll-like receptors in sepsis: from bench to clinical trials.* Antioxidants & Redox Signaling, 2021. **35**(15): p. 1324-1339.
37. O'Neill, L.A. and A.G. Bowie, *The family of five: TIR-domain-containing adaptors in Toll-like receptor signalling.* Nat Rev Immunol, 2007. **7**(5): p. 353-64.

Chapter 2

(Background and Significance)

Chapter 2: Background and Significance

2.1. Graphical summary

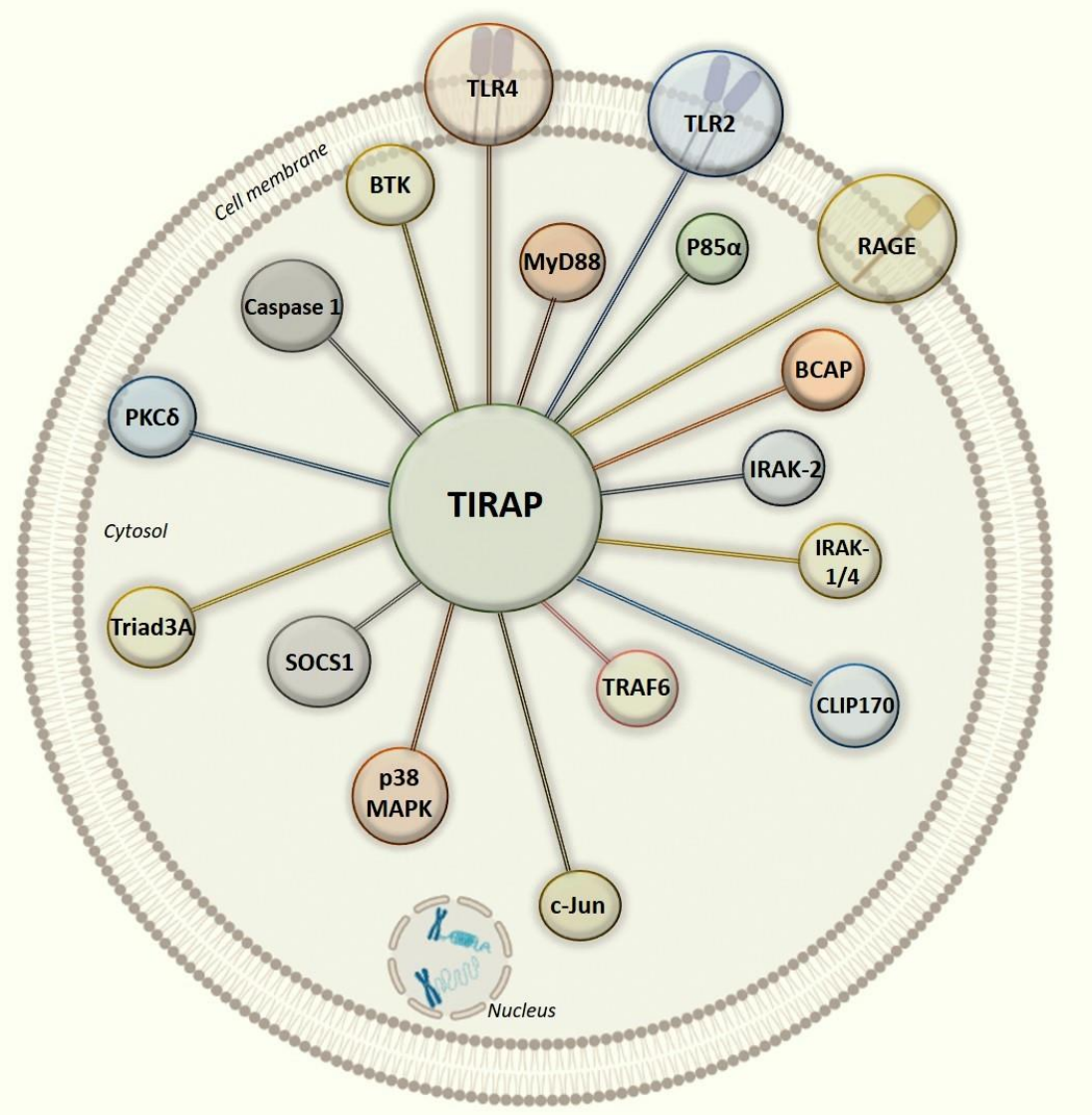

Figure 2. 1. *Representing the total network of TIRAP protein-protein interactions in macrophages inflammatory signalling since its discovery mere as an adaptor protein bridging MyD88 and TLR4/2 further highlights the significance as the master regulator of inflammation.*

2.2. TIRAP: Discovery and Emergence

The second adaptor in the TIR-domain-containing adaptor family TIRAP/MAL was discovered as the adaptor required for signalling by TLR4 and TLR2, serving as a bridge to recruit MyD88. Accumulating evidence suggests the specific role of TIRAP was confirmed in TIRAP-deficient mice, which were shown to be defective in TLR4 and TLR2 signalling in terms of cytokine induction. This led to the conclusion that TIRAP is required for signalling only by TLR4 and TLR2. For TLR4 signalling, the phenotype in TIRAP-deficient cells was the same as that for MyD88-deficient cells — involving a delay in NF-κB and p38 MAPK activation while no role in the activation of IRF3 and so the conclusion was drawn that TIRAP is an essential component of the inflammatory pathway [1].

Besides, many other features of TIRAP have also been uncovered that distinguish it from other adaptors mainly MyD88, for example, TIRAP has a TRAF6-binding motif and it also undergoes tyrosine phosphorylation for activation, which has a role in both TLR4 and TLR2 signalling, and in turn leads to the increased activity of NF-κB, which is required for cytokines gene expression. Since the discovery of TIRAP in 2001, initial studies were mainly focused on its role as an adaptor protein that couples MyD88 with TLR4/2, to activate MyD88-dependent TLRs signalling. Subsequent studies highlighted and delineated TIRAP's role as a transducer of signalling events through its interactions with several non-TLR signalling mediators. Indeed, the ability of TIRAP to interact with an array of intracellular signalling mediators suggests its central role in various immune responses. Therefore, continued studies that elucidate the molecular basis of various TIRAP-protein interactions and how they affect the signalling magnitude should provide key information on the inflammatory disease mechanisms.

TIRAP-deficient mice have not been tested in as many disease models as MyD88-deficient mice. However, TIRAP has been shown to be crucial for early immune responses to *Escherichia coli* and LPS in the lung, and also in the induction of antimicrobial peptides in the lung in response to *Klebsiella pneumoniae*, but not to

Pseudomonas aeruginosa. LPS-induced airway hyper-reactivity has also been shown to involve TIRAP [1]. Therefore, the TIRAP holds a huge potential for further study in disease conditions where it may make differential interactions to regulate the signalling. Hence understanding TIRAP protein-protein interactions and its function in signalling could be therapeutically significant and novel in chronic inflammatory diseases. Therefore, we attempted to summarize all the protein-protein interactions of TIRAP since its discovery to understand the overall inflammatory signalling mechanism mediated by TIRAP.

2.3. TIRAP-mediated protein-protein interactions in inflammation

The table (**Table 2.1**) below summarizes the total number of partner proteins making interactions with TIRAP as well as the nature of such interaction whether modulating positively or negatively the function of TIRAP.

Table 2. 1. The significance of TIRAP interaction with the partner proteins in the cellular process.

Sr No.	Interactions	Nature of Response	Role of the Interaction in Inflammatory Pathways	References
1	TIRAP-TLR4	Pro-inflammatory response	Interaction transduces downstream signaling via MyD88 dependent pathway. It bridges MyD88 to TLR4 and hence activates NF-κB and AP-1 nucleus translocation and cytokines expression.	[2-5]
2	TIRAP-TLR2	Proinflammatory response	Like TLR4, this interaction also bridges TRL2 to MyD88 and leads to the production of the inflammatory cytokines via the activation of NF-κB, AP-1, and MyD88-independent PI3k-Akt pathway too.	[3, 6, 7]
3	TIRAP-MyD88	Proinflammatory response	In the MyD88 dependent pathway, the TIRAP acts as the	[2-5, 8, 9]

			bridging protein to bring the MyD88 to TLR4/2 inflammatory signaling.	
4	TIRAP-CLIP170	Inhibitory	Bacterial protein TcpB interacts with TIRAP and allows CLIP170 interaction which leads to TIRAP ubiquitination and promotes proteasomal degradation and hence reduced NF-κB and AP-1 response.	[10]
5	TIRAP-RAGE	Proinflammatory response	The stimulated RAGE receptor, similar to TLR4, binds TIRAP to activate MyD88 dependent NF-κB and AP-1 inflammatory pathways.	[11]
6	TIRAP-TRAF6	Proinflammatory response	In the stimulated TLR4 pathway, the interaction leads to the transactivation of p65 by its direct phosphorylation at serine-536 (p-S536) residue.	[12]
7	TIRAP-p85α	Proinflammatory response	TIRAP interacts with PI3K subunit p85α in response to the TLR2-TLR1/6 heterodimer response to activate the PI3K-Akt pathway.	[7, 13]
8	TIRAP-Triad3A	Inhibitory	In overexpressed conditions, Triad3A, an E3 ubiquitin ligase, observed to interact with TIRAP for its U&PD	[14]
9	TIRAP-SOCS1	Inhibitory	SOCS1 interacts with BTK phosphorylates TIRAP to negatively regulate it by U&PD	[15-17]
10	TIRAP-BTK	Proinflammatory response	In stimulated TLR4/2 pathways, the interaction of BTK is crucial for TIRAP	[6, 18-20]

			activation by its TIR domain tyrosine phosphorylation and leads to downstream NF-κB and AP-1 activation	
11	TIRAP-PKCδ	Proinflammatory response	The interaction leads to phosphorylation and activation of TIRAP which promotes the downstream p38 MAPK and NF-κB response in stimulated macrophages.	[19, 21, 22]
12	TIRAP-p38 MAPK	Proinflammatory response	Interaction leads to activation of AP-1 and pro-inflammatory cytokines response in stimulated macrophages	[21, 23]
13	TIRAP-c-Jun	Proinflammatory response	In stimulated TLR4 pathway, interaction leads to the transactivation of c-Jun and its nucleus translocation for proinflammatory genes expression	[24]
14	TIRAP-IRAK2	Proinflammatory response	In the TLR4/2 pathway, interaction activates NF-κB independent of MyD88 via TRAF6 and TAK protein and hence the pro-inflammatory response	[2, 20]
15	TIRAP-Caspase1	Inhibitory	Caspase1 interaction leads to cleavage of TIRAP at D198 for its activity in TLR4/2 pathways for NF-κB activity. In contrast study, D198E, however, functions normally and hence demands more study.	[25, 26]
16	TIRAP-IRAK1/4	Inhibitory	In stimulated TLR4/2 pathways, TIR domain	[27]

			mediated interaction leads to mainly T28 and probably other sites phosphorylation in TIRAP leading to its U&PD	
17.	TIRAP-BCAP	Inhibitory	This interaction negatively regulates TLR signaling. Dimeric BCAP interferes with the TLR-PI3K signalling and associates with the TIR domain-containing protein of TLR signalosome mainly TIRAP to negatively regulates the inflammatory response.	[28-31]

2.3.1. TIRAP and Bruton's tyrosine kinase (BTK)

For TIRAP to carry out its function as a TLR adaptor protein in inflammatory signaling, it must be recruited to the membranes' activated receptors. This occurs upon binding to PIP2 before its interaction with TLRs[32]. Subsequent interaction with TLRs' TIR domain is facilitated by tyrosine phosphorylation of selected TLRs and their adaptor molecules by several tyrosine kinases, including Bruton's tyrosine kinase (BTK), Src, Lyn, Syk, etc[33, 34]. For example, phosphorylation of the cytoplasmic tail of the TLR4 TIR domain at Y674 and Y680 and phosphorylation of TIRAP tyrosine residues at positions 86, 106, 159, and 187 by BTK are required for TLR4-TIRAP-MyD88 interaction and activation of NF-κB and MAPK (mitogen-activated protein kinase) signaling leading to proinflammatory responses (**Figure 2.2**) [6, 20, 35, 36]. BTK interaction with TIRAP and its tyrosine phosphorylation in the TIR domain is crucial for TIRAP to function. Six conserved tyrosine (Y) residues in the TIR domain of human TIRAP are the potential phosphor-receptor site. The four residues Y86, Y106, Y159, and Y187 in TIRAP are experimentally identified as the sites for BTK-mediated phosphorylation. Meanwhile, the mutation of these tyrosine

residues either with alanine or phenylalanine describes them as the crucial sites for BTK-mediated phosphorylation, as after stimulation, the mutation impaired the BTK association with TIRAP, similar to the previously reported P125H variant of TIRAP. Also, these mutations play a dominant negative role and impair NF-κB activation [6, 20, 37]. Several studies hence concluded the significance of tyrosine sites on TIRAP in the TIR domain for association with BTK immediately on LPS stimulation. However, it is important to have a detailed understanding of the mechanism of TIRAP-BTK interaction and the role of tyrosine phosphorylation in regulating downstream signaling. The prerequisite step in the TIRAP phosphorylation by BTK is its activation itself. In stimulated macrophages, src kinase is reported to activate BTK as well as PKCδ (protein kinase C delta) [18, 19, 21, 38-40]. Structural analysis of BTK and PKCδ interaction with TIRAP suggests that Y106 of TIRAP is phosphorylated by the action of both BTK and PKCδ[19]. Both phosphorylation sites promote the activation of downstream p38-MAPK, NF-κB pathways, and the associated cytokine response, but due to ubiquitin-dependent degradation of phosphorylated TIRAP mediated by SOCS1 (suppressor of cytokine signaling 1), TIRAP tyrosine phosphorylation by BTK is transient [17]. With the critical molecules poised to become activated at the membrane, BTK-mediated TIRAP phosphorylation and activation, followed by degradation of phospho-TIRAP, results in a rapid yet balanced inflammatory response, avoiding prolonged TLR4 or TLR2 signaling that would otherwise result in chronic inflammation and associated diseases [17]. A recently concluded study on BCR-TLR interplay suggests that the high expression of BTK in TLR signaling leads to the development of pathology in a Btk-dependent model for systemic autoimmune disease [41].

2.3.2. TIRAP and Receptor for advanced glycation end-products (RAGE)

The Receptor for advanced glycation end-products (RAGE) is a multi-ligand cell membrane receptor implicated in diverse chronic inflammatory states such as cardiovascular disease, cancer, neurodegeneration, and diabetes [42-44]. RAGE is activated by diverse damage-associated molecular pattern molecules (DAMPs), which

include advanced glycation end products (AGEs), high mobility group box-1 (HMGB1), and S100 proteins [43-45]. Upon ligand binding, Protein Kinase C-z (PKC-z) phosphorylates the cytosolic domain of RAGE on Ser391, mediating interaction with the TIR domain TIRAP [11]. As with TLR signaling, TIRAP acts as a bridge to MyD88. In this way, RAGE activation inducesMyD88-dependent proinflammatory signaling [11] (**Figure 2.2**). The soluble RAGE is generated after either the proteolytic cleavage of its transmembrane domain to generate sRAGE or alternative splicing to give endogenous soluble RAGE (esRAGE). These proteins have distinct roles in inflammation and disease (compared to RAGE), with neither capable of inducing signaling upon binding RAGE targets. Instead, sRAGE blocks RAGE signaling effectively and appears to prevent or reduce inflammatory conditions [42, 43, 46]. As mutations in the TIR domain of TIRAP result in the inhibition of downstream inflammatory signaling and the role of RAGE in inducing a proinflammatory immune response during disease[11]. The RAGE signalling plays a vital role in many inflammatory-associated diseases (acute lung injury, sepsis, inflammatory bowel disease, atherosclerosis, cancer and other chronic infectious and noninfectious diseases). Many ligands (e.g., HMGB1, s100, etc) activate both RAGE and TLR4 leading to the same inflammatory pathway via TIRAP interaction, a direct cross-talk between both signalling has also been highlighted [47, 48]. It should now be explored in detail whether the therapeutic intervention of TIRAP and RAGE represents a means to treat these diseased states. An earlier study on neuronal cells has been reported to disrupt this interaction through decoy RAGE peptide (RAGE-I) targeting TIRAP and abrogating the activation of cdc42, inhibiting cell migration and invasion and protecting cell death [49].

2.3.3. TIRAP and phosphatidylinositol3′-kinase p85 and b-cell adaptor for phosphoinositide 3-kinase (BCAP)

The interaction of p85a, a regulatory subunit of phosphoinositide3-kinase (PI3K) with TIRAP, is a MyD88-independent response of the TLR2 receptor upon stimulation with bacterial lipoproteins (**Figure 2.2**) [7, 13]. This interaction is highly significant in

TLR2 and TLR6heterodimer signaling, resulting in the activation of PI3K dependent phosphorylation of Akt, PIP3 [phosphatidylinositol(3,4,5)P3] generation, and polar shape changes of the macrophage [7]. Signaling is initiated when TLR2 heterodimers with TLR6 are bound by diacylated lipoprotein ligands, or when TLR1/2 heterodimers are bound by triacylated lipoproteins [50]. Ligand binding induces conformational changes within the receptor that bring their TIR domains close to downstream signal transduction [1, 51, 52]. Upon diacylated lipoprotein stimulation of TLR2/6, TIRAP, but not MyD88, is essential for PI3K activity and NF-κB activation[7]. Upon stimulation of macrophages, TIRAP interacts with p85a, and these proteins colocalize at the plasma membrane [7]. Whereas MyD88 is not required for interaction of TIRAP with p85a, the efficiency ofPI3K activity, and therefore downstream activation of Akt and NF-κB, as well as macrophage polarization, becomes delayed inMyD88 deficient cells [7]. This suggests that the TIRAP interaction with p85a is direct but that MyD88 might accelerate the kinetics of Akt phosphorylation and PIP3 generation. MALP-2 induced activation of the TLR2/6 pathway in THP-1cells also induces the interaction of TIRAP with p85a, and this is essential for the induction of Heme Oxygenase-1 (HO-1) via Akt phosphorylation and Nrf2 activation [13]. Similar to the above study, this study also reported that MyD88 deficiency resulted in decreased Akt phosphorylation but at earlier time points post activation (60 minutes). HO-1 expression upon MALP-2 stimulation also involves c-Src and BTK, which are other binding partners of TIRAP. These proteins are likely to form a complex consisting of c-Src, BTK, TIRAP, and p85a upon stimulation, and together, they represent a potentially important target for pharmacotherapy during various chronic inflammatory diseases. In contrast, a multi-modular protein, B-cell adaptor for phosphoinositide 3-kinase (PI3K) (BCAP) has been reported to negatively regulate the TLR4/2-PI3K signalling, suggesting its association with TLR and downstream TIR domain of TIRAP, leading to its recruitment to TLR signalosome by TIR-TIR interactions [29-31]. BCAP also interacts with p85a suggesting its role in regulating the downstream signalling [31]. BCAP is a dimeric protein and its oligomerization depends on its ANK (ankyrin repeat) and DBB (Dof/BANK1/BCAP) domains. A recently concluded study clearly defines the

importance of DBB domain in dimerization and its role in TIRAP-BCAP interaction [28]. The monomeric BCAP, though fails to negatively regulate the TLR signaling suggesting that only domain dimerization drives the negative response. The TIRAPTIR domain is reported to assemble to form filament complex invitro, an event critical for signal transduction. Such a filament could be disrupted by dimeric, and not monomeric, BCAP. Another angle suggests BCAP phosphoinositide metabolism, which cleaves PIP2 to DAG and IP3 and hence deprives TIRAP for its membrane anchor required for TLR signaling [28]. Overall, the BCAP association mainly with TIRAP and p85a provides novel directions for regulatory pathways in inflammation.

2.3.4. TIRAP and Protein kinase C-delta (PKCδ)

As mentioned above, PKCδ represents an interacting partner of TIRAP that is required for TLR2- and TLR4-induced activation of p38 MAPK, NF-κB and proinflammatory cytokine expression (**Figure 2.2**) [21, 38]. Mice harboring PKCδ-deficiency reduces the bacterial killing function of macrophages, showing decreased NO, ROS, and H2O2, resulting in hyper-susceptible animals to infection with mycobacterium tuberculosis with increased mortality[53]. Mechanistically, PKCδ constitutively interacts with and phosphorylates Y106 in the TIR domain of TIRAP as described above, and BTK phosphorylates TIRAP at Y106, as well as Y86 [19]. Accordingly, Baig et al., 2017 reported a novel heterotrimeric complex consisting of TIRAP, PKCδ, and p38MAPK required for AP1-mediated inflammatory responses in macrophages in response to LPS stimulation [21]. Thus, TIRAP activity is regulated in response to receptor stimulation. In this situation, TIRAP was not required for the phosphorylation of PKCδ but was required for cytokine production [21]. In summary, PKCδ activation is likely required downstream of TIRAP; however, it remains unclear how PKCδ activation is regulated in macrophages upon LPS stimulation.

2.3.5. TIRAP and Cytoplasmic linker protein 170 (CLIP170)

Cytoplasmic linker protein 170 (CLIP170), containing two conserved cytoskeleton-associated protein Glycine rich (CAPGly)domains and two tandem repeats of zinc

knuckle motifs (also called CCHC zinc fingers), is a multifunctional protein that binds to and regulates the dynamics of the growing plus end of microtubules [54-56]. In addition, CLIP170 acts as a negative regulator of TLR4 by inducing TIRAP ubiquitination (both mono and polyubiquitination) and promoting its proteasomal degradation (**Figure 2.2**). Accordingly, this activity of CLIP170 decreased downstream signaling activity, including reduced NF-κB, and MAPK activity. Further, the activity of CLIP170 is specific to TIRAP, with MyD88 levels unaltered upon overexpression of CLIP170 [10]. Analogous to many negative regulators, CLIP170expression is induced upon stimulation with LPS. Interestingly, the pathogenic bacteria Brucella species viz. *Brucella melitensis, Brucella abortus,* and *Brucella ovis* inhibit TIRAP activity by encoding a TIR domain-containing effector protein TcpB, also called Btp1 [57]. TcpB, like TIRAP, shares phosphoinositide binding properties and resemblance in its TIR domain; however, functionally, TcpB impairs TLR-4 and TLR-2 induced NF-κB activation inflammatory responses [10, 57]. Mechanistically, TcpB interacts with TIRAP and promotes CLIP170-dependent polyubiquitination and subsequent proteasomal degradation of TIRAP [10]. CLIP170 is also of therapeutic interest; Pregnenolone, a steroid hormone precursor, suppresses TLR4 and TLR2 mediated inflammation by promoting CLIP170-mediated ubiquitination and degradation of TIRAP [58].

2.3.6. TIRAP and c-Jun

Delivery of bacterial-derived pathogenic LPS to TLR4 has been shown to activate AP-1 through a series of phosphorylation events on serine/threonine residues mediated by upstream MAPKs(extracellular signal-regulated kinases; ERK, c-Jun N-terminal kinase; JNK, and p38 mitogen-activated protein kinases; p38kinase) [59]. For example, c-Jun, which contains a transactivation domain, is phosphorylated at Ser 63 and 73 by JNKs, resulting in its activation [59]. c-Jun can form homo and heterodimers with otherAP-1 family members, including c-Fos or ATF (Activating transcription factor) to make transcriptionally active complexes [60-63]. These transcriptionally active dimeric components of AP-1 now control the activation of critical

proinflammatory cytokine genes such as TNF-a, IL-12, IL-23, and other proinflammatory cytokines [64-67]. In recent findings, TIRAP was found to interact with the AP-1 subunit c-Jun in endotoxin-induced macrophages. This drives the transactivation of c-Jun, its translocation to the nucleus, and a proinflammatory immune response (**Figure 2.2**) [24]. Careful analysis of the molecular docking of a TIRAP-c-Jun crystal structure with immunoprecipitation experiments revealed the direct interaction of TIRAP with c-Jun[24]. The pharmacological inhibitor Gefitinib, which abrogates the interaction of TIRAP with c-Jun, specifically reveals the importance of TIRAP-mediated c-Jun transactivation; treatment with Gefitinib drastically reduced the expression of several proinflammatory cytokines (IL-12, IL-23, TNF-a) in both bone-marrow-derived macrophages and in animals [24].

2.3.7. TIRAP and p38 mitogen-activated protein kinase (MAPK)

As mentioned above, p38 MAPK is one of three members of the MAPK protein family, that in response to LPS, induces the expression of proinflammatory cytokines (IL-12, IL-23, TNF-a, IL-6, and IL-1b) through activation of the downstream transcription factor AP-1 [23]. In addition, the MyD88-dependent TLR4/TLR2 induced activation of MAPKs and NF-κB and subsequent proinflammatory response is well characterized [4, 8, 23, 68, 69]. Interestingly, this inflammatory response is also regulated through the direct interaction of TIRAP with p38 MAPK and PKCδ in LPS-stimulated macrophages (**Figure 2.2**) [21] and suggests that TIRAP has multiple functions in the induction of MAPK signaling.

2.3.8. TIRAP and Caspase-1

Two reports on the interaction of TIRAP with Caspase-1 have highlighted the importance of this interaction to macrophage signaling events [25, 26]. Caspases are evolutionarily conserved enzymes with aspartate-specific, cysteine-dependent proteolytic activity, which are involved in inflammation and apoptosis[70, 71]. Caspase-1, formerly called IL-1beta converting enzyme (ICE), is synthesized as a zymogen precursor and is cleaved into its p20 (20kDa) and p10 (10kDa) active

catalytic subunits and a non-catalytic Caspase Activation and Recruitment Domain (CARD) [72, 73]. Active caspase-1, often found in a multi-protein complex called the inflammasome, cleaves the inactive pro-forms of IL-1b and IL-18 to generate active cytokines. This function of caspase-1, as well as activation of gasdermin-D (GSDMD), is critical for the inflammatory immune response of LPS-primed macrophages [73, 74]. TIRAP first found to interact with caspase-1 by yeast two-hybrid, is not required for the activation of Caspase-1 (**Figure 2.2**) [25]. Instead, caspase-1appears to cleave TIRAP (but not MyD88), and this is required for TLR4, and TLR2 mediated NF-κB, p38 MAPK activation, and cytokine production but not IL-1 and TLR7 signaling, which is TIRAP independent [25, 26]. After LPS stimulation of macrophages, caspase-1 was reported to cleave after D198 in the C-terminal region of TIRAP. However, the significance of this cleavage was questioned by another study, which found that cleavage was not required for NF-κB activity [26]. Instead, it appears that mutation of D198A disrupts TLR4 mediated signaling due to the loss in the acidic amino acid at this site and not due to the loss of caspase-1 cleavage. Indeed, TIRAP-D198E remained functional, suggesting that TIRAP is functional in its full-length form [26]. Therefore, whether the caspase-1-TIRAP interaction is of biological relevance requires further study.

2.3.9. TIRAP and Tumor necrosis factor receptor (tnfr)-associated factor 6 (TRAF6)

A novel role for TIRAP in NF-κB p65 trans-activation was described after the identification that TIRAP interacts with TRAF-6 [12]. The interaction following the activation of TLR2 or TLR4 is direct in nature and independent of membrane localization (**Figure 2.2**). The TRAF family of adaptor proteins and E3 ubiquitin ligases comprises 6 members, viz., TRAF1, TRAF2, TRAF3, TRAF4, TRAF5, and TRAF6, with each member having distinct functions in the regulation of immune signaling [75]. A short motif, Pro-X-Glu-X-X-Z (X: any amino acid; Z: aromatic/acidic residue), acts as a TRAF6 binding motif that is found in various receptors and adaptor proteins [75].TIRAP contains a TRAF6 binding domain, with

mutation of this motif (TIRAP-E190A), abolishing interaction with TRAF6 and preventing signal transduction [12]. Functionally, the interaction of TIRAP with TRAF6 promotes serine-536 phosphorylation of the p65 subunit of NF-κB, which regulates its transcriptional activation, rather than nuclear translocation [12]. In contrast, a recent study based on a mathematical data model suggests that TIRAP-independent MyD88 activation and Myddosome complex formation in TLR4 signaling does not require TRAF6 [76].

2.3.10. TIRAP and TRIAD3A

LIGASE RNF216 (TRIAD3A) Triad3A is a RING finger-type E3 ubiquitin-protein ligase that recognizes and interacts with the TIR domain of TLRs, promoting their proteolytic degradation [14, 77]. Specifically, Triad3A causes K48-linked ubiquitination and degradation of TLR4 and TLR9. In addition, Fearns et al. (2006) demonstrated that overexpressed Triad3A directly interacts with and results in the degradation of the TLR4 adaptor proteins TIRAP, TRIF, and RIP1 but no other adaptor proteins such as MyD88 and TRAM (**Figure 2.2**) [14]. This suggests that TIRAP is post-translationally regulated via different E3 ligases (CLIP170 and Triad3A). Future work should determine the relative contributions and functions to pro-inflammatory immune signaling.

2.3.11. TIRAP and Interleukin-1 receptor-associated kinase-like 2 (IRAK-2)

The interleukin-1 receptor-associated kinase (IRAK) family protein kinase consists of four members, IRAK-1, IRAK-2, IRAK-3/M, and IRAK-4 [78]. The sequential activation and recruitment of IRAKs, excluding IRAK-M, in MyD88-dependent signaling is well studied and reported in TLR signaling [69, 79-81]. In the TLR-4-TIRAPMyD88mydossome complex, active MyD88 interacts with the N-terminal death domains of IRAK4, triggering a series of phosphorylation events and recruitment of IRAK-1 and IRAK-2, which are required for TRAF-6 ubiquitination, activation, and downstream activation of NF-κB (**Figure 2.2**) [82, 83]. In addition, IRAK-2, but

not IRAK-1, directly interacts with TIRAP, and this results in NF-κB activation [2, 20]. Further evidence for the critical role of IRAK-2 comes from the observation that a dominant-negative variant blocks TIRAP-induced NF-κB activation. The precise residues that mediate the TIRAP-IRAK-2 interaction remain unknown, but the critical tyrosine residues of TIRAP (Y86, Y106, and Y159) are not required [20]. Further research is required to understand the precise physiological role of the IRAK-2-TIRAP signaling axis and test whether it represents a means for developing targeted therapeutics that control inflammation.

2.3.12. TIRAP and Interleukin-1 receptor associated kinase-like 1/4 (IRAK1/4)

Interestingly, the interaction of TIRAP with IRAK-4 and IRAK-1 can result in TIRAP degradation following its phosphorylation and ubiquitination, and therefore inhibition of signaling (**Figure 2.2**). In this way, IRAK-1/-4 negatively regulates TLR-4/2 signaling by expressing an auto-active IRAK4 inducing TIRAP degradation[27]. The interaction appears to be mediated by the TIR domain of TIRAP, with mutation of proline at position 125 (P125H) in the BB loop abolishing the interaction. Both IRAK-4 and IRAK-1 phosphorylate multiple sites, including T28 on TIRAP, are required for subsequent ubiquitination and degradation [27]. Additional research is required to dissect the additional phosphorylation sites within TIRAP, as well as the ubiquitination sites that control TIRAP degradation. Furthermore, the selective role of IRAK-4 and IRAK-1 both as positive and negative regulators is an important consideration in the investigation of inflammation. It is interesting to speculate that over time IRAK-1 and IRAK-4 switch from a positive role inMyD88 dependent inflammatory signaling to a negative one, helping to dampen signaling and prevent too much inflammation. What controls this switch should be investigated using a dose-dependent endotoxin challenge over time, with careful monitoring of TIRAP complex composition.

2.3.13. TIRAP and Suppressor of cytokine signaling 1 (SOCS1)

The suppressor of cytokine signaling (SOCS1) serves as a key physiological regulator of both innate and adaptive immunity acting through macrophages, dendritic cells, B-

cells, and T-cells[84]. Structurally, the eight intracellular members of the SOCS family, SOCS1-SOCS7 and CIS, have a central SH2 domain, N-terminal extended SH2 subdomain and a variable region, and C-terminal40 amino acid SOCS box. The SOCS box recruits factors for E3 ubiquitin ligase-mediated target protein ubiquitination followed by proteasomal degradation [84, 85]. Previous studies described SOCS1 as a negative intracellular regulator in the cytokine-induced JAK-STAT pathway; however, subsequent studies have addressed the role of SOCS1 that is associated with TLR4 and TLR2 signaling as an E3 ligase that polyubiquitinates TIRAP along with other proteins such as p65and IRAK1, causing their 26S proteasomal degradation [15-17]. Analogous to PEST (Proline, Glutamic acid, Serine, and Threonine) motif-containing proteins such as IκB, the PEST region of TIRAP mediates its phosphorylation, lysine polyubiquitination, and degradation, after LPS and Pam3Cysinduced TLR4 and TLR2 signaling, but not following TLR7and TLR9. Unlike TIRAP, MyD88 does not contain a PEST domain. This degradation appears dependent on SOCS1; a mutant SOCS1 (SH2 and SOCS Box) variant, as well as SOCS1deficient macrophages, are unable to target and degrade TIRAP in response to LPS ligation, whereas wild-type SOCS1 interacted and degraded TIRAP as early as 15 to 30 minutes post LPS stimulation [17]. As tyrosine phosphorylation of TIRAP is required for SOCS1-mediated degradation, it appears that TIRAP is degraded only after BTK has been activated and has phosphorylated TIRAP [15, 17]. Further, the tyrosine phosphorylated TIRAP generates a binding site for the SH2-domain of SOCS1[15]. Accordingly, SOCS1 mediates the negative regulation of TIRAP to prevent sustained NF-κB and MAPK activities in macrophages [17]. In addition to TIRAP phosphorylation, SOCS1 functional activity also depends on NOS1-derived NO production [66, 86]. In response to LPS inTLR4 signaling, NOS1-derived NO production resulted in the degradation of wild-type SOCS1 post-S-nitrosation, whereas pharmacological inhibition of NOS1 resulted in increasedSOCS1 expression and a concomitant increase in TIRAP degradation [66]. Therefore, it will be a rewarding effort to elucidate how the NOS1 axis, propagating sustained TIRAP

activation, balances with TIRAP degradation mediated via BTK and SOCS1 during different inflammatory events (**Figure 2.2**).

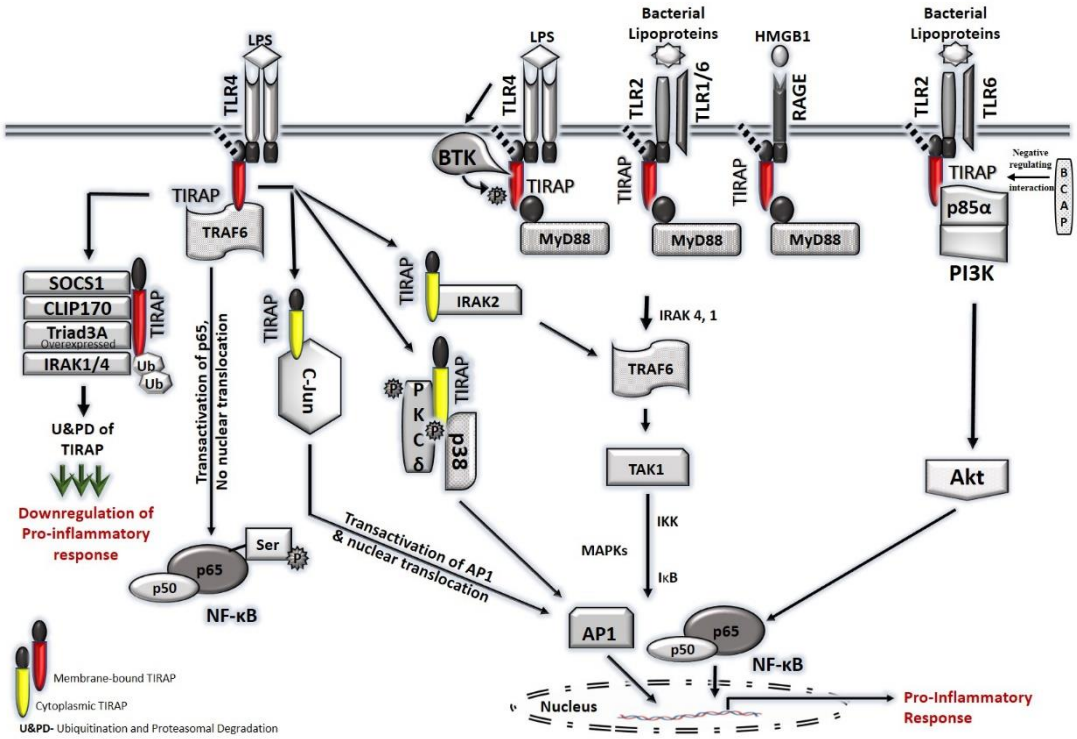

Figure 2. 2. TIRAP in the mechanism of inflammation.

2.4. TIRAP- TIR domain

Studies have described the role of TIRAP in modifying the innate immune response elicited largely by endotoxin. However, the increasing number of TIRAP partner proteins and their role in the activation of inflammatory response pose great potential as therapeutic targets, demanding further structural elucidation. Here we have attempted to give a brief insight into the basic architecture of TIRAP and its protein binding domain.

In our preliminary analysis, we dissected the TIRAP structure and its key sites making it possible for so many protein-protein interactions as discussed above. In Chapter 1, we have briefly shown the domains of the TIR domain-containing adaptor proteins. Further, as the study emphasizes the TIRAP, we studied the TIRAP in detail. The

human TIRAP gene encodes a 221 amino acid protein [87]. Segregating the TIRAP protein sequence gives us an N-terminal region spanning from the 1st to 83rd amino acid containing the PBD (Phosphatidylinositol 4,5-bisphosphate(PIP2) Binding Domain) from the 15th to 35th amino acid sequence that is rich in lysine residues. A C-terminal region mainly encodes the TIR Domain, spanning 130 amino acids long from the 84th to the 213th position [37, 87, 88]. Also, we used the Motif search tool at www.genome.jp (https://www.genome.jp/tools/motif/) to obtain the domain details from different databases as produced by the tool search results.

Interestingly, in all the interactions discussed above **(Figure 2.2)**, it is interesting to note that the TIR domain is centrally involved in making interactions with the TIRAP partner proteins. So, we propose to dissect the key sites in TIRAP which can modulate these interactions. Though, there may be numerous post-translational modifications that can regulate TIRAP interactions, however, the experimental evidence of tyrosine phosphorylation in the TIR domain is one of the most common and validated. Besides, the macrophages largely produce NOS (Nitric oxide synthase) mediated NO (nitric oxide) which has a crucial role in regulating inflammatory responses, for example, NOS1 protects TIRAP degradation from SOCS1 [66, 86]. Unlike phosphorylation, there is no experimental evidence of NO-mediated nitrosylation sites yet in TIRAP, however, we may presume that the presence of Cystine S-nitrosylation site in the TIR domain may be another key factor in regulating the interaction and signaling events. However, S-glutathionylation of cysteine at C91 in the TIR domain has been shown to increase the interaction of TIRAP with MyD88 [89]. Besides the known phosphorylation sites, the TIR domain might also encompass other sites which might be crucial for a string of TIRAP-mediated interactions. Hence, in the current analysis, we attempted to computationally predict the major post-translational modifications- (i) Serine/threonine/tyrosine phosphorylation and (ii) S-nitrosylation sites, respectively in TIRAP.

Briefly, the human TIRAP TIR domain sequence retrieved from UniProt (UniProtKB-P58753) was used for the prediction and study. We searched the protein

phosphorylation database PhosphoSitePlus server (https://www.phosphosite.org/homeAction) and the same sites were retrieved for the human TIRAPTIR domain. Further, the predictions of possible phosphorylation sites in the TIR domain were obtained from kinase-based phosphorylation prediction tools; GPS-phosphorylation (http://gps.biocuckoo.cn/) [90] and NetPhos 3.1 (http://www.cbs.dtu.dk/services/NetPhos/) [91]. Including the experimentally proved sites, both tools predicted the same number of a total of 21 probable phosphorylation sites (10 serine sites, 05 threonine sites, and 06tyrosine sites) **(Figure 2.3)**. Similarly, the S-Nitrosylation (SNO) sites in the TIR domain were predicted from three different computational tools [GPS-SNO (http://sno.biocuckoo.org) [92], DeepNitro (www.deepnitro.renlab.org) [93] and SNOSite (http://csb.cse.yzu.edu.tw/SNOSite/predict.php)] [94]. Interestingly, all the SNO sites predicted from these three independent tools were found similar **(Figure 2.3).** The graphical representation of TIRAP and its domains, as presented in Supplementary Figure 1, was further depicted using the DOG Domain illustrator tool (http://dog.biocuckoo.org/). In support of these predictions, the tyrosine residues Y86, Y106, Y159, and Y187 have been reported to be the experimentally confirmed phosphorylation sites that modulate the interaction of TIRAP with BTK protein and downstream transcription factors activation. Since the discovery of TIRAP, it has been shown to have an elaborate role in inflammatory signalling. As summarized in this review, many investigators have identified its diverse functions other than that of its role as an adaptor protein. The dynamic nature of TIRAP interaction with several upstream and downstream signaling proteins in varied inflammatory pathways draws immense curiosity towards the post-translational modifications in its TIR domain.

Interestingly, a recent study described the interaction of TIRAP andMyD88 with IL1R1 (interleukin-1 receptor like-1) receptor in response to Helicobacter pylori released stimuli [95]. Though this study focuses on experimentally validated phosphorylation sites of the TIRAP TIR domain, it would be interesting to

experimentally identify novel modification sites on TIRAP which may reveal other crucial interactions involved in signaling pathways.

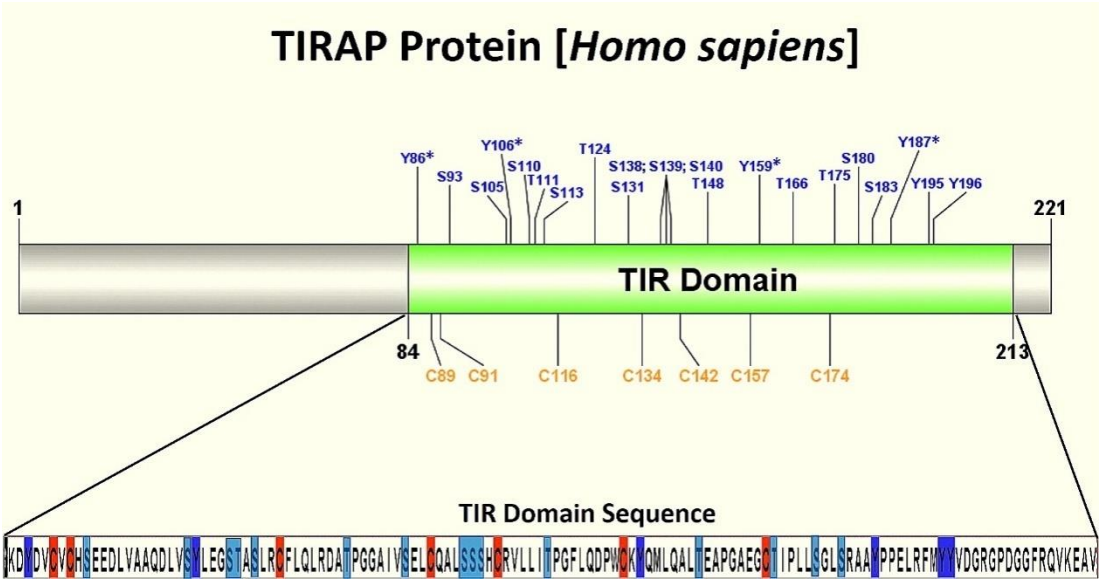

Figure 2. 3. Representation of TIRAP TIR (Toll/Interleukin-1 Receptor) domain and computational prediction of serine (S), threonine (T), and tyrosine (Y) phosphorylation and cysteine (C) S-nitrosylation (SNO) positions. The TIRAP protein containing an N-terminal PBD and C-terminal TIR domain are highlighted. The predicted phosphorylation sites on top and SNO sites at bottom of the domain map are indicated in blue and light brown colors, respectively. The experimentally proved phosphorylation sites (Y86, Y106, Y159, and Y187) are marked with an asterisk. The predicted phosphorylation sites were obtained from kinase-based computational tools GPS-Phosphorylation (http://gps.biocuckoo.cn/) and NetPhos 3.1 (http://www.cbs.dtu.dk/services/NetPhos/). For cysteine (C) SNO sites, computational tools GPS-SNO (http://sno.biocuckoo.org/index.php), DeepNitro (www.deepnitro.renlab.org), and SNOSite (http://csb.cse.yzu.edu.tw/SNOSite/predict.php) were used.

Since the phosphorylation of TIRAP is the most crucial modification for its activation and downstream function as also discussed above, we were curious to focus our study on understanding the TIRAP protein interactions with kinases and its activation. The TIRAP, though known well to be phosphorylated by BTK for its activation and downstream signalling in MyD88 dependent pathway. However, the TIRAP-PKCδ interaction and TIRAP activation by its phosphorylation is not well established whereas the TIRAP-PKCδ sigalling axis mediated pathway is not studied in detail.

Henceforth, it was very interesting to dissect the signalling mechanism and to use this as a therapeutic approach for inflammatory diseases. So further studies focused on the PKCδ and BTK-mediated TIRAP activation. Therefore, it is imperative to discuss these two kinases' background and significance in inflammatory signalling and sepsis.

2.5. Role of PKCδ in inflammation and sepsis

Protein Kinase C (PKC) was first identified by Nishizuka and coworkers in 1977. It is a family composed of phospholipid-dependent serine/threonine kinases that play a crucial role in infections and are one of the master regulators of inflammatory signaling. These kinases are composed of a highly conserved catalytic domain (C-terminus) and a regulatory domain (N-terminus) that demonstrates considerable variability across family members. Based on structural elements and cofactor requirements for activation, mammalian PKCs are classified into three broad categories comprising (i) classical/conventional PKCs (cPKCs: PKC-α, β-I, β-II, and γ isoforms)require Calcium (Ca2+) and the lipid second messenger diacylglycerol (DAG), (ii) novel PKCs (nPKCs: PKC-δ, ε, η, and θ isoforms)require DAG but are calcium-independent, (iii) atypical PKCs (aPKCs: PKC-ι and ζ isoforms), do not require Ca2+ or DAG for activation, but are sensitive to other lipid second messengers such as phosphatidylserine (PS) [96-99]. The different PKCs share several common structural features. The catalytic domain (C3 and C4), located at the C-terminus, contains the ATP binding site, as well as the substrate binding sites. A hinge region connects the catalytic domain to the regulatory domain (C1 and C2) at the N-terminus, which is a domain that regulates the activation state of the kinase through a pseudo-substrate region. PKCs also contain five variable regions, which are poorly conserved across the different PKCs **(Figure 2.4)** [97, 98, 100].

PKCs isoforms are implicated in a wide range of cellular functions and a plethora of diseases. Initial evidence for the involvement of PKC in TLR signaling came from observations that altering PKC activity in cells of the innate immune system affected cytokine secretion. Subsequently, LPS and other TLR ligands were shown to activate most of the PKC isoforms expressed in monocytes, macrophages, dendritic cells, and neutrophils. PKCδ is a unique nPKC that plays a significant role in several diseases, including cancer, diabetes, ischemic heart disease, and neurodegenerative diseases and recent studies have shown that PKCδ is also a critical regulator of the inflammatory response in sepsis. Though the role of PKCδ in sepsis is established, less is known about the PKCδ activation during the inflammatory response [96, 99].

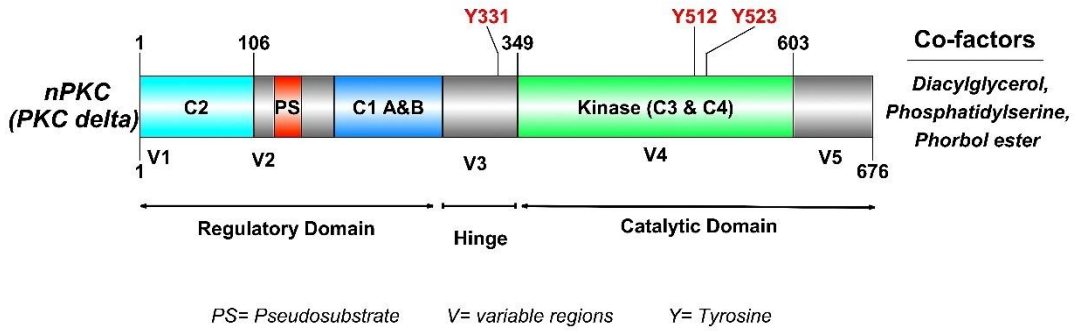

Figure 2. 4. Schematic representation of nPKC (PKC delta) domains and crucial tyrosine phosphorylation sites.

PKCδ activity is regulated by phosphorylation patterns, subcellular translocation, and cleavage in a context-dependent manner. The three main conserved threonine and serine phosphorylation sites for PKCδ are Threonine-505 (Thr-505, activation loop), Serine-643 (Ser-643, turn motif), and Serine-662 (Ser-662, hydrophobic motif). Unlike other members of the PKC family, PKCδ is unique in its regulation and activation by tyrosine phosphorylation, activation mechanisms, and multiple subcellular targets. Human PKCδ contains 20 tyrosine residues (19 for mice and 21 for rats) and includes phosphorylation sites in the regulatory domain (Tyr-52, Tyr-64, Tyr-155, and Tyr-187), the hinge region (Tyr-311 and Tyr-332), and the catalytic domain (Tyr-505, Tyr-512, and Tyr-523) [39, 97]. Tyrosine phosphorylation of the catalytic domain increases PKCδ activity, while tyrosine phosphorylation in the

regulatory domain influences cellular actions rather than catalytic competence.Tyr-311, Tyr-332, and Tyr-512 are important phosphorylation sites for kinase activation and subcellular localization and are phosphorylated during sepsis and play key roles in sepsis-induced lung injury. Inhibition of PKC-δ with Rottlerin, or its downregulation, consistently decreases activation of NF-κB, secretion of inflammatory cytokines, and production of nitric oxide by cells in TLR4 and TLR2 pathway underscores its importance in signaling via these receptors. Also, studies with PKCδ−/− mice and PKCδ inhibitors indicate a role for PKCδ in regulating neutrophil trafficking to the lung in response to inflammation triggered by bacterial sepsis, asbestos, stroke/reperfusion injury, LPS, or pancreatitis [96, 101, 102].

2.6. Role of BTK in inflammation and sepsis

Btk was first identified as the gene responsible for X-linked agammaglobulemia (XLA), an immune disorder characterized by a lack of circulating B lymphocytes as a result of a pro- to pre-B cell transition during B cell ontogeny and an absence of immunoglobulins (Ig) of all classes. It is critically important for B-cell development as well as mature B-cell activation and survival [18].

Non-receptor tyrosine kinases are involved in signalling in response to diverse stimuli but are perhaps most studied in the context of immune regulation. They are typified by the Src kinase family of protein tyrosine kinases (PTK), which are best understood for their role downstream of receptors such as the T cell receptor (TCR) and B cell receptor (BCR). Ligation of either of these receptors activates Src family members associated with them, a consequence of which is the trans-phosphorylation of tyrosine residues on the receptor complex. This results in the recruitment of additional kinases and downstream signalling molecules to the receptor complex via the interaction of their Src-homology-2(SH2) domains with the phosphorylated tyrosine.

The Tec family of protein tyrosine kinases, of which Bruton's tyrosine kinase (Btk) is a prototypical member, is involved in a vast array of signaling pathways in cells of hematopoietic lineage. The Tec kinases are similar to the Src family, but in addition to an SH2 (src-homology 2), SH3, and kinase domain in their C terminal half, they also possess an N terminal pleckstrin homology (PH) domain, responsible for membrane localization due to its high affinity for phosphatidylinositol lipids **(Figure 2.5)**. This domain is followed by the Tec homology (TH)region, unique to each family member. This is a proline-rich region, which has been implicated in the autoregulation of the Tec kinases. Similar to the Src family they are expressed mainly in hematopoietic cells and are key signalling proteins downstream of Src kinases [18, 36, 41].

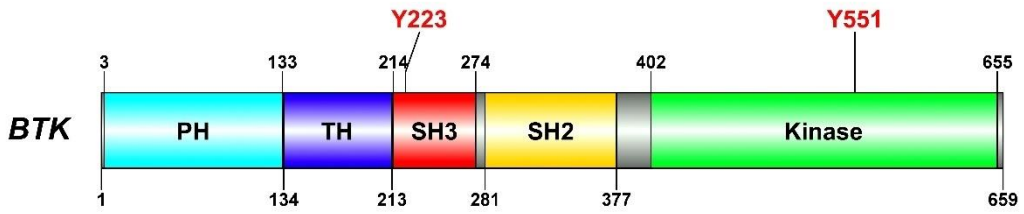

Figure 2. 5. Schematic representation of BTK domains with crucial tyrosine phosphorylation sites activating BTK protein.*PH, pleckstrin homology domain; TH, Tec homology region; SH3, Src-homology 3 domain; SH2, Src-homology 2 domain; Kinase, kinase domain.*

Btk is by far the most studied member of this family and is expressed in myeloid, mast, and B cells, but not in T lymphocytes and natural killer cells. In a resting cell, the majority of the Btk is localized in the cytosol and rapidly recruited to the plasma membrane when it becomes phosphorylated and its tyrosine kinase activity subsequently activated. Btk activation is a two-step process. The first and prerequisite step for its activation is membrane targeting where the PH domain binds selectively to the phosphatidylinositol 3-kinase (PI3K) product PIP3 or is presumed that associated with TLR4 promotes membrane localization. The second step in Btk activation is phosphorylation on its activating loop by a tyrosine kinase and subsequent

autophosphorylation of the SH3 domain. Phosphorylation of Y551 results in the association of R544 with the newly acquired phosphate group, thus releasing E445, allowing it to relocate to the active site and take part in the catalytic reaction. Src kinases such as Lyn are responsible for the transphosphorylation of Btk. This transphosphorylation event results in the autophosphorylation of tyrosine 223 in the SH3 domain of Btk, and subsequent activation of downstream signalling pathways [18, 36].

In particular, it has been shown that Btk interacts with the TIR domains of TLRs 4, 6, 8, and 9 and was also found to specifically associate with MyD88, Mal, and IL-1 receptor-associated kinase 1 (IRAK-1) [18]. LPS induces tyrosine phosphorylation of Btk and activates its kinase activity, and monocytes from patients with X-linked agammaglobulinemia, which contain mutant Btk, are unresponsive to LPS [6, 103]. TIRAP is tyrosine phosphorylated during TLR2 and TLR4 signaling. Btk is identified as the responsible tyrosine kinase and therefore TIRAP adaptor protein is the first substrate for Btk in TLR signaling to be identified, its phosphorylation by Btk being an important mechanism in signaling by TLR2 and TLR4 [6].

2.7. Scope and Objectives of the Study

The study proposes to understand the significance of TIRAP-mediated signaling in the TLR4 pathway of macrophages to develop a novel therapeutic strategy for sepsis. The TIRAP shows huge therapeutic potential due to its key involvement in several inflammatory pathways and hence could be a novel target in pathophysiological conditions. Besides the regulation of pathogenic agents, the host-specific target is crucial to curb the uncontrolled inflammation in response to infections which play a central role in initiating the sepsis condition. Therefore, it would be therapeutically beneficial to pursue the TIRAP-mediated signalling in response to various infectious stimulants and identify the candidate molecules targeting TIRAP to dampen the exaggerated response. In sepsis, we proposed to reveal the novel TIRAP-PKCδ mediated signalling and understand the TIRAP-BTK interaction and hence identify potential drug candidates targeting host-specific molecule TIRAP in sepsis conditions.

Drug identification is a tedious and time-consuming process. However, advancements in various biological, chemical, and mainly computational technologies have paved the drug discovery process faster and more economical. In the same process is drug repurposing. The urgency of an effective drug for sepsis may be answered through drug repurposing which will hugely cut down the time and cost. We, therefore, proposed to include the identification of approved small molecules to repurpose as a potential anti-inflammatory agent to tackle sepsis conditions. Collectively, we propose to study the importance of the TIR domain in TIRAP as a key interface involved in protein interactions which could hence serve as a therapeutic target to dampen the extent of acute and chronic inflammatory conditions.

Henceforth, the study's main objective is focused on exploring the TIRAP activation by its protein-protein interaction with two upstream kinases BTK and PKCδ, and TIRAP-mediated inflammatory signaling in macrophages. The following major aims are therefore proposed for it:-

- **Aim 1:-**To understand the TIRAP protein interaction with PKCδ in the LPS/TLR4 pathway to regulate the chronic inflammatory signaling and identification of small molecules through in-silico study for validation as an anti-sepsis agent through in-vitro and in-vivo model study.
- **Aim 2:-**To understand the tyrosine phosphorylation in the TIRAP TIR domain in relation to p38 MAPK interaction and its activation using in silico approaches.
- **Aim 3:-** To understand the non-phosphorylated and phosphorylated state of upstream kinases BTK and PKCδ interaction with TIRAP for identification of consensus interface of TIRAP and drug targeting for simultaneous inhibition of interactions.

2.8. References

1. O'Neill, L.A. and A.G. Bowie, *The family of five: TIR-domain-containing adaptors in Toll-like receptor signalling.* Nat Rev Immunol, 2007. **7**(5): p. 353-64.
2. Fitzgerald, K.A., et al., *Mal (MyD88-adapter-like) is required for Toll-like receptor-4 signal transduction.* Nature, 2001. **413**(6851): p. 78-83.
3. Bernard, N.J. and L.A. O'Neill, *Mal, more than a bridge to MyD88.* IUBMB Life, 2013. **65**(9): p. 777-86.
4. Chow, J.C., et al., *Toll-like receptor-4 mediates lipopolysaccharide-induced signal transduction.* J Biol Chem, 1999. **274**(16): p. 10689-92.
5. Lu, Y.C., W.C. Yeh, and P.S. Ohashi, *LPS/TLR4 signal transduction pathway.* Cytokine, 2008. **42**(2): p. 145-151.
6. Gray, P., et al., *MyD88 adapter-like (Mal) is phosphorylated by Bruton's tyrosine kinase during TLR2 and TLR4 signal transduction.* 2006. **281**(15): p. 10489-10495.
7. Santos-Sierra, S., et al., *Mal connects TLR2 to PI3Kinase activation and phagocyte polarization.* EMBO J, 2009. **28**(14): p. 2018-27.
8. Balka, K.R. and D. De Nardo, *Understanding early TLR signaling through the Myddosome.* J Leukoc Biol, 2019. **105**(2): p. 339-351.
9. Ohnishi, H., et al., *Structural basis for the multiple interactions of the MyD88 TIR domain in TLR4 signaling.* Proc Natl Acad Sci U S A, 2009. **106**(25): p. 10260-5.
10. Jakka, P., et al., *Cytoplasmic Linker Protein CLIP170 Negatively Regulates TLR4 Signaling by Targeting the TLR Adaptor Protein TIRAP.* J Immunol, 2018. **200**(2): p. 704-714.
11. Sakaguchi, M., et al., *TIRAP, an adaptor protein for TLR2/4, transduces a signal from RAGE phosphorylated upon ligand binding.* PLoS One, 2011. **6**(8): p. e23132.
12. Verstak, B., et al., *MyD88 adapter-like (Mal)/TIRAP interaction with TRAF6 is critical for TLR2- and TLR4-mediated NF-kappaB proinflammatory responses.* J Biol Chem, 2009. **284**(36): p. 24192-203.
13. You, X., et al., *Macrophage-activating lipopeptide-2 requires Mal and PI3K for efficient induction of heme oxygenase-1.* PLoS One, 2014. **9**(7): p. e103433.
14. Fearns, C., et al., *Triad3A regulates ubiquitination and proteasomal degradation of RIP1 following disruption of Hsp90 binding.* J Biol Chem, 2006. **281**(45): p. 34592-600.
15. Fujimoto, M. and T. Naka, *SOCS1, a Negative Regulator of Cytokine Signals and TLR Responses, in Human Liver Diseases.* Gastroenterol Res Pract, 2010. **2010**.
16. Kinjyo, I., et al., *SOCS1/JAB is a negative regulator of LPS-induced macrophage activation.* Immunity, 2002. **17**(5): p. 583-91.
17. Mansell, A., et al., *Suppressor of cytokine signaling 1 negatively regulates Toll-like receptor signaling by mediating Mal degradation.* Nat Immunol, 2006. **7**(2): p. 148-55.
18. Jefferies, C.A. and L.A. O'Neill, *Bruton's tyrosine kinase (Btk)-the critical tyrosine kinase in LPS signalling?* Immunol Lett, 2004. **92**(1-2): p. 15-22.
19. Paracha, R.Z., et al., *Structural evaluation of BTK and PKCdelta mediated phosphorylation of MAL at positions Tyr86 and Tyr106.* Comput Biol Chem, 2014. **51**: p. 22-35.
20. Piao, W., et al., *Tyrosine phosphorylation of MyD88 adapter-like (Mal) is critical for signal transduction and blocked in endotoxin tolerance.* J Biol Chem, 2008. **283**(6): p. 3109-19.
21. Baig, M.S., et al., *Heterotrimeric complex of p38 MAPK, PKCdelta, and TIRAP is required for AP1 mediated inflammatory response.* Int Immunopharmacol, 2017. **48**: p. 211-218.
22. Kubo-Murai, M., et al., *Protein kinase Cdelta binds TIRAP/Mal to participate in TLR signaling.* Mol Immunol, 2007. **44**(9): p. 2257-64.
23. Yang, Y., et al., *Functional roles of p38 mitogen-activated protein kinase in macrophage-mediated inflammatory responses.* Mediators Inflamm, 2014. **2014**: p. 352371.
24. Srivastava, M., et al., *Inhibition of the TIRAP-c-Jun interaction as a therapeutic strategy for AP1-mediated inflammatory responses.* 2019. **71**: p. 188-197.
25. Miggin, S.M., et al., *NF-κB activation by the Toll-IL-1 receptor domain protein MyD88 adapter-like is regulated by caspase-1.* 2007. **104**(9): p. 3372-3377.

26. Ulrichts, P., et al., *Caspase-1 targets the TLR adaptor Mal at a crucial TIR-domain interaction site.* J Cell Sci, 2010. **123**(Pt 2): p. 256-65.
27. Dunne, A., et al., *IRAK1 and IRAK4 promote phosphorylation, ubiquitination, and degradation of MyD88 adaptor-like (Mal).* J Biol Chem, 2016. **291**(47): p. 24802.
28. Lauenstein, J.U., et al., *Negative Regulation of TLR Signaling by BCAP Requires Dimerization of Its DBB Domain.* 2020. **204**(8): p. 2269-2276.
29. Ni, M., et al., *B-cell adaptor for PI3K (BCAP) negatively regulates Toll-like receptor signaling through activation of PI3K.* 2012. **109**(1): p. 267-272.
30. Troutman, T.D., et al., *Role for B-cell adapter for PI3K (BCAP) as a signaling adapter linking Toll-like receptors (TLRs) to serine/threonine kinases PI3K/Akt.* 2012. **109**(1): p. 273-278.
31. Halabi, S., et al., *Structure of the Toll/interleukin-1 receptor (TIR) domain of the B-cell adaptor that links phosphoinositide metabolism with the negative regulation of the Toll-like receptor (TLR) signalosome.* 2017. **292**(2): p. 652-660.
32. Patra, M.C. and S. Choi, *Insight into Phosphatidylinositol-Dependent Membrane Localization of the Innate Immune Adaptor Protein Toll/Interleukin 1 Receptor Domain-Containing Adaptor Protein.* Front Immunol, 2018. **9**: p. 75.
33. Leifer, C.A. and A.E.J.J.o.l.b. Medvedev, *Molecular mechanisms of regulation of Toll-like receptor signaling.* 2016. **100**(5): p. 927-941.
34. Lannoy, V., et al., *Phosphatases in toll-like receptors signaling: the unfairly-forgotten.* 2021. **19**(1): p. 1-15.
35. Chattopadhyay, S. and G.C. Sen, *Tyrosine phosphorylation in Toll-like receptor signaling.* Cytokine Growth Factor Rev, 2014. **25**(5): p. 533-41.
36. Jefferies, C.A., et al., *Bruton's tyrosine kinase is a Toll/interleukin-1 receptor domain-binding protein that participates in nuclear factor kappaB activation by Toll-like receptor 4.* J Biol Chem, 2003. **278**(28): p. 26258-64.
37. Lin, Z., et al., *Structural insights into TIR domain specificity of the bridging adaptor Mal in TLR4 signaling.* PLoS One, 2012. **7**(4): p. e34202.
38. Kubo-Murai, M., et al., *Protein kinase Cδ binds TIRAP/Mal to participate in TLR signaling.* Molecular immunology, 2007. **44**(9): p. 2257-2264.
39. Steinberg, S.F., *Distinctive activation mechanisms and functions for protein kinase Cdelta.* Biochem J, 2004. **384**(Pt 3): p. 449-59.
40. Gschwendt, M., et al., *Tyrosine phosphorylation and stimulation of protein kinase C delta from porcine spleen by src in vitro. Dependence on the activated state of protein kinase C delta.* FEBS Lett, 1994. **347**(1): p. 85-9.
41. Rip, J., et al., *Toll-like receptor signaling drives Btk-mediated autoimmune disease.* 2019. **10**: p. 95.
42. Chavakis, T., A. Bierhaus, and P.P. Nawroth, *RAGE (receptor for advanced glycation end products): a central player in the inflammatory response.* Microbes Infect, 2004. **6**(13): p. 1219-25.
43. Hudson, B.I. and M.E. Lippman, *Targeting RAGE Signaling in Inflammatory Disease.* Annu Rev Med, 2018. **69**: p. 349-364.
44. Sparvero, L.J., et al., *RAGE (Receptor for Advanced Glycation Endproducts), RAGE ligands, and their role in cancer and inflammation.* J Transl Med, 2009. **7**: p. 17.
45. Bierhaus, A., et al., *Understanding RAGE, the receptor for advanced glycation end products.* J Mol Med (Berl), 2005. **83**(11): p. 876-86.
46. Kierdorf, K. and G. Fritz, *RAGE regulation and signaling in inflammation and beyond.* J Leukoc Biol, 2013. **94**(1): p. 55-68.
47. Prantner, D., S. Nallar, and S.N.J.T.F.J. Vogel, *The role of RAGE in host pathology and crosstalk between RAGE and TLR4 in innate immune signal transduction pathways.* 2020. **34**(12): p. 15659-15674.
48. Watanabe, M., et al., *Differential contribution of possible pattern-recognition receptors to advanced glycation end product–induced cellular responses in macrophage-like RAW264. 7 cells.* 2020. **67**(2): p. 265-272.

49. Putranto, E.W., et al., *Inhibition of RAGE signaling through the intracellular delivery of inhibitor peptides by PEI cationization.* 2013. **32**(4): p. 938-944.
50. Ishii, K.J., et al., *Host innate immune receptors and beyond: making sense of microbial infections.* Cell Host Microbe, 2008. **3**(6): p. 352-63.
51. Jin, M.S., et al., *Crystal structure of the TLR1-TLR2 heterodimer induced by binding of a tri-acylated lipopeptide.* Cell, 2007. **130**(6): p. 1071-82.
52. Henneke, P., et al., *Lipoproteins are critical TLR2 activating toxins in group B streptococcal sepsis.* J Immunol, 2008. **180**(9): p. 6149-58.
53. Parihar, S.P., et al., *Protein kinase C-delta (PKCdelta), a marker of inflammation and tuberculosis disease progression in humans, is important for optimal macrophage killing effector functions and survival in mice.* Mucosal Immunol, 2018. **11**(2): p. 579-580.
54. Dixit, R., et al., *Microtubule plus-end tracking by CLIP-170 requires EB1.* Proc Natl Acad Sci U S A, 2009. **106**(2): p. 492-7.
55. Maekawa, H. and E. Schiebel, *CLIP-170 family members: a motor-driven ride to microtubule plus ends.* Dev Cell, 2004. **6**(6): p. 746-8.
56. Pierre, P., et al., *CLIP-170 links endocytic vesicles to microtubules.* Cell, 1992. **70**(6): p. 887-900.
57. Sengupta, D., et al., *Subversion of innate immune responses by Brucella through the targeted degradation of the TLR signaling adapter, MAL.* J Immunol, 2010. **184**(2): p. 956-64.
58. Murugan, S., et al., *The neurosteroid pregnenolone promotes degradation of key proteins in the innate immune signaling to suppress inflammation.* J Biol Chem, 2019. **294**(12): p. 4596-4607.
59. Atsaves, V., et al., *AP-1 transcription factors as regulators of immune responses in cancer.* 2019. **11**(7): p. 1037.
60. Eferl, R. and E.F. Wagner, *AP-1: a double-edged sword in tumorigenesis.* Nat Rev Cancer, 2003. **3**(11): p. 859-68.
61. Kerppola, T.K. and T. Curran, *Fos-Jun heterodimers and Jun homodimers bend DNA in opposite orientations: implications for transcription factor cooperativity.* Cell, 1991. **66**(2): p. 317-26.
62. Wisdom, R., *AP-1: one switch for many signals.* Exp Cell Res, 1999. **253**(1): p. 180-5.
63. Chida, K., S. Nagamori, and T. Kuroki, *Nuclear translocation of Fos is stimulated by interaction with Jun through the leucine zipper.* Cell Mol Life Sci, 1999. **55**(2): p. 297-302.
64. Liu, W., et al., *AP-1 activated by toll-like receptors regulates expression of IL-23 p19.* J Biol Chem, 2009. **284**(36): p. 24006-16.
65. Liu, X., et al., *LPSinduced proinflammatory cytokine expression in human airway epithelial cells and macrophages via NFkappaB, STAT3 or AP1 activation.* Mol Med Rep, 2018. **17**(4): p. 5484-5491.
66. Srivastava, M. and M.S. Baig, *NOS1 mediates AP1 nuclear translocation and inflammatory response.* Biomed Pharmacother, 2018. **102**: p. 839-847.
67. Schonthaler, H.B., J. Guinea-Viniegra, and E.F. Wagner, *Targeting inflammation by modulating the Jun/AP-1 pathway.* Ann Rheum Dis, 2011. **70 Suppl 1**: p. i109-12.
68. Kawai, T. and S. Akira, *The role of pattern-recognition receptors in innate immunity: update on Toll-like receptors.* Nat Immunol, 2010. **11**(5): p. 373-84.
69. Abraham, C., S.N. Vogel, and D.J. Perkins, *Signaling Mechanisms Regulating Innate Immune Responses*, in *Mucosal Immunology*. 2015, Elsevier. p. 605-622.
70. Boatright, K.M., et al., *A unified model for apical caspase activation.* Mol Cell, 2003. **11**(2): p. 529-41.
71. Lamkanfi, M., et al., *Caspase-1 activates nuclear factor of the kappa-enhancer in B cells independently of its enzymatic activity.* J Biol Chem, 2004. **279**(23): p. 24785-93.
72. Broz, P., et al., *Differential requirement for Caspase-1 autoproteolysis in pathogen-induced cell death and cytokine processing.* Cell Host Microbe, 2010. **8**(6): p. 471-83.
73. Martinon, F., A. Mayor, and J. Tschopp, *The inflammasomes: guardians of the body.* Annu Rev Immunol, 2009. **27**: p. 229-65.

74. Thornberry, N.A., et al., *A novel heterodimeric cysteine protease is required for interleukin-1βprocessing in monocytes.* 1992. **356**(6372): p. 768-774.
75. Xie, P., *TRAF molecules in cell signaling and in human diseases.* J Mol Signal, 2013. **8**(1): p. 7.
76. Li, X., et al., *Data-Driven Modeling Identifies TIRAP-Independent MyD88 Activation Complex and Myddosome Assembly Strategy in LPS/TLR4 Signaling.* 2020. **21**(9): p. 3061.
77. Chuang, T.H. and R.J. Ulevitch, *Triad3A, an E3 ubiquitin-protein ligase regulating Toll-like receptors.* Nat Immunol, 2004. **5**(5): p. 495-502.
78. Janssens, S. and R. Beyaert, *Functional diversity and regulation of different interleukin-1 receptor-associated kinase (IRAK) family members.* Mol Cell, 2003. **11**(2): p. 293-302.
79. Flo, T.H. and A. Aderem, *Pathogen Recognition by Toll-like Receptors*, in *NeuroImmune Biology*, L. Bertók and D.A. Chow, Editors. 2005, Elsevier. p. 167-182.
80. de Diego, R.P. and C. Rodríguez-Gallego, *Chapter 34 - Other TLR Pathway Defects*, in *Stiehm's Immune Deficiencies*, K.E. Sullivan and E.R. Stiehm, Editors. 2014, Academic Press: Amsterdam. p. 687-710.
81. Kumar, H., O. Takeuchi, and S. Akira, *Toll-Like Receptors*, in *Encyclopedia of Biological Chemistry (Second Edition)*, W.J. Lennarz and M.D. Lane, Editors. 2013, Academic Press: Waltham. p. 396-401.
82. Mandraju, R., T.D. Troutman, and C. Pasare, *Toll-Like Receptor Function and Signaling*, in *Reference Module in Biomedical Sciences*. 2014, Elsevier.
83. Biswas, C., *Chapter 18 - Inflammation in Systemic Immune Diseases: Role of TLR9 Signaling and the Resultant Oxidative Stress in Pathology of Lupus*, in *Immunity and Inflammation in Health and Disease*, S. Chatterjee, W. Jungraithmayr, and D. Bagchi, Editors. 2018, Academic Press. p. 223-237.
84. Yoshimura, A., T. Naka, and M. Kubo, *SOCS proteins, cytokine signalling and immune regulation.* Nat Rev Immunol, 2007. **7**(6): p. 454-65.
85. Sharma, J. and J. Larkin, 3rd, *Therapeutic Implication of SOCS1 Modulation in the Treatment of Autoimmunity and Cancer.* Front Pharmacol, 2019. **10**: p. 324.
86. Baig, M.S., et al., *NOS1-derived nitric oxide promotes NF-kappaB transcriptional activity through inhibition of suppressor of cytokine signaling-1.* J Exp Med, 2015. **212**(10): p. 1725-38.
87. Belhaouane, I., et al., *Paradoxical Roles of the MAL/Tirap Adaptor in Pathologies.* Front Immunol, 2020. **11**: p. 569127.
88. Zhao, X., et al., *Membrane targeting of TIRAP is negatively regulated by phosphorylation in its phosphoinositide-binding motif.* Sci Rep, 2017. **7**: p. 43043.
89. Hughes, M.M., et al., *Solution structure of the TLR adaptor MAL/TIRAP reveals an intact BB loop and supports MAL Cys91 glutathionylation for signaling.* Proc Natl Acad Sci U S A, 2017. **114**(32): p. E6480-E6489.
90. Xue, Y., et al., *GPS 2.1: enhanced prediction of kinase-specific phosphorylation sites with an algorithm of motif length selection.* 2011. **24**(3): p. 255-260.
91. Blom, N., et al., *Prediction of post-translational glycosylation and phosphorylation of proteins from the amino acid sequence.* 2004. **4**(6): p. 1633-1649.
92. Xue, Y., et al., *GPS-SNO: computational prediction of protein S-nitrosylation sites with a modified GPS algorithm.* PLoS One, 2010. **5**(6): p. e11290.
93. Xie, Y., et al., *DeepNitro: prediction of protein nitration and nitrosylation sites by deep learning.* 2018. **16**(4): p. 294-306.
94. Lee, T.-Y., et al., *SNOSite: exploiting maximal dependence decomposition to identify cysteine S-nitrosylation with substrate site specificity.* 2011. **6**(7): p. e21849.
95. Fulgione, A., et al., *Interaction between MyD88, TIRAP and IL1RL1 against Helicobacter pylori infection.* 2020. **10**(1): p. 1-13.
96. Yang, Q., et al., *The Role of Tyrosine Phosphorylation of Protein Kinase C Delta in Infection and Inflammation.* Int J Mol Sci, 2019. **20**(6).

97. Steinberg, S.F., *Structural basis of protein kinase C isoform function.* Physiol Rev, 2008. **88**(4): p. 1341-78.
98. Mellor, H. and P.J. Parker, *The extended protein kinase C superfamily.* Biochem J, 1998. **332 (Pt 2)**(Pt 2): p. 281-92.
99. Loegering, D.J. and M.R. Lennartz, *Protein kinase C and toll-like receptor signaling.* Enzyme Res, 2011. **2011**: p. 537821.
100. Newton, A.C., *Protein kinase C: structural and spatial regulation by phosphorylation, cofactors, and macromolecular interactions.* Chem Rev, 2001. **101**(8): p. 2353-64.
101. Kilpatrick, L.E., et al., *Protection against sepsis-induced lung injury by selective inhibition of protein kinase C-δ (δ-PKC).* J Leukoc Biol, 2011. **89**(1): p. 3-10.
102. Mondrinos, M.J., et al., *Pulmonary endothelial protein kinase C-delta (PKCδ) regulates neutrophil migration in acute lung inflammation.* Am J Pathol, 2014. **184**(1): p. 200-13.
103. Horwood, N.J., et al., *Bruton's tyrosine kinase is required for lipopolysaccharide-induced tumor necrosis factor α production.* The Journal of experimental medicine, 2003. **197**(12): p. 1603-1611.

Chapter 3

(Dorzolamide (DZD) suppresses PKCδ-TIRAP-p38 MAPK signalling axis to dampen the inflammatory response)

Chapter 3: Dorzolamide (DZD) suppresses PKCδ-TIRAP-p38 MAPK signalling axis to dampen the inflammatory response

3.1. Graphical Abstract

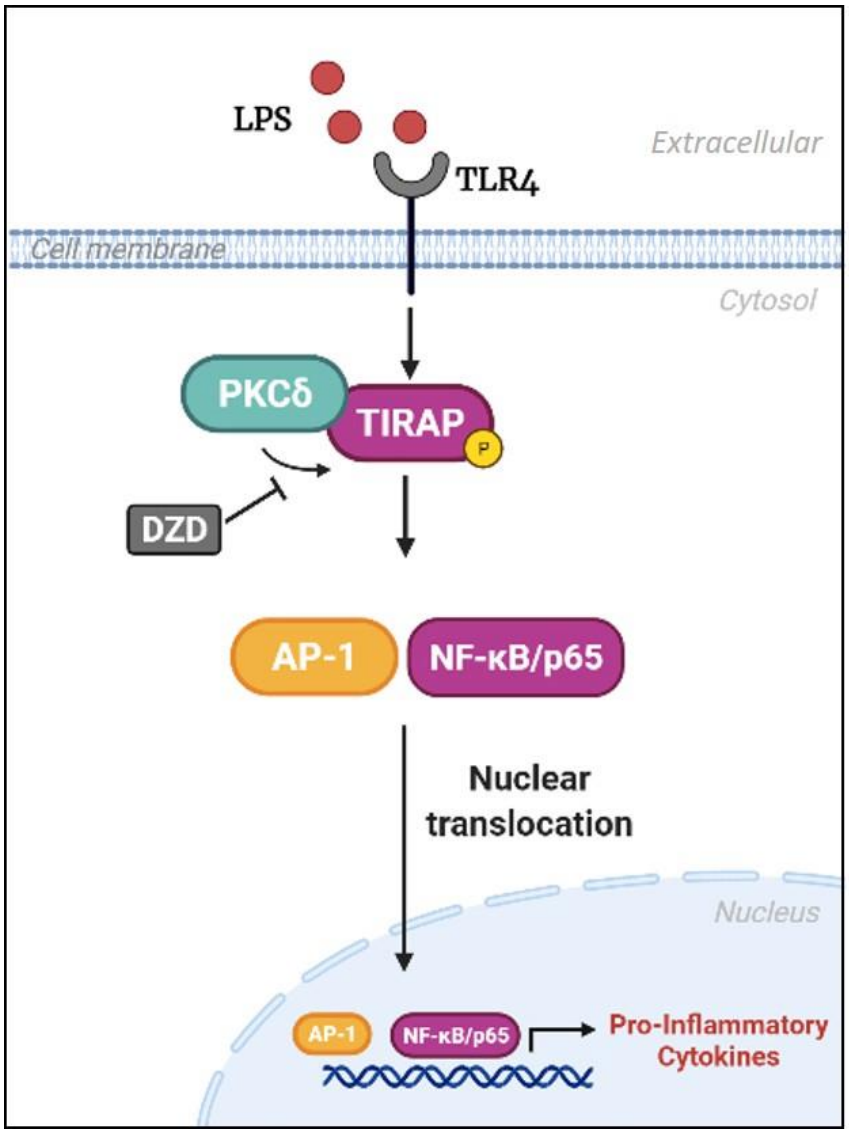

Figure 3. 1. *Underlying signaling mechanism of TIRAP and PKCδ in LPS stimulated macrophages via TLR4 and repurposing of dorzolamide (DZD) as an anti-inflammatory agent targeting TIRAP interface to disrupt its interaction with upstream kinase PKCδ.*

3.2. Summary

In this study, we show the indispensable role of TIRAP interaction with protein kinase C delta (PKCδ) in inducing p38 mitogen-activated protein kinase (MAPK)-mediated activation of nuclear factor kappa-light-chain-enhancer of activated B cells (NF-κB) and activator protein 1 (AP-1) transcription factors and pro-inflammatory cytokines expression. Through virtual screening, we have identified that dorzolamide (DZD), a food and drug administration (FDA)-approved drug for glaucoma, inhibits the interaction of TIRAP with PKCδ which dampens the pro-inflammatory response. Hence, targeting TIRAP and PKCδ interaction by DZD is a novel therapeutic approach for treating sepsis.

3.3. Introduction

Inflammation is a protective response of the host body against harmful stimuli such as infectious agents, damaged tissue, and irritants [1-3]. Typically, the inflammatory response involves tight control of several cellular and molecular events, including mitogen-activated protein kinases (MAPKs). MAPKs act as a node for activating several transcription factors (TFs) including nuclear factor kappa-light-chain-enhancer of activated B cells (NF-κB) and activator protein 1 (AP-1) [3]. MAPKs are activated after the interaction of a stimulus such as bacterial lipopolysaccharide (LPS), also known as pathogen-associated molecular patterns (PAMPs), with their cognate receptor(s) such as the toll-like receptors (TLRs), termed pattern recognition receptors (PRRs) [4]. The inflammatory response against infectious stimuli is an essential mechanism of innate immunity and a prerequisite for eliminating pathogens, followed by affected tissue repair and regeneration [5]. However, long-lasting inflammation leads to chronic inflammation [2, 6]. In the late stage, chronic inflammation compromises lung functions and manifests into organ failure and death[7]. Macrophages, localized throughout the human body in a resident and circulatory form, are the most sentinel cell type involved in triggering innate immune responses against pathogens [8, 9]. These macrophages predominantly express TLRs on their cell surface and in intracellular vesicles, which initiate immune signaling pathways upon sensing

pathogens [4]. In TLR4 signaling, LPS binding initiates signaling via its toll/interleukin-1 (IL-1) receptor (TIR) domain and interaction with Toll/interleukin-1 receptor domain-containing adapter protein (TIRAP) [10, 11]. TIRAP then recruits myeloid differentiation primary response 88 (MyD88) on the cell membrane to mediate protein-protein interactions and post-translational modifications, leading to the activation of transcription factors [12, 13]. In addition, TIRAP has a significant role in the rapid activation of transcription factors AP-1 and NF-kB through a MyD88-independent pathway [14-20]. We recently summarized the critical role of TIRAP in inducing macrophage signaling via its multi-protein interactions [21]. Understanding such protein-protein interactions will identify potential therapeutic targets for treating inflammatory diseases. One such interaction is between TIRAP and PKCδ, which occurs following LPS stimulation of TLR4 [20, 22]. In this study, we determine how TIRAP's interaction with protein kinase C delta (PKCδ) shapes the inflammatory response via the activation of NF-κB and AP-1. Our in-vitro and in-silico studies suggest TIRAP and PKCδ interaction as the driver of LPS-induced inflammatory signaling. We show that this interaction facilitates p38 MAPK phosphorylation and activation to further activate NF-κB and AP-1. The significance of this study holds the promise to disrupt TIRAP and PKCδ interaction to dampen macrophage inflammatory signaling, pushing the response toward resolution and repair would be the significant importance of this study.

3.4. Materials and Methods

3.4.1. Cell Culture

The murine macrophage RAW 264.7 cell line was obtained from the cell repository of the National Centre for Cell Science (NCCS), Pune, India. Mice were sacrificed, and femur bone was obtained for bone marrow-derived macrophages (BMDM) culture. The RAW 264.7 and BMDM cells were grown in Dulbecco's minimal essential medium (DMEM) (11965118, Gibco) supplemented with heat-inactivated 10% fetal bovine serum (FBS) (10270106, Gibco) and 100U/ml penicillin and 100µg/ml streptomycin (15140122, Gibco). For BMDM, 20% of L929 conditioned media was

added to complete the media, and fresh media was replenished on the third day of the culture. To get maximum confluency, all cells were cultured in a humidified incubator with 5% CO2 at 37ºC. For all the experiments with treatment, cells were treated with 250ng/ml of lipopolysaccharide (LPS; Sigma L2630) and 1μM of dorzolamide (DZD, Sigma SML0468) for indicated time points, unless mentioned otherwise.

3.4.2. Immunofluorescence

Cells were grown on sterile coverslips to 70-75% confluency and treated with LPS and DZD as indicated. Before fixation, cells were washed twice with PBS (pH-7.4) at room temperature, then fixed in freshly prepared 4% paraformaldehyde (PFA) (pH-7.2) in PBS for 15min at room temperature. Subsequently, cells were permeabilized using 0.01% Triton-X prepared in 1X-PBS for 10min at room temperature and then washed three times with gentle shaking in PBS. Next, the blocking was carried out with gentle shaking in freshly prepared 5% non-fat blocking milk (1706404, BioRad) for 1h at room temperature, and cells were washed three times with TBST buffer for 5min each. For immunostaining, the primary antibodies, anti-TIRAP (sc-166149, Santa Cruz Biotechnology), anti-PKCδ (sc-213, Santa Cruz Biotechnology), or anti-NF-κB/p65 (sc-8008, Santa Cruz Biotechnology) were added at a dilution 1:200 prepared in TBST buffer, then incubated at 4ºC for overnight. After incubation, the excess antibody was removed from cells by washing three times with gentle shaking in TBST buffer. Then, fluorescence-conjugated secondary antibodies Alexa Fluor 594 Chicken anti-rabbit (A21441, Invitrogen) and Alexa Fluor 488 Goat anti-mouse (A11001, Invitrogen) were applied at a dilution of 1:200 in TBST buffer and incubated at room temperature for one h in the dark. Excess antibodies were removed by washing three times in TBST buffer for 5min. Cells were stained with DAPI (F6057, Sigma) for nuclear counterstaining and mounted on coverslips. Cells were studied using a confocal laser scanning microscope (Olympus), and ImageJ and its plugin JACoP were used for colocalization analysis.

3.4.3. Co-Immunoprecipitation

For the co-immunoprecipitation study, the RAW 264.7 cells were seeded in six-well plates and after growth, the cells were treated as indicated. After the incubation period, the cells were lysed in non-denaturing Co-IP lysis buffer (25mM Tris pH 8.0, 150mM KCl, 5mM EDTA, 0.5% Triton-X100) along with a protease and phosphatase inhibitor cocktail (1mM NaF, 1mM Na2VO3, and 1mM PMSF) by scrapping on ice followed by 30secs of three vortexes. Further, the samples were centrifuged at 16,200 ×g for 20min at 4°C to remove the cell debris. The supernatant was collected in fresh pre-chilled tubes. The protein concentration was estimated by Bradford assay as per the manufacturer's protocol (BioRad). An equal concentration of protein was taken for each condition and 2µg of primary antibody (anti-PKCδ, sc-213, Santa Cruz Biotechnology) was added to each sample and incubated at 4°C overnight with gentle shaking. Later, the agarose beads were added and the samples were again incubated on the shaker at 4°C for at least 4h or overnight. The samples were centrifuged at 600 ×g for 5min at 4°C and the agarose beads were washed twice with Co-IP lysis buffer. For elution and immunoblotting, 40µl of 2X protein loading dye was added to washed samples and boiled at 95°C for 5min followed by short centrifugation. For immunoblotting, anti-PKCδ (sc-213, Santa Cruz Biotechnology), and anti-TIRAP (PA5-88657, Invitrogen) primary antibodies followed by Rabbit anti-Mouse HRP conjugate (Invitrogen), and Goat anti-Rabbit HRP conjugate (626120, Invitrogen) secondary antibodies were used, respectively.

3.4.4. Molecular modelling

A homology-based approach was applied to model the 3D protein structure of PKCδ and loop modelling of the TIRAP TIR domain. Before modelling, the sequences and functional domain information were retrieved from the UniProt database for human PKCδ (UniProtKB-Q06187). We used MODELLER 9.24 for modelling and loop refinement of the structure[23, 24]. The structure was modelled by a multi-template comparative method. The crystal structures of human protein kinase C theta (PDB ID 4Q9Z and 2JED) were used as the templates for model prediction of the kinase domain

of PKCδ. The templates were aligned with the target sequence in PIR format in ExpasyClustalW[25]. To run MODELLER 9.24, the alignment file was prepared as described above, and a total of 20 models were developed for PKCδ. The analysis was performed through PROCHECK [26] and ERRAT [27]. The outlier residues in the Ramachandran plot were corrected through loop refinement in MODELLER 9.24. The DOPE (discrete optimized potential energy) score was used to select the best model for in silico stereochemical quality assessment and docking studies. Finally, GalaxyWeb was used for the overall refinement of the modelled structure [28]. The final structural analysis was performed by Swiss-model structure assessment [29] (generating the Ramachandran plot and QMEAN score), ERRAT, and ProTSAV (Protein structure analysis and validation) [30], which calculates multiple stereochemical parameters and predicts the overall quality and resolution of the structure. Chimera 1.13.1 was used to minimize the structure energetically and perform the target and template structure superimposition for comparative analysis [31]. For the TIRAP TIR domain structure, the missing residues from 110 to 127 in the target structure (PDB: 3UB2) were completed by the loop modelling function of MODELLER 9.24 using the structure of another human TIRAP TIR domain (PDB: 5UZB) as a template and was refined as mentioned above. The TIRAP crystal structure 5UZB was not used due to its poor resolution (7 Å) compared to 3UB2 (2.4 Å).

3.4.5. Molecular docking and virtual screening

The TIRAP and PKCδ protein-protein molecular docking was performed in pyDockWEB (https://life.bsc.es/servlet/pydock/) [23]. The interface residues of the complex within the 3Å region were studied in the Chimera tool [24], and PDBePISA (https://www.ebi.ac.uk/pdbe/pisa/) [25]. For the virtual screening study, the ZINC15 database (https://zinc15.docking.org/) was used, and in-stock compounds, including the Food and Drug Administration (FDA), approved compounds, were retrieved for docking. The interacting residues of TIRAP were targeted for virtual screening in the Autodock Vina tool [26]. Blind docking was performed with a grid box size of 40×36×34 (x×y×z), covering the complete structure of TIRAP. Each compound was

docked for ten poses and analyzed for screening in Discovery Studio Visualizer [27] through the receptor-ligand interaction tool. Compounds with binding specificity to the TIRAP interacting residues and higher dock scores were selected. The protein-protein and protein-drug complexes were visualized and represented using Pymol version 1.5.0 (https://www.pymol.org) [28].

3.4.6. qRT-PCR

The total RNA was isolated from macrophages (RAW 264.7 and BMDM) and mice lung tissue by RNAiso Plus reagent (9109, Takara Bio Inc.) according to the manufacturer's instructions. Mice lung tissue was snap-frozen and homogenized. The concentration and purity of isolated RNA were determined through nanodrop reading. For cDNA preparation, a total of 1000ng of RNA was reverse transcribed (RT) using the cDNA Synthesis Kit (AB-1453, Invitrogen) according to the manufacturer's datasheet. The real-time PCR (qPCR) was performed using SYBR green master mix (A25742, Applied Biosystems) in StepOnePlus Real-Time PCR Systems (Applied Biosystems). The experiment was performed in at least three independent sets for the gene expression of GAPDH, TNF-α, IL-1β, IL-6, IL-12, and IL-23. The primer sequences are provided in **Supplementary Table S3.1**. The ct value was analyzed using the $2^{-\triangle\triangle Ct}$ method for the relative cytokine expression, while GAPDH was regarded as a reference gene to standardize the relative expression levels of cytokine genes.

3.4.7. Molecular dynamics (MD) simulation

To provide insights into the inhibition of the TIRAP-PKCδ protein-protein complex by DZD, several molecular dynamics (MD) simulations were performed. Initially, systems for the MD simulations were prepared by solvating them in a rectangular truncated octahedron filled with TIP4P-EW [29] water molecules. Na+ and Cl- ions were used to neutralize the simulation system. The protein, solvent, and ion parameters were assigned using the Amber ff14SB force field [30]. The parameters for DZD were generated using antechamber and parmchk2 tool (https://ambermd.org). Initially, the water and ions were subjected to the steepest-descent energy minimization to relax

their initial configuration, while restraining the protein atoms using harmonic position restraints of 10kcal/mol/Å2. In the next step, all restraints were removed, and the complete system was minimized by 2000 steps. The systems were then gradually heated in the canonical ensemble from 0 to 300K over the course of 500ps and then equilibrated for the period of 5ns. System relaxation and equilibration MD simulations were performed using the Amber18 package. Finally, for all systems, 500ns production MD simulations were performed using Gromacs 5.0.4 package (https://www.gromacs.org) [31]. ParmEd package was employed to convert AMBER topologies to Gromacs topologies [32]. MD simulations were performed using an NPT ensemble at a constant temperature of 300 K. SHAKE algorithm was used to constrain all hydrogen atoms. A time step of 2fs was used for the simulations. A cut-off of 10Å was used for short-range interactions, while Particle-Mesh Ewald (PME) method was used to handle long-range interactions. The MD trajectory was processed and analyzed using Gromacs utilities, MDAnalysis[33], MDTraj[34], and scikitlearn[35] python libraries. MM-PBSA binding energy calculations were performed using the g_mmpbsa program [36]. Intermolecular contacts were analyzed from the MD simulation trajectories using GetContacts (https://getcontacts.github.io/). Graphics were prepared using Matplotlib python library [37], R (https://www.r-project.org), and Pymol version 1.5.0 (https://www.pymol.org) [28].

3.4.8. Immunoblotting

The RAW 264.7 cells were washed with PBS and lysed in radioimmunoprecipitation assay (RIPA) lysis buffer containing protease and phosphatase inhibitors (1mM each of PMSF, NaF, and Na3VO4) for whole cell lysate. For cytoplasmic and nuclear protein, a Nuclear/Cytosol Fractionation Kit (K266-100, BioVision, CA) was used and isolated per the manufacturer's protocol. Protein concentration was estimated by Bradford assay dye reagent (500-0006, BioRad) as per the manufacturer's instruction. Equal protein was prepared in 4X protein loading dye and resolved in 10% of Sodium Dodecyl Sulfate Polyacrylamide Gel Electrophoresis (SDS-PAGE), blotted onto nitrocellulose membrane (1620112, BioRad), blocked with 5% non-fat milk (1706404,

BioRad) for 1h at room temperature (RT) and probed with primary antibodies at 4°C for overnight and/or 4h at RT. After incubation, the membrane was washed thrice in Tris-buffered saline/Tween 20 (TBST) buffer and incubated in horseradish peroxidase (HRP)-tagged secondary antibody for 1h at RT. The blots were washed again in TBST and detected using enhanced chemiluminescence (ECL) HRP Substrate (170-5061, BioRad) in Gel documentation system (Image Quant LAS 4000), and band intensities were analyzed using ImageJ (National Institutes of Health; Schneider et al., 2012). The list of primary and secondary antibodies used for immunoblot analysis are anti-TIRAP (PA5-88657, Invitrogen), anti-phospho Y86 TIRAP (PA5-40297, Invitrogen), anti-p38α MAPK (9212, CST), anti-phospho T180/Y182 p38α MAPK (9211, CST), anti-ERK1/2 (9102, CST), anti-phospho ERK1/2 (9101, CST), anti-JNK1/2 (92952, CST), anti-phopsho JNK1/2 (9251, CST), anti-IκBα (sc-847, Santa Cruz Biotechnology), anti-NF-κB/p65 (sc-8008, Santa Cruz Biotechnology), anti-phosphor-NF-κB/p65 (3033, CST), anti-β-Actin (Invitrogen), anti-HDAC1 (A300-713A, Bethyl Laboratories, Inc.), Goat anti-Rabbit HRP conjugate (626120, Invitrogen) and Rabbit anti- Mouse HRP conjugate (Invitrogen).

3.4.9. Murine model

All the animal studies were conducted on wild-type Swiss albino mice. The mice used in the study were 6 to 8 weeks old, weighing around ~ 28g, and were kept in pathogen-free conditions with an optimum temperature of 22-25°C and relative humidity of 55-60%. The light and dark cycle was maintained for 14:10h. The mice had ad libitum access to mice feed (dry pellet) and clean water. All the experiments were conducted under the Institutional Animal Ethics Committee (IAEC) of Acropolis Institute of Pharmaceutical Education and Research and following the policies of the Committee for Control and Supervision of Experiments on Animals (CPCSEA), Govt. of India. The mice survival study was conducted in LPS induced endotoxemia model. The male mice were randomly divided into four groups with twelve mice in each group, namely Control, LPS treated, and LPS+DZD treated groups. All treatments were given through the intraperitoneal (i.p) route of injection. The total number of mice in each

group was 12 (n=12). A single lethal dose of 25mg/kg of LPS was injected for inducing sepsis. A single dose of DZD of 20mg/kg was administered 1h before the LPS injection. The control group of mice only received the vehicle PBS and/or DMSO solution. The survival rate was recorded every 12h till 96h (4 days). Mice lung tissue was isolated at 12h after treatment (as discussed above in the survival study, n=3 per group), washed with sterile PBS, and placed in 10% formalin for slide preparation. The lung tissue section was dehydrated and embedded in paraffin for sectioning of 5μm-thick sections. Haematoxylin and eosin (H&E) staining were then performed. Images were captured under the white light microscope at 40X magnification.

3.4.10. Statistical analysis

The experimental data were plotted using GraphPad Prism 7.0 (GraphPad Software, USA) and represented as means ± SEM from three independent sets of the experiment. Statistical analysis was performed by Student's t-test for comparing two groups, while one-way ANOVA was followed by Tukey's multiple group comparisons. A value of $p<0.05$ was considered statistically significant. The Kaplan-Meier plot was used for survival analysis (GraphPad Prism).

3.5. Results

3.5.1. TIRAP interaction with PKCδ increases in LPS-stimulated macrophages

The TIRAP upstream kinase PKCδ and Bruton's tyrosine kinase (BTK) play an imperative role in LPS-induced macrophage inflammatory signaling[38, 39]. Though the interaction of TIRAP with PKCδ has been delineated in earlier studies, including ours[22, 40, 41], the TIRAP and PKCδ mediated downstream signaling mechanisms are not well studied. We first sought to understand the interaction of TIRAP and PKCδ in LPS-stimulated macrophages. We found an enhanced interaction of TIRAP with PKCδ in response to LPS-stimulated macrophages through immunofluorescence and co-immunoprecipitation **(Figure 3.2A-F)**. The overlay of immunostained TIRAP and PKCδ was analyzed to estimate Pearson's correlation coefficient (PCC), which lies

between 0 to 1. Our result suggests that the colocalization of TIRAP and PKCδ is significantly higher in the cytoplasm, while untreated macrophages don't show such colocalization **(Figure 3.2A-D)**. As shown in (**Figures 3.2E-F)**, the immunoblotting of anti-PKCδ immunoprecipitated samples also indicates an increase in the interaction of TIRAP with PKCδ in LPS endotoxin-stimulated macrophages. Together, it suggests that the TIRAP interaction with PKCδ significantly increases in response to LPS stimulation. Henceforth, a detailed understanding of the molecular interaction between the TIRAP and PKCδ residues and their role in modulating LPS-induced inflammatory signaling through their inhibition in macrophages is warranted.

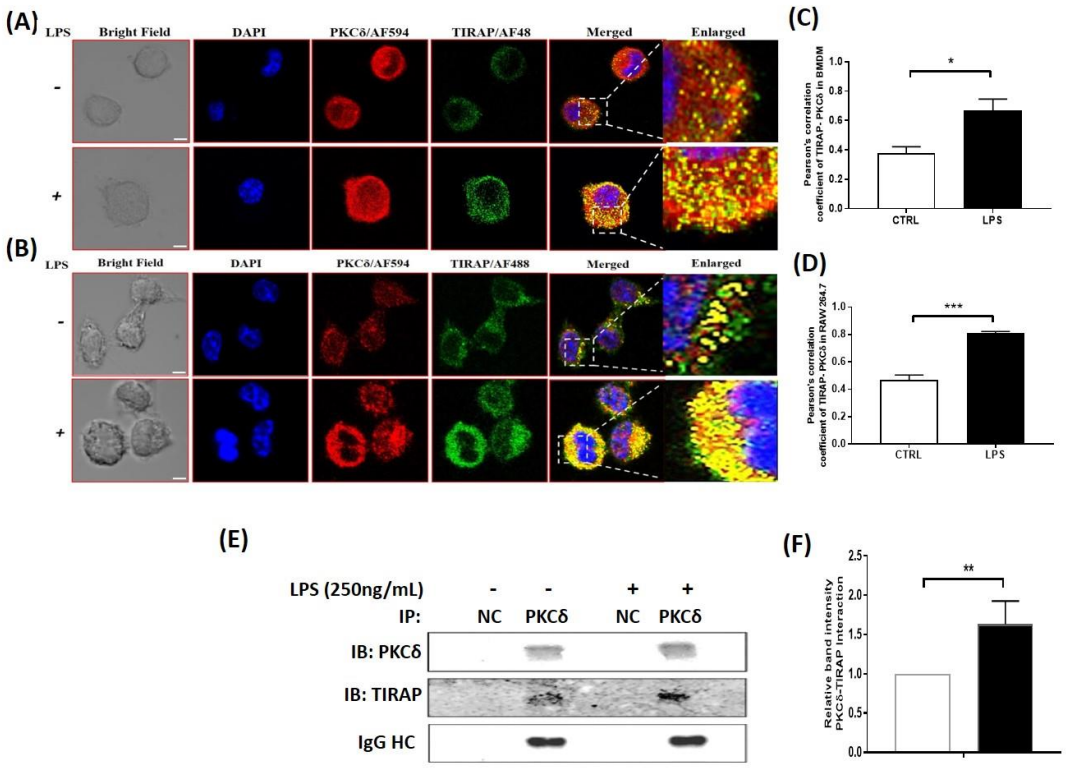

Figure 3. 2. Cellular interaction study of TIRAP with PKCδ in LPS stimulated macrophages exhibits an increase in their interaction. Immunofluorescence study of TIRAP and PKCδ for their cellular colocalization analysis in LPS stimulated **(A)** mouse BMDM and **(B)** RAW 264.7 cells with its Pearson's correlation coefficient (PCC) analysis **(C-D)** display enhanced interaction of TIRAP and PKCδ in compare to untreated cells. The macrophages were stimulated with LPS for 1h and immune-tagged with anti-PKCδ and anti-TIRAP primary antibodies followed by immunofluorescence tagging with secondary antibodies Alexa Fluor 594 (red) for PKCδ and Alexa Fluor 488 (Green) for TIRAP. The nucleus was counterstained with DAPI (blue) and cells were mounted on a glass slide for confocal microscopy. The PCC analysis of TIRAP and PKCδ overlay was performed in ImageJ through the JACoP plugin. **(E-F)** Co-immunoprecipitation of PKCδ by anti-PKCδ and immunoblot analysis by anti-PKCδ and anti-TIRAP for their interaction study in LPS stimulated RAW 264.7 cells also result in an increase in their interaction compared to untreated cells. All experiments were independently performed three times, and data represented as the mean ± S.E.M. Significance value, *$p<0.05$, **$p<0.005$, **$p<0.005$ versus untreated cells. Scale bar=10μm.

3.5.2. Molecular structure modelling of PKCδ

The modelling of PKCδ was completed to perform the structural interaction analysis with TIRAP. Initially, we analyzed the domains of PKCδ protein, which mainly consist of regulatory (C1 and C2 regions) and catalytic (C3 and C4 regions) domains connected through a hinge region acting as a pseudo-substrate region [19, 40]**(Figure 3.3)**. The PKCδ plays a significant role in the regulation of inflammatory signalling and unlike other PKCs, it is uniquely activated by multiple tyrosine phosphorylation alongside its regular threonine and serine phosphorylation. The catalytic domain containing most of these sites determines the PKCδ activation, localization, and substrate-binding specificity [40, 42]. Therefore, for further docking studies, we performed the homology-based structure modelling of the catalytic domain (region 349 to 676) of PKCδ as represented in **(Figure 3.3)**. Sequence matching through protein blast resulted in the highest similarity with the structures of two human PKC theta (PKCθ) homologs (PDB ID 2JED chain A and 4Q9Z chain A), which were selected as templates for homology modelling. The sequences were prepared as discussed above for BTK. A total of 20 models were prepared through MODELLER

9.24 for initial analysis. The model with the lowest DOPE score was chosen for further analysis. Using PROCHECK, we performed the Ramachandran plot analysis and identified the residues in the unfavoured region for loop refinement. A total of three small loop regions (469 to 474, 619 to 622, and 655 to 657) were corrected through MODELLER 9.24 loop modelling. Finally, the overall structure refinement was performed through the GalaxyRefine program of the GalaxyWeb tool. Based on their RMSD values, MolProbity and Ramachandran favoured value, out of a total of five models, PKCδ-Model 5 **(Figure 3.3)** was selected for further docking studies. In comparison to the Ramachandran value and ERRAT score of 96.9% and 83.02, respectively, for the initial model structure of PKCδ, the refined PKCδ-Model 5 structure had 98.8% residues in the most favourable region of the Ramachandran plot along with a significantly enhanced ERRAT quality factor score of 97.07. The QMEAN quality estimate score was also calculated as −0.29 in the Swiss model structure assessment. Additionally, the overall quality assessment by the ProTSAV tool cumulatively measuring several stereochemical parameters resulted in a satisfactory resolution of the structure with a 2–2.5 Å RMSD value. Finally, the final PKCδ-Model 5 **(Figure 3.3)** was superimposed with their templates to determine the RMSD, which was only 0.378 Å with 4Q9Z and 0.922 with 2JED, respectively.

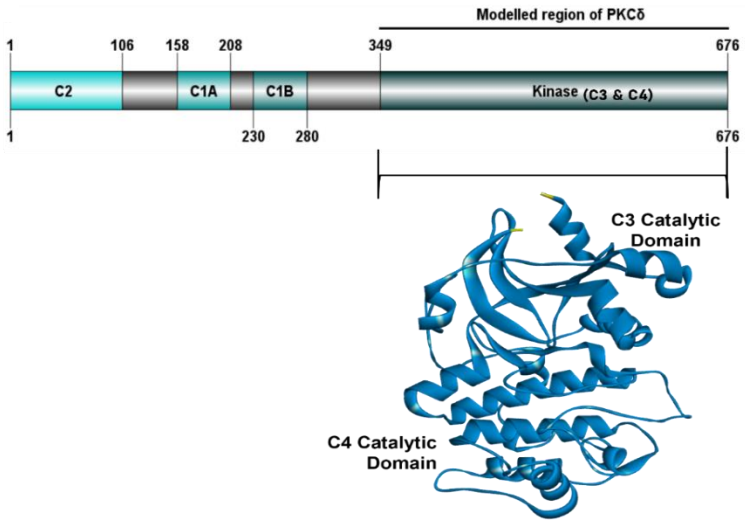

Figure 3. 3. Homology-based 3D structure modelling of protein kinase C delta (PKCδ) by MODELLER 9.24. The domain map and modelled 3D structure of PKCδ protein representing the region modelled for docking studies.

5.5.3. Loop modelling of TIRAP molecule

The available TIRAP structures in the PDB database were analyzed to ascertain their suitability for docking studies with BTK and PKCδ. The human TIRAP TIR domain X-ray crystallographic structure with PDB ID 3UB2 had the lowest resolution (2.4 Å) and was selected over the other human TIRAP structure with PDB ID 5UZB (7 Å). The 221 amino acid TIRAP protein exhibits an extreme N-terminal phosphatidylinositol 4,5-bisphosphate (PIP2) binding domain (PBD) and a C-terminal TIR domain **(Figure 3.4)**. Excluding the PBD, known for its cellular localization and membrane attachment function for the TIRAP protein, the region of our interest was the TIR domain actively involved in an interaction with several of its intracellular upstream and downstream protein molecules and signal transduction [43, 44]. However, the TIRAP structure from 3UB2 was missing residues from regions 110 to 127, referred to as the AB loop, and was thus required to be modelled **(Figure 3.4)**. We performed the loop modelling of this region using the best-matched template 5UZB (human TIR domain of TIRAP) containing the solved crystal structure for these missing residues. As described earlier, a protein blast was performed and the PIR format of sequence alignment was prepared along with the script required for the modelling tool. Again, the MODELLER 9.24 [45, 46] was employed for loop modelling. Out of the five models, the best one was selected based on its lowest DOPE score. The initial analysis of the Ramachandran plot in PROCHECK and Swiss-model structure assessment as well as correctness in the pattern of atomic interaction resulted in 92.6% residues in the most favoured region of the Ramachandran plot with ERRAT quality factor scores of 82.963, respectively. Furthermore, the TIRAP structure was subjected to refinement in the GalaxyRefine program of the GalaxyWeb server tool. A total of five refined structures were produced mainly based on their RMSD values, MolProbity and Ramachandran favoured values. We finally chose the best loop-modeled TIRAP structure after re-analyzing its ERRAT score and Swiss model structure assessment. The TIRAP-Model 2 **(Figure 3.4)** obtained from GalaxyRefine with an enhanced Ramachandran score of 98.6% in favoured region and no outlier

residues, −0.04 QMEAN score, and the ERRAT quality factor score of 97.037 was finally selected for further docking studies **(Figure 3.4)**. The ProTSAV overall quality assessment for the TIRAP model showed that the structure was within the range of 2–3 Å RMSD value. Estimating the RMSD in loop-modelled TIRAP and templates, the superimposition of TIRAP-Model 2 with 3UB2 and 5ZUB showed only 0.8 Å and 0.39 Å of RMSD value in the chimera 1.13.1 tool.

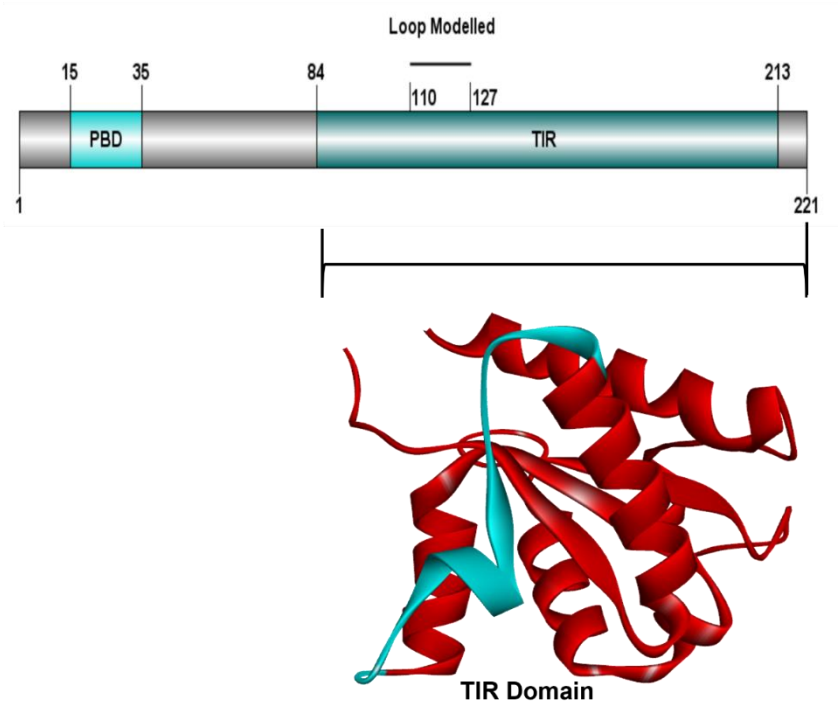

Figure 3. 4. Homology-based 3D loop modelling of TIRAP-TIR domain by MODELLER 9.24. The domain map and loop modelled 3D structure of TIRAP protein representing the loop region modelled for docking studies.

3.5.4. DZD perturbs the TIRAP and PKCδ interaction in virtual screening

The molecular interaction between TIRAP and PKCδ was studied through a protein-protein molecular docking tool pyDockWEB. Out of 100 output complexes from pyDockWEB, the complex with the most favorable docking energy (-44.593) was selected for further analysis. The docking complex indicates that TIRAP contacts the groove of the C3 and C4 catalytic domains of PKCδ**(Figure 3.5A)**. Further, we

analyzed the molecular interaction between the interface residues of TIRAP and PKCδthrough Chimera [24] and PDBePISA[25] and obtained the interface and interacting residues within the 3Å region as summarized in (**Figure 3.5B)**. Among the primary interfacial residues within the TIRAP and PKCδ docking complex are E167, E190, R215, and T219 of TIRAP as well as S359, Q440, D552, and E553 of PKCδ. Considering this interface and interacting residues of TIRAP as a major target site, we further proceeded with a virtual screening of the potential compounds in Autodock Vina 4.0 for disruption of the TIRAP-PKCδ complex. The ZINC15 database was utilized to obtain the compounds by applying the filter of in-stock, FDA-approved, and reactive compounds. The obtained small molecules and TIRAP structure were prepared in the pdbqt format for docking in Autodock Vina 4.0. Each molecule was allowed to dock in ten poses, which were ranked according to the docking scores in decreasing order. For the binding specificity of compounds interacting in the TIRAP-PKCδ interface, the top pose of each molecule was selected for interaction analysis. Further, the binding site for each molecule was individually analyzed in the Discovery Studio Visualizer. Out of 1615 compounds, we shortlisted three compounds, based on their best Autodock Vina docking scores at the first pose and binding site on the TIRAP interface **(Figure 3.5C and Table 3.1)**. The known pharmacological function, molecular weight, 2D structure, commercial name, and other details are provided in (**Table 3.1)**. Based on these parameters, we chose dorzolamide (DZD) for further in-vitro analysis.

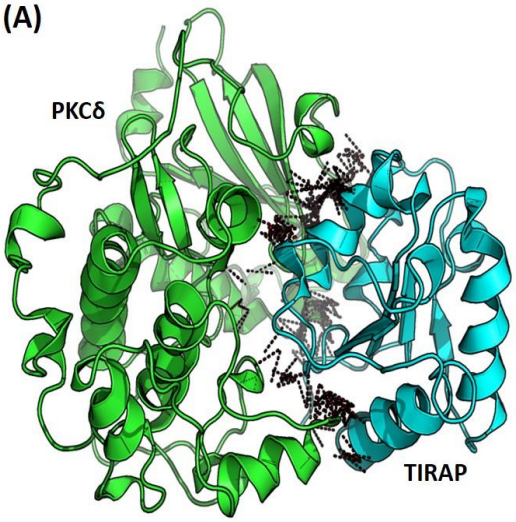

(B)

Docking Suit	Interacting Residues and its position in TIRAP and PKCδ complex		No of Residue
pyDockWEB	TIRAP	R81, W82, V130, K158, Y159, L162, Q163, L165, T166, E167, P169, E172, P189, E190, F193, M194, Y195, R215 and T219	19
	PKCδ	K355, G356, S357, I385, D386, D387, D388, M434, I437, Q438, D475, P510, D511, G542, Q543, S544, H547, G548, D549, D550, E551, D632, E634, F635 and E638	25

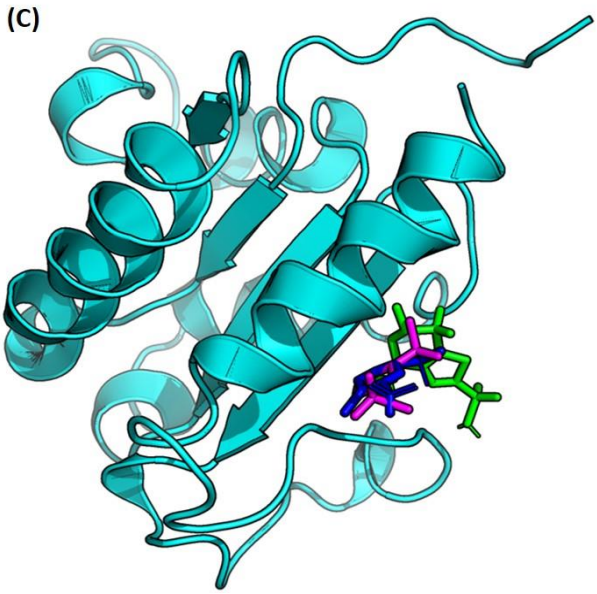

Figure 3. 5. In-silico interaction analysis of TIRAP and PKCδ through molecular docking and virtual screening of small molecules targeting TIRAP at the binding interface site of PKCδ. **(A)** The protein-protein molecular docking complex of TIRAP TIR domain and PKCδatalytic domain from pyDockWEB tool. The TIRAP is represented in cyan and PKCδ in green, while the black dotted lines represent all the interactions within the 4Å region, **(B)** Analysis of interface and interacting residues of TIRAP and PKCδ within the 4Å region from Chimera and PDBePISA tool, and **(C)** Representation of molecular docking from Autodock Vina 4.0 of TIRAP (cyan) with virtually screened three shortlisted small molecules ZINC01530621 (dorzolamide) in green, ZINC95696967 in magenta, and ZINC00897236 (Trichlormethiazide) in blue displaying their binding on TIRAP at the interface site of PKCδ.

S. No.	ZINC Id	Chemical Name	Commercial Name	Molecular Formula	Molar Mass (g/mol)	AutoDock Binding Energy (kcal/mol)	Known Target/ Function	2D Structure
1.	ZINC01530621	(4S,6S)-4-(ethylamino)-6-methyl-5,6-dihydro-4H-thieno[2,3-b]thiopyran-2-sulfonamide 7,7-dioxide	Dorzolamide	$C_{10}H_{16}N_2O_4S_3$	324.449	-5.7	Carbonic anhydrase (CA) inhibitor to treat high intraocular pressure in ocular hypertension and open-angle glaucoma	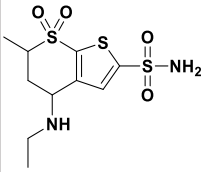
2.	ZINC95696967	3-(methylsulphonyl) benzenesulphonyl chloride	-	$C_7H_7ClO_4S_2$	254.716	-5.6	Prostaglandin G/H synthase 2 inhibitor	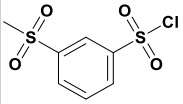
3.	ZINC00897236	6-Chloro-3-(dichloromethyl)-3,4-dihydro-2H-1,2,4-benzothiadiazine-7-sulfonamide 1,1-dioxide	Trichlormethiazide	$C_8H_8Cl_3N_3O_4S_2$	380.662	-5.5	Thiazide diuretic to treat oedema & hypertension	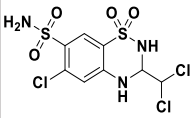

Table 3. 1. List of virtually screened small molecules from the ZINC15 database targeting TIRAP at the binding interface of PKCδ. The virtual screening was performed in Autodock Vina 4 and docked molecules were shortlisted based on their binding pose and Autodock binding energy (kcal/mol). The 2D structure of the below-listed molecules is drawn in ChemDraw 15.0 while their molecular details and known functions are obtained from the ZINC15 and Drugbank database.

3.5.5. DZD attenuates the expression of the pro-inflammatory cytokines in LPS-stimulated macrophages

The expression of pro-inflammatory cytokines is an endpoint marker to evaluate the response of inflammatory signaling pathways and plays an important role in regulating the host immune response. We, therefore, determined the impact of several LPS-induced, NF-κB and AP-1 dependent, pro-inflammatory cytokines upon treatment with DZD. Interestingly, DZD significantly suppressed the mRNA expression of TNF-α, IL-1β, IL-6, IL-12, and IL-23 in both primary bone-marrow-derived macrophages (BMDM) and RAW 264.7 macrophage cells, respectively **(Figure 3.6A-B)**. These findings suggest that the interaction of TIRAP with PKCδ mediates downstream inflammatory signaling and cytokines expression and that DZD inhibits this.

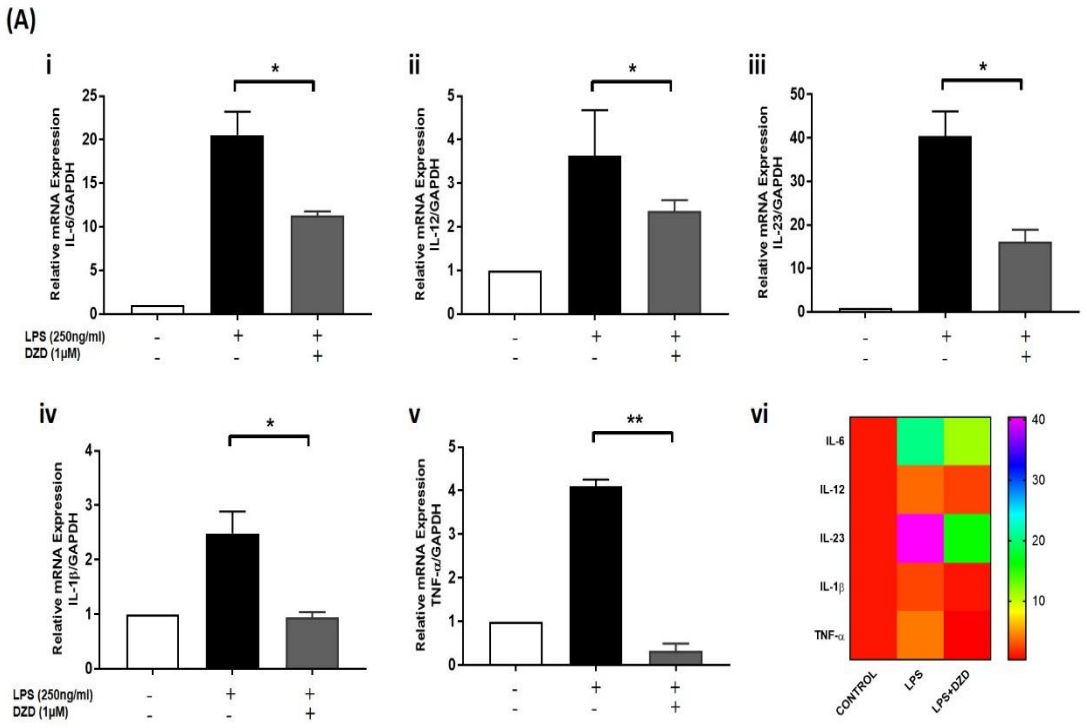

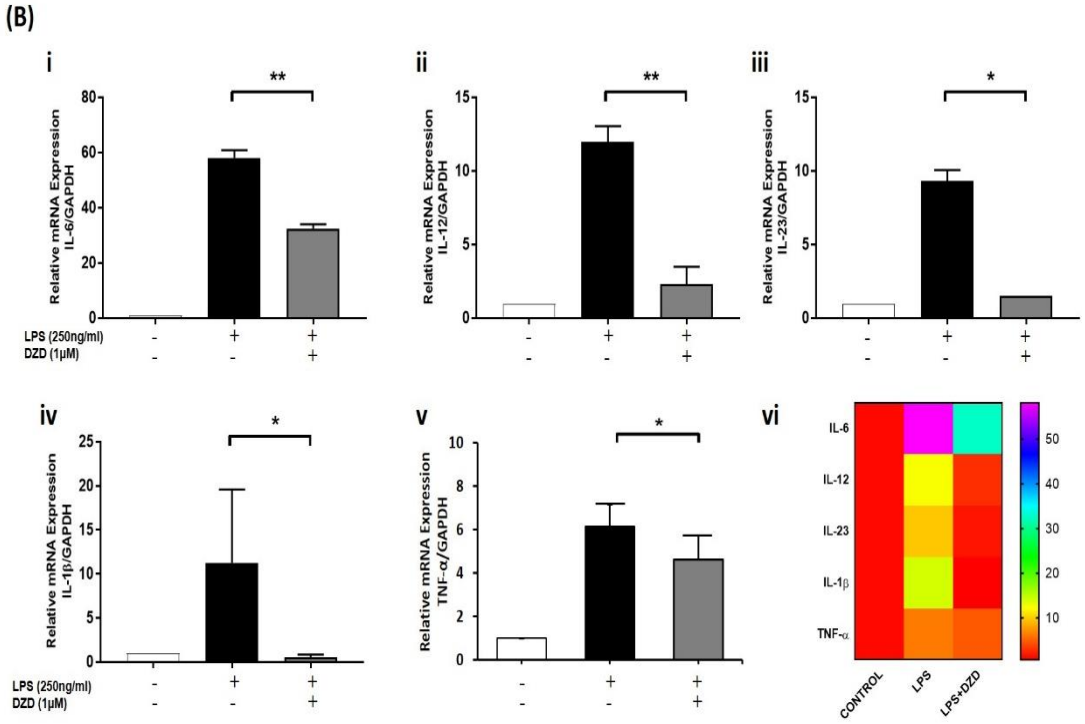

Figure 3. 6. Effect of dorzolamide (DZD) on pro-inflammatory cytokines expression in LPS induced mouse bone marrow-derived macrophages (BMDM) and RAW 264.7 cell. The total RNA was isolated and 1μg from each sample was used for single-stranded cDNA preparation as per the manufacturer's instruction. Prepared cDNA was used as the template for real-time PCR and relative mRNA expression of pro-inflammatory cytokines was estimated with respect to GAPDH. **(A) & (B)** Relative mRNA expression of **(i)** IL-6, **(ii)** IL-12, **(iii)** IL-23, **(iv)** IL-1β, **(v)** TNF-α, and **(vi)** heatmap for all cytokines (i-v) in BMDM and RAW 264.7 cells, respectively. All experiments were independently performed three times, and data represented as the mean ± S.E.M. Significance value, *p<0.05, **p<0.005, versus LPS stimulated cells.

3.5.6. MD simulation reveals stable TIRAP and DZD binding

To test the hypothesis that DZD inhibits LPS-induced cytokine production by disrupting the interaction between TIRAP and PKCδ we used in silico methods to analyse the binding stability of DZD with TIRAP using molecular dynamics (MD) simulation **(Figure 3.7A)**. In addition, an MD simulation of the apo form of TIRAP was also performed. MD simulation of 500ns was performed using the GROMACS

program. Analysis of root mean squared deviations (RMSD) throughout the MD trajectory suggested no significant fluctuations for the DZD from its initial docking predicted position **(Figure 3.7B)**. Similarly, no significant fluctuations were observed for TIRAP suggesting the overall stability of the protein-ligand complex. Furthermore, higher fluctuation of amino acid residues was observed mostly near the N and C-terminal tail **(Figure 3.7C)**. Interestingly, the comparison of MD trajectories for apo TIRAP and DZD-bound TIRAP revealed restricted protein movements upon ligand binding **(Figure 3.7D)**. Although, TIRAP-DZD MD simulation suggests stable binding, the free energy landscape generated by projecting the first two principal components revealed multiple energy minima indicating weak binding of DZD to TIRAP **(Figure 3.7E)**. To further estimate the energetics of DZD binding to TIRAP, MM-PBSA analysis was performed using a full 500ns MD trajectory which revealed favorable binding free energy for DZD **(Figure 3.7F)**. Our TIRAP-PKCδ and TIRAP-DZD docking calculations suggested the binding of DZD at one of the major contact regions between TIRAP and PKCδ **(Figure 3.8A)**. TIRAP amino acid residues such as Tyr195, Gln208, Arg215, and Tyr216 which form key interactions with DZD are also predicted to be involved in TIRAP-PKCδ protein-protein interaction **(Figure 3.8B-C)**. Hence, we hypothesized that DZD binding might interfere with the TIRAP-PKCδ protein-protein complex formation. To get insights into the inhibitory mechanisms, we performed two MD simulations starting from the DZD bound and unbound form of the TIRAP-PKCδ complex. We expected that the DZD bound TIRAP-PKCδ complex will either start to dissociate with the simulation progression or will not be as stable as the TIRAP-PKCδ complex. Indeed, the free energy landscape constructed by projecting the first two principal components from the 500ns MD trajectory revealed that the TIRAP-PKCδ complex was comparatively more stable with two energy minima **(Supplementary Figure S3.1A)**. On the other hand, higher collective movements were observed in the case of the DZD bound TIRAP-PKCδ complex as exemplified by several low-energy wells indicating a less stable system **(Supplementary Figure S3.1B)**. To further shed light on the inhibition of the TIRAP-PKCδ complex by DZD, we next calculated the hydrogen bonds, salt bridges, and van

der Waals contacts between TIRAP and PKCδ throughout the MD trajectory and plotted their occurrence frequency as a heatmap. As shown in (**Figure 3.8D-E)** and **Supplementary Figure S3.2-S3.5**, there is a significant decrease in the contacts between TIRAP and PKCδ in the case of the DZD bound complex. Specifically, almost all hydrogen bonds and salt bridges disappeared and van der Waals contacts decreased significantly indicating the dissociation/destabilization of the TIRAP and PKCδ complex **(Figure 3.8D-E and Supplementary Figure S3.2-S3.5)**. Interestingly, most of the contacts that vanished during the MD simulations lay in the contact region where DZD is predicted to bind **(Figure 3.8A-C)**. Among these contacts, TIRAP Arg215 is predicted to interact with a patch of several negatively charged residues (Asp551, Asp552, Glu553, and Asp554) on the PKCδ interacting surface **(Figure 3.8F)**. Comparison of the C_β-C_β distance between TIRAP Arg215 and negatively charged residues on PKCδ interacting surface in DZD bound simulation was found to be higher than in the TIRAP-PKCδ MD simulation **(Figure 3.8G)**. The binding of DZD with two sulphonyl groups appears to repel two proteins (PKCδ and TIRAP) away from each other **(Figure 3.8H)**. Comparison of C_β-C_β distance (C_α-C_β for Gly550-Tyr195 interaction) for other interacting residues at or around the DZD binding interface also revealed a similar trend **(Supplementary Figure S3.6)**.

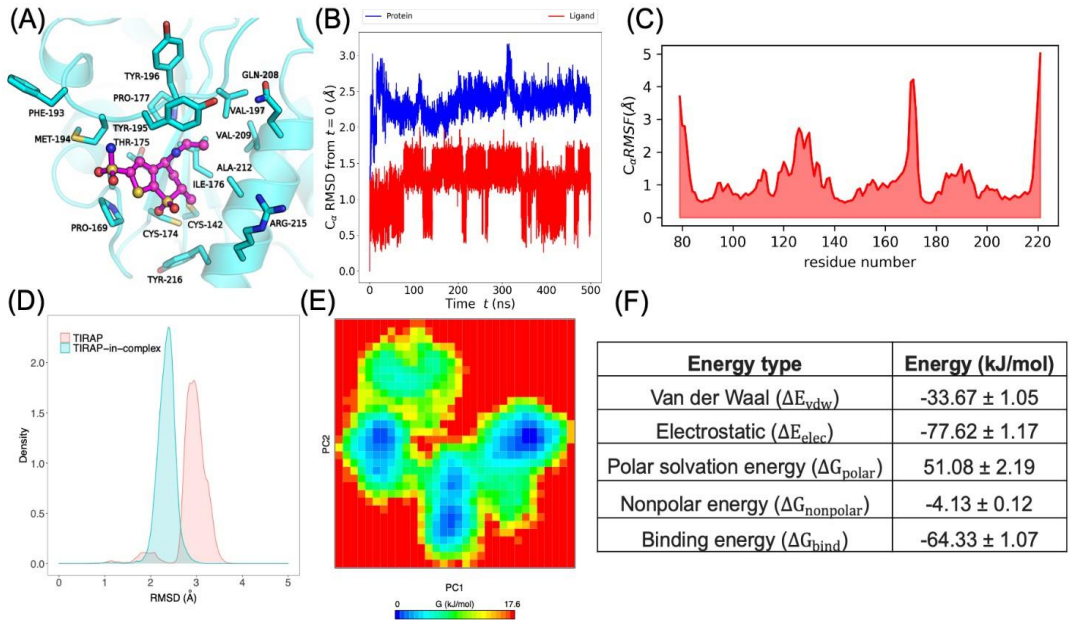

Energy type	Energy (kJ/mol)
Van der Waal (ΔE_{vdw})	-33.67 ± 1.05
Electrostatic (ΔE_{elec})	-77.62 ± 1.17
Polar solvation energy (ΔG_{polar})	51.08 ± 2.19
Nonpolar energy ($\Delta G_{nonpolar}$)	-4.13 ± 0.12
Binding energy (ΔG_{bind})	-64.33 ± 1.07

Figure 3. 7. Analysis of MD trajectory of TIRAP with docking predicted Dorzolamide (DZD). **(A)** Docking predicted the binding pose of DZD (magenta) with TIRAP (cyan). **(B)** RMSD of DZD (red) and TIRAP (blue) throughout 500ns MD trajectory. **(C)** RMSF of TIRAP residues throughout 500ns MD trajectory. **(D)** Comparison of RMSD of apo and DZD bound TIRAP. **(E)** Gibbs's free energy landscape is generated by plotting the first two principal components. **(F)** Table showing DZD binding free energy calculated using MM-PBSA method.

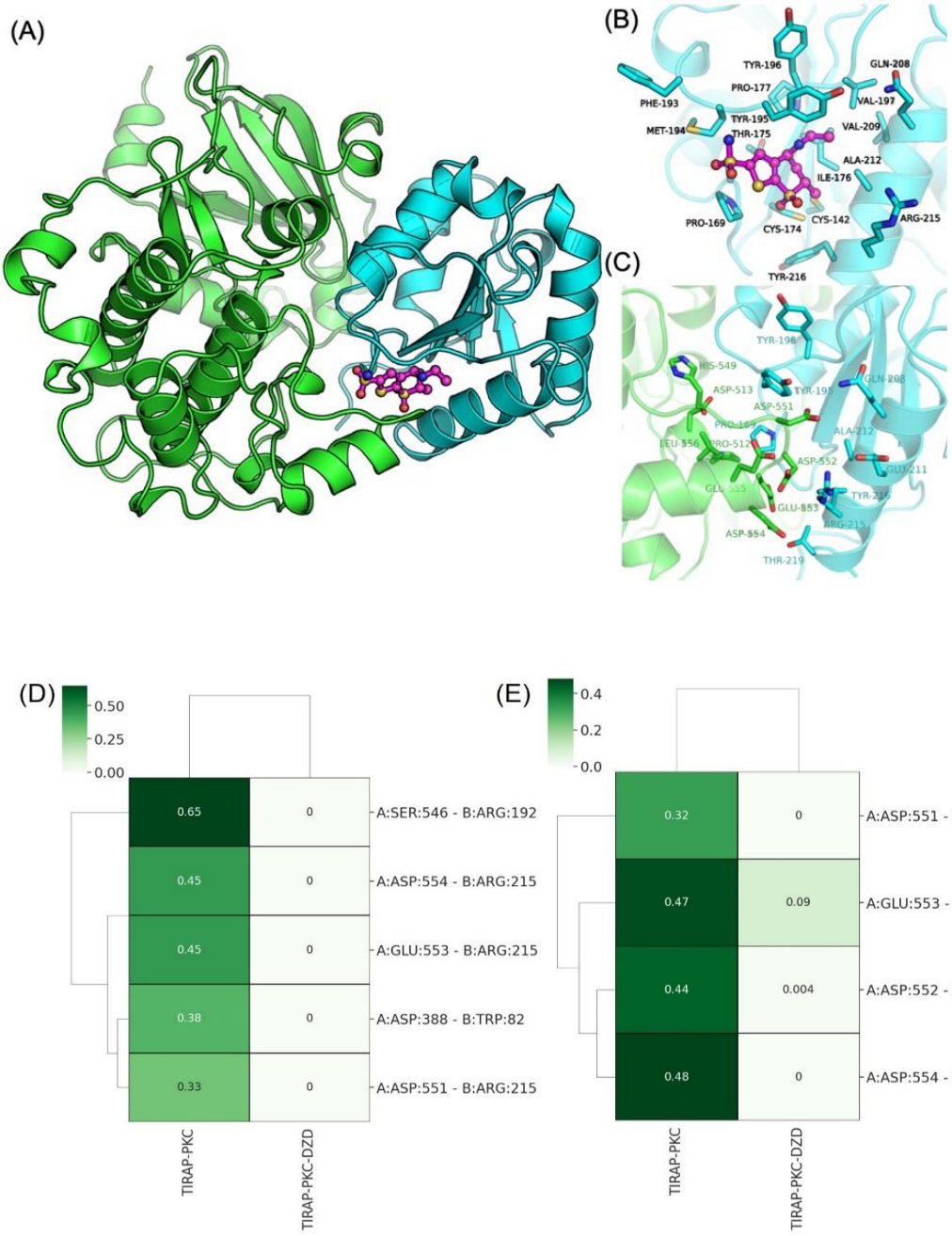

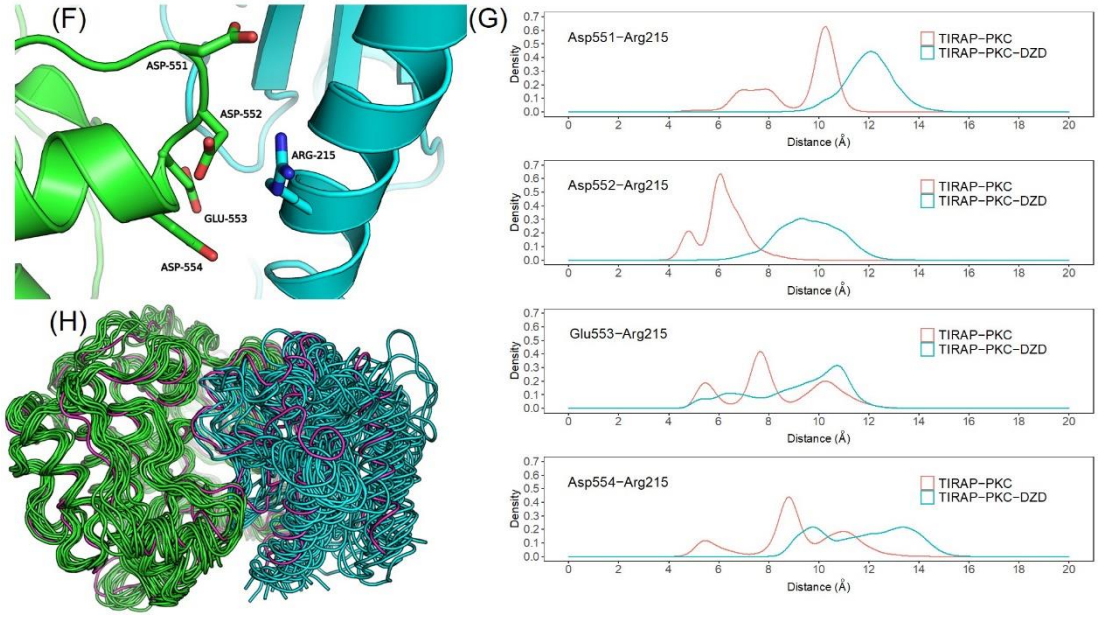

Figure 3. 8. (A) A cartoon figure of docking predicted complex of TIRAP (cyan) and PKCδ (green) with docking predicted binding pose of Dorzolamide (DZD). **(B)** A close-up view of docking predicted the binding pose of DZD (magenta atom color) to TIRAP. **(C)** PKCδ and TIRAP interacting interface near DZD predicted binding site. Frequency heatmaps of intermolecular contacts calculated between TIRAP and PKCδ throughout 500 ns MD trajectory**. (D)** Hydrogen bond and **(E)** Salt bridge**. (F)** A close-up view of the PKCδ region with a patch of negatively charged residues at the TIRAP-PKCδ predicted binding interface. **(G)** Distance between interacting residues was calculated throughout the 500 ns MD trajectory. **(H)** Overlay of 10 snapshots extracted from the 500 ns MD trajectory. TIRAP is shown in cyan color while PKCδ is shown in green. Docking predicted TIRAP-PKCδ complex is shown in magenta.

3.5.7. DZD inhibits TIRAP phosphorylation in LPS-stimulated macrophages

Upon LPS stimulation of macrophages, TLR4 and TIRAP are phosphorylated by kinases. Tyrosine phosphorylation of the TIRAP TIR domain is crucial for its downstream activity [19, 47, 48]. As our in-silico analysis suggested that DZD disrupts the interaction of TIRAP with the PKCδ kinase, we predict that DZD treatment will decrease TIRAP phosphorylation. Both Y86 and Y106 within the TIRAP TIR domain, represent crucial phosphorylation sites for PKCδ [40]. Phosphorylation of TIRAP at

Y86 (p-TIRAP) showed a modest increase over time and this was significantly decreased at 30min post LPS treatment in DZD-treated RAW 264.7macrophages **(Figure 3.9A-B)**. No changes in total TIRAP levels were observed (t-TIRAP, **Figure 3.9A**). Early, LPS-induced phosphorylation of TIRAP is also regulated by BTK, which competitively targets tyrosine sites in the TIRAP TIR domain and this might explain why no significant change in TIRAP phosphorylation is observed at 5min and 15min [19, 48]. However, the downregulation of TIRAP phosphorylation at 30min post LPS activation strongly suggests that DZD decreases TIRAP activation by blocking its interaction with PKCδ and subsequent phosphorylation by this kinase. Therefore, we next investigated the interaction of TIRAP with PKCδ at 30min post-LPS stimulation in RAW 264.7 macrophages through a co-immunoprecipitation study. As before, a modest increase in interaction between TIRAP and PKCδ was observed upon LPS treatment and this was significantly reduced in the presence of DZD **(Figure 3.9C-D)**. Together our data suggest that phosphorylation of TIRAP, induced by LPS, is inhibited by the addition of DZD, most likely due to the inhibition of the TIRAP-PKCδ interaction.

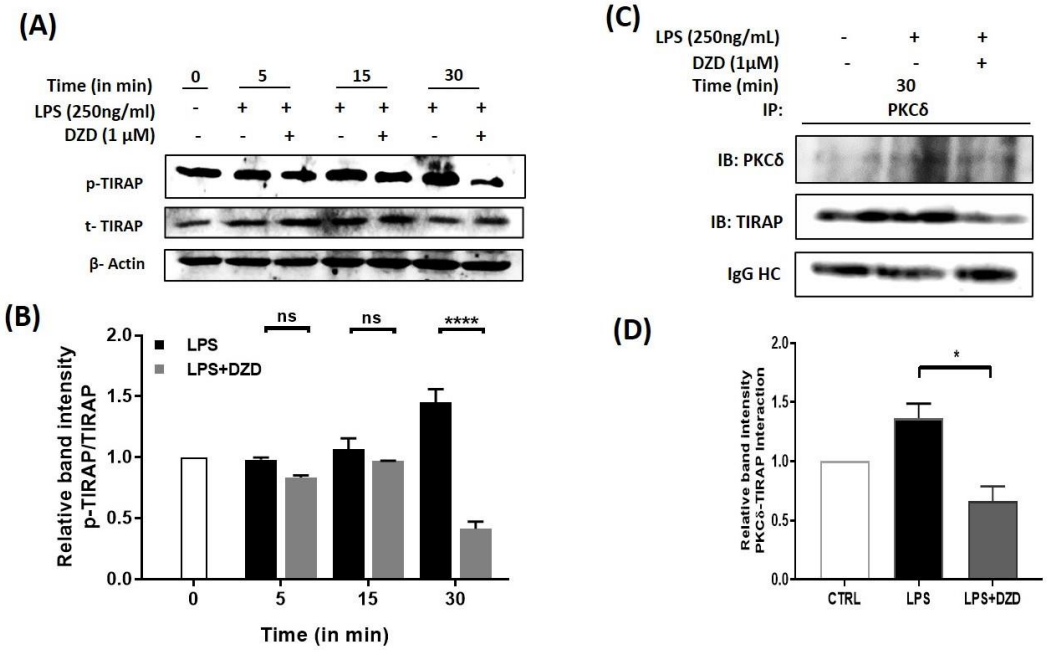

Figure 3. 9. Dorzolamide (DZD) downregulates the tyrosine phosphorylation of TIRAP and significantly disruption its interaction with upstream kinase PKCδ in LPS stimulated RAW 264.7 cells. **(A-B)** Immunoblot analysis of phosphorylated TIRAP at variable time points indicates the significant downregulation of TIRAP phosphorylation and **(C-D)** disruption of TIRAP interaction with PKCδ through co-immunoprecipitation study, respectively at 30 min time point. All experiments were independently performed three times, and data represented as the mean ± S.E.M. Significance value, ****p<0.00005, versus LPS-stimulated cells.

3.5.8. PKCδ-mediated TIRAP phosphorylation regulates p38 MAPK activation

To understand the downstream signalling mechanism and the possible factor responsible for the regulation of inflammatory cytokine responses mediated via TIRAP and PKCδ in LPS-induced macrophages we analyzed the protein expression and phosphorylation of different MAPKs. After 1h of LPS stimulation, phosphorylation of p38 MAPK and p-ERK were increased but only phosphorylation of p38 was significantly decreased when the cells were also treated with DZD **(Figure 3.10A-C)**. Only modest activation of p-JNK was observed at this time point and this was not decreased by DZD treatment (**Figure 3.10A and D**). This indicated that activation of p38 MAPK might lie downstream of PKCδ-TIRAP interaction and that phosphorylated TIRAP specifically activates the p38 MAPK. As p38 MAPK regulates NF-κB/p65 transcriptional activity and its nuclear translocation we next analyzed the negative regulator of NF-κB, IκB. IκB retains NF-κB in the cytosol but becomes degraded by the proteasome upon stimulation, allowing free transcription factors to be translocated to the nucleus and induce pro-inflammatory cytokines [49, 50]. Western blot analysis of IκB revealed the expected decrease in IκB protein levels in LPS-stimulated macrophages, with the lowest levels detected at 30min post-stimulation. This LPS-induced loss of IκB was prevented in the presence of DZD **(Figure 3.10E-F)**. To test if there was a concomitant increase in NF-κB/p65 phosphorylation and its release for nuclear translocation we analyzed NF-κB/p65 phosphorylation by immunoblot. NF-κB/p65 phosphorylation was significantly downregulated in the LPS+DZD-treated condition as compared to cell lysates prepared from macrophages stimulated with LPS+DMSO **(Figure 3.10G)**. Furthermore, immunofluorescence microscopy demonstrated that the nuclear translocation of NF-κB/p65, induced by

LPS treatment, was also largely inhibited by the addition of DZD **(Figure 3.10H-I)**. In line with this finding, cell lysate fractionation demonstrated that LPS-induced nuclear translocation of phosphorylated NF-κB/p65 is reversed significantly in the LPS+DZD-treated condition **(Figure 3.10J)**. Together, the data indicate that DZD disrupts the PKCδ/TIRAP interaction and subsequently blocks the p38 MAPK and NF- κB/p65 signaling axis which is critical for LPS-induced pro-inflammatory cytokine responses in macrophages.

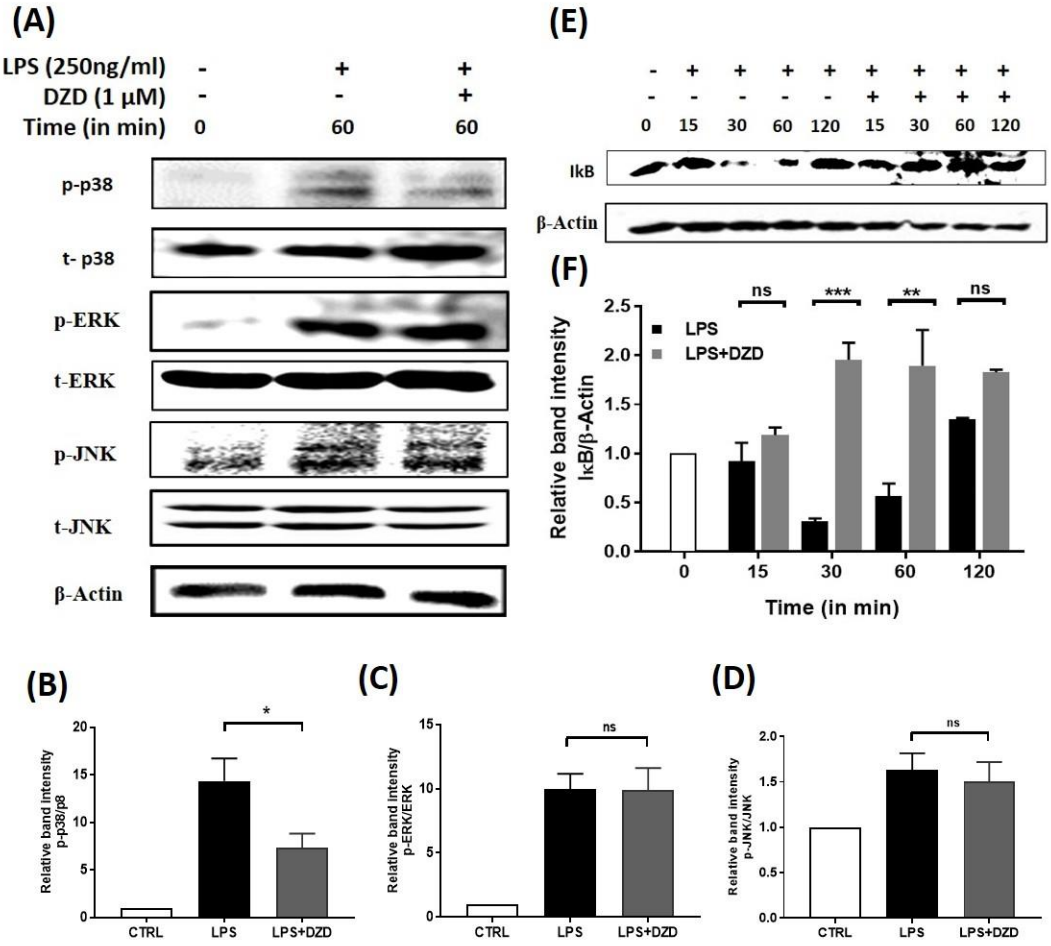

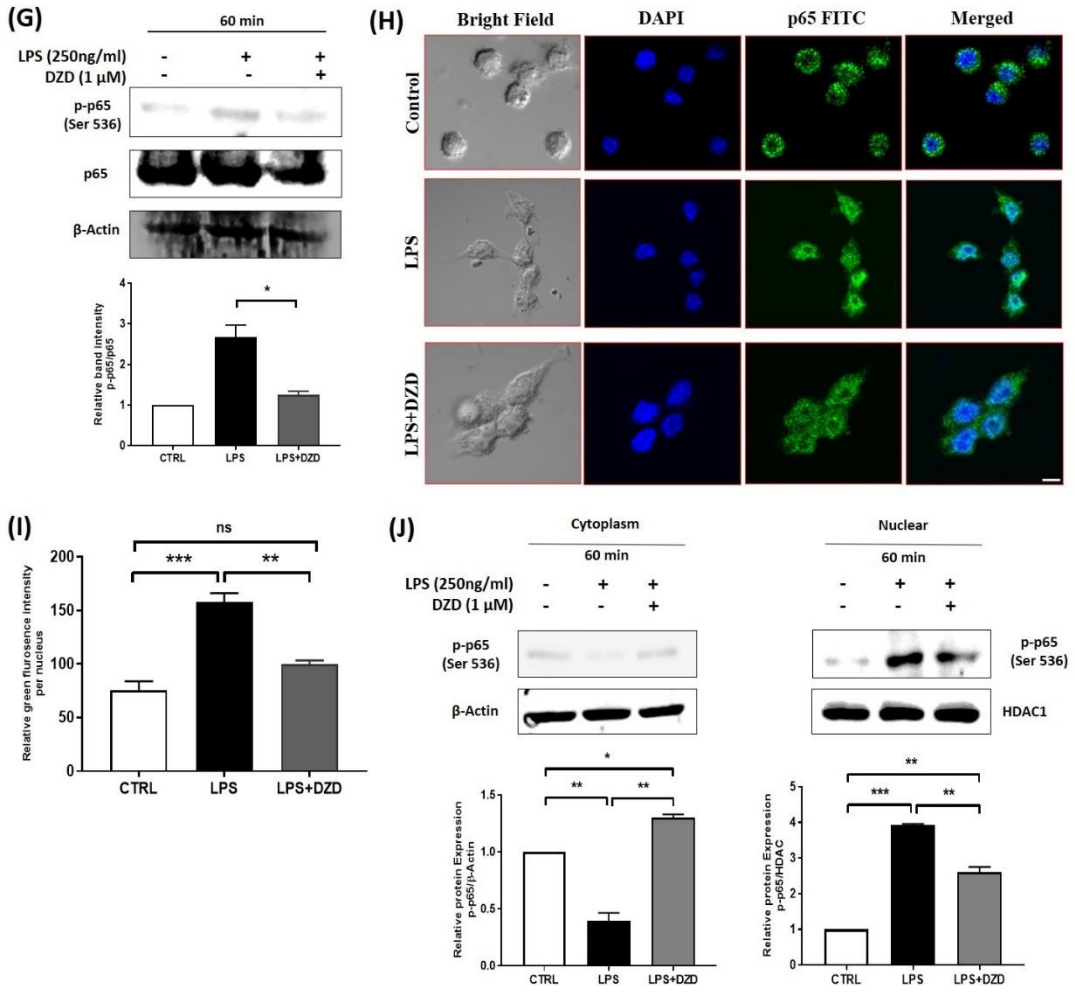

Figure 3. 10. Effect of dorzolamide (DZD) in TIRAP-PKCδ mediated downstream signalling in LPS-stimulated TLR4 signaling in RAW 264.7 cells. **(A-D)** Immunoblot analysis of MAPKs indicates the significant downregulation of p38 MAPK phosphorylation while ERK and JNK phosphorylation remains unchanged in DZD-treated macrophages, and **(E-F)** Immunoblot analysis of IκB indicates the effect of DZD to reduce its proteasomal degradation. **(G)** Immunoblot analysis of NF-κB/p65 shows decrease in its phosphorylation in DZD-treatment. **(H-I)** Immunofluorescence data indicates the inhibition of nuclear translocation of NF- κB/p65 in DZD-treated cells. **(J)** Immunoblot analysis of cytoplasmic and nuclear fraction of phopsho-NF-κB/p65 displays the translocation of p-p65 in nucleus in LPS treated macrophages while reduced phosphorylation of p65 in DZD-treated condition shows inhibition in its nuclear translocation. All experiments were independently performed three times, and data were represented as the mean ± S.E.M. Significance value, *p<0.05, **p<0.005, ***p<0.0005, versus LPS-stimulated cells. Scale bar=10µm.

3.5.9. DZD treatment protects mice from septic injury and mortality

To investigate whether DZD can prevent toxic shock induced by LPS we exploited the LPS-induced sepsis model in mice. The survival rate across three groups of mice (n=12) was assessed to determine the efficacy of DZD over a 96h period. The control group received vehicle DMSO and/or PBS only, the LPS group received the LPS lethal dose of 25mg/kg body weight with DMSO vehicle control, and the LPS+DZD group received a single dose of DZD (20mg/kg)1h before the LPS infection. All the injections were administered through the intraperitoneal (IP) route and mice survival was recorded every 12h for a total of 96h for each group. The survival rate for the LPS group sharply reduced to 30% at 24h post-injection (pi) with a further decrease to ~8% at 48h, which was maintained until 96h pi **(Figure 3.11A)**. In contrast, the DZD-treated mice display a higher survival rate of ~65% at 24h to an overall 42% survival rate at the end of the 96h study **(Figure 3.11A)**. Besides, the higher survival rate when compared to the LPS group, the mortality of mice in the DZD-treated group was also delayed as compared to the LPS group as presented in the Kaplan Meier survival curve **(Figure 3.11A)**. The mice in the control displayed no changes and all survived till the end of the experiment. Overall, the survival rate study suggests a protective role of DZD in LPS-treated mice, significantly reducing LPS-induced toxic shock **(Figure 3.11A)**. To further investigate the protective nature of DZD in alleviating LPS-induced lung injury, a histology study of the lung tissue section in each group was performed. The lungs are one of the primary sites of inflammation which undergo damage due to the infiltration of immune cells and inflammatory responses. The lung tissue from each group of mice described above was isolated 12h after IP injection. The lung tissues were then fixed in 10% formalin and used for the preparation of 5μm thin sections on a glass slide for hematoxylin and eosin (H&E) staining and detection. The lung tissues were observed under the light microscope and images were captured at 40X **(Figure 3.11B i-iii)**. Interestingly, the lung histomorphology of the DZD-treated mice resembled the control group of the mice lung tissue as evidenced by the intact epithelial lining, the disappearance of the alveolar septum, and interstitial edema, and significantly decreased infiltration of inflammatory cells **(Figure 3.11B-D)**. In

contrast, the lung tissue of LPS-challenged mice shows alveolar haemorrhage, thickening of alveolar septum, distorted epithelial and endothelial cell structure, and increased infiltration of inflammatory cells and pulmonary edema **(Figure 3.11B-D)**. Finally, pro-inflammatory cytokine expression in lung tissue was also analyzed by qRT-PCR. We observed that the cytokines IL-6, IL-12, IL-23, IL-1β, and TNF-α expression in DZD-treated mice lung tissue was downregulated as compared to LPS-only challenged mice lung tissue **(Figure 3.11E-J)**. In conclusion, DZD administration effectively alleviated LPS-induced lung tissue injury and inflammation as well as death in mice.

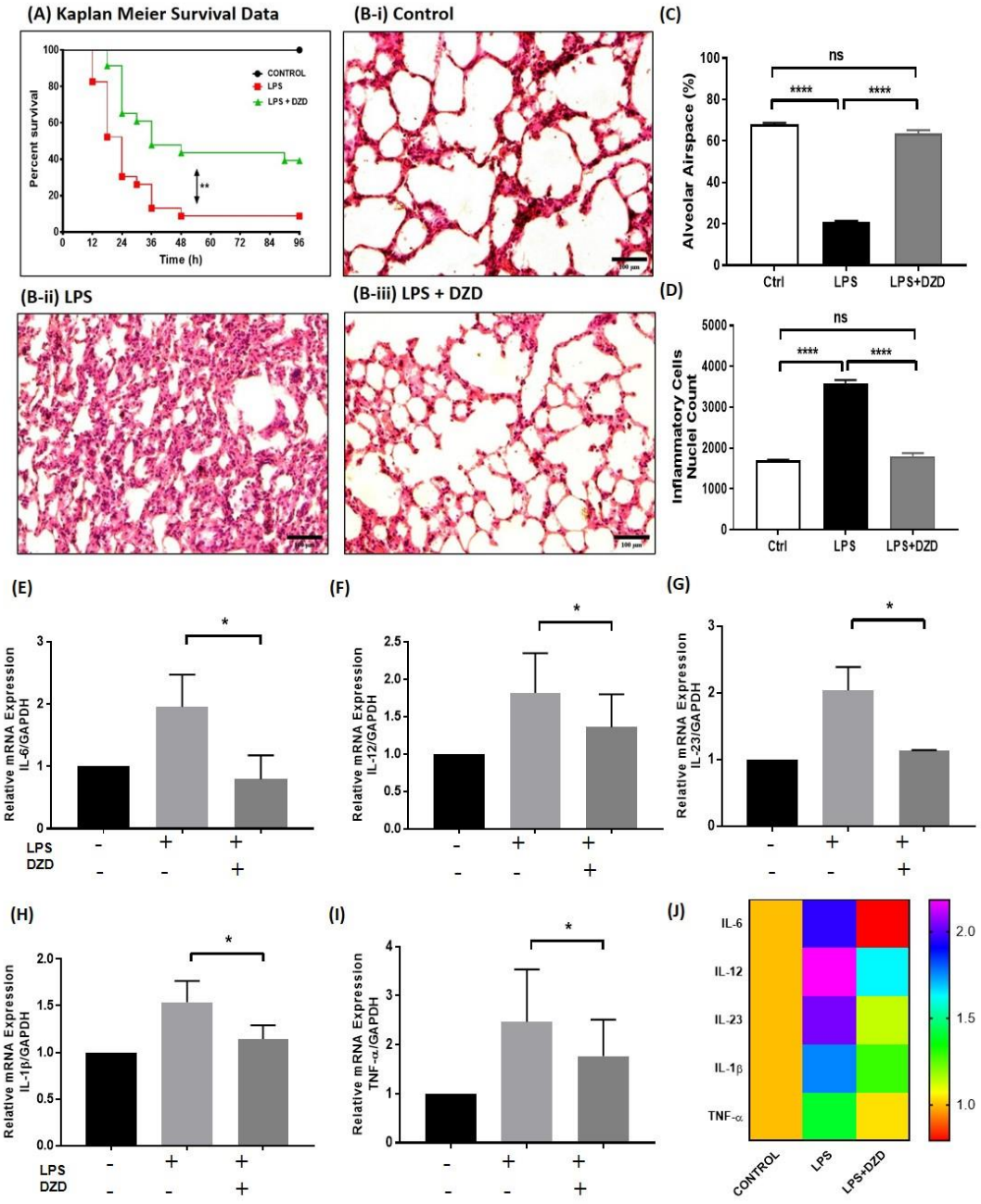
(A) Kaplan Meier Survival Data
Percent survival
Time (h)
CONTROL
LPS
LPS + DZD
(B-i) Control
(B-ii) LPS
(B-iii) LPS + DZD
(C)
Alveolar Airspace (%)
ns
****
Ctrl
LPS
LPS+DZD
(D)
Inflammatory Cells Nuclei Count
(E)
Relative mRNA Expression IL-6/GAPDH
(F)
Relative mRNA Expression IL-12/GAPDH
(G)
Relative mRNA Expression IL-23/GAPDH
(H)
Relative mRNA Expression IL-1β/GAPDH
(I)
Relative mRNA Expression TNF-α/GAPDH
LPS
DZD
(J)
IL-6
IL-12
IL-23
IL-1β
TNF-α
CONTROL
LPS
LPS+DZD

Figure 3. 11. Administration of dorzolamide (DZD) in mice protects the septic mice mortality and alleviates the lung injury induced by LPS**. (A)** Kaplan Meier survival curves of mice from three different treatment groups (Control, LPS, and LPS+DZD; n=12 per group). In the control group, all mice received the vehicle DMSO/PBS only. In the LPS group, mice were challenged with a single dose of LPS (25 mg/kg) to induce sepsis. In LPS+DZD, a single dose of DZD (20 mg/kg) was pre-administered 1h before the LPS challenge. The mortality of mice was recorded every 12h consecutively for 4 days (96h). All injections were given through the intraperitoneal (i.p) route. The data represented as the mean ± S.E.M from two sets of independent experiments and significance value, **p<0.005, versus LPS challenged mice. **(B)** The histomorphology study from the lung tissue section was performed to access the LPS-induced lung damage and the effect on the lung from the administration of DZD. The **(B-i)** Control, **(B-ii)** LPS, and **(B-iii)** LPS+DZD group of mice were treated as described for **(A)** for 12h (n=3 per group) and sacrificed for lung tissue isolation and fixed in 10% formalin for preparation of 5μm thin section on a glass slide. The tissue sections were stained in haematoxylin and eosin **(H&E)** and imaged under a light microscope at 40X magnification. qRT-PCR for relative mRNA expression of **(E)** IL-6, **(F)** IL-12, **(G)** IL-23, **(H)** IL-1β, and **(I)** TNF-α and **(J)** heatmap for all cytokines **(E-I)** in mice lung tissue at 12h as indicated. All experiments were independently performed three times, and data represented as the mean ± S.E.M. Significance value, *p<0.05, **p<0.005, ***p<0.0005, versus LPS stimulated cells. Scale bar=100μm.

3.6. Discussion

The role of the TIR domain-containing adaptor proteins in the TLR signaling pathway is crucial for the modulation of downstream inflammatory signaling. There are five major TIR domains containing adaptor proteins, which take part in macrophage TLR signaling [12, 51, 52]. Stimulation of TLR4/2 signaling by their classical ligands LPS/lipoproteins leads to subsequent recruitment and activation of the cytoplasmic adaptor proteins like TIRAP andMyD88 for further activation of downstream transcription factors and hence the expression of cytokines. Initially, TIRAP's role was thought to be mainly to recruit the MyD88 to TLR4/2 and to act as a bridging protein for the myddosome complex. [10, 11, 13, 53-55]. However, further studies suggested the diverse roles of TIRAP in the independent activation of signalling mediators and downstream inflammatory responses, besides the myddosome complex [17, 21]. Activation of TIRAP is, however, also regulated by upstream kinases upon

macrophage stimulation. In TLR4 signaling, stimulation with LPS leads to the activation of numerous kinases, such as syk, srk, lyn, src, BTK, PKCδ, etc., which act on phosphorylation of the TIR domain [47, 56]. The tyrosine phosphorylation of the TIRAP TIR domain is crucial for its activation and function [48]. Earlier, most of the studies focused on BTK for TIRAP tyrosine phosphorylation and this kinase is well-studied in the regulation of TIRAP activation [19, 57]. However, the role of another tyrosine-protein kinase, abundantly present in macrophages, PKCδ, in phosphorylation and activation of TIRAP in TLR4 signaling is not studied much, whereas limited information is available on the PKCδ-TIRAP mediated signaling axis. Few earlier studies, including ours, emphasized the importance of PKCδ in the activation of TIRAP, which leads to downstream inflammatory response as well as the competitive interaction between BTK and PKCδ with TIRAP for its activation [22, 40, 41]. Studies suggest that the Y86 and Y106 in the TIR domain of TIRAP are competitively phosphorylated by BTK as well as by PKCδ [41]. Such interactions likely regulate inflammatory responses in the host through various pathways via TIRAP. In summary, the TIRAP is playing a central role in inflammation and a detailed study on its growing number of interactions with proteins, including PKCδ and other kinases or non-kinase proteins, may open many unexplored avenues in inflammatory signaling and could be therapeutically beneficial in pathophysiological conditions. In an attempt to do so, we investigated the TIRAP-PKCδ mediated signaling axis in the TLR4 pathway and discovered a novel inhibitor of TIRAP that can control and subside prolonged inflammation.

In the current study, we found that the interaction of TIRAP with PKCδ in response to LPS is accentuated, which eventually leads to activation of downstream p38 MAPK and increased expression of pro-inflammatory cytokines through AP-1 and NF-κB transcription factors, whereas DZD significantly attenuated the underlying signaling via inhibition of TIRAP interaction with PKCδ **(Figure 3.1)**. We confirmed the interaction of TIRAP with PKCδ through immunoblotting of co-immunoprecipitated and co-localization by immunofluorescence techniques in LPS-stimulated mouse

macrophage cells **(Figure 3.2A-F)**.The data suggest that TIRAP interaction with PKCδ increases in LPS-stimulated macrophages **(Figure 3.2B, D, and F)**. This increase indicates that the association of TIRAP and PKCδ is an important event in inflammatory signaling. To study the possible effect of this interaction on TIRAP and its downstream function, we decided to disrupt binding to PKCδ with small molecules. We, therefore, identified the interface and interacting residues in the TIRAP-PKCδ complex through in-silico analysis. Molecular docking is a powerful technique to decipher the interactions at residue and atomic levels and greatly helps in drug development. Therefore, we performed the high-quality homology-based-3D structure modelling of PKCδ **(Figure 3.3)** and loop modelling of TIRAP's missing residues in the TIR domain **(Figure 3.4)**. Further, we performed molecular docking of TIRAP and PKCδ structures in pyDockWEB and identified the protein-protein interface and interacting residues through Chimera and PDBePISA **(Figure 3.5A-B)**. Drug development is a very long process and needs to go through many stages before the drug can be approved for use. However, the repurposing of approved drugs has been largely appreciated and can improve the cost and time of drug development, increase safety and efficacy, etc. Therefore, we used a library of approved for clinical use small molecules from the ZINC15 database for virtual screening against the TIRAP interface with PKCδ. Notably, we shortlisted three molecules based on their binding specificity and high docking scores **(Figure 3.5C and Table 3.1)**. We advanced the best molecule DZD to test in macrophages. DZD is currently approved as a carbonic anhydrase (CA) inhibitor to treat elevated intraocular pressure (IOP) associated with open-angle glaucoma and ocular hypertension. It is indicated to work by blocking the enzyme in the ciliary process that regulates ion balance and fluid pressure in the eyes. The expression of cytokines is an end-point marker of an inflammatory pathway and modulates the microenvironment in the host. So, we first sought to investigate the effect of DZD on the expression of pro-inflammatory cytokines (IL-6, IL-12, IL-23, IL-1β, and TNF-α) via the TIRAP and PKCδ signaling axis. Interestingly, we observed that DZD could significantly attenuate the cytokines expression in LPS-stimulated mouse BMDM and RAW 264.7 cells, respectively **(Figure 3.6A-B)**. The DZD effect

on cytokines expression raised the curiosity to understand the stability of DZD binding with TIRAP and in complex with PKCδ as well as its role in regulating the TIRAP activation. The molecular dynamic simulation of the complex of DZD with TIRAP and in the TIRAP-PKCδ complex was extensively performed for 500ns, which demonstrated that the DZD binding is energetically stable (ΔG_{bind} = -64.33) and DZD diminishes the hydrogen bonds and salt bridges between TIRAP and PKCδ **(Figure 3.7 and Figure 3.8)**. As discussed earlier, tyrosine phosphorylation of TIRAP is crucial for its activity and PKCδ is reported to phosphorylate TIRAP mainly at Y86. We, therefore, checked the phosphorylation of Y86 in TIRAP in the presence of DZD. Interestingly, phosphorylation of TIRAP increases with time in response to LPS and is significantly downregulated at 30 min in presence of DZD, while no major change was observed at the earlier time point of 5 and 15 min with DZD **(Figure 3.9A-B)**. This may be due to the actions of other kinases being active in TIRAP phosphorylation. BTK, being the key kinase, may contribute to the immediate phosphorylation of TIRAP in response to LPS, whereas such response was diminished at a later time due to the action of DZD blocking its interaction with PKCδ [19, 48]. To further confirm this, we performed co-immunoprecipitation at 30 min time point and observed that the interaction of TIRAP with PKCδ was significantly reduced in presence of DZD **(Figure 3.9C-D)**. Thus, disruption of TIRAP interaction with PKCδ by DZD leads to a decrease in TIRAP's Y86 phosphorylation, reversing the effect of LPS on macrophages. However, it would be very interesting to investigate the inhibitory effect on both BTK and PKCδ in the phosphorylation of TIRAP. Therefore, in another study, we will identify a small molecule with the potential to inhibit the TIRAP interaction simultaneously with both BTK as well as PKCδ to understand the combined effect of ceasing its phosphorylation and downstream action [58]. DZD treatment of LPS-stimulated macrophages reduced expression of pro-inflammatory cytokines via decreasing TIRAP interaction with PKCδ and its tyrosine phosphorylation. To reveal the downstream signaling and transcription factors responsible for gene expression, we investigated MAPK activity. Activation of MAPKs has a major role in macrophage inflammatory signaling and is mainly responsible for the activation of transcription

factors [42, 43]. Notably, we found that the DZD-treated RAW 264.7 macrophages display a significant decrease in p38 MAPK in comparison to LPS-stimulated macrophages, while the other two MAPKs ERK and JNK remained unchanged **(Figure 3.10A-D)**. This indicates that the TIRAP-PKCδ binary complex leads to the activation of p38 MAPK where TIRAP might be playing a crucial role in the activation of p38 MAPK. In agreement with our previous study describing the role of phosphorylated TIRAP in the activation of p38 MAPK [44], it may be that activated TIRAP promotes activation of p38 MAPK, whereas DZD blocks TIRAP's interaction with PKCδ and reduces activation of p38 MAPK at 1h. Activated p38 MAPK leads to the activation of transcription factors, primarily AP-1 and NF-κB[45, 49, 50]. The negative regulator IκB degradation leads to the nuclear translocation of NF-κB and cytokine response. We observed that IκB was protected and protein expression mainly recovered at 1h upon DZD treatment **(Figure 3.10E-F)**. Subsequently, we checked for phosphorylation and nuclear translocation of NF-κB/p65 through immunoblotting and immunofluorescence and observed that its phosphorylation, as well as nuclear translocation, are significantly inhibited in DZD-treated RAW 264.7 macrophages **(Figure 3.10G-I)**. Further, this was confirmed through the immunoblot analysis of cytoplasmic and nuclear protein fraction of phosphorylated NF-κB/p65 **(Figure 3.10J)**. Overall, our in-vitro investigation indicates that the TIRAP-PKCδ mediated signaling axis in the LPS-stimulated TLR4 pathway regulates p38 MAPK activation and NF-κB activity for pro-inflammatory gene expression. Moreover, the in-vivo study of the protective role of DZD in septic mice indicates the significance of TIRAP-PKCδ signaling. Importantly, inhibition of this signaling by DZD in LPS-induced septic mice significantly reduced the mortality rate as well as alleviated the LPS-induced lung injury and inflammation **(Figure 3.11A-I)**. Our study further highlights the central role of TIRAP and PKCδ mediated responses in different pathophysiological conditions associated with inflammation and proposes harnessing the inhibitory effect of TIRAP in the regulation of inflammation. Besides, more studies on DZD at the biophysical level with TIRAP and in-vivo level will pave the way for repurposing this as a potential anti-inflammatory agent.

3.8. References

1. Majno, G. and I. Joris, *Cells, tissues, and disease: principles of general pathology*. 2004: Oxford University Press.
2. Medzhitov, R., *Origin and physiological roles of inflammation.* Nature, 2008. **454**(7203): p. 428-435.
3. Chen, L., et al., *Inflammatory responses and inflammation-associated diseases in organs.* Oncotarget, 2018. **9**(6): p. 7204-7218.
4. Kawasaki, T. and T. Kawai, *Toll-like receptor signaling pathways.* Front Immunol, 2014. **5**: p. 461.
5. Nathan, C. and A. Ding, *Nonresolving inflammation.* Cell, 2010. **140**(6): p. 871-882.
6. Serhan, C.N. and J. Savill, *Resolution of inflammation: the beginning programs the end.* Nature immunology, 2005. **6**(12): p. 1191-1197.
7. Wynn, T.A. and K.M. Vannella, *Macrophages in tissue repair, regeneration, and fibrosis.* Immunity, 2016. **44**(3): p. 450-462.
8. Fujiwara, N. and K. Kobayashi, *Macrophages in inflammation.* Current Drug Targets-Inflammation & Allergy, 2005. **4**(3): p. 281-286.
9. Conway, E.M., et al., *Macrophages, inflammation, and lung cancer.* American journal of respiratory and critical care medicine, 2016. **193**(2): p. 116-130.
10. Lu, Y.C., W.C. Yeh, and P.S. Ohashi, *LPS/TLR4 signal transduction pathway.* Cytokine, 2008. **42**(2): p. 145-151.
11. Fitzgerald, K.A., et al., *Mal (MyD88-adapter-like) is required for Toll-like receptor-4 signal transduction.* Nature, 2001. **413**(6851): p. 78-83.
12. Kawasaki, T. and T. Kawai, *Toll-like receptor signaling pathways.* Frontiers in immunology, 2014: p. 461.
13. Latty, S.L., et al., *Activation of Toll-like receptors nucleates assembly of the MyDDosome signaling hub.* Elife, 2018. **7**.
14. Horng, T., et al., *The adaptor molecule TIRAP provides signalling specificity for Toll-like receptors.* 2002. **420**(6913): p. 329-333.
15. Horng, T., G.M. Barton, and R. Medzhitov, *TIRAP: an adapter molecule in the Toll signaling pathway.* Nature immunology, 2001. **2**(9): p. 835-841.
16. Verstak, B., et al., *MyD88 adapter-like (Mal)/TIRAP interaction with TRAF6 is critical for TLR2- and TLR4-mediated NF-kappaB proinflammatory responses.* J Biol Chem, 2009. **284**(36): p. 24192-203.
17. Bernard, N.J. and L.A. O'Neill, *Mal, more than a bridge to MyD88.* IUBMB Life, 2013. **65**(9): p. 777-86.
18. Dunne, A., et al., *IRAK1 and IRAK4 promote phosphorylation, ubiquitination, and degradation of MyD88 adaptor-like (Mal).* J Biol Chem, 2010. **285**(24): p. 18276-82.
19. Gray, P., et al., *MyD88 adapter-like (Mal) is phosphorylated by Bruton's tyrosine kinase during TLR2 and TLR4 signal transduction.* 2006. **281**(15): p. 10489-10495.
20. Kubo-Murai, M., et al., *Protein kinase Cδ binds TIRAP/Mal to participate in TLR signaling.* Molecular immunology, 2007. **44**(9): p. 2257-2264.
21. Rajpoot, S., et al., *TIRAP in the Mechanism of Inflammation.* Front Immunol, 2021. **12**: p. 697588.
22. Baig, M.S., et al., *Heterotrimeric complex of p38 MAPK, PKCdelta, and TIRAP is required for AP1 mediated inflammatory response.* Int Immunopharmacol, 2017. **48**: p. 211-218.

23. Jimenez-Garcia, B., C. Pons, and J. Fernandez-Recio, *pyDockWEB: a web server for rigid-body protein-protein docking using electrostatics and desolvation scoring.* Bioinformatics, 2013. **29**(13): p. 1698-9.
24. Pettersen, E.F., et al., *UCSF Chimera--a visualization system for exploratory research and analysis.* J Comput Chem, 2004. **25**(13): p. 1605-12.
25. Krissinel, E. and K.J.J.M.B. Henrick, *Protein interfaces, surfaces and assemblies service PISA at European Bioinformatics Institute.* 2007. **372**: p. 774-797.
26. Trott, O. and A.J. Olson, *AutoDock Vina: improving the speed and accuracy of docking with a new scoring function, efficient optimization, and multithreading.* J Comput Chem, 2010. **31**(2): p. 455-61.
27. BIOVIA, D.S., *BIOVIA Discovery Studio 2020.* San Diego: Dassault Systemes, 2020.
28. DeLano, W.L.J.C.N.o.p.c., *Pymol: An open-source molecular graphics tool.* 2002. **40**(1): p. 82-92.
29. Horn, H.W., et al., *Development of an improved four-site water model for biomolecular simulations: TIP4P-Ew.* The Journal of chemical physics, 2004. **120**(20): p. 9665-9678.
30. Maier, J.A., et al., *ff14SB: improving the accuracy of protein side chain and backbone parameters from ff99SB.* Journal of chemical theory and computation, 2015. **11**(8): p. 3696-3713.
31. Abraham, M.J., et al., *GROMACS: High performance molecular simulations through multi-level parallelism from laptops to supercomputers.* SoftwareX, 2015. **1**(1): p. 19-25.
32. Shirts, M.R., et al., *Lessons learned from comparing molecular dynamics engines on the SAMPL5 dataset.* Journal of computer-aided molecular design, 2017. **31**(1): p. 147-161.
33. Michaud-Agrawal, N., et al., *MDAnalysis: a toolkit for the analysis of molecular dynamics simulations.* 2011. **32**(10): p. 2319-2327.
34. McGibbon, R.T., et al., *MDTraj: a modern open library for the analysis of molecular dynamics trajectories.* 2015. **109**(8): p. 1528-1532.
35. Pedregosa, F., et al., *Scikit-learn: Machine learning in Python.* 2011. **12**: p. 2825-2830.
36. Kumari, R., et al., *g_mmpbsa□ A GROMACS tool for high-throughput MM-PBSA calculations.* J. Chem. Inf. Model., 2014. **54**(7): p. 1951-1962.
37. Hunter, J.D.J.I.A.o.t.H.o.C., *Matplotlib: A 2D graphics environment.* 2007. **9**(03): p. 90-95.
38. Parihar, S.P., et al., *Protein kinase C-delta (PKCdelta), a marker of inflammation and tuberculosis disease progression in humans, is important for optimal macrophage killing effector functions and survival in mice.* Mucosal Immunol, 2018. **11**(2): p. 579-580.
39. Serrero, M., R. Planes, and E. Bahraoui, *PKC-delta isoform plays a crucial role in Tat-TLR4 signalling pathway to activate NF-kappaB and CXCL8 production.* Sci Rep, 2017. **7**(1): p. 2384.
40. Kubo-Murai, M., et al., *Protein kinase Cdelta binds TIRAP/Mal to participate in TLR signaling.* Mol Immunol, 2007. **44**(9): p. 2257-64.
41. Paracha, R.Z., et al., *Structural evaluation of BTK and PKCdelta mediated phosphorylation of MAL at positions Tyr86 and Tyr106.* Comput Biol Chem, 2014. **51**: p. 22-35.
42. Meng, A., X. Zhang, and Y. Shi, *Role of p38 MAPK and STAT3 in lipopolysaccharide-stimulated mouse alveolar macrophages.* Exp Ther Med, 2014. **8**(6): p. 1772-1776.
43. Yang, Y., et al., *Functional roles of p38 mitogen-activated protein kinase in macrophage-mediated inflammatory responses.* Mediators Inflamm, 2014. **2014**: p. 352371.
44. Rajpoot, S., et al., *TIRAP-mediated activation of p38 MAPK in inflammatory signaling.* Sci Rep, 2022. **12**(1): p. 5601.

45. Olson, C.M., et al., *p38 mitogen-activated protein kinase controls NF-kappaB transcriptional activation and tumor necrosis factor alpha production through RelA phosphorylation mediated by mitogen- and stress-activated protein kinase 1 in response to Borrelia burgdorferi antigens.* Infect Immun, 2007. **75**(1): p. 270-7.
46. Jiménez-García, B., C. Pons, and J.J.B. Fernández-Recio, *pyDockWEB: a web server for rigid-body protein–protein docking using electrostatics and desolvation scoring.* Bioinformatics, 2013. **29**(13): p. 1698-1699.
47. Chattopadhyay, S. and G.C. Sen, *Tyrosine phosphorylation in Toll-like receptor signaling.* Cytokine Growth Factor Rev, 2014. **25**(5): p. 533-41.
48. Piao, W., et al., *Tyrosine phosphorylation of MyD88 adapter-like (Mal) is critical for signal transduction and blocked in endotoxin tolerance.* J Biol Chem, 2008. **283**(6): p. 3109-19.
49. Kim, H.J., et al., *p38 Mitogen-activated protein kinase up-regulates LPS-induced NF-kappaB activation in the development of lung injury and RAW 264.7 macrophages.* Toxicology, 2006. **225**(1): p. 36-47.
50. Liu, S., et al., *p38MAPK inhibition attenuates LPS-induced acute lung injury involvement of NF-kappaB pathway.* Eur J Pharmacol, 2008. **584**(1): p. 159-65.
51. O'Neill, L.A. and A.G. Bowie, *The family of five: TIR-domain-containing adaptors in Toll-like receptor signalling.* Nat Rev Immunol, 2007. **7**(5): p. 353-64.
52. Kumar, H., O. Takeuchi, and S. Akira, *Toll-Like Receptors*, in *Encyclopedia of Biological Chemistry (Second Edition)*, W.J. Lennarz and M.D. Lane, Editors. 2013, Academic Press: Waltham. p. 396-401.
53. Balka, K.R. and D.J.J.o.l.b. De Nardo, *Understanding early TLR signaling through the Myddosome.* 2019. **105**(2): p. 339-351.
54. Chow, J.C., et al., *Toll-like receptor-4 mediates lipopolysaccharide-induced signal transduction.* J Biol Chem, 1999. **274**(16): p. 10689-92.
55. Mandraju, R., T.D. Troutman, and C. Pasare, *Toll-Like Receptor Function and Signaling*, in *Reference Module in Biomedical Sciences*. 2014, Elsevier.
56. Medvedev, A.E., et al., *Role of TLR4 tyrosine phosphorylation in signal transduction and endotoxin tolerance.* J Biol Chem, 2007. **282**(22): p. 16042-53.
57. Jefferies, C.A. and L.A. O'Neill, *Bruton's tyrosine kinase (Btk)-the critical tyrosine kinase in LPS signalling?* Immunol Lett, 2004. **92**(1-2): p. 15-22.
58. Rajpoot, S., et al., *Identification of novel inhibitors targeting TIRAP interactions with BTK and PKCδ in inflammation through an in silico approach.* SAR and QSAR in Environmental Research, 2022. **33**(3): p. 141-166.

Chapter 4

(TIRAP-mediated activation of p38 MAPK in inflammatory signaling)

Chapter 4: TIRAP-mediated activation of p38 MAPK in inflammatory signaling

4.1. Graphical Abstract

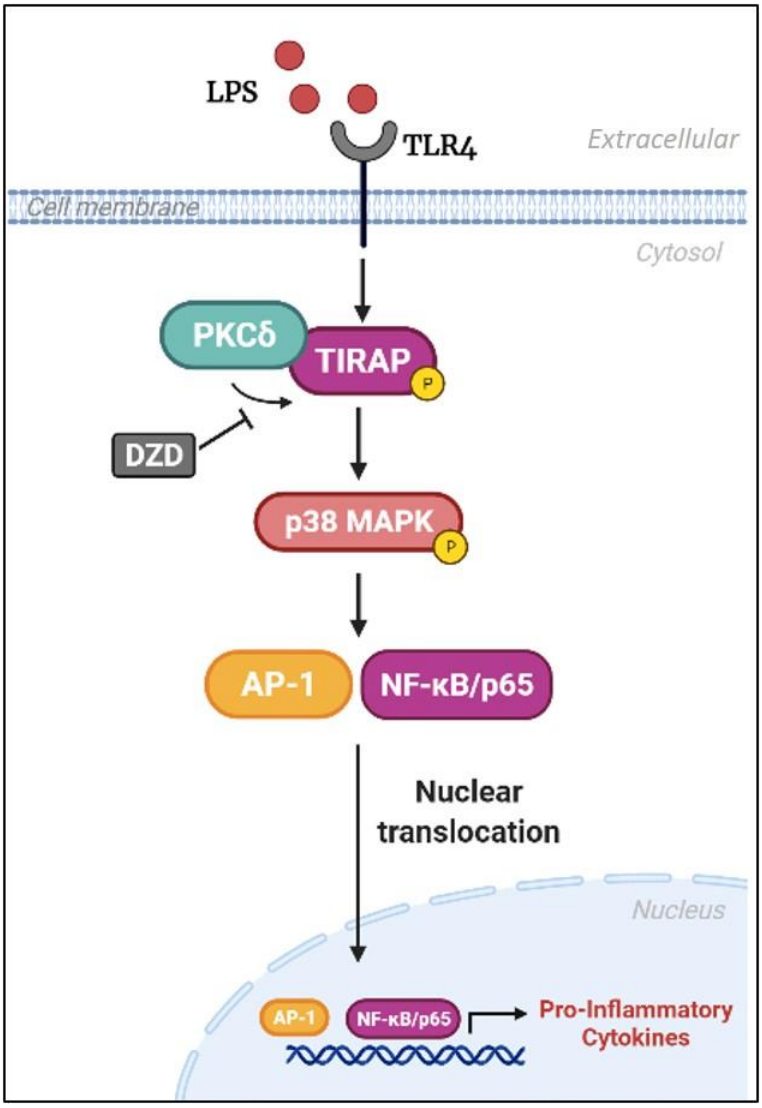

Figure 4.1. *Schematic representation of TIRAP mediated activation of p38 MAPK leading to downstream signaling and transcription factors activation. The downregulation of p38 MAPK phosphorylation in TIRAP-PKCδ axis is shown to be associated with enhanced binding of activated (phosphorylated) TIRAP with p38 MAPK leading to its activation.*

4.2. Summary

In toll-like receptor (TLR) 4/2 signalling, Bruton's tyrosine kinase (BTK) and Protein kinase C delta (PKCδ) are known to phosphorylate the Y86, Y106, Y159, and Y187 of TIRAP which is crucial for the downstream function of MAPKs (mitogen-activated protein kinases) activation. In this structural study, we performed an in-silico molecular docking and immunofluorescence to unravel the interaction between TIRAP and p38 MAPK. Further, in-silico phosphorylation of TIRAP tyrosine's; Y86, Y106, Y159, and Y187 was created to study the conformational changes in protein docking and their binding affinities with p38 MAPK in comparison to non-phosphorylated state. Our molecular docking and 500ns of molecular dynamic (MD) simulation study demonstrates that the Y86 phosphorylation (pY86) in TIRAP is crucial in promoting the higher binding affinity (ΔG_{bind}) with p38 MAPK. The conformational changes due to the tyrosine phosphorylation mainly at the Y86 site pull the TIRAP closer to the active site in the kinase domain of p38 MAPK and plays a significant role at the interface site which is reversed in its dephosphorylated state. Our findings may further be validated in an in-vitro system and would be crucial for targeting the TIRAP and p38 MAPK interaction for therapeutic purposes against the chronic inflammatory response and associated diseases.

4.3. Introduction

Macrophages are crucial immune cells responsible for the initiation, activation, and resolution of inflammatory signalling in the host defensive system. They perform extensive roles in providing first-line defense through recognition of vast intra- and extracellular stimuli such as damaged cells or various extracellular pathogens patterns through their specialized pattern-recognizing receptors (PRRs) [1-4]. The group of Toll-like receptors (TLRs) is one of the important members of PRRs which play critical roles in mediating the host's innate immune response and help in the initiation of the adaptive immune response. The activation of TLR4 in macrophages in response to its extracellular stimulus such as lipopolysaccharide (LPS) triggers its ectodomain

dimerization and conformational changes in its cytoplasmic Toll/Interleukin-1 receptor (TIR) domain allowing it to initiate the recruitment of TIR domain-containing adaptor proteins. The process subsequently activates several downstream protein kinases, transcription factors such as AP-1 and NF- κB, and eventually the production of inflammatory cytokines [5-10]. Out of the five known adaptor proteins, toll/interleukin-1 receptor domain-containing adapter protein **(**TIRAP) is identified as one of the most vital and actively involved TIR domain-containing proteins in TLR4/2 signaling pathways [11-14]. The initiation of intracellular signalling through TIRAP is complex and involves multiple protein–protein interactions through its TIR domain [15]. Structurally, protein phosphorylation is one the most vital and common post-translational modifications occurring in the majority of signal transduction in response to a robust stimulus. Similarly, tyrosine phosphorylation of TIRAP is crucial for its function and interaction with its partner protein [15-17]. In mammalian cells, the phosphor-proteomic analysis suggests that although most proteins undergo phosphorylation, some contain only a few phosphorylation sites, and some proteins have most of their serine, threonine, and tyrosine residues phosphorylated. Among the proteins, serine is by far, the most phosphorylated residue (86%), followed by phosphorylation of threonine (12%) and tyrosine residues (2%) [17, 18]. However, tyrosine phosphorylation serves a plethora of functions and in phosphor-tyrosine signalling, the protein–protein interaction is one important module. The accumulating study suggests that the phospho-tyrosine binding module possesses substrate or ligand recognition specificity to narrow down the potential interacting partners [19-22]. The TIR domain of TIRAP contains a total of six tyrosine residues (Y86, Y106, Y159, Y187, Y194, and Y195) where the initial four significantly undergo phosphorylation modification, leading to the regulation of the downstream response [15, 23]. In the presence of LPS, macrophages activate many tyrosine kinases including Src, Hck, and Lyn, acting on TLRs [16, 24]. However, a study has revealed the presence of a tec family kinase burton's tyrosine kinase (BTK) as a key tyrosine kinase that regulates the phosphorylation of TIRAP at tyrosine Y86, Y106, Y159, and Y187 including TLR4, TLR2, and MyD88 [25-27]. In addition, protein kinase C delta (PKCδ) has also

been established to act upon the tyrosine residues of TIRAP for its phosphorylation [28]. The effect of tyrosine phosphorylation on TIRAP is observed during the downstream signalling which regulates its interaction with MyD88, IRAK-2, and TRAF6, leading to activation of MAPKs, mainly on p38 MAPK and transcription factor NF-kB [15, 29-37]. A dominant-negative response has been observed in LPS-stimulated macrophage signalling where tyrosine mutant TIRAP fails to induce the downstream kinase p38 MAPK and transcription factors such as NF-κB activation as compared to the wild-type [23]. In macrophage-mediated inflammatory response, p38 MAPK is a major player whose expression is upregulated besides undergoing tyrosine phosphorylation [36, 37].

The p38 MAPK family consists of four subtypes (p38α MAPK, p38β MAPK, p38γ MAPK, and p38δ MAPK) [37, 38]. As with TIRAP, the p38 MAPK is critical in LPS-induced macrophage signalling and its targeted deletion impairs cytokines expression [39]. From a disease perspective, the evidence suggests that p38 MAPK mediates the decisive role in inflammation of the lung, kidney, liver, and brain and is termed a critical player in macrophages-mediated inflammatory diseases such as gastritis, colitis, arthritis, etc. [37, 38] Like TIRAP, the tyrosine residue of the p38 MAPK is also crucial for its activation and macrophages stimulation leads to the high expression of its active form of p38 MAPK phosphorylated at a tyrosine residue. The p38 MAPK subtypes are also expressed in other cells like endothelial cells, neutrophils as well as CD4+ T cells. Structurally, the 38 kDa of p38 MAPK is comprised of a 135 amino acid long, secondary β-sheets N-terminal domain and a 225 amino acid long, secondary α-helical C-terminal domain while the catalytic site is located in between adjoining these two domains. The catalytic site contains a 13 amino acid phosphorylation lip from leucine (L171) to valine (V183) in which the phosphorylation of threonine (T180) and tyrosine (Y182) activates the p38 MAPK [37, 40]. The activated p38 MAPK in stimulated macrophages leads to the production of several pro-inflammatory cytokines such as IL-1β, TNF-α, IL-12, COX-2, IL-8, IL-6, etc. which are implicated with the inflammatory diseases as mentioned above as well as others like granuloma, diabetes, and acute lung inflammation [37, 41]. Therefore,

several studies have signified the p38 MAPK as a crucial anti-inflammatory target, and a range of natural and chemical inhibitors are investigated such as AMG-548, SC-80036, SC-79659, quercetin, mycoepoxydiene, losmapimod, etc. and few also went through clinical trials [37, 38, 42, 43]. Besides their role in inflammation, the p38 MAPK has also an imperative role in cell proliferation, differentiation, and apoptosis [37, 38]. The p38 MAPK is activated by different environmental stimuli and cellular stress and hence understanding their molecular mechanism of activation is more beneficial for deciding the target in disease-specific conditions, developing novel drugs, and countering the diseases effectively. In this *in-silico* study, the structural changes and impact of TIRAP tyrosine phosphorylation on p38 MAPK interaction are analyzed. The effect of phosphorylation of each tyrosine residue of TIRAP mentioned above and the complex conformational changes leading to a better binding affinity for interaction with p38 MAPK was also investigated to understand the interaction that may be important to understand its activation and when designing anti-inflammatory drugs.

4.4. Materials and methods

4.4.1. 3D structure preparation and molecular docking of TIRAP and p38 MAPK

Molecular docking of TIRAP and p38 MAPK crystal structures was performed to investigate their protein–protein interaction. The solved crystal structures of the TIRAP TIR domain (PDB ID 3UB2) and p38 MAPK (PDB ID 1WBV) were obtained from the RCSB PDB database (https://www.rcsb.org/) and were prepared for the docking studies. Both structures were prepared by removing the water, heteroatoms, and any co-crystallized ligand groups followed by the addition of polar hydrogen atoms. The prepared structure with a single chain for the TIRAP TIR domain in 3UB2 or p38 MAPK in 1WBV was finally saved in a PDB file format. The protein–protein molecular docking of TIRAP and p38 MAPK was performed in four docking platforms which include HADDOCK 2.4 [44], pyDockWEB [45], ClusPro 2.0 [46], and ZDOCK 3.0.2 [47] for confirmation. The interaction interface was analyzed in the chimera

v1.13.1 tool [48]. Finally, the images of the interactions were prepared in a Discovery Studio Visualizer v21.1.0.20298[49].

4.4.2. In-vitro cell culture for immunofluorescence staining and confocal microscopy

RAW 264.7 murine macrophage cell line was obtained from the cell repository of the National Centre for Cell Science (NCCS), Pune, India. For cellular colocalization of TIRAP and p38 MAPK in macrophages, RAW 264.7 murine macrophages cells (1. 104) were seeded on sterile coverslips in the well plate and grown for 24 h in Dulbecco's minimal essential medium (DMEM) (11,965,118, Gibco) complete media supplemented with heat-inactivated 10% fetal bovine serum (FBS) (10,270,106, Gibco) and 1%penicillin–streptomycin (15,140,122, Gibco) in a humidified incubator with 5% CO2 at 37 °C. Before the experiment, the cells were washed with sterile 1X phosphate-buffered saline (PBS) at room temperature (RT) and replenished with fresh DMEM complete media. For the immunofluorescence study, cells were stimulated with 250 ng/ml of lipopolysaccharide (LPS; Sigma L2630) for 1 h. After treatment, cells were rinsed twice with PBS and fixed in 4% paraformaldehyde for 15 min at RT. Cells were again washed thrice with PBS (5 min each) and then permeabilized in 0.1% Triton X-100 in PBS for 10 min at RT. After three more washing, cells were then blocked with 5% bovine serum albumin (BSA) prepared in PBST (0.1% Tween-20 in PBS) for 1 h at RT. After blocking, the cells were briefly washed with PBST and incubated in the primary antibodies at 4 °C overnight. The anti-TIRAP (sc-166149, Santa Cruz Biotechnology, Inc.) and anti-p38 MAPK (9212, CST) were used in 1:200 dilution in PBST. After three washes with PBST, cells were incubated in secondary antibody for 1 h in dark using the goat anti-mouse Alexa Fluor 488 (A11001, Invitrogen) and chicken anti-rabbit Alexa Fluor 594 (A21442, Invitrogen) at 1:200 dilution in PBST. Finally, cells were washed thrice and mounted on glass slides over fluoro-shield mounting media containing DAPI for nuclear staining (F6057, Sigma) and stored at 4 °C for imaging. The confocal microscopy was performed using Olympus confocal laser scanning microscope (FV 1200 MPE Olympus) at 20X 2.5z

and 100X 2.0z magnification. For colocalization analysis, ImageJ [50], and its plugin JACoP [51] were used. The data were plotted using GraphPad Prism 7.0 (GraphPad Software, USA) and presented as mean ± SEM while Student's -test was performed for comparing the two groups.

4.4.3. In-silico TIRAP phosphorylation/dephosphorylation and molecular docking

The site-specific phosphorylation of tyrosine residue was obtained in the crystal structure of the TIRAP TIR domain (PDB 3UB2) through the Discovery Studio tool. The tyrosine residue at positions Y86, Y106, Y159, and Y187 was replaced with the phosphorylated tyrosine residue pY86, pY106, pY159, and pY187, and the files were saved in PDB formats. Single tyrosine as well as all four-tyrosine phosphorylated (pYall04) TIRAP structures were prepared. For sequential dephosphorylation study, TIRAP structure was generated with one non-phosphorylated tyrosine at a time followed by the remaining three phosphorylated conformations and subsequently, renamed as dpY86/pYall03, dpY106/pYall03, dpY159/pYall03, and dpY187/pYall03. All these PDB files of structures were energetically minimized in a Chimera v1.13.1 tool. The molecular docking of phosphorylated tyrosine TIRAP and non-phosphorylated p38 MAPK (PDB 1WBV) was performed in a HADDOCK 2.4 [44] supporting the docking of phosphorylated residues.

4.4.4. Molecular dynamic (MD) simulation analysis

The TIRAP and p38 MAPK protein structures as well as the tyrosine-phosphorylated and non-phosphorylated TIRAP molecular docking complexes with p38 MAPK were selected as the initial starting point for the MD simulation study. The TIRAP and p38 MAPK protein structures as well as each complex were placed into a dodecahedron box before being solvated in TIP3P water molecules. The MD simulation system was neutralized by adding Na + or Cl − ions. CHARMM 27 force field was employed to assign parameters for the protein, solvent, and ion molecules [52]. The parameters for

phosphorylated tyrosine were obtained from the Swiss Side Chain database (https://www.swisssidechain.ch). Classical MD simulation was performed using GROMACS program v5.0.4 following typical energy minimization, equilibration, and production runs [53]. Initially, 50,000 steps of steepest-descent energy minimization were performed to relax the MD system. Energy minimization was followed by 1 ns equilibration under NVT and NPT ensemble respectively. Finally, 500 ns production MD runs were performed at a constant temperature of 300 K for each system. The simulations were performed using a time step of 2 fs. A cut-off of 10 A was used for short-range interactions while the long-range interactions were handled using Particle-Mesh Ewald (PME) method. MDAnalysis [54], MDTraj [55], and scikit-learn [56] python libraries were used to process and analyze MD trajectories. Principal component analysis (PCA) was performed using the MODE-TASK program [57]. Intermolecular contacts were analyzed from the MD simulation trajectories using GetContacts (https://getcontacts.github.io/). Graphics were prepared using Matplotlib python library[58], [59], and PyMOL v2.3.460.

4.5. Results and discussion

4.5.1. TIR domain of TIRAP interacts with p38 MAPK

In the recent past, the TIRAP's crucial role in TLR4 and TLR2 inflammatory signalling pathways has been investigated beyond its adaptor protein function. It is experimentally established that TIRAP interacts with several other proteins other than MyD88, which results in the regulation of the downstream signalling as well as the activation of NF-kB and AP-1 transcription factor [15, 30]. Based on our prior research work [34], the structural conformation and mechanism of TIRAP to interact and regulate the downstream p38 MAPK, which is mainly responsible for the activation of transcription factors in inflammatory pathways, has been investigated here. TIRAP protein, mostly known as an adaptor protein for TLR4 and TLR2, has two domains regulating its overall activity. Besides the N-terminal PBD (PIP2 binding domain)

domain governing its subcellular location, the TIR domain is most crucial for TIRAP activity to regulate the interactions and/or signalling. Since many previous reports of TIRAP interaction with other proteins demonstrate the involvement of the TIR domain in all known interactions, we sought to understand its binding pattern with p38 MAPK. The *in-silico* approach was applied to establish the protein complex of TIRAP and p38 MAPK as well as to determine the best binding pattern and key residues involved at the interface. We extensively performed the docking study of the TIRAP TIR domain crystal structure (PDB Id 3UB2) and full-length crystal structure of p38 MAPK protein (PDB Id 1WBV) **(Figure 4.1A)**. Both proteins were prepared by removing any water molecules and ligands followed by polar hydrogens addition before the protein–protein docking. First, the protein–protein docking tool HADDOCK 2.4 [44] was used for their blind docking and the topmost binding pose was analyzed. The HADDOCK 2.4 results were produced in a cluster form in order of high to low based on their Z-score with each cluster containing the four best poses. We analyzed the topmost pose from the highest-ranked cluster which was of interest since TIRAP specifically fit into the active region of p38 MAPK **(Figure. 4.1A).** Additionally, to validate the yielded binding pose of TIRAP and p38 MAPK, we included other docking methods to confirm the obtained pattern of the TIRAP and p38 MAPK complex. Therefore, three more docking suits pyDockWEB [45], ZDOCK 3.0.2 [47], and ClusPro 2.0 [46] were used for the study **(Figure 4.1A).** Similar to the findings based on HADDOCK 2.4, only the topmost complex was selected for analysis. As a consensus, all docking produced similar binding poses for TIRAP and p38 MAPK complex suggesting that they are the best-fit solution **(Figure. 4.1A)**. Next to the binding pattern, the interacting residues at the interface of both TIRAP and p38 MAPK were identified from each docking result as the most favoured within the 3 A region **(Table 4.1).** Interestingly, the interface residues revealed that the crucial tyrosine residues Y86, Y106, Y159, and Y187 occur in the TIR domain of TIRAP **(Figure 4.1B)** whereas the p38 MAPK active site tyrosine residue Y182 **(Figure. 4.1B)** in its kinase domain is in the proximity at the interface site besides actively participating in the interaction.

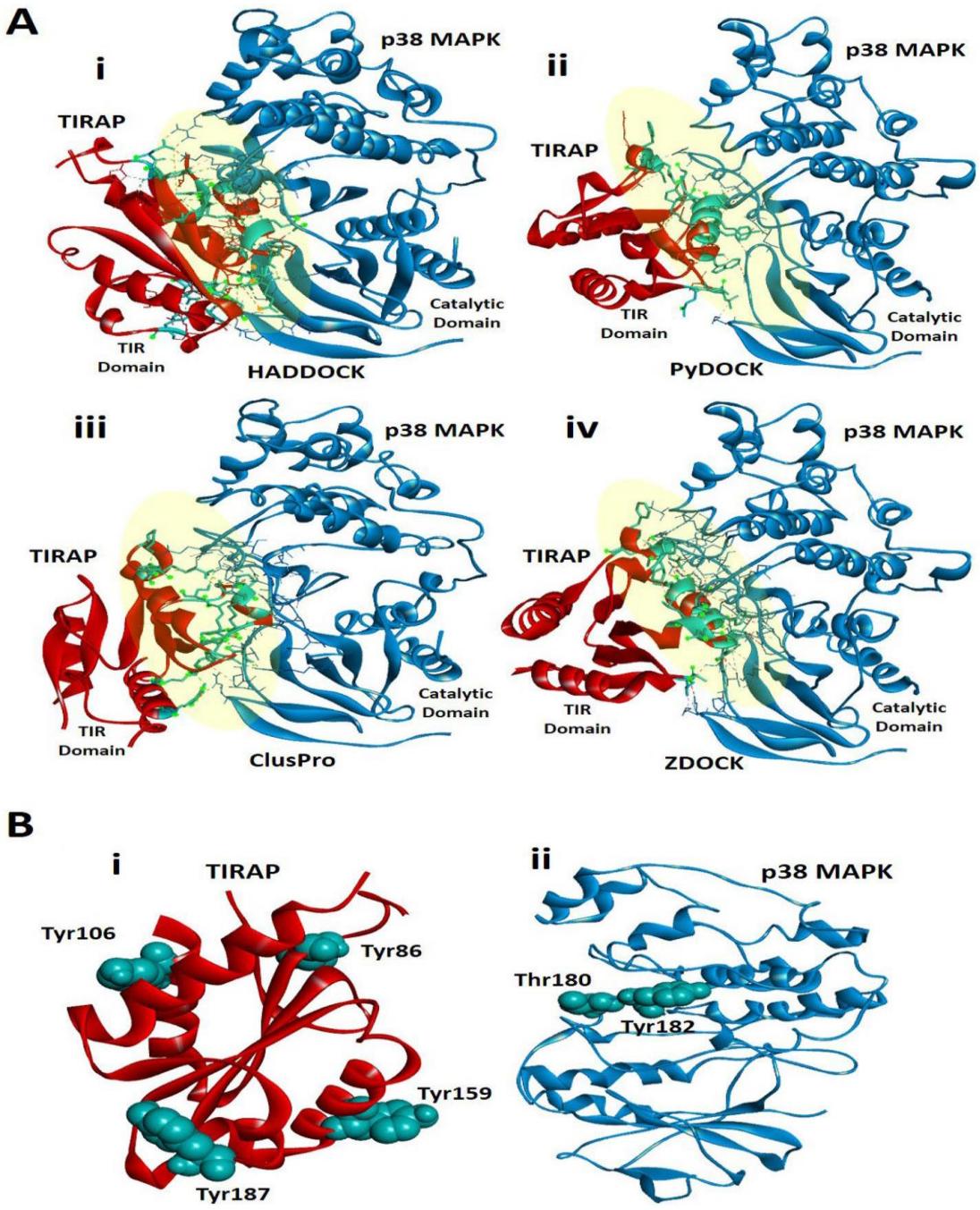

Figure 4. 2. The protein–protein interaction of TIRAP and p38 MAPK. (**A**) The molecular docking complexes of TIRAP TIR domain (red) and full-length p38α MAPK protein (blue) as obtained from (i) HADDOCK 2.4 (ii) pyDockWEB (iii) ClusPro and (iv) ZDOCK 3.0.2. (**B**) Illustration of crucial tyrosine residues of (i) TIRAP TIR domain (red) Y86, Y106, Y159, and Y187, and (ii) p38 MAPK (blue) active site Y182 residue in spacefilling cpk (Corey-Pauling-Koltun), espectively. The images were prepared using a Discovery studio Visualizer v21.1.0.20298.

Docking Suits	TIRAP & p38 MAPK complex	TIRAP Interacting and Interface Residues Position	No. of interface Residue
HADDOCK 2.4	TIRAP	D85, Y86, E94, E95, D96, L97, A100, Q101, E108, G109, S131, E132, L133, Q135, L179, S180, G181, Y187, D198, G199, R200, D203 and Y106	22
	p38 MAPK	E12, N14, K15, N26, S28, P29, S32, R49, M109, G110, D112, N114, N115, K118, C119, Q120, K152, S153, A184, R220, Y182, V183, and T185	23
pyDockWEB	TIRAP	Q135, A136, L137, W156, Y159, Q160, M161, L162, Q163, L165, T166, E167, A168, P169, G170, P189, E190, F193, and M194.	19
	p38 MAPK	K15, G31, S32, G33, L171, A172, T175, D177, E178, and Y182	19
ClusPro 2.0	TIRAP	P155, K158, Y159, P169, G170, S183, R184, P189, E190, R192, M194, Y195, Y196, Q208, R215	15
	p38 MAPK	N14, K15, P29, V30, S32, G33, R49, N114, K118, D168, F169, D177, Y182, V183, and T185	15
ZDOCK 3.0.2	TIRAP	A136, L137, L152, Q153, P155, W156, K158, Y159, Q163, L165, T166, E167, P188, P189, E190, F193, and M194.	17
	p38 MAPK	K15, V30, G31, S32, M109, G110, A111, D112, N114, N115, K118, F169, G170, L171, A172, D177, E178, Y182, V183, and W187	20

Table 4. 1. The interacting residues of TIRAP and p38 MAPK were identified using the UCSF Chimera v1.13.1 and PDBePISA within the 3 A region. The p38 MAPK phosphorylation site Y182 in the kinase domain is involved in the interaction at the interface while the tyrosine-phosphorylation sites of the TIRAP TIR domain are involved on the other side.

Further, to confirm the interaction of TIRAP and p38 MAPK at the cellular level, we performed the cellular colocalization of TIRAP and p38 MAPK in macrophages through stimulation of TLR4 signaling with LPS. The murine macrophage cell line RAW 264.7 cells were treated with 250 ng/ml of LPS for 1 h and stained with antibodies. The confocal images at 100X magnification were analyzed and interestingly we observed the significant colocalization of TIRAP and p38 MAPK in macrophages cytoplasm in LPS-treated cells when compared to untreated cells **(Figure 4.2 and Supplementary Figure S4.1).** Combinedly, this provided us the direct evidence of the signaling of TIRAP with p38 MAPK in the TLR4 pathway and provided us the strong evidence to understand its structural binding conformation in phosphorylated states of TIRAP. As also mentioned earlier that the previous studies found the tyrosine residues in the TIR domain to be the most important residues of TIRAP for its activation and they mainly undergo a post-translational modification of phosphorylation to impart its downstream function[23, 24]. Similarly, the Y182 in the kinase domain of p38 MAPK protein, unburied and exposed outside making a surface turn, is the active site for its phosphorylation and activation making p38 MAPK catalytically active for several downstream signalling as well as transcription factor activation. In agreement with these previous studies, our docking findings for TIRAP and p38 MAPK complex undoubtedly suggested that the interaction of TIRAP in the kinase domain of p38 MAPK and the best-fit model in proximity with its active residue Y182 favor it to regulate its activation and downstream function. Therefore, to establish the fact further, the effect of phosphorylation on TIRAP tyrosine residues in relation to its binding affinity and stability with p38 MAPK was analyzed.

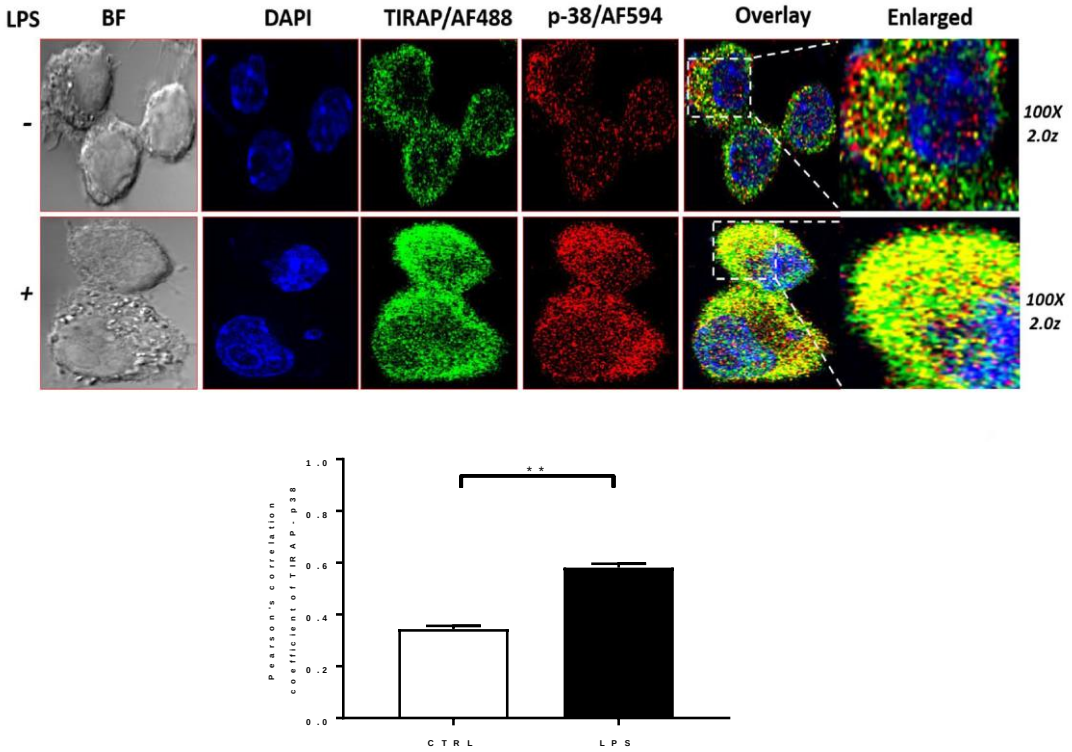

Figure 4. 3. The immunofluorescence staining of TIRAP and p38 MAPK for their cellular co-localization in RAW 264.7 murine macrophages through confocal microscopy. The RAW 264.7 cells were treated with 250 ng/ ml of lipopolysaccharide (LPS) for 1 h and immune-stained with mouse raised anti-TIRAP and rabbit raised anti-p38 MAPK antibody and probed with secondary antibody anti-mouse conjugated with Alexa Fluor 488 and anti-rabbit conjugated with Alexa Fluor 594. The images are captured in a confocal laser scanning microscope at 100X 2z magnification. The significant cellular colocalization of TIRAP and p38 MAPK is observed in cell cytoplasm in LPS treated cells in overlay image as compared to control cells and co-localization was quantified in ImageJ through the JACoP plugin. The data were plotted in GraphPad Prism 7 and presented as mean ± SEM. Student t-test was performed for significant difference (**$p < 0.05$). BF- Bright field; DAPI- 4′,6-diamidino-2-phenylindole.

4.5.2. The cumulative effect of multi-site tyrosine phosphorylation in the TIR domain of TIRAP significantly enhances its binding affinity with p38 MAPK

We performed the site-specific *in-silico* phosphorylation of tyrosine residues of TIRAP protein to investigate its impact on the binding affinity and the conformational

changes with p38 MAPK. The tyrosine residues mainly within the TIR domain of TIRAP, are imperative for its activation and downstream inflammatory signalling. The human TIR domain sequence (position 84 to 213, UniProtKB- P58753) which contains a total of six tyrosine sites (Y86, Y106, Y159, Y187, Y195, and Y196) was analyzed as confirmed by previous studies [23, 25, 27], which suggests that only the first four tyrosine residues are the key sites actively involved in the phosphorylation modification to impart its function. The four tyrosine sites (Y86, Y106, Y159, and Y187) of TIRAP are mainly investigated for their phosphorylation by the upstream tec-family kinase Bruton's Tyrosine Kinase (BTK)as well as by the protein kinase C delta (PKCδ). Since the phosphorylation modification of the final two tyrosine residues (Y195 and Y196) is not defined experimentally and has no effect on the downstream signalling and transcription factors activation, we proposed individual phosphorylation of the four-tyrosine residues followed by the cumulative phosphorylation of all four sites to perform the docking studies with p38 MAPK. The tyrosine sites (Y86, Y106, Y159, and Y187) were phosphorylated in BIOVIA Discovery Studio 2020, adding a phosphate group to the tyrosine residues. Subsequently, the structure was energetically minimized to prepare it for docking. Imitating the native form, we performed the docking of tyrosine phosphorylated TIRAP, considering it an active protein, with non-phosphorylated p38 MAPK in the HADDOCK 2.4 tool. Previous studies have shown that phosphorylation energy can either stabilize or destabilize the structure and the differences in the binding energy by 1–2 kcal/mol are significant enough to contribute to the stabilizing or destabilizing effect on complex conformation [60, 61]. Remarkably, our docking results were promising in terms of enhanced binding energy. In order to understand the effect of the energy for tyrosine phosphorylation of TIRAP with p38 MAPK interaction as compared to the non-phosphorylated TIRAP, the total binding energy (ΔGbind) of the non-phosphorylated TIRAP and p38 MAPK complex, as well as the binding energy (ΔGbind) of phosphorylated TIRAP and p38 MAPK complex, was calculated using a PDBePISA tool **(Figure 4.3A–F)**. As compared to − 10 kcal/mol (ΔGbind) for the non-phosphorylated TIRAP and p38 MAPK complex, phosphorylation of Y86 (pY86)

displayed the most significant decrease in binding energy (− 15.0 kcal/mol), followed by pY187 (− 12.0 kcal/mol), pY159 (− 11.7 kcal/mol) and pY106 (− 10.9 kcal/mol), respectively. It is evident that the phosphorylation of all these four tyrosine residues in the TIR domain of TIRAP has led to more strong binding between the complex where pY86 exerted the highest energetic effect while pY106 showed a modest effect. Multisite phosphorylation is explained to expand the regulation patterns and modulate the conformational changes more accurately whereas cooperatively increases the binding affinity to other proteins [17, 62, 63]. Henceforth, to confirm the effect, the cumulative response of all four phosphorylated tyrosine residues in the complex was further investigated. As expected, pYall04 TIRAP and p38 MAPK complex **(Figure 4.3F)** produced binding energy (ΔGbind) of − 20.5 kcal/mol suggesting the cooperative response of phosphorylated sites which attains a better conformation in the complex.

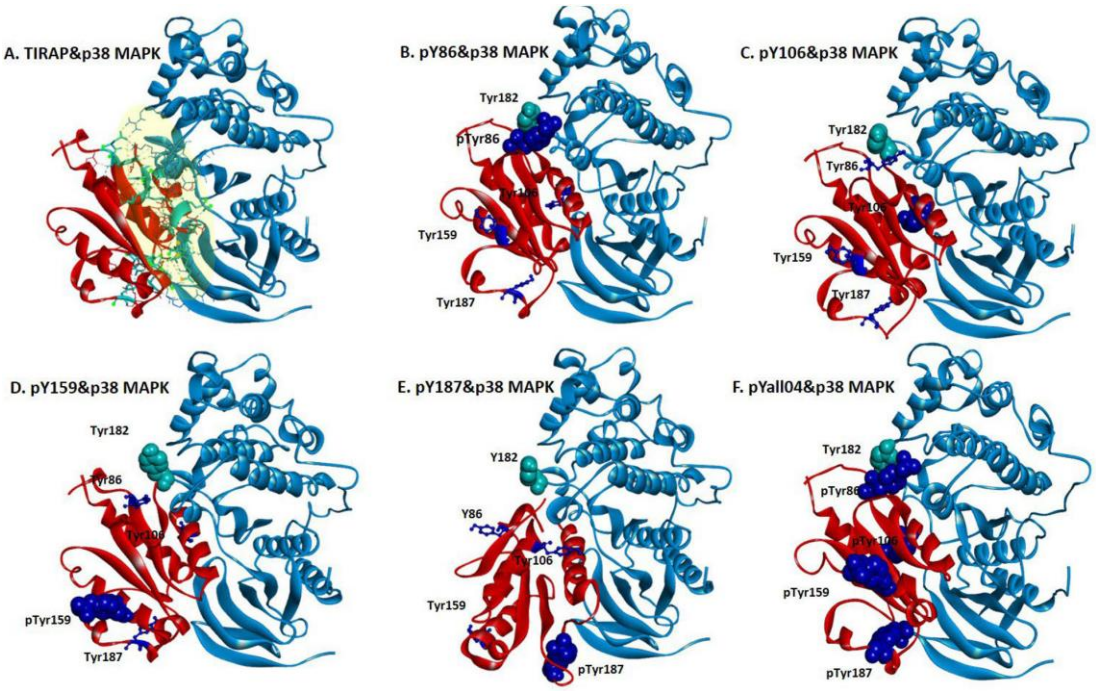

Figure 4. 4. The molecular docking complex of p38 MAPK and tyrosine-phosphorylated (pY) TIRAP from the HADDOCK 2.4 tool. The complex of non-phosphorylated TIRAP (red) and p38 MAPK (light blue) (**A**) was further investigated in a comparative analysis with a docking complex of p38 MAPK

(light blue) and TIRAP (red) phosphorylated tyrosine pY86 (dark blue) (**B**), pY106 (dark blue) (**C**), pY159 (dark blue) (**D**), pY187 (dark blue) (**E**) and all four phosphorylated site pYall04 (dark blue) (**F**), respectively. The complexes were the top pose result of HADDOCK 2.4 docking, and the images were prepared using a Discovery studio Visualizer v21.1.0.20298. The tyrosine residues of TIRAP (dark blue) were represented in ball and stick format whereas the phosphorylated tyrosine residue in TIRAP (blue) and p38 MAPK (cyan) were represented in cpk (Corey- Pauling-Koltun) format. The interacting interface residues between both proteins were analyzed with the 3 A region in a Chimera v1.13.1 tool (Supplementary Table S4.1).

4.5.3. Phosphorylated tyrosine in the TIR domain at the binding interface of TIRAP and p38 MAPK complex mainly modulates the binding conformation

The TIR domains are rather conserved in the TIR domain-containing proteins [64-66]. Similar to the TIR domain of TIRAP, most phospho-tyrosine residues are located in conserved protein domains [60, 67]. However, unlike most serine and threonine sites found in the flexible region and are exposed to the surfaces of the structure, the hydrophobic tyrosine is more likely to be embedded in a structured region and phospho-tyrosine signalling is important in protein–protein interaction module [19, 60]. We sought to understand the conformational dynamics of this phosphorylated tyrosine in TIRAP and p38 MAPK complexes. Interestingly, we observed that Y86 and Y187 in the TIR domain are mainly at the flexible loop of the structure when compared to the two other sites **(Figure 4.1B)**. As represented in **(Figure 4.3)**, in these protein–protein complexes, phosphorylated Y86 conformation specifically obtains an orientation closest to the active site residues T180 and Y182 of p38 MAPK, respectively.

In contrast, the binding orientation of pY187 TIRAP with p38 MAPK complexes **(Figure 4.3E)** was distinct from the other three complexes **(Figure 4.3B–D)**, suggesting that phosphorylation of Y187 not only brings the c-terminal loop closer to the other regions of p38 MAPK but pulls the n-terminal loop carrying Y86 distant from the active site of p38 MAPK. Moreover, the change in the free binding energy (of − 2 kcal/mol) is also marginal in phosphorylated Y187 conformation when compared to the significant decrease (− 5 kcal/mol) in the pY86 conformation from the total binding

energy of non-phosphorylated TIRAP and p38 MAPK binding conformations (ΔG_{bind} = − 10 kcal/mol) **(Table 4.2 and Figure 4.5).** Besides, phosphorylation of Y106 and Y159 has shown no dominant effect in regulating the binding conformation of two proteins and were mainly like the pY86 complex conformation but have a marginal energetic effect which promotes a better binding of TIRAP and p38 MAPK in the phosphorylated conformation. The finding indicates the significance of Y86 phosphorylation which modulates towards a favorable complex conformation between these two proteins–protein interactions and attained the highest decrease in the binding energy of the complex while all three other phosphorylated sites (Y106, Y159, and Y187) show a very close decrease in binding energy change. Nevertheless, it is notable that such an effect is reversed when all four tyrosine sites of TIRAP were phosphorylated in the complex where the total binding energy (ΔG_{bind} = − 20.5 kcal/mol) was comparably very much high than that of other complexes **(Figure. 4.3F, 4.5, and Table 4.2)**. The interacting interface residues play imperative roles in influencing the change of such binding energy. Also, the study reports that mapping of experimentally identified phosphorylation sites on the crystal structure of human homo – and hetero-protein complexes indicated that protein interface sites are more enriched with phosphorylation sites as compared to non-interface surfaces. Additionally, such sites at the binding interfaces of hetero-protein complex exert larger changes in the binding affinity than that for other sites on the interface [17, 60]. Therefore, we also analyzed the interacting residues of each complex within the 3Å region **(Supplementary Table S 4.1)** and as discussed above we found that both pY86 TIRAP and pY187 TIRAP complexes with p38 MAPK have changes in their interface residues in which the pY86 TIRAP and p38 MAPK complexes have more of the N-terminal residues including Y86 which is opposite of the pY187 TIRAP and p38 MAPK complexes in which more C-terminal residues participate in the interaction. Importantly, the interaction involved mainly pY86 and pY106 from TIRAP where T180 and Y182 from p38 MAPK were the only phosphorylation sites present among the interface residues in pY86 TIRAP and p38 complexes, and pY106 TIRAP and p38 MAPK complexes, respectively **(Supplementary Table S 4.1)**. In the other two

complexes (pY159 TIRAP and p38 MAPK and pY187 TIRAP and p38 MAPK), neither pY159 nor pY187 of TIRAP and neither T180 nor Y182 of p38 MAPK was present at the interfaces **(Supplementary Table S4.1)**. Interestingly, pY86 was observed again at the interface of pYall04 TIRAP and p38 MAPK complexes **(Supplementary Table S 4.1)**. The hydrogen bonds between the interfaced residues are one of the major factors contributing to the change in the binding affinity. Also at the interfaces, the phosphorylated sites contribute to the complex stability by making more hydrogen bonds than other non-phosphorylated residues on the interface. Henceforth, we further analyzed all hydrogen bonds along with their bond distances between the phosphorylated TIRAP and p38 MAPK interface residues using the PDBe PISA tool **(Supplementary Table S 4.2)**. In agreement with the above discussion, it was established that among all phosphorylated tyrosine, pY86 is the only one involved in the hydrogen bonding with R220 and T221 in p38 MAPK. Also, none of the three tyrosine residues present either in phosphorylated or non-phosphorylated forms formed any hydrogen bonds with p38 MAPK residues **(Supplementary Table S 4.2)**. In pY86 TIRAP and p38 MAPK complexes, pY86 was found to make a single hydrogen bond with T221 within 2.89Å. Remarkably, in pYall04 TIRAP and p38 MAPK, pY86 makes three hydrogen bonds (one very strong bond with R220 within 1.64Å and the other two with T221 within 3.39Å and 3.76Å, respectively) **(Supplementary Table S 4.2)**. The phenomenon strongly suggests that the presence of pY86 at the interface site largely influences the binding affinity and favors a stable conformation between TIRAP and p38 MAPK. Therefore, it is concluded that the highest increase in ΔGbind in TIRAP and p38 MAPK complex is a cumulative response of all four tyrosine phosphorylation sites, although it is imperative to determine if pY86 plays any dominant roles. Hence, we further sought to investigate the destabilizing effect of these four tyrosine residues in the complex which will uncover the site-specific significance of these tyrosine residues.

Sr No.	TIRAP-p38 MAPK complex	Phosphorylated site(s) in TIRAP	Total BE (ΔG_{bind}) (kcal/mol)	Change in ΔG_{bind} (kcal/mol)
1.	TIRAP-p38 MAPK	-	-10.0	-
2.	p-Y86 and p38 MAPK	Y86	-15.0	-5
3.	p-Y106 and p38 MAPK	Y106	-10.9	-0.9
4.	p-Y159 and p38 MAPK	Y159	-11.7	-1.7
5.	p-Y187 and p38 MAPK	Y187	-12.0	-2
6.	p-all04 and p38 MAPK	Y86, Y106, Y159 and Y187	-20.5	-10.5

Table 4. 2. The energetic effect of phosphorylation of tyrosine residues (Y86, Y106, Y159, and Y187) in the TIR domain of TIRAP were calculated in terms of change in the free binding energy (BE) of TIRAP and p38 MAPK complexes. Phosphorylation of tyrosine residues significantly decreases the binding energy (ΔG_{bind}) of TIRAP and p38 MAPK complex, with the highest decrease seen with pY86 while the modest seen with pY106 as analyzed from the PDBePISA tool.

4.5.4. Tyrosine 86 phosphorylation (pY86) is crucial for binding affinities of TIRAP and p38 MAPK and its dephosphorylation has a destabilizing impact on the binding conformation and affinity

In this section, we discuss the reciprocal effect of phosphorylated tyrosine sites of the TIR domain in the complex of TIRAP and p38 MAPK through sequential dephosphorylation events. Earlier, we observed the conformational and energetic significance of pY86 as compared to other tyrosine sites. However, to confirm the site-specific significance of phosphorylation among the multiple study sites, we perform the sequential dephosphorylation of each tyrosine site to calculate the destabilizing effect in terms of the adverse change in the binding energy as compared to all four phosphorylated tyrosine (pYall04) TIRAP and p38 MAPK complexes. Therefore, we

prepared four different TIRAP structures each with three tyrosine sites phosphorylated (p) while one was dephosphorylated (dp) at a time [dpY86/pYall03, dpY106/pYall03, dpY159/pYall03, and dpY187/pYall03] for docking with p38 MAPK. As mentioned in the above sections, the docking was performed in the HADDOCK 2.4 tool and the yielded results were analyzed using PDBePISA and Chimera v1.13.1 tools. Again, the top pose complex of each docking result (dpY86/pYall03 and p38 MAPK, dpY106/pYall03 and p38 MAPK, dpY159/ pYall03 and p38 MAPK, and dpY187/pYall03 and p38 MAPK) **(Figure 4.4C–F)** were investigated and the total binding energy (ΔGbind) of the complex **(Table 4.3 and Figure 4.5)** calculated. As expected, pY86 has unfavorable dephosphorylation, both in terms of stabilizing effect and binding conformation. The binding conformation of TIRAP in dpY86/pYall03 and p38 MAPK was in total inverse to that for pYall04 TIRAP and non-phosphorylated TIRAP complex with p38 MAPK, respectively **(Figure 4.4A–C)**. Additionally, the total binding energy adversely changed to − 7.1 kcal/mol with a shift of − 13.4 kcal/mol when compared to the total binding energy of − 20.5 kcal/mol of pYall04 TIRAP and p38 MAPK **(Table 4.3)**. It was interesting to observe that next to dpY86, dpY159 was second to show the destabilizing effect as evident both from conformational and binding energy change **(Figure 4E and Table 4.3)**. Meanwhile, a modest effect was observed with the dephosphorylation of pY106 and pY187. In addition, there was almost no conformation change in dpY106/pYall03 and p38 MAPK **(Figure 4.4D)**. As discussed and observed earlier about the significance of the interface residues, the change may suggest that there exists an interface whose intermolecular bonding stabilizes dpY106/pYall03 complex key residues. In contrast, despite the presence of a conformational change of TIRAP orientation in dpY187/pYall03 and p38 MAPK complexes, there was a modest destabilizing effect in the form of change in binding energy as compared to dpY86/pYall03 and dpY159/pYall03. Dephosphorylation of both pY106 and pY187 complexes of dpY106/pYall03 and dpY187/ pYall03 with p38 MAPK displayed total binding energies of − 16.2 and − 15.5 kcal/mol, respectively with slight shift of − 4.3 and − 5 kcal/mol from the total binding energy of pYall04 TIRAP and p38 MAPK complex,

when compared to dpY86/pYall03 and dpY159/pYall03 **(Table 4.3)**. Therefore, this fact clearly defines the crucial role of Y86 site-specific phosphorylation in TIRAP and p38 MAPK complexes, indicating that dephosphorylation change adversely has a destabilizing effect on the complex. Secondly, Y159 phosphorylation may also be deemed critical in this complex. Additionally, we also sought to confirm the presence of phosphorylated tyrosine at the interface residues interaction. Hence, as before, the hydrogen bonding of interface residues from each complex was analyzed. It was interesting to observe that Y86 was absent at the interface residues. Importantly, there were no hydrogen bonds found with Y86 in dpY86/pYall03 TIRAP and p38 MAPK complexes which is not what was observed with phosphorylated pY86 earlier **(Table 4.2 and Supplementary Table S 4.2)** and it directly indicates the sharpest increase in binding energy and destabilizing effect in the complex. Moreover, the same pattern was also observed for Y159. In dpY159/pYall03 TIRAP and p38 MAPK complex too, none of the phosphorylated tyrosine nor hydrogen bonds were present at the interface. On the other hand, it was the interface phosphorylated tyrosine residues pY86 in dpY106/pYall03 and pY159 in dpY187/pYall03 complex with p38 MAPK which were present and making the hydrogen bonds. This fact not only suggests the significance of the presence of phosphorylated tyrosine at the interface but also the dominant effect of pY86 in modulating the favorable binding conformation and providing the larger binding affinity in terms of enhanced binding energy. Nevertheless, although the presence and bonding of pY159 at the interface in the dpY187/pYall03 complex maintain the stabilizing effect, it fails to favor the binding conformation of TIRAP in the complex. Therefore, it is plausible that the tyrosine phosphorylation of TIRAP is crucial in the protein–protein binding to confer a better cumulative effect on the stability of the complex. However, it is pY86 that plays the most vital part in TIRAP and p38 MAPK complexes and is highly crucial for the binding conformation and affinity.

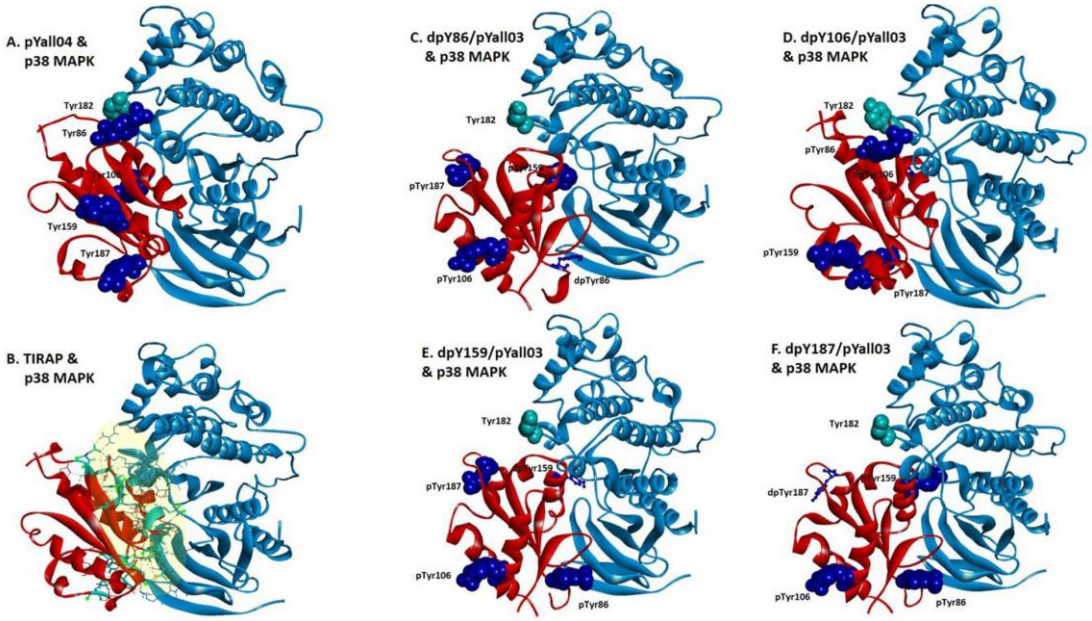

Figure 4. 5. The molecular docking complex of p38 MAPK and conditionally phosphorylated tyrosine (pY) of TIRAP TIR domain from HADDOCK 2.4. The complex of non-phosphorylated and all four-tyrosine site phosphorylated TIRAP structure (red) and p38 MAPK (light blue) (**A**) and (**B**) are represented for a comparative purpose with a docking complex of p38 MAPK (light blue) and tyrosine-phosphorylated TIRAP (red) with de-phosphorylated (dp) tyrosine dpY86pYall03 (dark blue) (**C**), dpY106pYall03 (dark blue) (**D**), dpY159pYall03 (dark blue) (**E**) and dpY187pYall03 (dark blue) (**F**), respectively. The complexes are the top pose result of HADDOCK 2.4 docking and images are prepared in Discovery studio Visualizer. The tyrosine residues of TIRAP (dark blue) and p38 MAPK (cyan) are represented in a ball and stick and cpk (Corey-Pauling-Koltun) format. The images were prepared using a Discovery studio Visualizer v21.1.0.20298. The interacting interface residues between both proteins were analyzed with the 3 A region in the Chimera v1.13.1 tool (Supplementary Table S4.1).

Sr No.	TIRAP-p38 MAPK complex	Dephosphorylated site in TIRAP	Total BE (ΔG_{bind}) (kcal/mol)	Change in ΔG_{bind} (kcal/mol)
6.	pYall04 and p38 MAPK	-	-20.5	-10.5
7.	dpY86/pYall03 and p38 MAPK	Y86	-7.1	-13.4
8.	dpY106/pYall03 and p38 MAPK	Y106	-16.2	-4.3
9.	dpY159/pYall03 and p38 MAPK	Y159	-9.6	-10.9
10.	dpY187/pYall03 and p38 MAPK	Y187	-15.5	-5

Table 4. 3. The destabilizing effect of dephosphorylation of tyrosine residues (Y86, Y106, Y159, and Y187) in the TIR domain of TIRAP were calculated in terms of change in the free binding energy (BE) of TIRAP and p38 MAPK complexes. The sequential dephosphorylation shows the highest destabilizing effect occurs with dephosphorylation of Y86 and Y159 while the modest with Y106, as evident from the change in the ΔG_{bind} obtained from the PDBePISA tool.

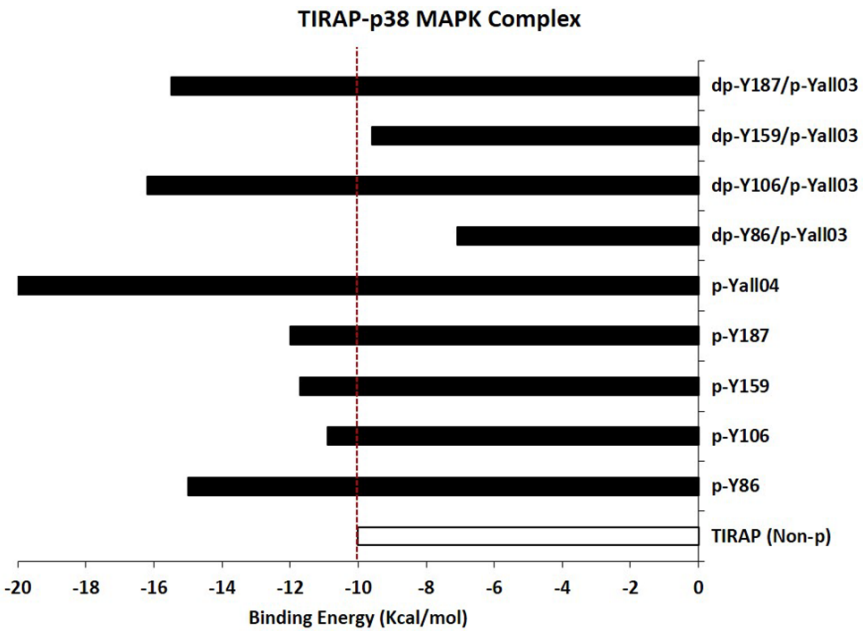

Figure 4. 6. Graphical representation of the energetic effect of phosphorylation/dephosphorylation of tyrosine residues (Y86, Y106, Y159, and Y187) in TIR domain of TIRAP calculated in terms of the change in the free binding energy (BE) of TIRAP and p38 MAPK complexes. The changes in BE of phosphorylated tyrosine TIRAP and p38 MAPK complexes are compared with that for the non-phosphorylated TIRAP and p38 MAPK complex while the significance of each tyrosine residue by sequential dephosphorylation is compared with the complex of all four phosphorylated tyrosine TIRAP and p38 MAPK complexes.

4.5.5. Molecular dynamic (MD) simulation of tyrosine-phosphorylated TIRAP and p38 MAPK

To study the effect of tyrosine phosphorylation and dephosphorylation, the docked complexes of phosphorylated and non-phosphorylated TIRAP with p38 MAPK were further analyzed using a 500 ns MD simulation employing the GROMACS program. No significant changes from the docked conformation of TIRAP were observed as suggested by small root mean squared deviations (RMSD) **(Figure 4.6)**. Comparatively higher deviations were observed for p38 MAPK mostly due to the movement of the C and N-terminal residues during dynamics **(Figure 4.6)**. Interestingly, amino acid residues at the TIRAP-p38 MAPK protein–protein interface mainly around the active site residue Y182 also account for these higher structural

deviations **(Figure 4.7A)**. Specifically, in the case of pY86 TIRAP and p38 MAPK complex, conformational changes of the residues around Y182 were comparatively higher in contrast to dpY86pYall03 TIRAP and p38 MAPK complex **(Figure .7B)**. As these residues also form the protein–protein interface in pY86 TIRAP and p38 MAPK complex **(Figure 4.7C)**, Y86 phosphorylation in TIRAP leads to the formation of additional protein–protein contacts and thereby provided stability to the protein–protein complex.

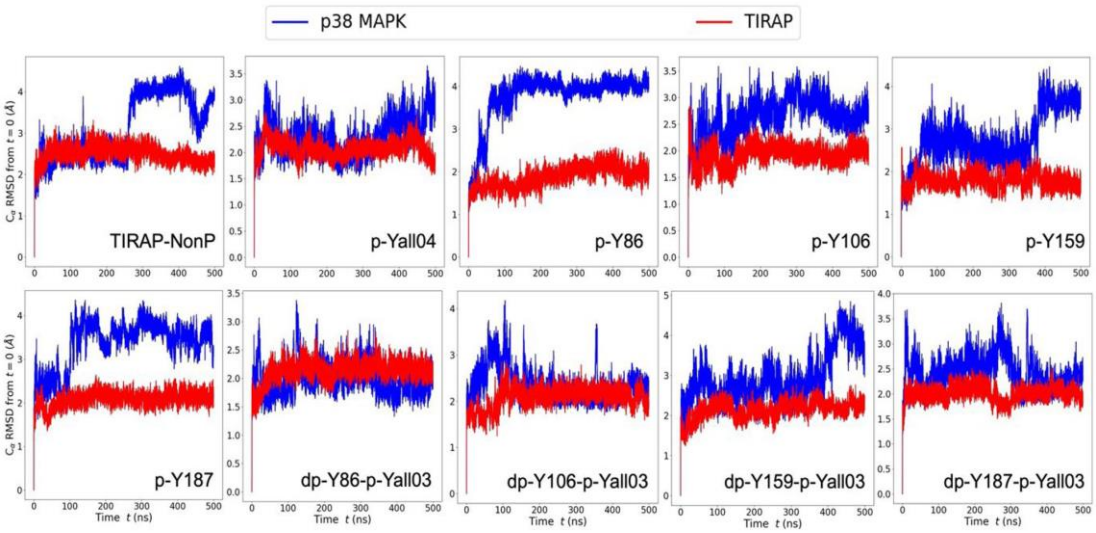

Figure 4. 7. The root mean squared deviations (RMSD) of p38 MAPK and phosphorylated and non-phosphorylated TIRAP complexes. The RMSD plot of TIRAP (red) and p38 MAPK (blue) Cα atoms and their nine different molecular complexes for a total simulation time of 500 ns is shown.

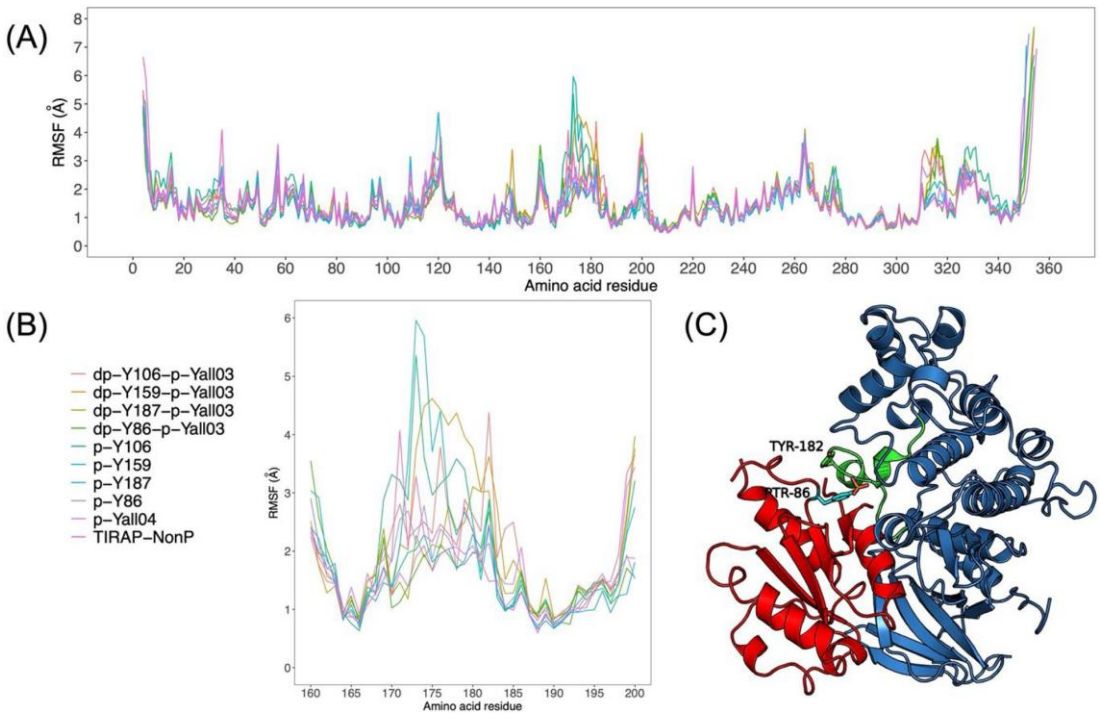

Figure 4. 8. The root mean squared fluctuations (RMSF) of p38 MAPK in phosphorylated and non-phosphorylated TIRAP and p38 MAPK complexes. (**A**) RMSF of full p38 MAPK residues throughout the 500 ns MD trajectory. (**B**) RMSF of TIRAP interacting p38 MAPK residues throughout the 500 ns MD trajectory and (**C**) A cartoon diagram of TIRAP (red) and p38 MAPK (blue) complex prepared in PyMOL v2.3.4 tool showing the TIRAP interacting region (green) around the catalytic residue.

To further study the effect of tyrosine phosphorylation on TIRAP structure, PCA using Cartesian coordinates and a singular value decomposition approach was performed. Analysis of the first two principal components **(Supplementary Figure S4.2)** revealed no major conformational change. Instead, in agreement with RMSD and RMSF analysis, tyrosine phosphorylation on TIRAP structure was associated with conformational changes in p38 MAPK **(Supplementary Figure S4.3)**. As structural deviations were detected mainly in the region forming the protein–protein interface in p38 MAPK, the conformational changes might be attributed to additional contacts formed as a result of tyrosine phosphorylation in TIRAP. To analyze the dynamics of the protein–protein contacts, the frequency of all hydrogen bonds, van der Waals contacts, and salt bridges between TIRAP and p38 MAPK were calculated throughout

the MD trajectory. As shown in **(Figure 4.7)**, the higher number of stable hydrogen bonds (occurrence frequency > 0.8) between pY86 TIRAP and p38 MAPK complex was observed when compared to pY106, pY159, pY187, and non-phosphorylated TIRAP. A similar pattern was also observed in the case of salt bridges and van der Waals contacts (Supplementary Figs. S4 and S5). One key contact was the hydrogen bond between pY86 and K118 of p38 MAPK with almost 100% occupancy during MD **(Figure 4.8)**. It was interesting to see that instead of TIRAP's pY86 as predicted by docking, D85 interacted with p38 MAPK residue R220 by forming hydrogen bonding and van der Waals contacts **(Figure 4.8 and Supplementary Figure S4.5)**. In agreement with our docking studies, MD also highlighted the importance of phosphorylation of Y86 as being the only tyrosine among all that interacted with p38 MAPK. In summary, taken together with the phosphorylated TIRAP interaction with p38 MAPK, it is plausible that the interaction provides a more stable conformation which significantly validates the fact that phosphorylation of tyrosine residues in the TIRAP TIR domain is crucial and greatly impacts the interaction with the downstream p38 MAPK.

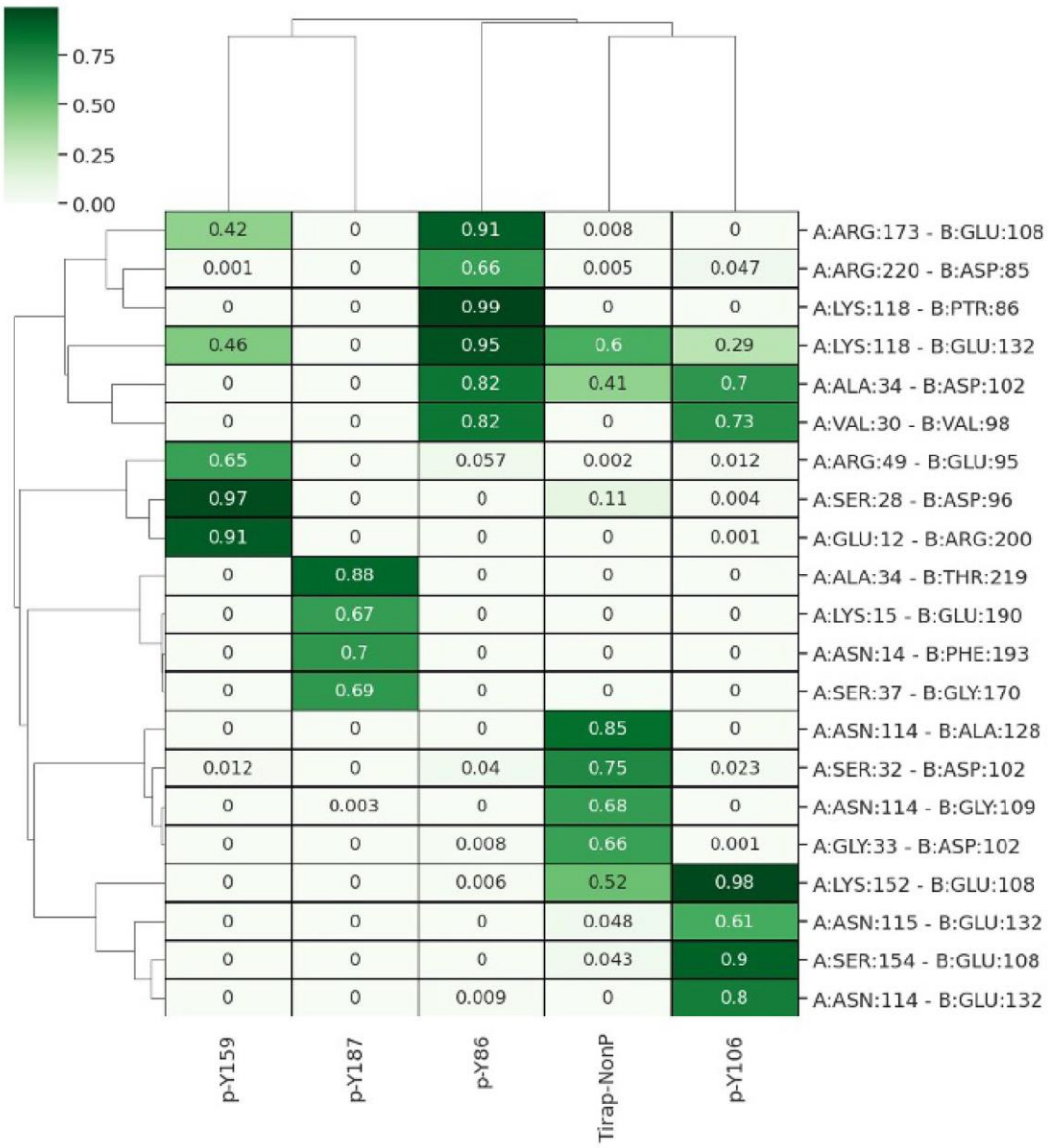

Figure 4. 9. A heatmap showing the frequency of hydrogen bonding contacts between TIRAP and p38 MAPK calculated throughout the 500 ns MD trajectory. Contacts with more than 60% occurrence frequency (frequency value = 0.6) for either of the complexes are shown.

4.6. Discussion

Overall, signalling events are tightly controlled in cellular settings and are highly regulated by several mechanisms which govern the normal functioning and

maintenance of the body's homeostasis [5, 11, 68]. The major event in signalling is the transduction of messenger signals to downstream molecules which mainly involves the communication between signalling mediators [15, 69, 70]. Protein–protein interaction which can either be a kinase-kinase or kinase-non-kinase protein interaction is one of the major events which play a crucial role between the start and the end of the signalling process. The dynamic regulations are achieved through post-translational modifications. Phosphorylation is one of the crucial post-translational modifications where the phospho-residues serine, threonine, and tyrosine regulate the function of the proteins. The importance of phospho-tyrosine residues is associated with protein–protein interaction in signalling events. Meanwhile, the presence of tyrosine residues at the binding interface has been shown to enhance the binding stability and energy of the protein complex [17-19, 60]. We have performed the structural analysis of TIRAP and p38 MAPK interaction through multiple molecular docking studies in HADDOCK 2.4, pyDockWEB, ClusPro 2.0, and ZDOCK 3.0.2, and the same has also been validated at the cellular level through *in-vitro* immunostaining study to colocalize both the proteins in murine macrophages RAW 264.7 cells. Previous studies have emphasized the crucial role of TIRAP tyrosine residue phosphorylation in TLR4/2 signaling[16, 23, 25]. Therefore, we further sought to understand the effect of TIRAP tyrosine phosphorylation on p38 MAPK interaction and created the in-silico site-specific phosphorylated structures of TIRAP through the discovery studio platform. Our *in-silico* data suggest that the phosphorylated Y86 of TIRAP is crucial in maintaining the structural stability of the complex since its dephosphorylation negatively impacts the binding affinity with p38 MAPK. Interestingly, phosphorylation of all four tyrosine sites jointly enhances TIRAP binding when compared to the non-phosphorylated TIRAP which is also mainly through the pY86. The phosphorylated Y86 shows to pull the TIRAP closer to the active site region in the kinase domain of p38 MAPK (T180 and Y182) while the docking of phosphorylated Y187 conformation keeps it away from the active region of p38 MAPK. Notably, the molecular docking and further molecular simulation study of 500 ns also define the highest stable hydrogen bonds in the complex with the

phosphorylated Y86 TIRAP. The structural evaluation provides insight into the importance of tyrosine phosphorylation of TIRAP mainly at Y86 for p38 MAPK interaction. Additionally, it provides a platform for their therapeutic interventions by targeting these hydrogen bonds such as the strongest between Y86 in TIRAP and K118 in p38 MAPK for the regulation of downstream signaling and prolonged inflammatory responses responsible for several inflammatory-associated diseases.

4.7. References

1. Abraham, C., S.N. Vogel, and D.J. Perkins, *Signaling Mechanisms Regulating Innate Immune Responses*, in *Mucosal Immunology*. 2015, Elsevier. p. 605-622.
2. Kumar, V., *Macrophages: the potent immunoregulatory innate immune cells.* Macrophage Activation-Biology and Disease, 2019.
3. Oishi, Y. and I. Manabe, *Macrophages in inflammation, repair and regeneration.* International immunology, 2018. **30**(11): p. 511-528.
4. Viola, A., et al., *The metabolic signature of macrophage responses.* Frontiers in immunology, 2019. **10**: p. 1462.
5. Beutler, B.A., *TLRs and innate immunity.* Blood, The Journal of the American Society of Hematology, 2009. **113**(7): p. 1399-1407.
6. Chow, J.C., et al., *Toll-like receptor-4 mediates lipopolysaccharide-induced signal transduction.* J Biol Chem, 1999. **274**(16): p. 10689-92.
7. Kawai, T. and S. Akira, *TLR signaling.* Cell Death & Differentiation, 2006. **13**(5): p. 816-825.
8. Kawasaki, T. and T. Kawai, *Toll-like receptor signaling pathways.* Front Immunol, 2014. **5**: p. 461.
9. El-Zayat, S.R., H. Sibaii, and F.A. Mannaa, *Toll-like receptors activation, signaling, and targeting: an overview.* Bulletin of the National Research Centre, 2019. **43**(1): p. 1-12.
10. Takeda, K. and S. Akira, *Toll-like receptors in innate immunity.* International immunology, 2005. **17**(1): p. 1-14.
11. Akira, S., *TLR signaling.* From innate immunity to immunological memory, 2006: p. 1-16.
12. O'Neill, L.A. and A.G. Bowie, *The family of five: TIR-domain-containing adaptors in Toll-like receptor signalling.* Nat Rev Immunol, 2007. **7**(5): p. 353-64.
13. Horng, T., et al., *The adaptor molecule TIRAP provides signalling specificity for Toll-like receptors.* Nature, 2002. **420**(6913): p. 329-333.
14. O'Neill, L.A.J., K.A. Fitzgerald, and A.G. Bowie, *The Toll–IL-1 receptor adaptor family grows to five members.* Trends in immunology, 2003. **24**(6): p. 286-289.
15. Rajpoot, S., et al., *TIRAP in the Mechanism of Inflammation.* 2021. **12**(2722).
16. Chattopadhyay, S. and G.C. Sen, *Tyrosine phosphorylation in Toll-like receptor signaling.* Cytokine Growth Factor Rev, 2014. **25**(5): p. 533-41.
17. Nishi, H., A. Shaytan, and A.R. Panchenko, *Physicochemical mechanisms of protein regulation by phosphorylation.* Frontiers in genetics, 2014. **5**: p. 270.
18. Ardito, F., et al., *The crucial role of protein phosphorylation in cell signaling and its use as targeted therapy.* International journal of molecular medicine, 2017. **40**(2): p. 271-280.

19. Kaneko, T., et al., *Phosphotyrosine recognition domains: the typical, the atypical and the versatile.* Cell Communication and Signaling, 2012. **10**(1): p. 1-20.
20. Songyang, Z. and L.C. Cantley, *Recognition and specificity in protein tyrosine kinase-mediated signalling.* Trends in biochemical sciences, 1995. **20**(11): p. 470-475.
21. Wolf-Yadlin, A., M. Sevecka, and G. MacBeath, *Dissecting protein function and signaling using protein microarrays.* Current opinion in chemical biology, 2009. **13**(4): p. 398-405.
22. Wavreille, A.-S., et al., *Defining SH2 domain and PTP specificity by screening combinatorial peptide libraries.* Methods, 2007. **42**(3): p. 207-219.
23. Piao, W., et al., *Tyrosine phosphorylation of MyD88 adapter-like (Mal) is critical for signal transduction and blocked in endotoxin tolerance.* J Biol Chem, 2008. **283**(6): p. 3109-19.
24. Medvedev, A.E., et al., *Role of TLR4 tyrosine phosphorylation in signal transduction and endotoxin tolerance.* J Biol Chem, 2007. **282**(22): p. 16042-53.
25. Gray, P., et al., *MyD88 adapter-like (Mal) is phosphorylated by Bruton's tyrosine kinase during TLR2 and TLR4 signal transduction.* 2006. **281**(15): p. 10489-10495.
26. Jefferies, C.A., et al., *Bruton's tyrosine kinase is a Toll/interleukin-1 receptor domain-binding protein that participates in nuclear factor kappaB activation by Toll-like receptor 4.* J Biol Chem, 2003. **278**(28): p. 26258-64.
27. Jefferies, C.A. and L.A. O'Neill, *Bruton's tyrosine kinase (Btk)-the critical tyrosine kinase in LPS signalling?* Immunol Lett, 2004. **92**(1-2): p. 15-22.
28. Paracha, R.Z., et al., *Structural evaluation of BTK and PKCdelta mediated phosphorylation of MAL at positions Tyr86 and Tyr106.* Comput Biol Chem, 2014. **51**: p. 22-35.
29. Verstak, B., et al., *MyD88 adapter-like (Mal)/TIRAP interaction with TRAF6 is critical for TLR2- and TLR4-mediated NF-kappaB proinflammatory responses.* J Biol Chem, 2009. **284**(36): p. 24192-203.
30. Bernard, N.J. and L.A. O'Neill, *Mal, more than a bridge to MyD88.* IUBMB Life, 2013. **65**(9): p. 777-86.
31. Fulgione, A., et al., *Interaction between MyD88, TIRAP and IL1RL1 against Helicobacter pylori infection.* 2020. **10**(1): p. 1-13.
32. Miggin, S.M., et al., *NF-κB activation by the Toll-IL-1 receptor domain protein MyD88 adapter-like is regulated by caspase-1*. 2007. **104**(9): p. 3372-3377.
33. Palsson-McDermott, E.M. and L.A. O'Neill, *Signal transduction by the lipopolysaccharide receptor, Toll-like receptor-4.* Immunology, 2004. **113**(2): p. 153-62.
34. Baig, M.S., et al., *Heterotrimeric complex of p38 MAPK, PKCdelta, and TIRAP is required for AP1 mediated inflammatory response.* Int Immunopharmacol, 2017. **48**: p. 211-218.
35. Bode, J.G., C. Ehlting, and D. Haussinger, *The macrophage response towards LPS and its control through the p38(MAPK)-STAT3 axis.* Cell Signal, 2012. **24**(6): p. 1185-94.
36. Meng, A., X. Zhang, and Y. Shi, *Role of p38 MAPK and STAT3 in lipopolysaccharide-stimulated mouse alveolar macrophages.* Exp Ther Med, 2014. **8**(6): p. 1772-1776.
37. Yang, Y., et al., *Functional roles of p38 mitogen-activated protein kinase in macrophage-mediated inflammatory responses.* Mediators Inflamm, 2014. **2014**: p. 352371.
38. Yong, H.-Y., M.-S. Koh, and A. Moon, *The p38 MAPK inhibitors for the treatment of inflammatory diseases and cancer.* Expert opinion on investigational drugs, 2009. **18**(12): p. 1893-1905.
39. Kang, Y.J., et al., *Macrophage deletion of p38α partially impairs lipopolysaccharide-induced cellular activation.* The Journal of Immunology, 2008. **180**(7): p. 5075-5082.

40. Wang, Z., et al., *The structure of mitogen-activated protein kinase p38 at 2.1-Å resolution.* Proceedings of the National Academy of Sciences, 1997. **94**(6): p. 2327-2332.
41. Kaminska, B., *MAPK signalling pathways as molecular targets for anti-inflammatory therapy—from molecular mechanisms to therapeutic benefits.* Biochimica et Biophysica Acta (BBA)-Proteins and Proteomics, 2005. **1754**(1-2): p. 253-262.
42. Kumar, S., J. Boehm, and J.C. Lee, *p38 MAP kinases: key signalling molecules as therapeutic targets for inflammatory diseases.* Nature reviews Drug discovery, 2003. **2**(9): p. 717-726.
43. Schindler, J.F., J.B. Monahan, and W.G. Smith, *p38 pathway kinases as anti-inflammatory drug targets.* Journal of dental research, 2007. **86**(9): p. 800-811.
44. van Zundert, G.C. and A.M. Bonvin, *Modeling protein-protein complexes using the HADDOCK webserver "modeling protein complexes with HADDOCK".* Methods Mol Biol, 2014. **1137**: p. 163-79.
45. Jimenez-Garcia, B., C. Pons, and J. Fernandez-Recio, *pyDockWEB: a web server for rigid-body protein-protein docking using electrostatics and desolvation scoring.* Bioinformatics, 2013. **29**(13): p. 1698-9.
46. Kozakov, D., et al., *The ClusPro web server for protein–protein docking.* 2017. **12**(2): p. 255.
47. Pierce, B.G., et al., *ZDOCK server: interactive docking prediction of protein–protein complexes and symmetric multimers.* 2014. **30**(12): p. 1771-1773.
48. Pettersen, E.F., et al., *UCSF Chimera--a visualization system for exploratory research and analysis.* J Comput Chem, 2004. **25**(13): p. 1605-12.
49. BIOVIA, D.S., *BIOVIA Discovery Studio 2020.* San Diego: Dassault Systemes, 2020.
50. Schneider, C.A., W.S. Rasband, and K.W. Eliceiri, *NIH Image to ImageJ: 25 years of image analysis.* Nat Methods, 2012. **9**(7): p. 671-5.
51. Bolte, S. and F.P. Cordelières, *A guided tour into subcellular colocalization analysis in light microscopy.* J Microsc, 2006. **224**(Pt 3): p. 213-32.
52. Foloppe, N. and A.D. MacKerell, *All-atom empirical force field for nucleic acids: I. Parameter optimization based on small molecule and condensed phase macromolecular target data.* Journal of Computational Chemistry, 2000. **21**(2): p. 86-104.
53. Abraham, M.J., et al., *GROMACS: High performance molecular simulations through multi-level parallelism from laptops to supercomputers.* 2015. **1**: p. 19-25.
54. Michaud-Agrawal, N., et al., *MDAnalysis: a toolkit for the analysis of molecular dynamics simulations.* 2011. **32**(10): p. 2319-2327.
55. McGibbon, R.T., et al., *MDTraj: a modern open library for the analysis of molecular dynamics trajectories.* 2015. **109**(8): p. 1528-1532.
56. Pedregosa, F., et al., *Scikit-learn: Machine learning in Python.* 2011. **12**: p. 2825-2830.
57. Ross, C., et al., *MODE-TASK: large-scale protein motion tools.* 2018. **34**(21): p. 3759-3763.
58. Hunter, J.D.J.I.A.o.t.H.o.C., *Matplotlib: A 2D graphics environment.* 2007. **9**(03): p. 90-95.
59. Team, R.C., *R: A language and environment for statistical computing*. 2013: R Foundation for Statistical Computing, Vienna, Austria.
60. Nishi, H., K. Hashimoto, and A.R. Panchenko, *Phosphorylation in protein-protein binding: effect on stability and function.* Structure, 2011. **19**(12): p. 1807-1815.
61. Devanand, T., P. Venkatraman, and S. Vemparala, *Phosphorylation promotes binding affinity of Rap-Raf complex by allosteric modulation of switch loop dynamics.* Scientific reports, 2018. **8**(1): p. 1-15.

62. Kumar, P., et al., *Multisite phosphorylation disrupts arginine-glutamate salt bridge networks required for binding of cytoplasmic linker-associated protein 2 (CLASP2) to end-binding protein 1 (EB1).* Journal of Biological Chemistry, 2012. **287**(21): p. 17050-17064.
63. Ferreon, J.C., et al., *Cooperative regulation of p53 by modulation of ternary complex formation with CBP/p300 and HDM2.* Proceedings of the National Academy of Sciences, 2009. **106**(16): p. 6591-6596.
64. Lin, Z., et al., *Structural insights into TIR domain specificity of the bridging adaptor Mal in TLR4 signaling.* PLoS One, 2012. **7**(4): p. e34202.
65. Williams, S.J., et al., *Structure and function of the TIR domain from the grape NLR protein RPV1*. Frontiers in plant science, 2016. **7**: p. 1850.
66. Toshchakov, V.Y. and A.F. Neuwald, *A survey of TIR domain sequence and structure divergence.* Immunogenetics, 2020. **72**(3): p. 181-203.
67. Sugiyama, N., et al., *Large-scale phosphorylation mapping reveals the extent of tyrosine phosphorylation in Arabidopsis.* Molecular systems biology, 2008. **4**(1): p. 193.
68. Kawai, T. and S. Akira, *The role of pattern-recognition receptors in innate immunity: update on Toll-like receptors.* Nat Immunol, 2010. **11**(5): p. 373-84.
69. Balka, K.R. and D. De Nardo, *Understanding early TLR signaling through the Myddosome.* J Leukoc Biol, 2019. **105**(2): p. 339-351.
70. Mandraju, R., T.D. Troutman, and C. Pasare, *Toll-Like Receptor Function and Signaling*, in *Reference Module in Biomedical Sciences*. 2014, Elsevier.

Chapter 5

(Identification of novel inhibitors targeting TIRAP interactions with BTK and PKCδ in inflammation)

Chapter 5: Identification of novel inhibitors targeting TIRAP interactions with BTK and PKCδ in inflammation

5.1. Graphical Abstract

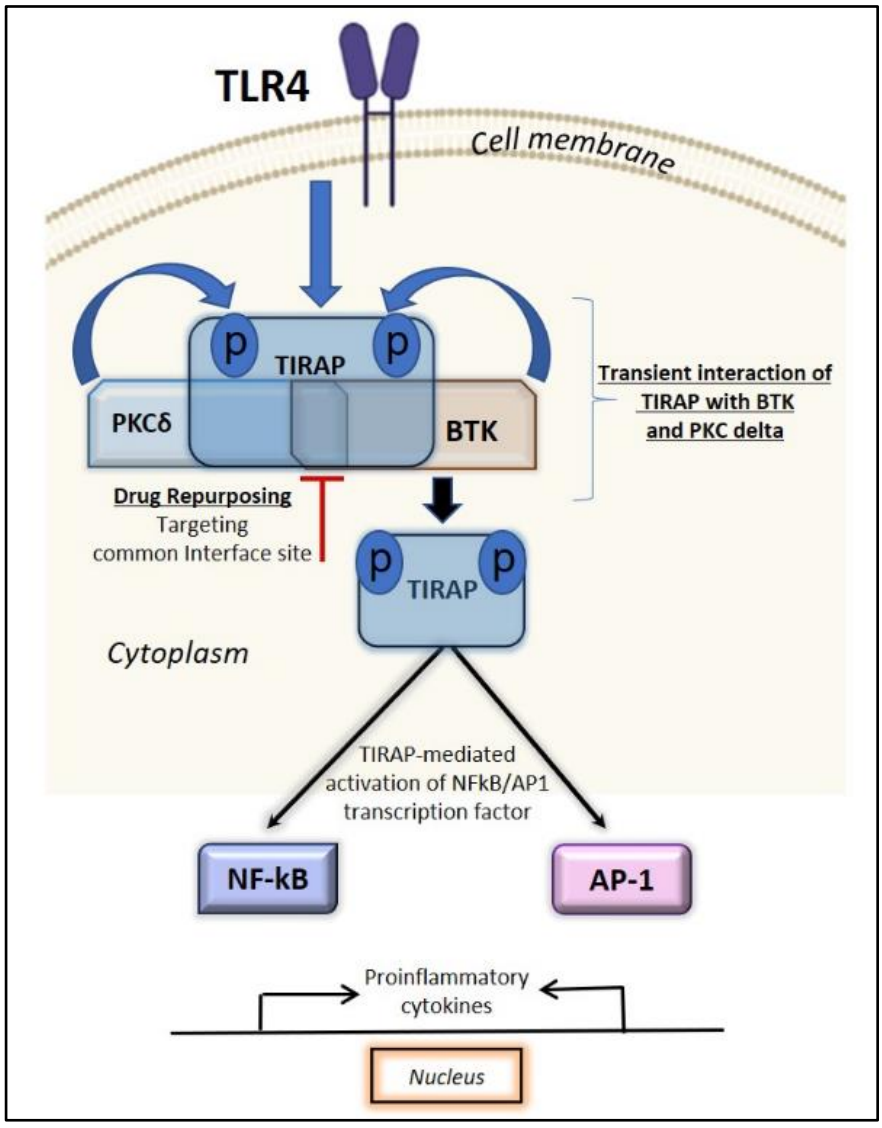

Figure 5. 1. *Illustration of TIRAP interactions with upstream kinases PKCδ and BTK, which is essential for TIRAP activation in TLR4 mediated inflammatory signalling and its dual inhibition through common interface could be highly effective therapy for sepsis.*

5.2. Summary

TIRAP interactions with other proteins in macrophage signalling are crucial components of severe or persistent inflammation. TIRAP activation through Bruton's tyrosine kinase (BTK) and Protein Kinase C delta (PKCδ) is essential for downstream inflammatory signalling. Therefore, we created homology-based structural models of BTK and PKCδ and studied their interactions in their non-phosphorylated and phosphorylated states with TIRAP to identify a common interface for drug targeting. Six FDA-approved drugs were identified and four were found to have stable interactions over a range of 100 ns MD simulation timescales. These drugs block the interactions of both kinases with TIRAP in silico. Hence, these drugs have the potential to completely block TIRAP activity which can dampen downstream inflammatory signalling and inflammation-mediated disease.

5.3. Introduction

Inflammation is termed as a complex biological and biochemical process of the host immune system involving several immune cells and a plethora of signalling mediators to respond against several stimuli such as pathogens and their toxins, damaged tissue or cells, irritants, etc. The initiation and resolution of inflammation are tightly regulated events, whereas dysregulated inflammatory signalling results in persistent inflammation associated with immunopathology [1, 2]. Triggered by stimuli, the unchecked host immune cell-mediated inflammation leads to the proinflammatory cytokine storm, increasing inflammatory mediators and inflammatory cells to control the pathogens. However, such an imbalance between pro- and anti-inflammatory responses leads to tissue damage, vascular dysfunction, multi-organ failure, and eventually death in many cases. Hence, pharmacotherapy of inflammation is globally essential and challenging. Macrophages are significant players in the host defense mechanism and critical immune cells in the inflammation process. They perform three major functions: antigen presentation, phagocytosis, and immunoregulation through the secretion of several cytokines and inflammatory mediators [1, 3]. Macrophages

pre-dominantly express Toll-like receptors (TLRs), which are pivotal in host immune defense. The cell-surface TLRs recognize a range of foreign pathogen-associated molecular patterns (PAMPs), which initiate a series of signals through their cytoplasmic TIR domain interaction with adaptor proteins and eventually result in the activation of transcription factors and the expression of inflammatory cytokines [4-8]. Toll/interleukin-1 receptor (TIR) domain-containing adapter protein (TIRAP), being one of the major adaptor proteins in TLR4/2 signaling, is the most upstream signalling molecule and extensively participates in the transduction and regulation of the downstream inflammatory signalling cascade [4, 5, 9]. Besides the adaptor protein role with TLRs, several studies, including ours, have revealed dozens of protein interactions of TIRAP TIR domains, governing its role in inflammatory responses [10-14]. The two major tyrosine kinase proteins, Bruton's tyrosine kinase (BTK) and Protein kinase C delta (PKCδ) interact with TIRAP for its downstream activity. BTK, a Tec family member protein similar to src protein members but with an additional N-terminal pleckstrin homology (PH) domain responsible for its membrane localization, is directly implicated downstream of TLR4/2, and activates TIRAP through multiple tyrosine phosphorylation in its TIR domain mainly at Y86, Y106, Y159 and Y187 [11, 15, 16]. However, the interaction of PKCδ with TIRAP is less studied but is known to regulate downstream signalling through TIRAP phosphorylation and activation [12]. PKCδ differs from other members of the protein kinase C family. It is uniquely activated by tyrosine kinase and has an imperative role in macrophage inflammation signalling [17-19]. The interactions of BTK and PKCδ with TIRAP are responsible for the downstream signal transduction and activation of transcription factors, mainly MAPK and NF-κB [12, 20, 21]. Therefore, abrogating these interactions is a possible therapeutic strategy for dampening inflammatory cytokines production. There is a paucity of drugs available for dysregulated inflammation and associated diseases, e.g., sepsis. [22]. PPI-based drug development has been challenging due to the intricacies of targeting the interface site and deciphering the critical interfacial residues of the complex. However, the emergence of computational tools has created a platform to accelerate the therapeutic development of small lead

molecules and repurposed drugs. Therefore, we performed the structural modelling of these kinase proteins BTK and PKCδ to understand their interaction and interface sites, serving as a potential therapeutic target. This study dissected the TIRAP interactions with BTK and PKCδ in both states of non-phosphorylated and phosphorylated active forms of heir structure. We computationally performed the structure-based screening of clinically approved drugs predicted to target this interaction as potential repurposed anti-inflammatory agents.

5.4. Materials and Methods

5.4.1. Molecular modelling

A homology-based approach was applied to model the 3D protein structure of BTK. Before modelling, the sequences and functional domain information were retrieved from the UniProt database for human BTK (UniProtKB-Q05655). We used MODELLER 9.24 for modelling and loop refinement of the structure [23, 24]. The kinase, SH2, and SH3 domains of BTK were modelled by a multi-template comparative method using PDB ID 4YHF, 6HTF, and 4XI2 as templates. The BTK modelling was similarly completed as described in chapter 3 materials and methods section. Meanwhile, the modeled structure of PKCδ and loop-modelled TIRAP structure was obtained from our previous study as mentioned in chapter 3 materials and methods section.

5.4.2. Structure preparation and molecular docking of TIRAP with BTK and PKCδ

The protein structures were prepared by adding the polar hydrogen atoms in Discovery Studio [25] and then energetically minimizing the structure in the Chimera 1.13.1 [26]. The default energy minimization option of the Chimera 1.13.1 tool was employed to perform single minimization of the structures, which includes the deletion of solvent, and replacement of incomplete sidechains, if any, using the Dunbrack rotamer library [27], followed by the addition of charges to standard residues using AMBER ff14SB force field. The tyrosine phosphorylated structure of BTK and PKCδ was also prepared

through the Discovery Studio function. Tyrosine residue was replaced with phosphor-tyrosine at transphosphorylation site Y551 in the catalytic domain and autophosphorylation site Y223 in the SH3 domain of BTK, while the transphosphorylation site Y512 in the catalytic domain of PKCδ. The prepared structures of BTK and PKCδ were docked with the TIRAP TIR domain structure in pyDockWEB [28], ClusPro 2.0 [29, 30], and HADDOCK 2.4 [31]. The HADDOCK 2.4 accepting phosphorylated residue was used for the docking of tyrosine phosphorylated structures. The topmost docking pose was selected for further analysis. The protein complexes were further analyzed in Chimera 1.13.1 to find out the interacting residues within the 4 Å region of the binding interface, and their interactions were visualized and represented through Discovery Studio Visualizer [25]. Virtual screening and analysis Food and Drug Administration (FDA)-approved drugs were obtained from the ZINC15 database [32] We applied 'purchasable' and 'in-stock drugs only' filters to FDA-approved drugs, which produced 1576 available drugs. For potential inhibitor site identification in TIRAP, the interaction interface of both BTK and PKCδ on TIRAP was identified to screen drugs with the potential to block those sites and inhibit their respective binding. The total interacting residues of TIRAP with BTK and PKCδ complexes identified within the 4 Å region of their interaction in the Chimera 1.13.1 tool [26] were analyzed. It was found that the residues from the c-terminal region of TIRAP contribute significantly to both interactions and hence were chosen for drug screening. The 1576 FDA-approved drugs were downloaded in 3D conformation in SDF format and processed and directed for blinding docking with the modelled TIRAP TIR domain structure in BIOVIA Discovery studio 2020 using the LibDock program [25]. For each protein-ligand complex, a LibDock Score was produced. After the initial results from LibDock, we employed another gold-standard docking program; AutoDock Vina [33] for re-confirming the binding conformations of ligands. To do so, the TIRAP structure was first converted to PDBQT format using the AutoDock tools, and the docking grid was defined as a − 38.356 x − 15.938 x 3.644 box fully encompassing the protein structure. Similarly, the drug structures were also converted to PDBQT file format. The

AutoDock Vina produced the binding affinity of the docked protein ligand complex in kcal/mol. The selection of drugs was based on the interactions with the target site and the binding score (LibDock score and binding affinity). Discovery Studio Visualizer 2020 [25] was used for the visualization and preparation of images of TIRAP-ligand complex and analysis of interactions.

5.4.3. In silico mutational study

Site-specific substitution mutations were created in the TIRAP TIR domain using the Discovery Studio tool [25]. To determine the significance of TIRAP's TIR domain key residues (P169, F193, M194, and Y195) involved in making bonds both with BTK and PKCδ, substitution mutations were created. These residues were substituted with Alanine (A), and mutated structures were energetically minimized. The mutated TIRAP (muTIRAP) structure P169A TIRAP, F193A TIRAP, M194A TIRAP, and Y195A TIRAP and simultaneously all four-alanine mutated TIRAP sites (all04A TIRAP) were (All04A TIRAP) were used for docking both with the non-phosphorylated and phosphorylated conformation of BTK and PKCδ structure in the HADDOCK 2.4 tool [31, 34]. Similarly, the importance of these residues in predicted drug binding was analyzed by a docking study in AutoDock Vina [33].

5.4.4. Molecular dynamics (MD) simulation analysis

MD simulation study was done to validate the stability of ligands within the active binding pocket of the TIRAP protein. Initially, a short MD simulation was performed for 1 ns in the Discovery studio tool [25], and further, an extended MD simulation was performed for 100ns with Gromacs 4.6 [35, 36]. For MD simulation in Gromacs 4.6, the topology files of macromolecules and small molecules were prepared by using the Amber99sb-ildn force field and the ANTECHAMBER module of AMBER Tools, respectively [37]. Initially, Apo (TIRAP only) or docked complexes (TIRAP and ligands) were placed in the center of a cubic box having a distance of 1.0 A° between the protein and the edge of the simulation box. Further, systems were solvated with TIP3P [44] explicit water molecules. Systems were neutralized by adding required numbers of Cl or Na ions in the Apo or ligand-bound systems. Each system was

minimized by using a steepest descent approach. Further NVT and NPT were also performed for 2 ns each to equilibrate the systems for constant volume, pressure (1 atm), and temperature (300 K). Generated trajectories were used for further analysis using Xmgrace [45].

5.4.5. qRT-PCR

The screened six drugs were experimentally tested for their potential effect on cytokines expression in LPS-stimulated macrophages through the TLR4 pathway. Briefly, the RAW264.7 cells were grown as described in chapter 3 and were stimulated with 500ng/ml of LPS for 1h before total RNA isolation. The methods and materials are the same as mentioned in chapter 3. Briefly, the total RNA was isolated from RAW 264.7 macrophage cell line by RNAiso Plus reagent (9109, Takara Bio Inc.) according to the manufacturer's instructions. The concentration and purity of isolated RNA were determined through nanodrop reading. For cDNA preparation, a total of 1000ng of RNA was reverse transcribed (RT) using the cDNA Synthesis Kit (AB-1453, Invitrogen) according to the manufacturer's datasheet. The real-time PCR (qPCR) was performed using SYBR green master mix (A25742, Applied Biosystems) in StepOnePlus Real-Time PCR Systems (Applied Biosystems). The experiment was performed in at least three independent sets for the gene expression of GAPDH, TNF-α, IL-1β, and IL-6. The primer sequences are provided in **Supplementary Table S3.1**. The ct value was analyzed using the $2^{-\triangle\triangle Ct}$ method for the relative cytokine expression, while GAPDH was regarded as a reference gene to standardize the relative expression levels of cytokine genes.

5.5. Results

5.5.1. Molecular structure modelling of BTK

We performed the homology-based 3D structure modelling of the catalytic region of the BTK to study its interaction with the TIRAP protein. The PDB database search of the human BTK sequence retrieved results only for its kinase domain. However, no

homologs are available in the PDB database for other important domains. Unlike the Src protein kinase, the protein tyrosine kinase BTK, a member of the Tec kinase family, bears an additional domain referred to as PH, responsible for its cellular localization and membrane attachment. Excluding the PH domain, the SH3, SH2, and the Kinase domain of BTK is the active region reported to undergo activation and is involved in protein-protein interaction [11]. Whereas the previous study has used the BTK with kinase domain only which may not represent actual interaction with TIRAP in order to define the interacting interface [16]. Therefore, we performed the homology modelling of BTK which includes these regions, as shown in (**Figure 5.1a)**. Briefly, templates matching with the target BTK sequence (region 214 to 659) were selected based on their NCBI protein blast [38] results against the RCSB PDB database [39]. Experimentally solved x-ray crystallographic structures with high resolution, maximum identity, and coverage with BTK target sequence were selected. The three templates including PDB Id 4YHF chain A (human BTK with 100% identity covering kinase domain only), 6HTF chain A (Human BTK with 100% identity covering SH2 domain only) and to further provide the support for structure modelling of the missing region, 4XI2 chain A (mouse BTK with 98.21% identities covering all three domains), were found suitable to construct a better model of BTK structure. The aligned FASTA sequences of 4YHF chain A, 6HTF chain A and 4XI2 chain A, retrieved from blast results were submitted to Expasy ClustalW [25] and a PIR format-based alignment was obtained for each sequence with the target BTK sequence. All sequences alignment in PIR format were serially placed in a single file and saved in the 'Ali file' format. Further, the missing residues from each PDB file of 4YHF, 6HTF and 4XI2, were identified and deleted from the aligned sequence file, replacing the gap with a hyphen exactly equal to the number of missing residues deleted. The presence of missing residues in the aligned file fails the modelling, and hence it is necessary to identify and replace them with a hyphen. However, to support near-native and better modelling of structure, we used multiple templates which have solved the structure for regions of the missing residues in another template. Several previous studies have determined that the approach of multiple templates significantly improves the

comparative (or homology) structure model yielding better performance and are appreciated in CASP (Critical Assessment of Techniques for Protein Structure Prediction) editions [[40-43]. The MODELLER 9.24 program [23, 24], serves as a convenient tool for such modelling protocols. We produced 20 model structures with a DOPE score from these aligned templates. The top one was selected based on the lowest DOPE score (the score value is negative). The initial analysis was performed in PROCHECK [26], and the outlier residues in the Ramachandran plot were further corrected by performing loop refinement of regions 59–66 and 44–45 in MODELLER 9.24. The loop refined model was reanalyzed in PROCHECK and Swiss model structure assessment [44] and ERRAT [45]. The 3D model structure shows 92.3% residues in the most favoured region of the Ramachandran plot and 81.735 quality factor scores from the ERRAT analysis. To further reduce the ERRAT error value by improving atomic interaction and increasing the Ramachandran value to bring the generously and additionally allowed region residue in the most favoured region, we performed the final refinement of the model in the GalaxyRefine program of GalaxyWeb server tool [46]. This resulted in a total of five improved models based on their RMSD value, MolProbity, and Ramachandran value. The final BTK structure for docking studies, out of these five refined models, was selected upon re-analysis in the Swiss-model structure assessment and ERRAT which showed an improved value for BTK_Model 2 **(Figure 5.1A)** as 98.2% for Ramachandran plot with no outlier residues, 0.23 as QMEAN (Qualitative Model Energy ANalysis) [47] quality estimate score and 96.4871 ERRAT quality factor score **(Supplementary Figure S5.1)**. Additionally, the quality assessment of the BTK-Model 2 structure in the ProTSAV tool determined its overall structural stability and improved quality parameters which cumulatively summarized in a good RMSD value of 2–3 Å for the structure **(Supplementary Figure S5.1)**. Finally, the selected BTK-Model 2 structure obtained from GalaxyRefine was compared with their template structure in chimera 1.13.1 and the RMSD was calculated as 0.69 Å with 4YHF, 0.387 Å with 6HTF, and 0.495 Å with 4XI2, respectively.

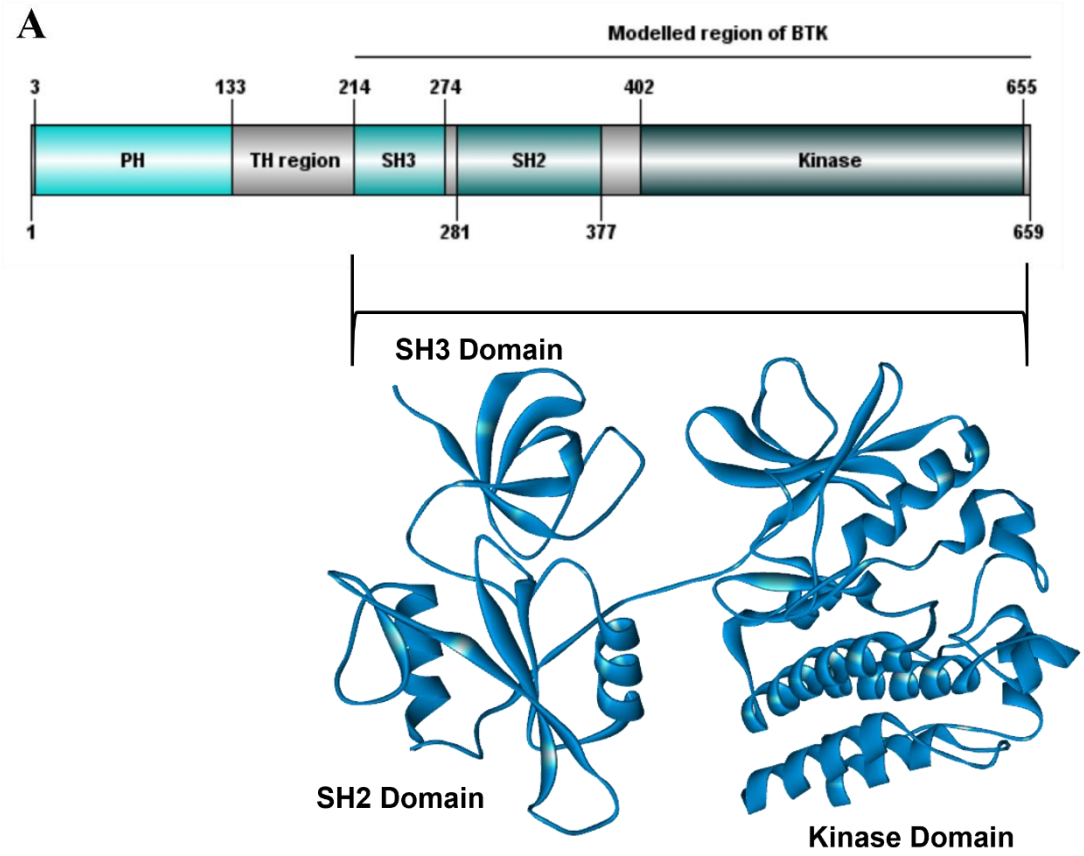

Figure 5. 2. Homology-based 3D structure modelling of bruton's tyrosine kinase (BTK) by MODELLER 9.24. The domain map and modelled 3D structure of BTK protein representing the region modelled for docking studies.

5.5.2. Docking study of TIRAP and BTK

The interactions of TIRAP with upstream kinase proteins are reported to be highly significant in terms of their activation and downstream signalling. Several previous experimental studies have revealed that active tyrosine phosphorylated BTK interacts with the TIR domain of TIRAP, leading to its site-specific tyrosine phosphorylation and downstream inflammatory signalling [11, 48]. However, to achieve therapeutic precision, the protein–protein interaction interface site requires characterization. We used molecular docking studies to achieve this. The modelled structures of BTK and TIRAP were initially prepared by adding polar hydrogens in BIOVIA Discovery Studio [25] and energy minimized in Chimera 1.13.1 tool [26]. To mimic the actual

binding, we also created a tyrosine phosphorylated form of the BTK structure. The tyrosine Y551 in the activating loop (A-loop) of the BTK kinase domain is an imperative phosphorylation site whose phosphorylation is reported by Src family kinases upon stimulation in macrophages or B-cells. The Y551 phosphorylated BTK leads to auto-phosphorylation of Y223 in the SH3 domain [11, 49]. Structurally, the A-loop of BTK structure in non-phosphorylated form adopts a very similar conformation to the active phosphorylated kinase domain for other kinases such as Lck and suggests that the non-phosphorylated conformation of the BTK A-loop does not limit the substrate binding [49]. However, we introduced the phosphorylated tyrosine (PTR) residues in the modelled BTK at Y551 and Y223 through BIOVIA Discovery Studio. Finally, they were subjected to docking in the pyDockWEB, ClusPro 2.0, and HADDOCK 2.4 docking platforms, all of which produced similar binding poses for the TIRAP and BTK complex. Due to the limitations of phosphorylated structure docking in pyDockWEB and ClusPro 2.0, phosphorylated Y551 and Y223 BTK and TIRAP were docked in HADDOCK 2.4. In all docking platforms, the TIR domain of TIRAP showed binding with the Kinase region of the BTK protein **(Figure 5.2a–d)**. We performed an interaction analysis to determine the residues involved at the binding interface site of the complex and identified the 4 Å region of the binding interface within the Chimera 1.13.1 tool both in TIRAP as well as BTK **(Table 5.1)**. The identification of closely interacting residues is imperative for the therapeutic design of inhibitor molecules. We observed the pattern of TIRAP interaction with the kinase region of BTK which is mainly through the c-terminal residues of TIRAP **(Table 5.1)**. Remarkably, the TIRAP residues A168, P169, R192, F193, M194, and Y195 were commonly present in all four docked complexes as obtained from each docking tool. Further, we applied the Molecular Mechanics/Generalized Born Surface Area (MM/GBSA) to calculate the free binding energy of the TIRAP-BTK docked protein complex, and was calculated through an in-built method from the HawkDock tool, which also predicts the individual binding energy contribution of each residue [50]. The ΔGbind (binding free energy) of −98.68 and −98.7 kcal/mol was computed for the TIRAP and BTK and TIRAP and p-Y551 & p-Y223 BTK complex, respectively. Also,

the above-listed residues were among the top ten residues contributing maximum towards the total free binding energy of this protein-protein complex. To determine the bonding between the residues of both proteins at the interface site, we applied the PDBePISA tool [51]. Both in phosphorylated and non-phosphorylated BTK complex with TIRAP, the hydrogen bonding was found between TIRAP's TIR domain residues (A168, R184, A185, R192, F193, M194, Y195, Y196, D198, P202, R207, Q208, and R215) and BTK kinase domain residues (S554, L569, Y571, T602, Q612, Y631, K637, A638, D639, and E640) within a distance of minimum 1.77 Å to maximum 3.55 Å. Beyond this, residues making salt bridge interaction were found between R184 and R192 of TIRAP and D639 and E640 of BTK.

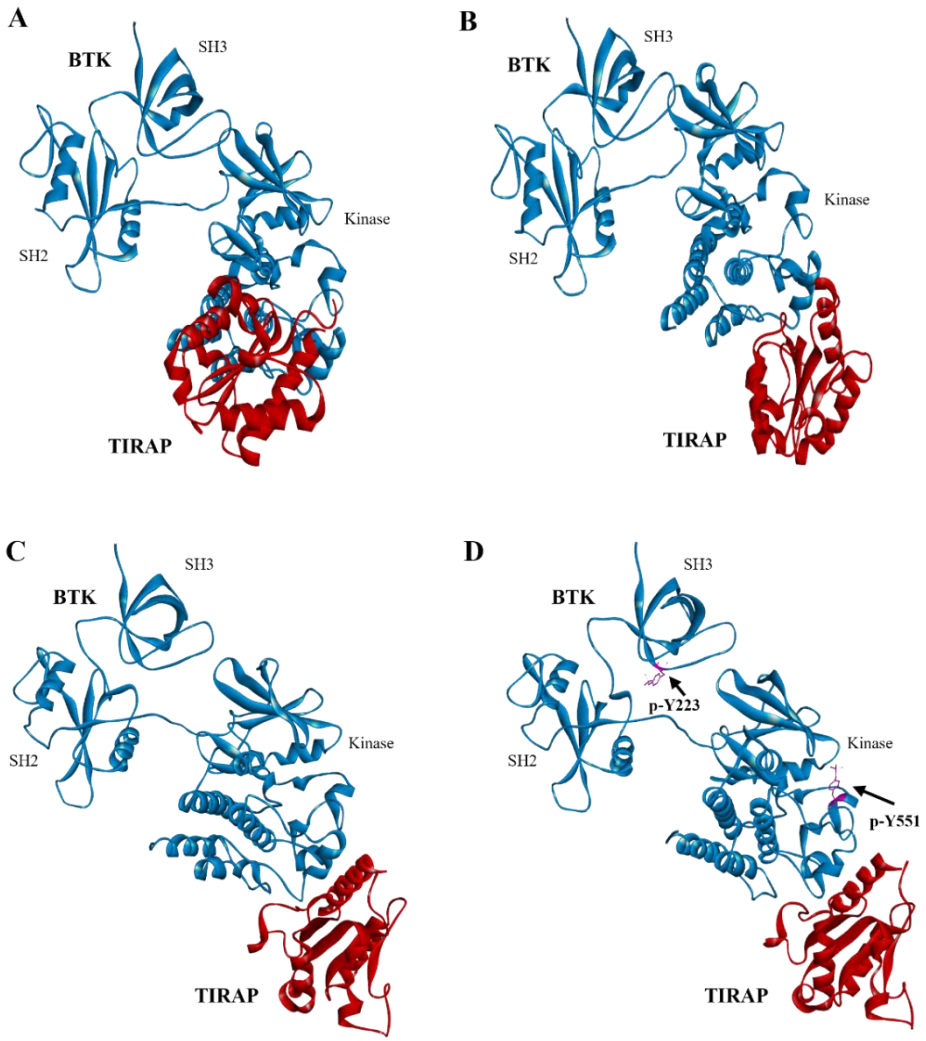

Figure 5. 3. Protein-protein docking complex of TIRAP and BTK. The results of TIRAP and BTK docking from (a) pyDockWEB, (b) ClusPro 2.0, and (c) HADDOCK 2.4 while (d) TIRAP and p-Y551 & p-Y223 BTK complex from HADDOCK 2.4 docking tools, respectively displayed in a similar interaction pattern in terms of the docked pose as well as the key residues participating at the interface site of the complex (Table 1). In all cases, the TIRAP shows to energetically favours the binding in the activation loop (A-loop) of both non-phosphorylated and phosphorylated state of BTK structure.

Docking Suits	**Interacting Residues and its position in TIRAP and BTK complex**		**No of Residue**
PyDock	TIRAP	Q163, L165, T166, E167, **A168, P169**, E172, P189, E190, **R192, F193, M194, Y195**, and T219	14
	BTK	M489, R492, F493, Q494, T495, L593, K595, E599, R618, H620, L621, A622, S623, and S659	14
ClusPro	TIRAP	L162, Q163, L165, T166, E167, **A168, P169, R192, F193, M194, Y195**, E211, A212, V213, R215, and Y216	16
	BTK	R600, F601, E605, H609, Q612, G613, L614, R615, Y617, R618, H620, Y627, Y631, and E636	14
HADDOCK 2.4	TIRAP	**A168, P169**, G170, C174, T175, I176, R184, A185, A186, Y187, **R192**, **F193, M194, Y195**, Y196, D198, P202, D203, G204, G205, F206, R207, Q208, E211, A212, R215, Y216, Q218, T219	29
	BTK	S554, V555, P566, L569, M570, Y571, KK573, T602, S604, E605, A607, E608, H609, A611, Q612, G613, L614, R615, Y631, H635, E636, K637, A638, D639, E640	25
HADDOCK 2.4	TIRAP	**A168, P169**, G170, C174, T175, R184, A185, Y187, **R192, F193, M194, Y195**, Y196, D198, P202, D203, G204, G205, G206, R207, Q208, E211, A212, R215, Y216, Q218, T219	27
	p-Y551 & Y223 BTK	S554, V555, G556, V561, P565, P566, E567, L569, M570, Y571, W581, N603, S604, E605, A607, E608, H609, I610, A611, Q612, G613, L614, R615, Y627, Y631, H635, E636, K637, A638, D639, E640, R641	32

Table 5. 1. Interacting residues in the TIRAP and BTK docking complex. The interacting residues at the interface site were identified within the 4 A region of their interaction through the Chimera 1.13.1 tool. The highlighted bold residues represent the key common residues from each docked complex of TIRAP and BTK obtained from all three docking platforms pyDockWEB, ClusPro 2.0, and HADDOCK 2.4.

5.5.3. Docking study of TIRAP and PKCδ

In addition to BTK, protein PKCδ actively participates in inflammatory signalling and plays a significant role in TIRAP-mediated inflammation in macrophages. In our previous study, we have experimentally reported that the direct interaction of PKCδ with TIRAP in macrophages regulates the downstream transcription factor activation and proinflammatory responses [21]. Other studies have also shown that the TIR domain of TIRAP is involved in the interaction with PKCδ and suggested its phosphorylation at tyrosine residues in the TIR domain [16, 52]. However, their interaction patterns and actual binding sites are not yet studied in the context of the therapeutic approach. Similar to BTK, both the non-phosphorylated and tyrosine phosphorylated PKCδ structure was prepared in BIOVIA Discovery Studio [25]. Unlike other PKC family member proteins, PKCδ is uniquely regulated and activated by tyrosine phosphorylation. The human PKCδ contains 20 tyrosine residues in different regions of the protein, including the regulatory domain, hinge region and the kinase domain. The tyrosine residue Y512 in the kinase domain of PKCδ is considered to be one of the most important phosphorylation sites for catalytic activation of PKCδ in inflammation [19]. Therefore, we incorporated the phosphorylated tyrosine at the Y512 site in the PKCδ structure to mimic the binding of activated PKCδ with TIRAP through docking studies. Finally, we performed molecular docking of TIRAP with non-phosphorylated and phosphorylated PKCδ to determine their novel interaction pattern and facilitate a drug targeting strategy. We followed the same docking methods as performed for TIRAP-BTK and analysed the best fit complex of TIRAP and PKCδ. The topmost docking results of the TIRAP and PKCδ complex obtained from pyDockWEB, ClusPro 2.0 and HADDOCK 2.4 tools were studied **(Figure 5.3a–d)**. Unlike the TIRAP-BTK complex, here both the N-terminal and C-terminal residues of the TIRAP TIR domain participate in binding with PKCδ kinase domain catalytic residues **(Table 5.2)**. In PKCδ, the C3 domain spans a short region containing the ATP binding sequence (from 356 to 371) while the major portion is covered by the C4 region containing the three phosphorylation sites T505, Y512, and Y523 in the activation loop (from 504 to 525) region [18, 19, 53]. As discussed above, the

phosphorylation of Y512 in the activation loop of the kinase domain predominantly regulates the catalytic activity. The sequence analysis of PKCδ interacting residues reveals that the C4 region of the kinase domain is mainly involved in the formation of the complex with the TIRAP TIR domain. The residues R81, P169, F193, M194, Y195, and R215 of TIRAP were commonly present in all of the docking outcomes. All the interacting residues of both the proteins were analysed only within the 4 Å region in the Chimera 1.13.1 tool **(Table 5.2)**. Finally, we performed the binding free energy calculation through the HawkDock in-built MM/GBSA calculation tool [50]. We obtained a ΔGbind of −72.48 and −70.31 kcal/mol for TIRAP and PKCδ complex and TIRAP and p-Y512 PKCδ complex, respectively. Also, the above-listed residues from TIRAP were among the top ten residues contributing highest to the binding free energy of the protein-protein complex. Furthermore, the bonding between residues of TIRAP and PKCδ determined from the PDBePISA tool [51] reveals that TIRAP TIR domain residues S79, R81, T166, A171, E172, P189, R192, F193, M194, R200, G201, and R215 makes hydrogen bonding with PKCδ kinase domain residues K355, G356, D387, D549, E551, E634, D646 and N648 within a distance of minimum 1.67 Å to maximum 3.84 Å. Also, the salt bridges interaction was found between R192, R200, R207, and R215 of TIRAP and D387, D549, and E634 of PKCδ.

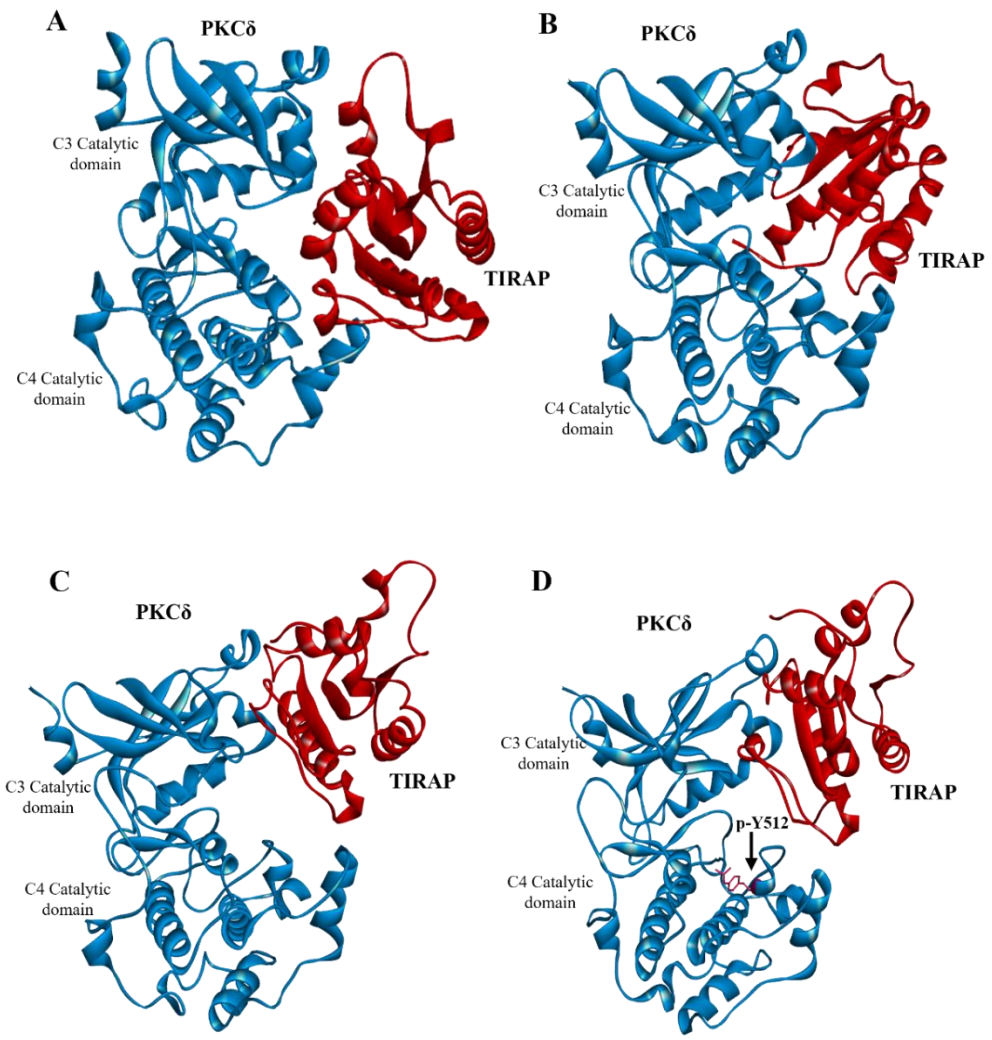

Figure 5. 4. Protein-protein docking complex of TIRAP and PKCδ. The results of TIRAP and PKCδ docking from (a) pyDockWEB, (b) ClusPro 2.0, and (c) HADDOCK 2.4 while (d) TIRAP and p-Y512 PKCδ complex from HADDOCK 2.4 docking tools, respectively displayed in a similar interaction pattern in terms of the docked pose as well as the key residues participating at the interface site of the complex (Table 1). In all cases, the TIRAP is shown to energetically favour the binding at C3-C4 catalytic sites closely sharing the active site residues in both non-phosphorylated and phosphorylated state of PKCδ structure.

Docking Suits	Interacting Residues and its position in TIRAP and PKCδ complex		No of Residue
PyDock	TIRAP	**R81,** W82, V130, K158, Y159, L162, Q163, L165, T166, E167, **P169,** E172, P189, E190, **F193, M194, Y195, R215** and T219	19
	PKCδ	K355, G356, S357, I385, D386, D387, D388, M434, I437, Q438, D475, P510, D511, G542, Q543, S544, H547, G548, D549, D550, E551, D632, E634, F635 and E638	25
ClusPro	TIRAP	S79, S80, **R81**, S83, K84, D85, D87, G109, S110, T111, A112, S113, L114, H141, **P169**, A171, C174, T175, I176, R192, **F193, M194, Y195**, Y196, V197, Q208, K210, A212, M214, **R215**, Y216, L217, Q218, T219, L220 and S221	36
	PKCδ	I385, D386, D387, V346, M492, N496, S504, T505, F506, I517, L522, Y523, E551, D552, F555, D646 and N648	17
HADDOCK 2.4	TIRAP	**R81**, L165, T166, E167, A168, **P169**, G170, A171, E172, P189, E190, R192, **F193, M194, Y195**, Y196, R200, G201, P202, R207, A212, **R215**, Y216	21
	PKCδ	K355, G356, S357, K360, D381, V382, I385, D386, D387, D549, D550, E551, D552, E634, F635, E638, R641, L642, S643, Y642, S645, D646, N648, L649	24
HADDOCK 2.4	TIRAP	S79, S80, **R81**, W82, **P169**, G170, A171, E172, R184, R192, **F193, M194, Y195**, Y196, G199, R200, G201, P202, A212, **R215**, Y216, T219, L220	23
	p-Y512 PKCδ	K355, G356, S357, D381, V382, L384, I385, D386, D387, P510, D549, D550, E551, D552, E634, F635, D646, K647, N648, L649, D651, S652	22

Table 5. 2. Interacting residues in the TIRAP and PKCδ docking complex. The interacting residues at the interface site were identified within the 4 A region of their interaction through the Chimera 1.13.1 tool. The highlighted bold residues represent the key common residues from each docked complex of TIRAP and PKCδ obtained from all three docking platforms pyDockWEB, ClusPro 2.0, and HADDOCK 2.4.

5.5.4. Virtual screening of drugs and in silico mutation study of the target protein

Previous studies on PKCδ and mainly on BTK interaction with TIRAP, including ours, focused on its downstream signalling only, and its therapeutic potential is not explored yet [16, 21, 54]. In this study, the structural analysis of TIRAP interaction with BTK

and PKCδ was focused on both understanding their interaction and eventually utilizing it as a potential therapeutic site. Therefore, the structural modelling of BTK and PKCδ with all necessary domains as discussed above, which were mostly excluded in previous studies, was very crucial here to establish the potential interface residue through protein–protein interaction. The modelled BTK and PKCδ containing the region of phosphorylation used to obtain the interacting complex with TIRAP in both states of non-phosphorylation and phosphorylation provided a very specific study of interface residues for the design of therapeutic sites. Based on this, the virtual screening was performed to identify drugs that potentially target these determined TIRAP sites that interact with BTK and PKCδ. We applied the concept of 'single drug dual action' to identify common sites in the TIRAP TIR domain where binding could competitively inhibit the interaction of both BTK and PKCδ. As discussed above in the docking results, all the TIRAP interacting residues in both docking complexes with BTK and PKCδ were determined within the 4 Å region of their binding using the Chimera 1.13.1 tool. To implement our concept of a common therapeutic site on TIRAP, we performed a comparative sequence analysis to determine the common residues in the TIR region involved in the interaction with both BTK and PKCδ in phosphorylated and non-phosphorylated states. Notably, the key residues P169, F193, M194, and Y195 from the C-terminal region were identified as the most promising region of TIRAP commonly involved in the interaction with both BTK and PKCδ in phosphorylated and non-phosphorylated states **(Figure 5.4a).** These residues are also among the top-most amino acids actively involved in complex stabilities as determined from their free binding energy (ΔGbind) contribution per residue, computed from MM/GBSA analysis of each protein-protein interaction in HawkDock tool [50]. However, to further validate the significance of these residues in complex with BTK and PKCδ, we performed a site-specific mutational study with these four residues of TIRAP. The residues were mutated with alanine (A) sequentially and combinedly at all four sites. The mutated TIRAP (muTIRAP) structures P169A TIRAP, F193A TIRAP, M194A TIRAP, Y195A TIRAP, and All04A TIRAP were docked both with BTK and PKCδ in their non-phosphorylated and phosphorylated state structures, and changes in the

binding energy were determined in comparison to the wild-type TIRAP (wtTIRAP) structure docking. Interestingly, the docking results obtained from HADDOCK 2.4 for each complex were analyzed in the PDBePISA tool for binding free energy, which displayed that the binding energies of muTIRAP structure complex with BTK and p-Y223 & p-Y551 BTK structure as well as with PKCδ and p-Y512 PKCδ structure were significantly reduced for most of the sites in comparison to the wtTIRAP docking complexes **(data shown in Supplementary Figure S5.2)**. The changes in the binding energy were obtained as −6, −5.9, −6.9, −10.7, and −7.1 kcal/mol as well as −5.7, −4.1, −8.1, −8.3, and −7.6 kcal/mol, respectively, between the docking complex of muTIRAP P169A, F193A, M194A, Y195A and All04A with BTK as well as p-Y223 & p-Y551 BTK when compared to −8.3 kcal/mol for both wtTIRAP and BTK as well as with p-Y223 & p-Y551 BTK complex. Similarly, it was obtained as −9.9, −6.5, −10.1, −11.1, and −7.1 kcal/mol as well as −9.7, −6.4, −8.3, −7.0, and −6.9 kcal/mol, respectively, between muTIRAP P169A, F193A, M194A, Y195A and All04A with PKCδ as well as p-Y512 PKCδ when compared to −11.9 and −8.6 kcal/ mol between wtTIRAP and PKCδ as well as p-Y512 PKCδ complex. Thus, reducing binding energies in the case of the muTIRAP structure signifies the importance of these residues at the site of the interacting interface and provides a therapeutic site to target the binding of both BTK and PKCδ with TIRAP and limit downstream signalling mediated via TIRAP. Therefore, for in silico screening of highly specific drug candidates, we performed unbiased blind docking of 1576 FDA-approved drugs with the TIRAP TIR protein structure. We utilized the ZINC15 drug database [32] to obtain the library of these approved drugs available commercially for purchase and hence subjected them to in silico screening. Potential candidates were screened, which could effectively block the site of TIRAP interaction with its activating partners BTK and PKCδ to regulate the downstream inflammatory signalling in macrophages. The TIRAP and drug blind docking were performed in the LibDock docking program of Discovery Studio 2020 [25]. The docked drug candidates were then arranged based on their LibDock score (in a higher to a lower value), and each drug candidate's interaction with TIRAP was studied in Discovery Studio Visualizer 2020 [25]. We

selected only those drug candidates that were specifically predicted to interact with most if not all the key residues of TIRAP **(Figure 5.4A)**. The top-scoring site-specific binding drug candidates shortlisted from this rigorous exercise were further filtered based on their known route of administration, where the candidates with the topical and other routes were excluded while retaining only the oral and intravenous drug candidates for further study. This exercise resulted in six FDA-approved drugs predicted to have potent TIPAP-BTK and TIRAP-PKCδ interaction-blocking activity: ZINC000036701290 (Ponatinib), ZINC000003939013 (Fosaprepitant), ZINC000027990463 (Lomitapide), ZINC000035902489 (Crizotinib), ZINC000003831151 (Montelukast), and ZINC000003816514 (Rolapitant). The interaction of all six drugs with the TIRAP target region is displayed together in **(Figure 5.4B)**. Furthermore, to cross-check the drug docking, we re-confirmed the blind docking of these six drugs through another docking platform, AutoDock Vina. The binding affinity of each drug with TIRAP was calculated in kcal/mol by AutoDock Vina and ranged from −9 kcal/mol to −7.2 kcal/mol. Thus, the docking results from Vina were consistent with our LibDock docking data. The details of all six drugs, their ZINC ID, common name, and known pharmacological actions along with the LibDock score (from Discovery Studio) and binding energy (from AutoDock Vina) are presented in **(Table 5.3)**.

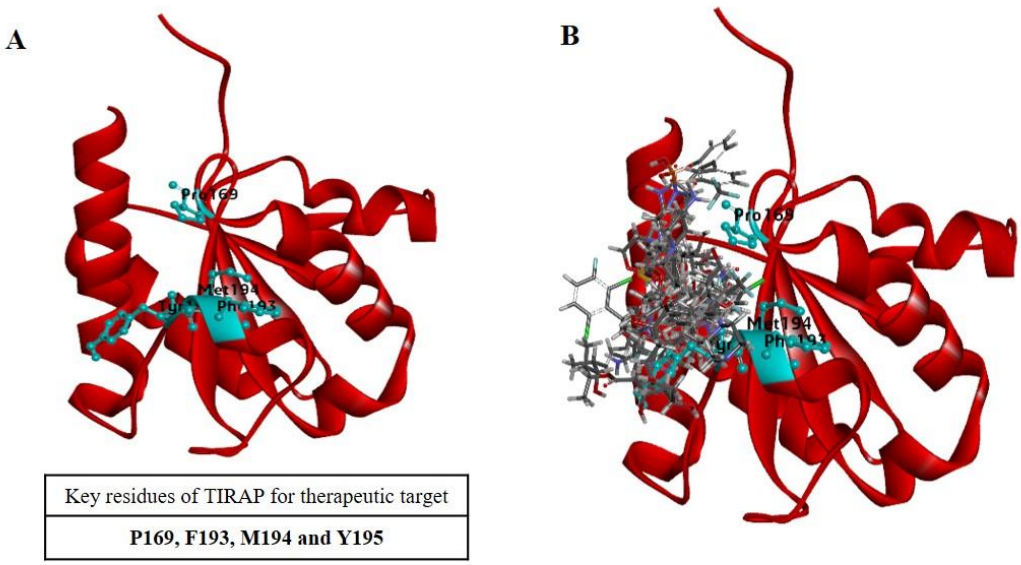

Figure 5. 5. Therapeutic target site on TIRAP TIR domain and interaction analysis of virtually screened drugs binding specifically to the key residues involved in the interaction with BTK and PKCδ kinase domains. (a) The key common interacting residues of TIRAP at the interface site of both BTK and PKC contributed significantly to the complex formation identified within the 4 A region (in the Chimera 1.13.1 tool) and were considered potential therapeutic targets for drug screening. (b) Docking pose of top-six screened drugs binding at the target region in TIRAP.

Individually, the TIRAP and each candidate drug interaction analysis were performed in Discovery Studio Visualizer. The candidate drugs were predicted to make several hydrogen bonds and other electrostatic bonding with the TIRAP target site residues **(Figure 5.5A–F)**. Docking of screened drugs with alanine mutated TIRAP (muTIRAP) shows reduced binding efficiency We re-performed the docking of the six FDA-approved screened drugs (Ponatinib, Fosaprepitant, Lomitapide, Crizotinib, Rolapitant, and Montelukast) with muTIRAP and their respective binding efficiencies to wtTIRAP in AutoDock Vina. The binding energy of all six drugs was reduced with the muTIRAP structure when compared to its wtTIRAP docking: wtTIRAP versus muTIRAP, −9 vs −7.9 kcal/mol for Lomitapide, −7.2 vs −7 kcal/mol for Crizotinib, −8.8 vs −7.8 kcal/mol for Rolapitant, and −8.4 vs −7.7 kcal/mol for Montelukast. These data provide further evidence for the significant role of the residues P169, F193,

M194, and Y195 in TIRAP as an optimal therapeutic target site efficient to block interaction both with BTK and PKCδ.

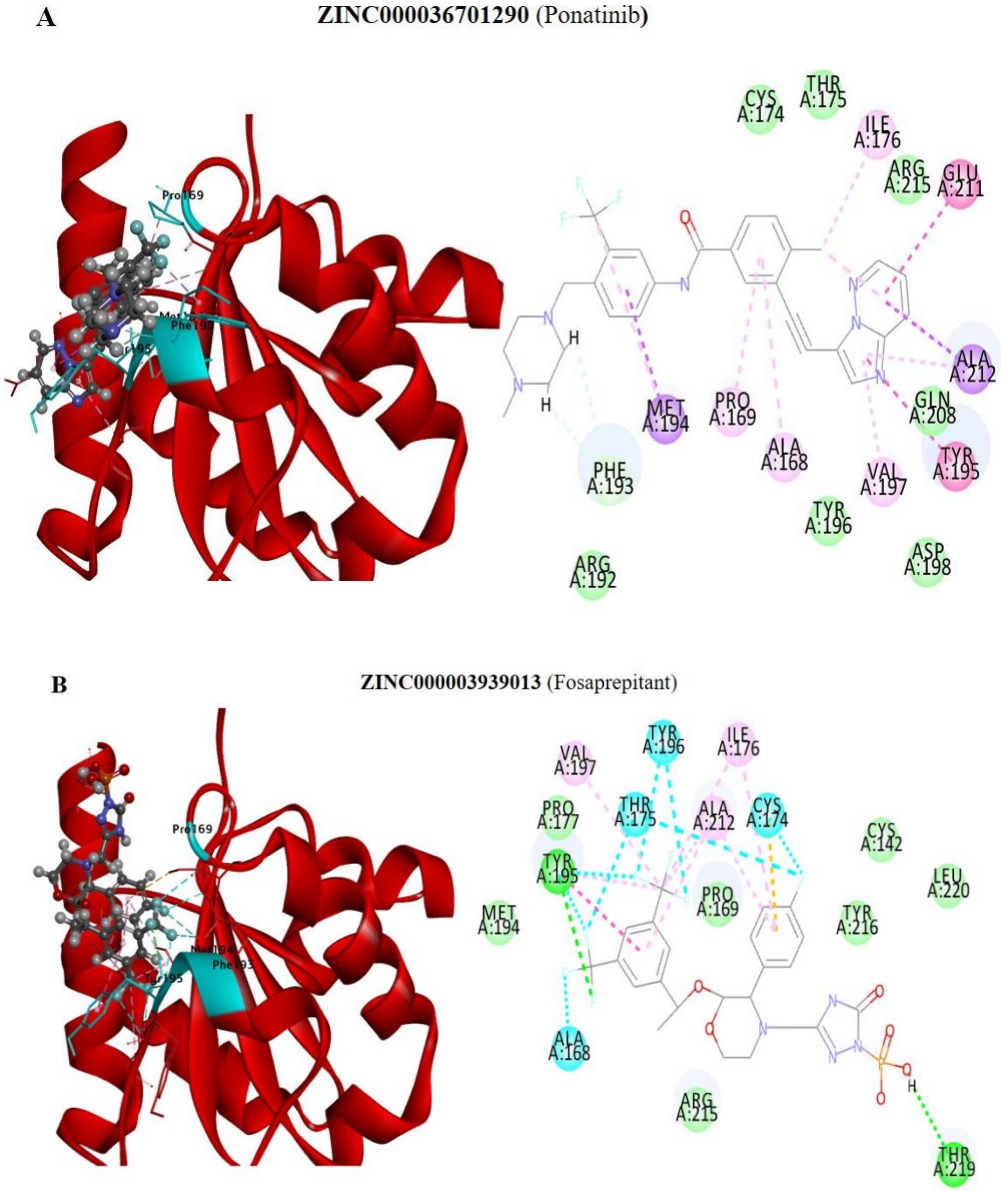

C **ZINC000027990463** (Lomitapide)

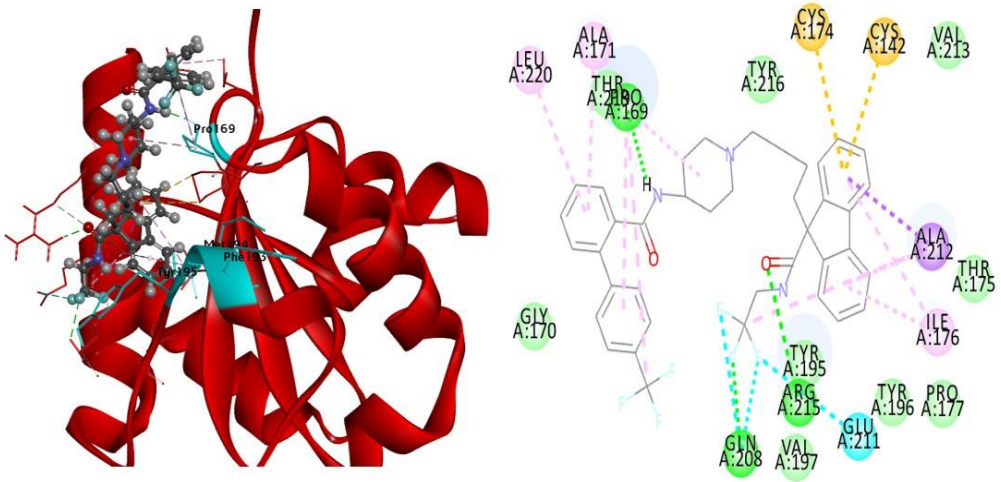

D **ZINC000035902489** (Crizotinib)

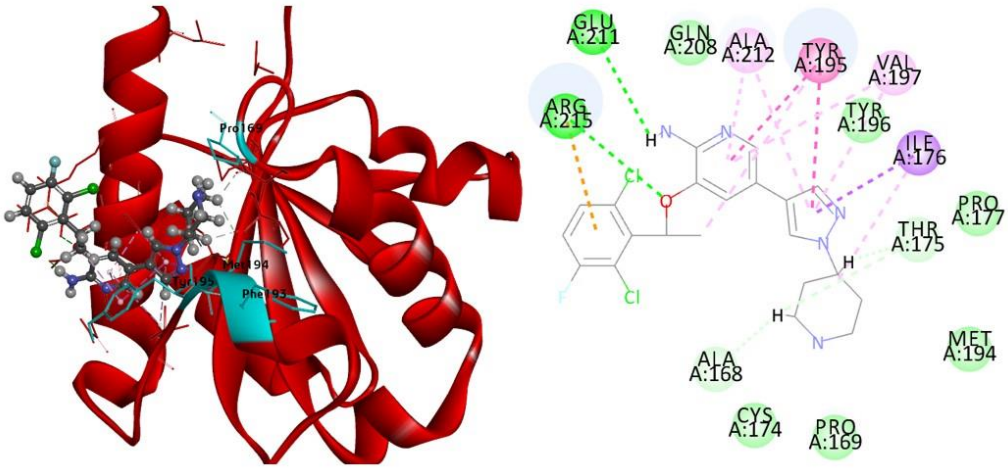

E **ZINC000003831151** (Montelukast)

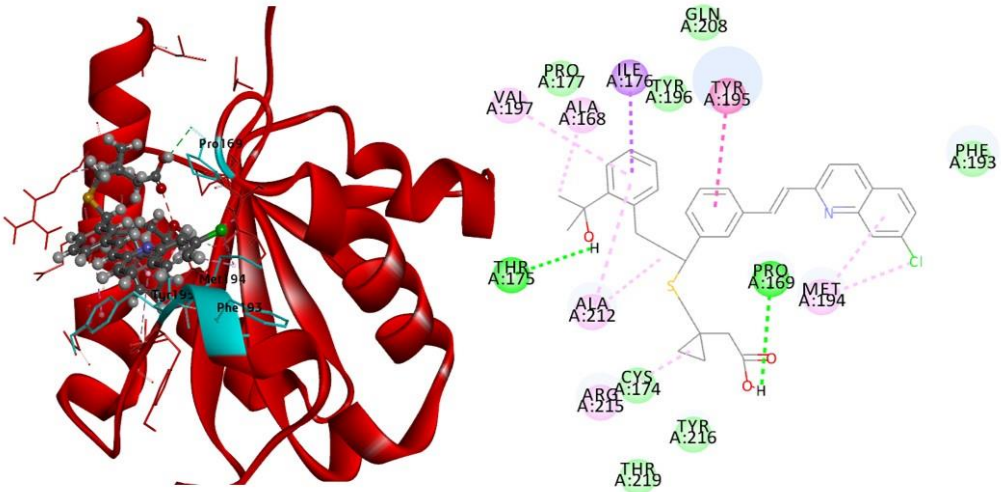

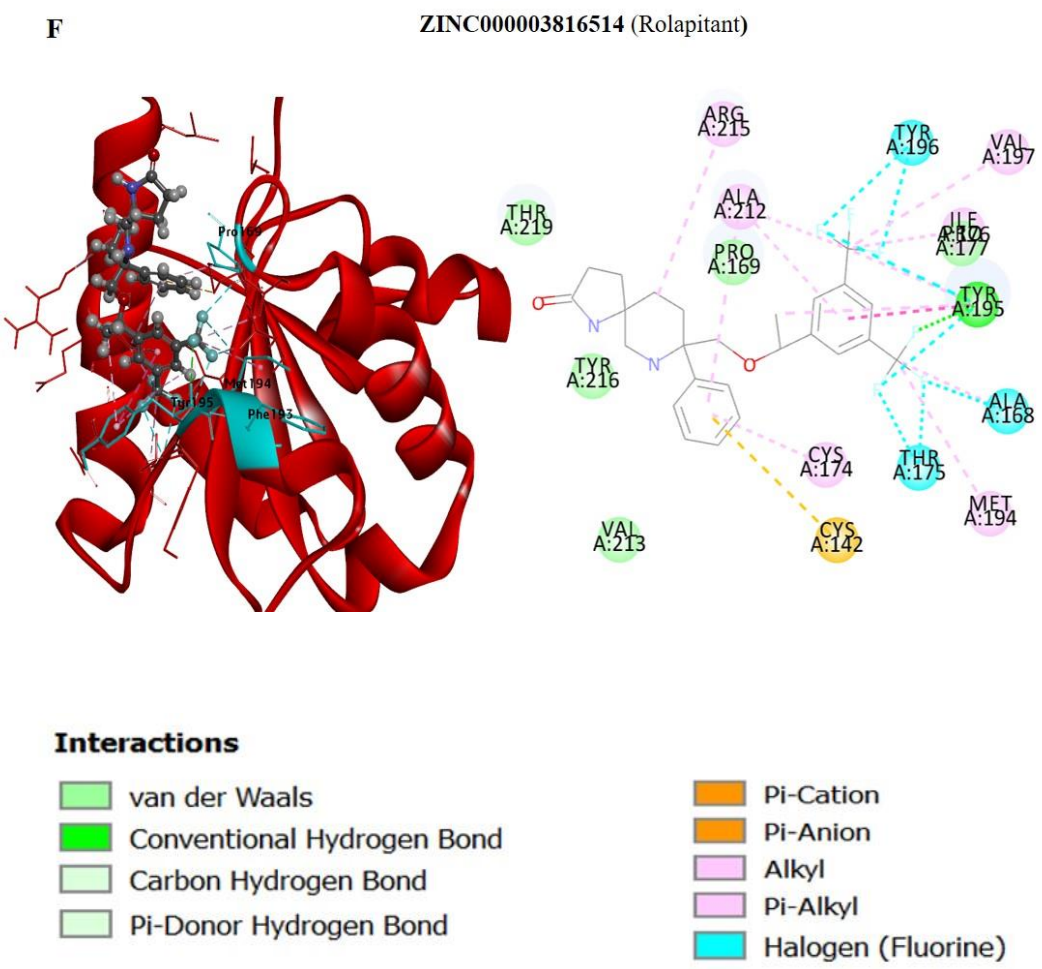

Figure 5. 6. The protein-ligand binding analysis of the top six virtually screened FDA-approved drug candidates for repurposing to inhibit TIRAP protein interaction with BTK and PKCδ. The images (A to F) represent the individual interaction pattern of each six drugs with TIRAP protein, presented both in 2D (2-Dimensional) and 3D (3-Dimensional) image format, reveals the identified key residues (P169, F193, M194, and Y195) of TIRAP being involved in the interaction with each of the drugs. Each drug-binding has been shown to make strong interaction with TIRAP which includes several hydrogen bonds along with other electrostatic interactions as identified from their specific colour code in 2D images. All the interactions are analysed in Discovery Studio visualizer tool.

Sr No.	ZINC Id	DS LibDock Score	AD Vina Binding Energy (kcal/mol)	Commercial Name	Route of Administration	Pharmacological Function	Mechanism of Action	References
1.	ZINC000036701290	130.419	-8.4	Ponatinib	Oral	Tyrosine kinase inhibitor	Targets Bcr-Abl tyrosine kinase protein and inhibits tyrosine activity of Abl.	[55-57]
2.	ZINC000003939013	124.109	-8.6	Fosaprepitant	Intravenous	Antiemetic drug for the prevention of acute and delayed nausea and vomiting associated with chemotherapy treatment.	Crosses the blood-brain barrier and occupies brain Neurokinin-1 (NK-1) receptors and acts as an antagonist	[58, 59]
3.	ZINC000027990463	123.773	-9	Lomitapide	Oral	Microsomal triglyceride transfer protein (MTP) inhibitor used in homozygous familial hypercholesterolemia (HoFH) patients	Inhibits MTP within the lumen of ER which prevents apolipoprotein B formation, and thus VLDL and chylomicrons as well	[60]
4.	ZINC000035902489	117.553	-7.2	Crizotinib	Oral	Tyrosine kinase receptor inhibitor for the treatment of non-small cell lung cancer (NSCLC)	In NSCLC, it inhibits anaplastic lymphoma kinase (ALK) resulting in decreased cell proliferation. Also inhibits hepatocyte growth factor receptor (HGFR, c-MET), and Recepteur d'Origine Nantais	[61]
5.	ZINC000003831151	116.719	-8.4	Montelukast	Oral	leukotriene receptor antagonist, prophylaxis and chronic treatment of asthma,exercise-induced bronchoconstriction (EIB)	Binds to CysLT type 1 receptor, which assists in inhibiting any physiological actions of CysLTs (Cysteinyl leukotrienes) at the receptor that may facilitate asthma or	[62]
6.	ZINC000003816514	116.701	-8.8	Rolapitant	Oral	NK-1 receptor antagonist prevents delayed chemotherapy-induced nausea and vomiting (CINV)	Binds to NK-1 receptor and prevents its binding with ligand Substance P which is released in the gut.	[63]

Table 5. 3. A list of six FDA-approved drugs virtually screened for repurposing as an inhibitor of TIRAP protein specifically targeting the region TIR domain involved in protein–protein interaction with BTK and PKCδ. The drug structures for the docking study were obtained from the ZINC15 database and their ZINC15 ID is mentioned along with their docking score with TIRAP protein as obtained in Discovery Studio (LibDock score) and AutoDock Vina (Binding energy) tools. Also, their pharmacological names, route of administration, known pharmacological functions, and mechanism of action are briefly described.

5.5.5. MD simulation of TIRAP and drugs complex

The docking complexes of TIRAP with ligands were used as the initial system for MD simulation to determine their stability in the protein-ligand complexes. Initially, a short MD simulation study for 1 ns (1000ps) was performed for all six drug complexes with TIRAP in the Discovery studio tool **(Supplementary Figure S5.3)**. An initial analysis of root mean square deviation (RMSD) from a simulation study of 1ns suggested that all the six drugs (ponatinib, fosaprepitant, lomitapide, crizotinib, rolapitant, and montelukast) complexes are stable with TIRAP with slight deviations and fluctuations in MD trajectories **(Supplementary Figure S5.3)**. Further, an extended MD simulation of 100 ns was performed for the Apo protein (TIRAP only) and each of the complexes using the Gromacs 4.6 program. The analysis of RMSD and root mean square fluctuation (RMSF) throughout the MD trajectory suggested no significant deviations and fluctuations in the Apo protein backbone structure and its binding interface residue as well as its complexes with four ligands **(Figure 5.6A–B)**. In complexes, the four ligands (lomitapide, crizotinib, rolapitant and montelukast) showed no deviation from the docking predicted binding mode, throughout the 100 ns simulation **(Figure 5.6A)**. However, the ponatinib and fosaprepitant complex simulation was not comparable with these four drugs and their MD trajectories showed some deviations and fluctuations. The lower deviation is associated with better conformational stability. The TIRAP complex with rolapitant and crizotinib showed no such deviations. In addition, the TIRAP-montelukast initially showed a slight fluctuation at around 10 ns while the same has been observed in the TIRAP and

lomitapide complex at around 70 ns **(Figure 5.6A)**. However, all the complexes were shown to converge with no deviations at the end of the simulation study and suggest the complex stability throughout the simulation of 100 ns. Slight conformational and positional rearrangements might have accounted for some of the deviations and fluctuations; however, ligands remained bound with TIRAP for the entire 100ns MD trajectory. The average RMSD for Apo (TIRAP) was 2.73 ± 0.46 Å while it was 3.49 ±0.50 Å, 2.70 ± 0.40 Å, 2.72 ± 0.34 Å, and 3.19 ± 0.33 Å for TIRAP complexes with lomitapide, crizotinib, rolapitant, and montelukast, respectively. To further estimate the energetics of these ligands binding to TIRAP, MM-PBSA analysis was performed using a full 100ns MD trajectory, which revealed their binding energies (ΔG_{bind}) **(Table 5.4)**. Therefore, based on the extended MD simulation study, we found these four drugs (lomitapide, crizotinib, rolapitant, and montelukast) to be more promising in stable binding with the TIRAP interface site, which could have the potential to block the interaction of the BTK and PKCδ kinases. Further validation in in-vitro and in-vivo models will be interesting for repurposing as an inflammatory agent.

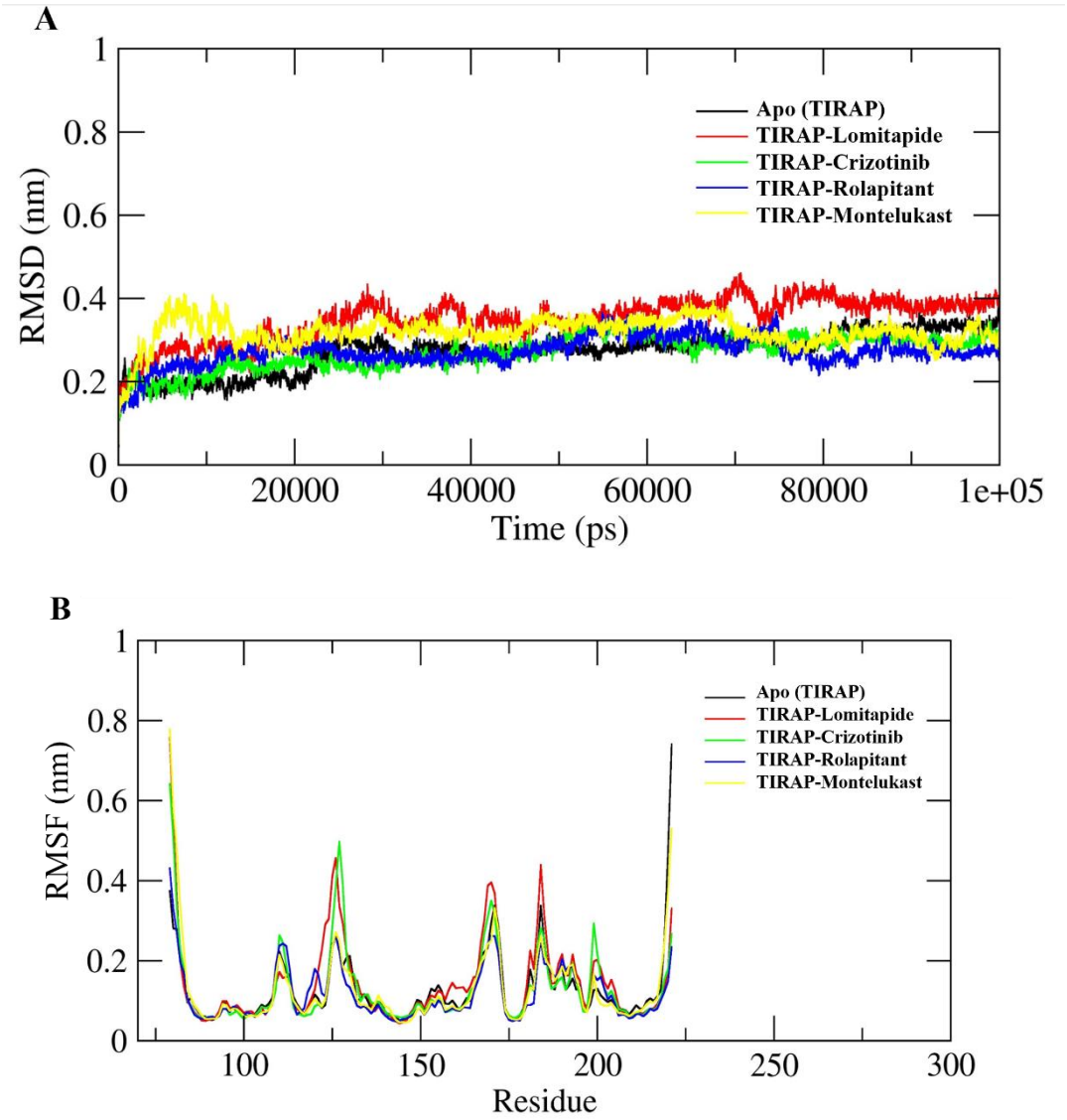

Figure 5. 7. Molecular Dynamic (MD) simulation of TIRAP and drugs complex. A total simulation of 100ns was performed in Gromacs 4.6 and all the complexes represent a stable complex conformation as represented in the plot of (a) RMSD (root mean square deviation) values against total simulation time, and (b) RMSF (root mean square fluctuation) values against the residue numbers.

5.5.6. Effect of drug treatment on cytokine expression in macrophages

We sought to test the potential effect of all six drugs at the cellular level through the analysis of end-point inflammatory cytokines expression in LPS-stimulated

macrophage cell line RAW 264.7. Similar to our previous study with DZD, we performed the analysis at an early time point of 1h for all six drugs. Interestingly, we observed that the mRNA expression of major pro-inflammatory cytokines, through the qRT-PCR experiment, was significantly downregulated in LPS-stimulated RAW264.7 macrophages for all the drugs **(Figure 5.8)**. This briefly indicates the anti-inflammatory effect of these drugs in the TLR4 pathway which is screened to dampen the interaction of TIRAP with both kinase BTK and PKCδ. However, further validation at the interaction level is warranted for its validation.

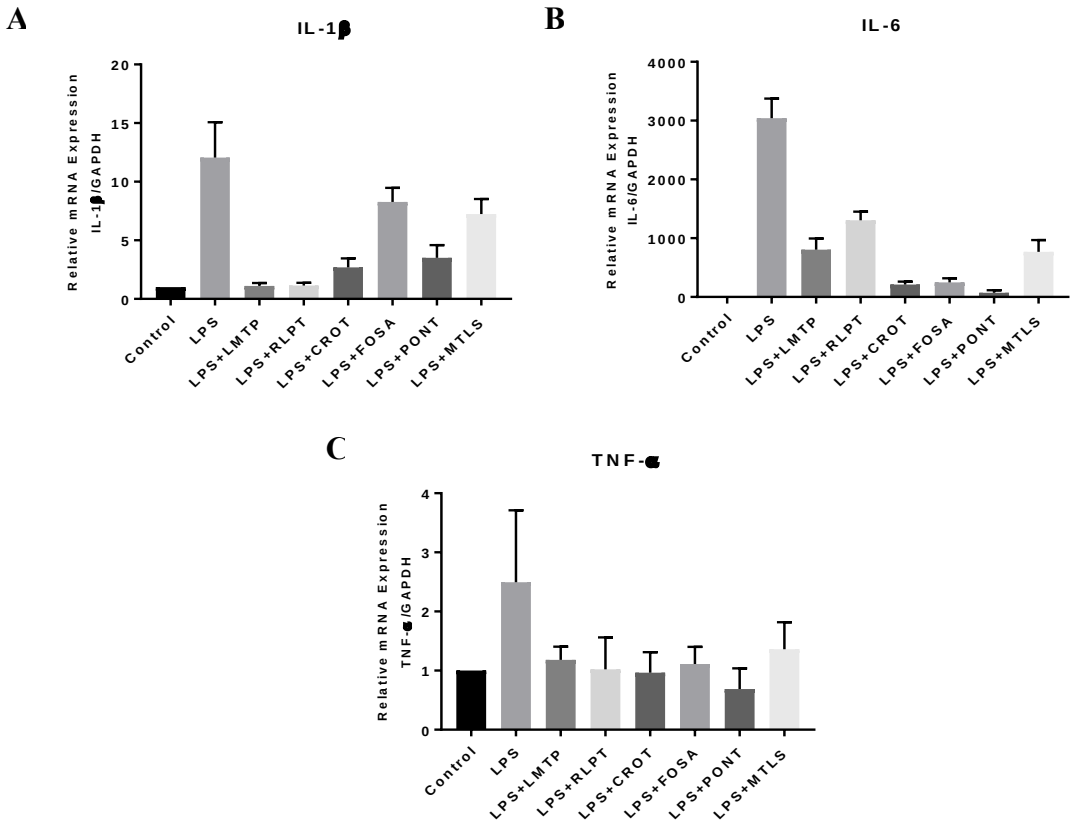

Figure 5. 8. Relative mRNA expression of pro-inflammatory cytokines in mouse RAW264.7 cells stimulated with LPS (500ng/ml) for 1h and treated with drugs (1μM each) 15min before LPS. The plot represents the (A) IL-1β, (B) IL-6, and (C) TNF-α mRNA expression normalized with housekeeping gene GAPDH at 1h. The data represents the three independent set of experiments. LMTP- Lomitapide; RLPT- Rolapitant; CROT- Crizotinib; FOSA- Fosaprepitant; PONT- Ponatinib; and MTLS- Montelukast.

5.6. Discussion

We have used an in-silico PPI-based strategy to identify the four drugs that are predicted to be stable in the TIRAP-binding pocket and could selectively block TIRAP-BTK and TIRAP–PKCδ interactions and therefore downstream inflammatory signalling in TLR4/2 expressing cells. In TLR4/2 signalling, the transduction of signals mainly initiates the interaction of the TIR domains of receptor and adaptor proteins. However, besides this TIR–TIR interaction, the upstream kinases BTK, as well as PKCδ, plays a crucial role in regulating downstream signalling via the adaptor protein TIRAP. The TIRAP subcellular localization mainly at the cell membrane and in cytoplasm uniquely allows it to interact with both membrane-bound and cytoplasmic proteins and hence leads to signalling, which may cause transactivation of transcription factors alongside its well-known bridging role in MyD88-dependent pathway leading to mainly NF-κB and AP-1 activation and hence pro-inflammatory responses [4, 64-66] **(Figure 5.7)**. Previous studies have reported the interaction of TIRAP with BTK and PKCδ in endotoxin-induced macrophages as a crucial step in inflammatory signalling, predominantly through TIRAP tyrosine phosphorylation and activation of the TIR domain. The activation of TLR4 by ligands, such as its classical ligand lipopolysaccharide (LPS), leads to the activation of a series of kinases such as Lck, Src, BTK, and PKCδ, which eventually phosphorylates the TLR4 as well as the TIRAP TIR domain. In LPS-stimulated macrophages, BTK is activated and regulates TIRAP function through tyrosine phosphorylation. Besides, the PKCδ has been equally appreciated in inflammatory signalling and its activation in LPS-stimulated TLR4 signalling also regulates the inflammatory response via TIRAP tyrosine phosphorylation **(Figure 5.7)** [11, 12, 15-17, 21]. Therefore, the understanding of TIRAP and tyrosine kinases BTK as well as PKCδ protein-protein interaction could be significant in regulating the inflammatory responses and may consider an effective therapeutic target. Several pharmacological inhibitors have been designed that either target BTK or PKCδ. Notably, direct inhibition of these two molecules may negatively impact other canonical signalling pathways, even in the absence of inflammation [67-70]. However, the adaptor protein TIRAP, which is central to TLR4 inflammatory

signalling, may serve as a potential upstream therapeutic target for several inflammatory-associated diseases. The precise molecular interaction of TIRAP with BTK and PKCδ, required to generate a selective therapeutic target, has not been previously described. A critical step in defining therapeutic sites is the structural analysis of interacting proteins and their binding complex. To obtain this, the prerequisite material is a suitable structure of these proteins. Unfortunately, the required crystal structure of BTK with SH3, SH2, and kinase domains and PKCδ with the kinase domain is not available in the protein database, and no such model structures with these domains are modelled previously. Hence, we focused to create high-quality homology-based 3D structure models of both the structures and completing the loop modelling of the TIRAP crystal structure missing important loops from residue positions 110 to 127 in the TIR structure. The crucial step in structure modelling is the selection of templates for modelling and structural analysis of the modelled structure because a low-quality structure and missing residues may negatively impact protein–protein docking studies and drug screening [71]. Therefore, we used a multi-template approach to obtain a modelled structure with proper folding supported by the matching templates. The multiple templates of high sequence identity with target protein provide a continuous platform for modelling tools for a better model structure without any loop or residue gap in the structure. Further, we performed a multi-step quality check of our modelled structure to obtain the structures, with the highest quality satisfying all the important stereochemical parameters. The modelled structure was subjected to several loop refinements for proper folding of certain outlier regions, and stereochemical parameters were re-confirmed to obtain a near-native folding based on the Ramachandran plot and other quality indexes. Further, the modelled structures were also subjected to an overall refinement process in the GalaxyWeb refine the tool and overall assessment and validation in the ProTSAV tool, which confirms that all three modelled structure quality scores are in the range of 2–3 Å. Finally, our modelled structures were compared with the templates to obtain the root mean square deviation (RMSD) between the modelled and experimentally solved crystal structures, which showed the RMSD significantly below 1 Å for all the three model structures of BTK,

PKCδ, and loop modelled TIRAP. Therefore, we further considered these modelled structures for our protein–protein docking studies to achieve the potential interface residues for the therapeutic target. In order to mimic the native conditions, the protein–protein docking complexes of TIRAP with inactive non-phosphorylated and active tyrosine-phosphorylated BTK and PKCδ were crucial in determining potential therapeutic sites. We used three different docking platforms (HADDOCK 2.4, pyDockWEB, and ClusPro 2.0) to cross-check the docking results of the complexes. Importantly, the structural analysis from all docking platforms confirms the TIRAP TIR domain interaction with the kinase domain of BTK and PKCδ. Therefore, for a therapeutic molecule to abolish both of these interactions, we determined closely interacting residues within the 4 Å region of TIRAP-BTK and TIRAP-PKCδ complex interfaces. Finally, the comparative analysis between their interacting residues was conducted to determine that the common residues of the TIRAP TIR domain P169, F193, M194, and Y195 from the C-terminal region significantly interacted with both the kinase domains from BTK and PKCδ. Hence, they were determined to serve as the best target site for drug repurposing. Structure-based drug screening against TIRAP was performed in the Discovery studio LibDock module. The proposed set of six virtually screened FDA-approved drugs with repurposing potential, block the interface site in the TIR domain of TIRAP which accommodates the key interacting residues involved in the interaction with both BTK and PKCδ. Moreover, these six drug candidates were re-confirmed with another docking platform AutoDock Vina, suggesting their specificity towards the determined target site on TIRAP. Further, the MD simulation study suggested the four drugs lomitapide, crizotinib, rolapitant and monteleukast as promising compounds in terms of their highly stable binding with TIRAP which remained bound to TIRAP throughout the simulation study with no deviations. The ponatinib and fosaprepitatnt simulation was not comparable with these four compounds in complex with TIRAP due to their deviations and fluctuations from the binding site. The strengths of this study are the novelty in describing the in silico structural and molecular PPI of TIRAP with BTK and PKCδ and the rigour of using more than one computational docking platform to confirm the findings. The weakness

of the study is that the potential repurposed drugs have not yet been tested in a biological system. The structural analysis of our above-studied interactions and repurposing of the in silico predicted FDA-approved drugs as anti-inflammatory agents targeting the TIRAP interactions hold a promising opportunity to counter the inflammatory responses in particular driven by macrophages signalling in the host. Therefore, we plan to perform the in vitro and in vivo validation of these drugs to harness their full therapeutic potential for better human health.

5.7. References

1. Fujiwara, N. and K. Kobayashi, *Macrophages in inflammation.* Current Drug Targets-Inflammation & Allergy, 2005. **4**(3): p. 281-286.
2. Rankin, J.A., *Biological mediators of acute inflammation.* AACN Clin Issues, 2004. **15**(1): p. 3-17.
3. Cohen, H.B. and D.M. Mosser, *Extrinsic and intrinsic control of macrophage inflammatory responses.* J Leukoc Biol, 2013. **94**(5): p. 913-9.
4. Barton, G.M. and R. Medzhitov, *Toll-like receptor signaling pathways.* Science, 2003. **300**(5625): p. 1524-5.
5. Sabroe, I., et al., *The role of TLR activation in inflammation.* J Pathol, 2008. **214**(2): p. 126-35.
6. Verstak, B., et al., *MyD88 adapter-like (Mal)/TIRAP interaction with TRAF6 is critical for TLR2- and TLR4-mediated NF-kappaB proinflammatory responses.* J Biol Chem, 2009. **284**(36): p. 24192-203.
7. O'Neill, L.A. and A.G. Bowie, *The family of five: TIR-domain-containing adaptors in Toll-like receptor signalling.* Nat Rev Immunol, 2007. **7**(5): p. 353-64.
8. Chen, L., et al., *Inflammatory responses and inflammation-associated diseases in organs.* Oncotarget, 2018. **9**(6): p. 7204-7218.
9. Kawasaki, T. and T. Kawai, *Toll-like receptor signaling pathways.* Front Immunol, 2014. **5**: p. 461.
10. Belhaouane, I., et al., *Paradoxical Roles of the MAL/Tirap Adaptor in Pathologies.* Front Immunol, 2020. **11**: p. 569127.
11. Jefferies, C.A. and L.A. O'Neill, *Bruton's tyrosine kinase (Btk)-the critical tyrosine kinase in LPS signalling?* Immunol Lett, 2004. **92**(1-2): p. 15-22.
12. Kubo-Murai, M., et al., *Protein kinase Cδ binds TIRAP/Mal to participate in TLR signaling.* Molecular immunology, 2007. **44**(9): p. 2257-2264.
13. Sakaguchi, M., et al., *TIRAP, an adaptor protein for TLR2/4, transduces a signal from RAGE phosphorylated upon ligand binding.* PLoS One, 2011. **6**(8): p. e23132.
14. Rajpoot, S., et al., *TIRAP in the Mechanism of Inflammation.* Front Immunol, 2021. **12**: p. 697588.
15. Lopez-Herrera, G., et al., *Bruton's tyrosine kinase--an integral protein of B cell development that also has an essential role in the innate immune system.* J Leukoc Biol, 2014. **95**(2): p. 243-50.
16. Paracha, R.Z., et al., *Structural evaluation of BTK and PKCdelta mediated phosphorylation of MAL at positions Tyr86 and Tyr106.* Comput Biol Chem, 2014. **51**: p. 22-35.
17. Loegering, D.J. and M.R. Lennartz, *Protein kinase C and toll-like receptor signaling.* Enzyme Res, 2011. **2011**: p. 537821.
18. Steinberg, S.F., *Structural basis of protein kinase C isoform function.* Physiol Rev, 2008. **88**(4): p. 1341-78.
19. Yang, Q., et al., *The Role of Tyrosine Phosphorylation of Protein Kinase C Delta in Infection and Inflammation.* Int J Mol Sci, 2019. **20**(6).
20. Gray, P., et al., *MyD88 adapter-like (Mal) is phosphorylated by Bruton's tyrosine kinase during TLR2 and TLR4 signal transduction.* 2006. **281**(15): p. 10489-10495.
21. Baig, M.S., et al., *Heterotrimeric complex of p38 MAPK, PKCdelta, and TIRAP is required for AP1 mediated inflammatory response.* Int Immunopharmacol, 2017. **48**: p. 211-218.

22. Vignon, P., et al., *New Agents in Development for Sepsis: Any Reason for Hope?* Drugs, 2020. **80**(17): p. 1751-1761.
23. Webb, B. and A. Sali, *Protein Structure Modeling with MODELLER.* Methods Mol Biol, 2021. **2199**: p. 239-255.
24. Webb, B. and A. Sali, *Comparative Protein Structure Modeling Using MODELLER.* Curr Protoc Protein Sci, 2016. **86**: p. 2 9 1-2 9 37.
25. BIOVIA, D.S., *BIOVIA Discovery Studio 2020.* San Diego: Dassault Systemes, 2020.
26. Pettersen, E.F., et al., *UCSF Chimera--a visualization system for exploratory research and analysis.* J Comput Chem, 2004. **25**(13): p. 1605-12.
27. Shapovalov, M.V. and R.L. Dunbrack Jr, *A smoothed backbone-dependent rotamer library for proteins derived from adaptive kernel density estimates and regressions.* Structure, 2011. **19**(6): p. 844-858.
28. Jimenez-Garcia, B., C. Pons, and J. Fernandez-Recio, *pyDockWEB: a web server for rigid-body protein-protein docking using electrostatics and desolvation scoring.* Bioinformatics, 2013. **29**(13): p. 1698-9.
29. Alekseenko, A., et al., *Protein-Protein and Protein-Peptide Docking with ClusPro Server.* Methods Mol Biol, 2020. **2165**: p. 157-174.
30. Comeau, S.R., et al., *ClusPro: a fully automated algorithm for protein-protein docking.* Nucleic Acids Res, 2004. **32**(Web Server issue): p. W96-9.
31. van Zundert, G.C. and A.M. Bonvin, *Modeling protein-protein complexes using the HADDOCK webserver "modeling protein complexes with HADDOCK".* Methods Mol Biol, 2014. **1137**: p. 163-79.
32. Sterling, T. and J.J. Irwin, *ZINC 15--Ligand Discovery for Everyone.* J Chem Inf Model, 2015. **55**(11): p. 2324-37.
33. Trott, O. and A.J. Olson, *AutoDock Vina: improving the speed and accuracy of docking with a new scoring function, efficient optimization, and multithreading.* J Comput Chem, 2010. **31**(2): p. 455-61.
34. van Zundert, G.C.P., et al., *The HADDOCK2.2 Web Server: User-Friendly Integrative Modeling of Biomolecular Complexes.* J Mol Biol, 2016. **428**(4): p. 720-725.
35. Hess, B., et al., *GROMACS 4: Algorithms for Highly Efficient, Load-Balanced, and Scalable Molecular Simulation.* J Chem Theory Comput, 2008. **4**(3): p. 435-47.
36. Van Der Spoel, D., et al., *GROMACS: fast, flexible, and free.* J Comput Chem, 2005. **26**(16): p. 1701-18.
37. Lindorff-Larsen, K., et al., *Improved side-chain torsion potentials for the Amber ff99SB protein force field.* 2010. **78**(8): p. 1950-1958.
38. Johnson, M., et al., *NCBI BLAST: a better web interface.* Nucleic Acids Res, 2008. **36**(Web Server issue): p. W5-9.
39. Rose, P.W., et al., *The RCSB Protein Data Bank: redesigned web site and web services.* Nucleic Acids Res, 2011. **39**(Database issue): p. D392-401.
40. Larsson, P., et al., *Using multiple templates to improve quality of homology models in automated homology modeling.* Protein Sci, 2008. **17**(6): p. 990-1002.
41. Chakravarty, S., et al., *Systematic analysis of the effect of multiple templates on the accuracy of comparative models of protein structure.* BMC Struct Biol, 2008. **8**: p. 31.
42. Cheng, J., *A multi-template combination algorithm for protein comparative modeling.* BMC Struct Biol, 2008. **8**: p. 18.

43. Fernandez-Fuentes, N., et al., *Comparative protein structure modeling by combining multiple templates and optimizing sequence-to-structure alignments.* Bioinformatics, 2007. **23**(19): p. 2558-65.
44. Arnold, K., et al., *The SWISS-MODEL workspace: a web-based environment for protein structure homology modelling.* Bioinformatics, 2006. **22**(2): p. 195-201.
45. Colovos, C. and T.O. Yeates, *Verification of protein structures: patterns of nonbonded atomic interactions.* Protein Sci, 1993. **2**(9): p. 1511-9.
46. Ko, J., et al., *GalaxyWEB server for protein structure prediction and refinement.* Nucleic Acids Res, 2012. **40**(Web Server issue): p. W294-7.
47. Benkert, P., M. Kunzli, and T. Schwede, *QMEAN server for protein model quality estimation.* Nucleic Acids Res, 2009. **37**(Web Server issue): p. W510-4.
48. Piao, W., et al., *Tyrosine phosphorylation of MyD88 adapter-like (Mal) is critical for signal transduction and blocked in endotoxin tolerance.* J Biol Chem, 2008. **283**(6): p. 3109-3119.
49. Kurosaki, T. and M. Kurosaki, *Transphosphorylation of Bruton's tyrosine kinase on tyrosine 551 is critical for B cell antigen receptor function.* J Biol Chem, 1997. **272**(25): p. 15595-8.
50. Weng, G., et al., *HawkDock: a web server to predict and analyze the protein-protein complex based on computational docking and MM/GBSA.* Nucleic Acids Res, 2019. **47**(W1): p. W322-W330.
51. Krissinel, E. and K.J.J.M.B. Henrick, *Protein interfaces, surfaces and assemblies service PISA at European Bioinformatics Institute.* 2007. **372**: p. 774-797.
52. Kubo-Murai, M., et al., *Protein kinase Cdelta binds TIRAP/Mal to participate in TLR signaling.* Mol Immunol, 2007. **44**(9): p. 2257-64.
53. Kronfeld, I., et al., *Phosphorylation of protein kinase Cdelta on distinct tyrosine residues regulates specific cellular functions.* J Biol Chem, 2000. **275**(45): p. 35491-8.
54. Jefferies, C.A., et al., *Bruton's tyrosine kinase is a Toll/interleukin-1 receptor domain-binding protein that participates in nuclear factor kappaB activation by Toll-like receptor 4.* J Biol Chem, 2003. **278**(28): p. 26258-64.
55. Cortes, J.E., et al., *Ponatinib in refractory Philadelphia chromosome–positive leukemias.* 2012. **367**(22): p. 2075-2088.
56. Ren, M., et al., *Novel FGFR inhibitor ponatinib suppresses the growth of non-small cell lung cancer cells overexpressing FGFR1.* 2013. **29**(6): p. 2181-2190.
57. O'Hare, T., et al., *AP24534, a pan-BCR-ABL inhibitor for chronic myeloid leukemia, potently inhibits the T315I mutant and overcomes mutation-based resistance.* 2009. **16**(5): p. 401-412.
58. Aapro, M., et al., *Aprepitant and fosaprepitant: a 10-year review of efficacy and safety.* 2015. **20**(4): p. 450.
59. Grunberg, S., et al., *Single-dose fosaprepitant for the prevention of chemotherapy-induced nausea and vomiting associated with cisplatin therapy: randomized, double-blind study protocol—EASE.* 2011. **29**(11): p. 1495-1501.
60. Sacks, F.M., M. Stanesa, and R.A.J.J.i.m. Hegele, *Severe hypertriglyceridemia with pancreatitis: thirteen years' treatment with lomitapide.* 2014. **174**(3): p. 443-447.
61. Timm, A. and J.M.J.A.j.o.h.-s.p. Kolesar, *Crizotinib for the treatment of non-small-cell lung cancer.* 2013. **70**(11): p. 943-947.
62. Zhang, Y.-J., et al., *Montelukast modulates lung CysLT1 receptor expression and eosinophilic inflammation in asthmatic mice.* 2004. **25**(10): p. 1341-1346.

63. Duffy, R.A., et al., *Rolapitant (SCH 619734): a potent, selective and orally active neurokinin NK1 receptor antagonist with centrally-mediated antiemetic effects in ferrets.* 2012. **102**(1): p. 95-100.
64. Kawasaki, T. and T. Kawai, *Toll-like receptor signaling pathways.* Frontiers in immunology, 2014: p. 461.
65. Kagan, J.C. and R. Medzhitov, *Phosphoinositide-mediated adaptor recruitment controls Toll-like receptor signaling.* Cell, 2006. **125**(5): p. 943-55.
66. Piao, W., et al., *Tyrosine phosphorylation of MyD88 adapter-like (Mal) is critical for signal transduction and blocked in endotoxin tolerance.* J Biol Chem, 2008. **283**(6): p. 3109-19.
67. Owen, C., et al., *Review of Bruton tyrosine kinase inhibitors for the treatment of relapsed or refractory mantle cell lymphoma.* Curr Oncol, 2019. **26**(2): p. e233-e240.
68. Soltoff, S.P., *Rottlerin: an inappropriate and ineffective inhibitor of PKCdelta.* Trends Pharmacol Sci, 2007. **28**(9): p. 453-8.
69. Wermuth, P.J., S. Addya, and S.A. Jimenez, *Effect of protein kinase C delta (PKC-delta) inhibition on the transcriptome of normal and systemic sclerosis human dermal fibroblasts in vitro.* PLoS One, 2011. **6**(11): p. e27110.
70. Mochly-Rosen, D., K. Das, and K.V. Grimes, *Protein kinase C, an elusive therapeutic target?* Nat Rev Drug Discov, 2012. **11**(12): p. 937-57.
71. Rodrigues, J.P., et al., *Defining the limits of homology modeling in information-driven protein docking.* Proteins, 2013. **81**(12): p. 2119-28.

Chapter 6

(Conclusion and Future Prospects)

Chapter 06: Conclusion and Future Prospects

6.1. Graphical Summary

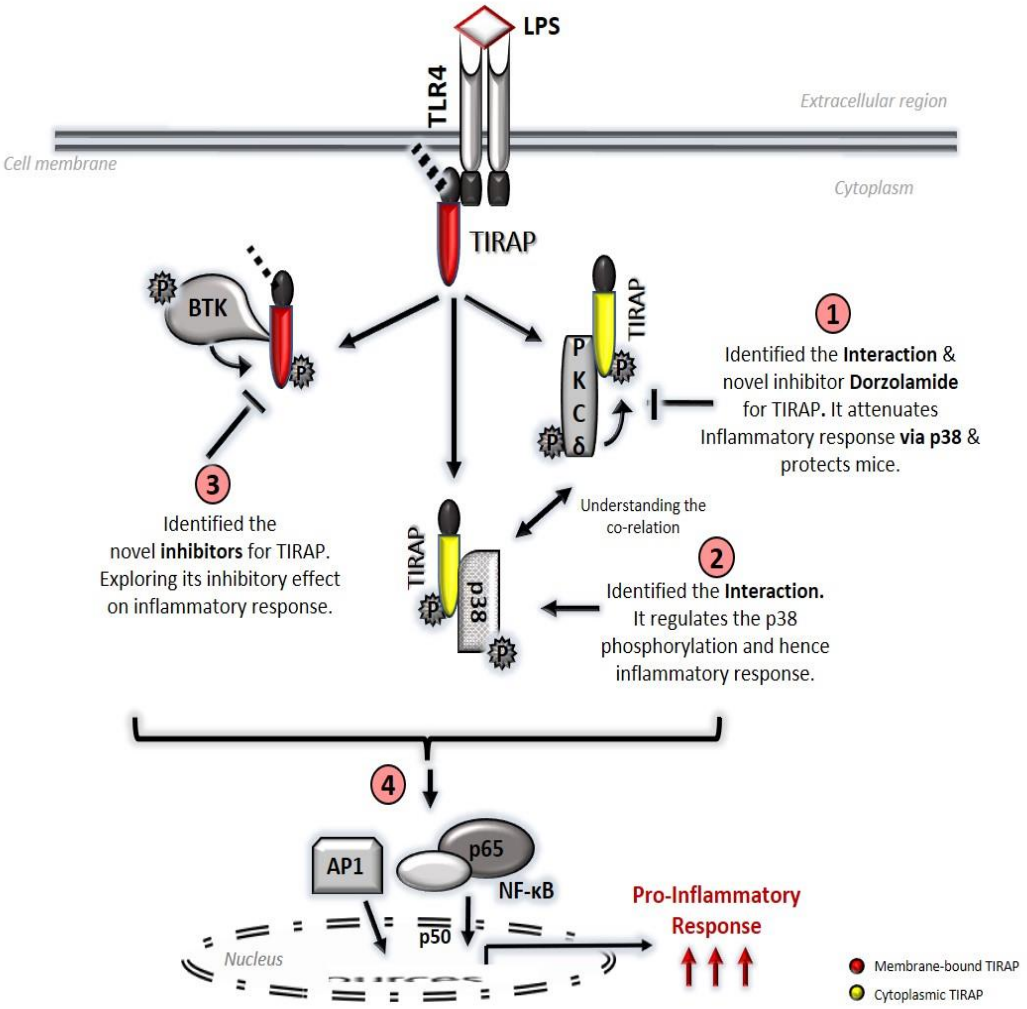

Figure 6. 1. *Overall therapeutic strategy against TIRAP-mediated inflammatory signaling in macrophage.*

6.2. Concluding key points

1. We identified a novel inflammatory pathway involved in TLR4-mediated signalling via the TIRAP and PKCδ interaction which leads to the upregulation of p38 MAPK and NF-κB activity. Meanwhile, the screened drug DZD shows effectively dampens the TIRAP-PKCδ interaction and attenuates the downstream pro-inflammatory response in cells and septic mouse model.
2. Further, another novel interaction between TIRAP and downstream p38 MAPK was identified. In macrophages, TIRAP shows enhanced interaction with p38 MAPK. A phosphorylated Y86 in the TIRAP TIR domain is found to be crucial in enhanced binding with p38 MAPK leading to its activation.
3. In addition to our newly identified TIRAP-PKCδ mediated inflammatory pathway in macrophages, TIRAP activation by its tyrosine phosphorylation is well known to be regulated by BTK. In sepsis pathophysiology, we proposed to completely block the known TIRAP activity by dampening its interaction with both upstream kinases PKCδ and BTK. We, therefore, identified six potential FDA-approved drugs that can simultaneously act on the common interface of TIRAP involved in interactions with BTK and PKCδ.
4. Our overall strategy is to regulate TIRAP involved in inflammatory signalling events through the activation of different downstream molecules which eventually regulate the expression of inflammatory cytokines and mediators via crucial transcription factors AP-1 and NF-κB

6.3. Overall Conclusion

The report that TIRAP acts as a second adaptor protein after MyD88 in the year 2001 was marked as a major discovery in the mechanism of TLR4-dependent inflammatory signaling. Subsequently, two more adaptor proteins, TRIF and TRAM, mostly responsible for IRF3 activation, were added to the family of TIR domain-containing adaptor proteins. However, more recent studies show that TIRAP not only acts as a bridging protein between TLR4/2 and MyD88 but also propagates the transduction of

downstream signaling events, sometimes in a MyD88-independent manner. Clearly, the ability of TIRAP to interact and collaborate with several signalling molecules in a context-dependent manner validates it as a major regulator of cell signalling.

Being central to innate immune response and canonically known for participation in inflammatory signaling mainly in macrophages, the TIRAP serves as a suitable and potential therapeutic target for the resolution of inflammation and its associated diseases. Recent reports indicate that there is no such drug that passed the clinical trials and is approved for sepsis that can work on host targets (57). Mostly, the treatment regimen includes the administration of antibiotics against foreign pathogens. However, ceasing the provoked and prolonged inflammation in response to such pathogens can not only be resolved by antibiotics but also by host target-specific drugs. Therefore, there is an urgent need to identify suitable targets in inflammation pathways and to develop target-specific drugs. In our study, TIRAP has been validated to be the one amongst others that could serve as an important target molecule in various inflammation-associated pathophysiological conditions. Its interaction profiling with other molecules in the early and late phases of inflammatory signalling has led us to understand the pattern of its regulation. We investigated a novel pathway of the TIRAP- PKCδ signalling axis via the p38 MAPK. This may further be studied in other sepsis models and patients. Further, DZD could be utilized to disrupt this interaction which would be beneficial in protection against inflammation However, DZD needs more biophysical, in-vivo, and clinical studies to establish its effect as an anti-inflammatory agent.

Our studies on TIRAP-PKCδ mediated signalling indicates the significance of downstream p38 MAPK activation. The inhibition of TIRAP-PKCδ interaction was directly associated with p38 MAPK phosphorylation and activation. Hence, we also studied the relation of TIRAP with p38 MAPK activation. We showed the significance of tyrosine phosphorylation of TIRAP-TIR dominant Y86 leading to an increase in p38 MAPK binding and activation. Henceforth, we combinedly propose the novel

PKCδ-TIRAP-p38 MAPK signalling axis as a potential therapeutic target that regulates the downstream activity of transcription factors in pathological conditions.

Furthermore, our study also explores the possibility of completely blocking the TIRAP activation by inhibiting its interaction with both the known upstream kinases; BTK and PKCδ. To do so, we employed a novel strategy of identifying the common interacting interface on TIRAP and identified six drugs that could potentially block their interactions with TIRAP thereby suppressing the chronic inflammatory responses. Interestingly, all the predicted drugs showed significant effects in attenuating the key pro-inflammatory cytokines in LPS-stimulated cells. However, these drugs need to be further tested through various experiments and in in-vivo models to identify the most suitable one with the highest efficacy. We propose to use these drugs as a combination therapy with in-use antibiotics for sepsis.

6.4. The future prospects

The TIRAP molecule holds a promising potential to study various pathological settings leading to inflammation-associated diseases. Our study is an attempt to reveal the numerous crucial activities of TIRAP in macrophage signaling besides its bridging role in the TLR pathway. This may attract many scientific communities to work more to explore TIRAP-mediated signalling as well as its regulation to counter uncontrolled inflammation. The idea to therapeutically target TIRAP is to solely develop host-target specific drug molecules for severe conditions like sepsis. In our study, we proposed to block the TIRAP activity by inhibiting its interaction with upstream kinases which are responsible for its tyrosine phosphorylation in the TIR domain and downstream function. The treatment of DZD represents a promising approach to targeting TIRAP-PKCδ inflammatory signaling. Meanwhile, six more drugs were tested in a preliminary set-up for their potential to completely block TIRAP activation by BTK as well as PKCδ. These approaches could be very crucial to counter the yet challenging and complex sepsis syndrome. We have chalked out key approaches which can help to

develop a novel host-specific therapy for sepsis through the regulation of master protein TIRAP.

6.4.1. Development of novel combination drug therapy for sepsis

The most interesting approach is to develop a novel combination drug therapy for sepsis which includes the use of both; in-market-in-use antibiotics along with DZD. The combination of the antibiotic and the target-specific drug may help to counter the conditions to subside both the pathogen load and host overstimulated immune response, respectively.

To mimic severe sepsis conditions, we also propose to develop a polymicrobial pathogen-infected mice model for sepsis. Cecal ligation puncture (CLP) is a time-consuming and tedious procedure and does not work well on large group experiments and is insufficient for studies on drug effect and survivability in-vivo. Hence, we propose to standardize the method through pathogen administration which can result in systemic sepsis condition.

6.4.2. Development of novel DZD derivatives for better efficacy

We have shown the potential of DZD as an anti-inflammatory agent. We are further interested to develop the derivatives or use the intermediates of DZD which can show an enhanced therapeutic potential and may be developed as novel drug molecules specific for TIRAP inhibition.

6.4.3. In-vitro and in-vivo validation of dual-inhibitors disrupting BTK and PKCδ interaction with TIRAP

The concept of completely blocking the TIRAP activation through its inhibition of interaction with upstream kinases; BTK and PKCδ holds a vast scope for future studies. We have shown the effect of drugs on cytokine expression at early time points only. Further, these drugs can be studied extensively to be validated as dual inhibitors.

6.4.4. TIRAP interaction profiling and Site-directed mutagenesis study

We propose to study the TIRAP interaction profiling at different stages of inflammation or in various pathological settings to understand its interaction pattern. Such profiling could provide us with knowledge of novel TIRAP interactions and would be beneficial to establish target-specific therapeutic molecules. We also plan to study and understand the effect of site-directed mutagenesis of crucial sites on TIRAP molecules involved in interactions with kinases and other proteins during the downstream inflammatory signaling pathways.

APPENDIX

(Supplementary Figures & Tables)

APPENDIX

Appendix A: Supplementary Figures

1. Supplementary Figures from Chapter 3: Dorzolamide (DZD) suppresses PKCδ-TIRAP-p38 MAPK signalling axis to dampen the inflammatory response

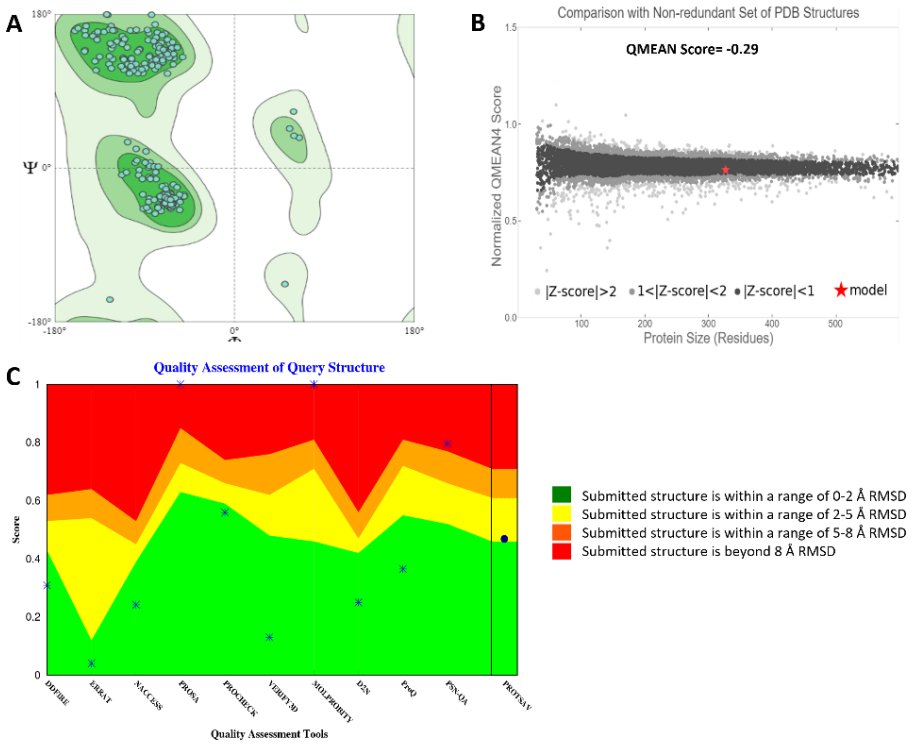

Supplementary Figure S3.1: Stereochemical analysis and structural validation of PKCδ model_5. (A) Ramachandran plot produced a 98.8% score for the model with no outlier residues in the unfavoured region, (B) QMEAN (Qualitative Model Energy ANalysis) quality factor normalized score with total protein size and its Z-score value, and (C) Overall structure assessment and validation by ProTSAV tools results in model structure quality score in the range of 2-2.5Å RMSD.

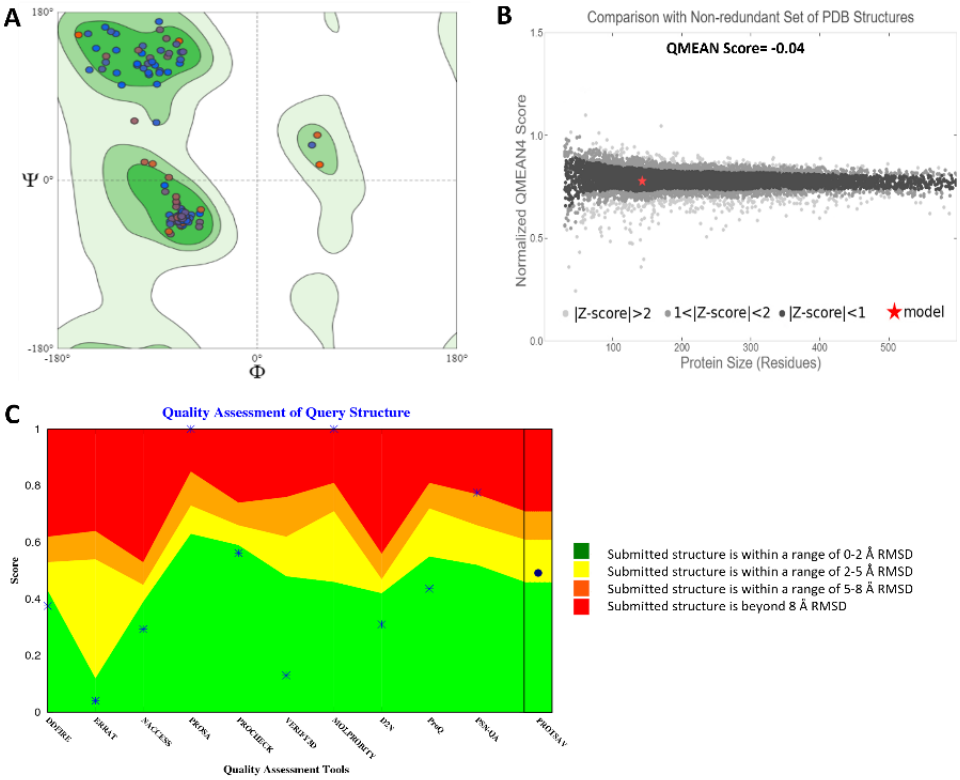

Supplementary Figure S3.2: Stereochemical analysis and structural validation of TIRAP model_2. (A) Ramachandran plot produced a 98.6% score for the model with no outlier residues in the unfavoured region, (B) QMEAN (Qualitative Model Energy ANalysis) quality factor normalized score with total protein size and its Z-score value, and (C) Overall structure assessment and validation by ProTSAV tools results in model structure quality score in the range of 2-3Å RMSD.

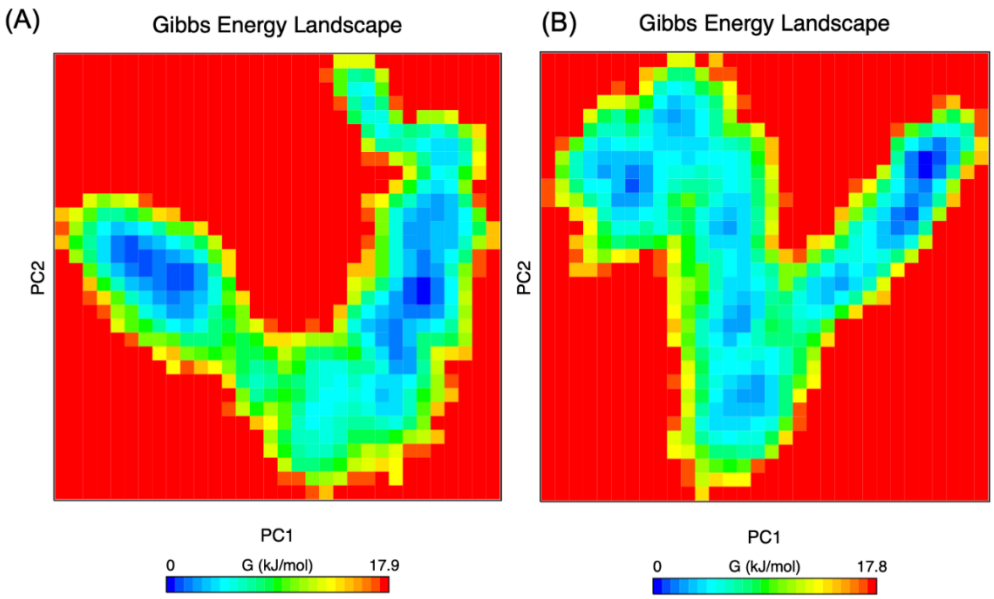

Supplementary Figure S3.3: Gibbs free energy landscape constructed by projecting the first two principal components from the 500 ns MD trajectory of (A) TIRAP-PKCδ and (B) TIRAP-PKCδ with Dorzolamide.

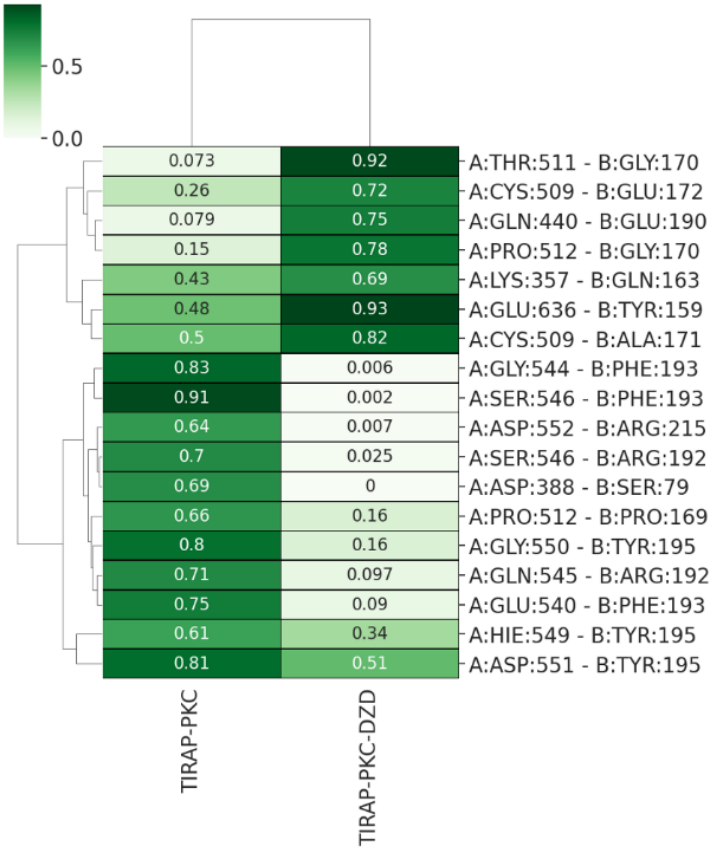

Supplementary Figure S3.4: Frequency heatmaps of intermolecular van der Waals contacts calculated between TIRAP and PKCδ throughout 500 ns MD trajectory.

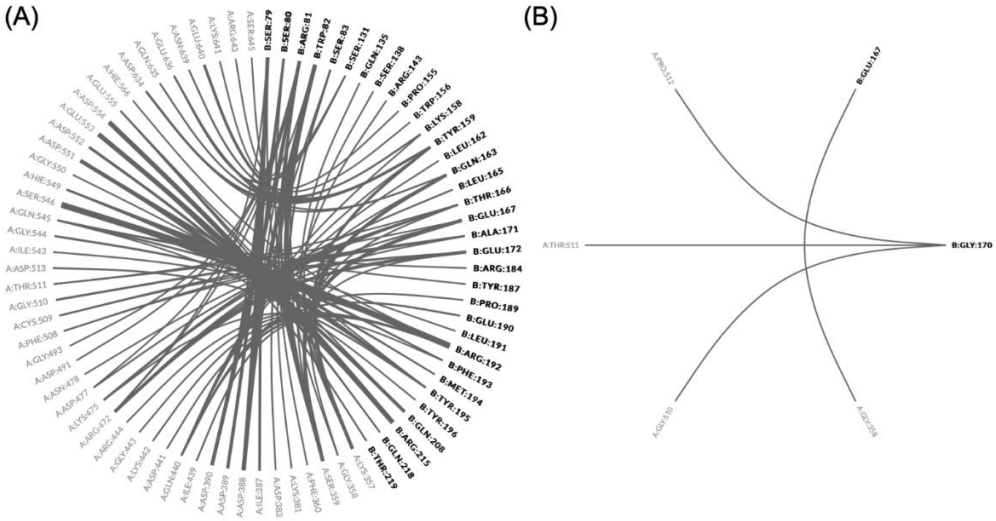

Supplementary Figure S3.5: Intermolecular hydrogen bond contacts calculated between TIRAP and PKCδ throughout 500 ns MD trajectory for (A) TIRAP-PKCδ and (B) TIRAP-PKCδ with Dorzolamide. The thickness of the line shows the occupancy of contact where thicker lines represent higher contact occupancy in 500 ns MD simulation.

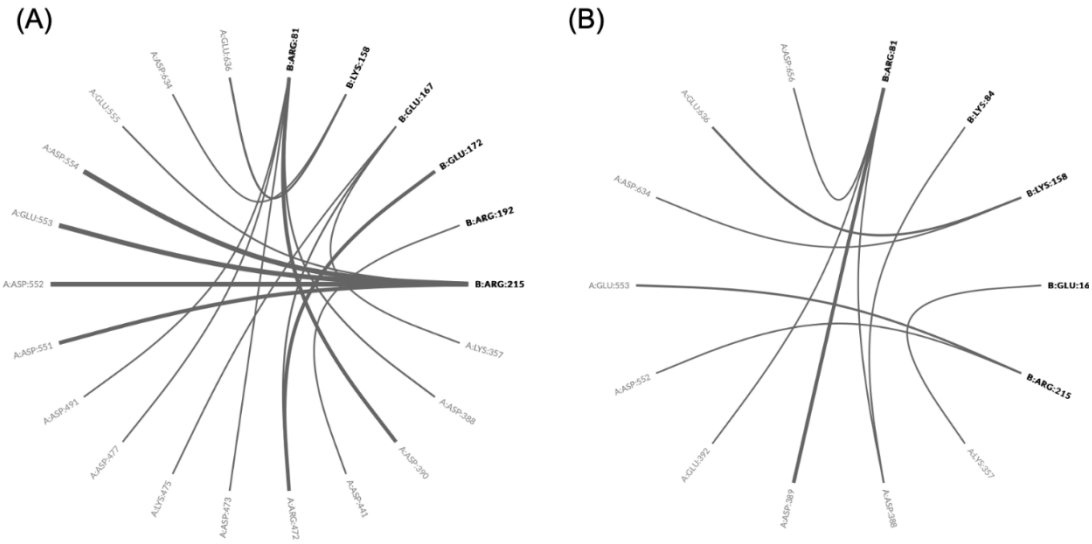

Supplementary Figure S3.6: Intermolecular salt bridges calculated between TIRAP and PKCδ throughout 500 ns MD trajectory for (A) TIRAP-PKCδ and (B) TIRAP-PKCδ with Dorzolamide. The thickness of the line shows the occupancy of contact where thicker lines represent higher contact occupancy in 500 ns MD simulation.

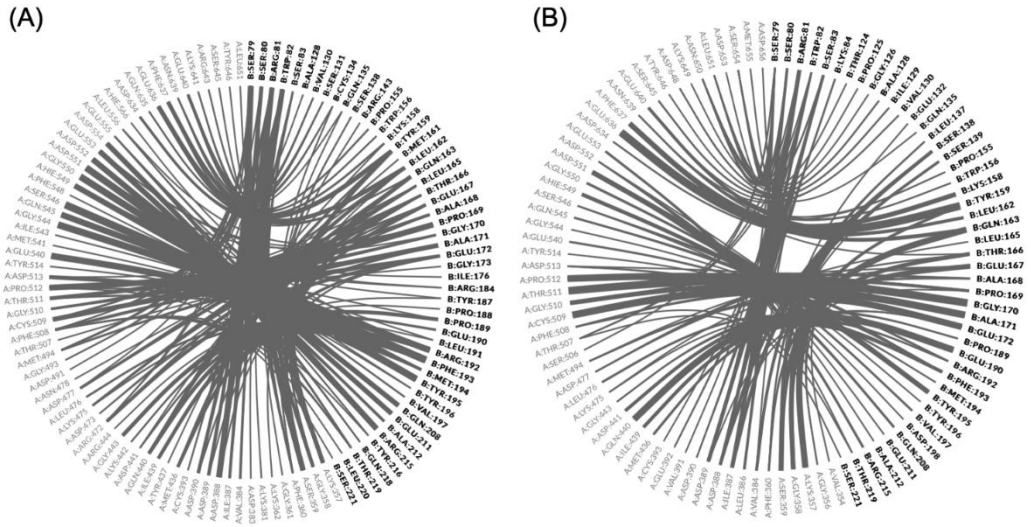

Supplementary Figure S3.7: Intermolecular van der Waals contacts calculated between TIRAP and PKCδ throughout 500 ns MD trajectory for (A) TIRAP-PKCδ and (B) TIRAP-PKCδ with Dorzolamide. Thickness of line shows the occupancy of contact where thicker lines represent higher contact occupancy in 500 ns MD simulation.

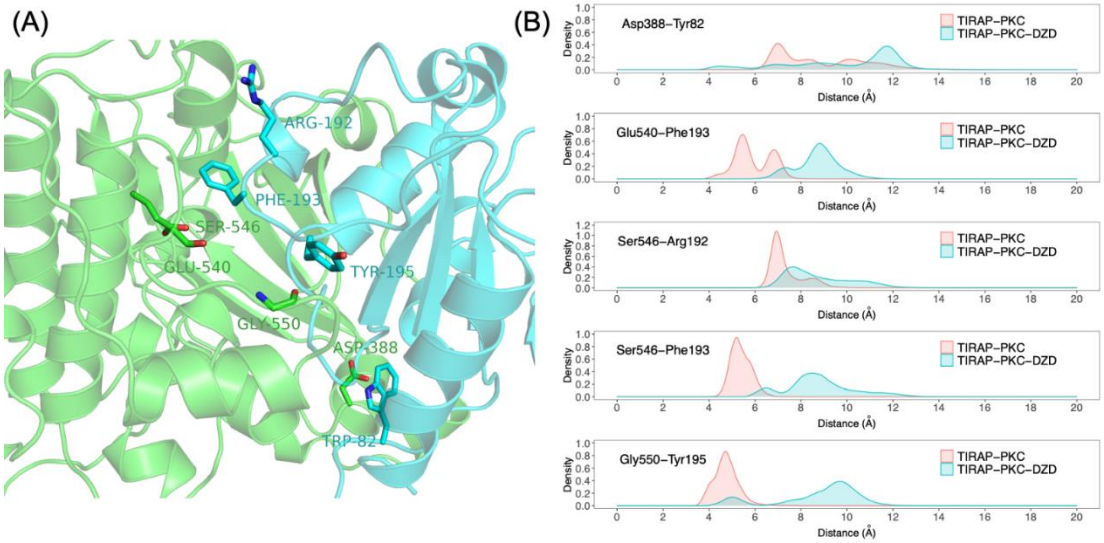

Supplementary Figure S3.8: (A) A close-up view of interacting residues at the TIRAP-PKCδ predicted binding interface. (B) Distance between interacting residues calculated throughout the 500 ns MD trajectory. TIRAP is shown in cyan color while the PKCδ is shown in green.

2. Supplementary Figures from Chapter 4: TIRAP-mediated activation of p38 MAPK in inflammatory signalling

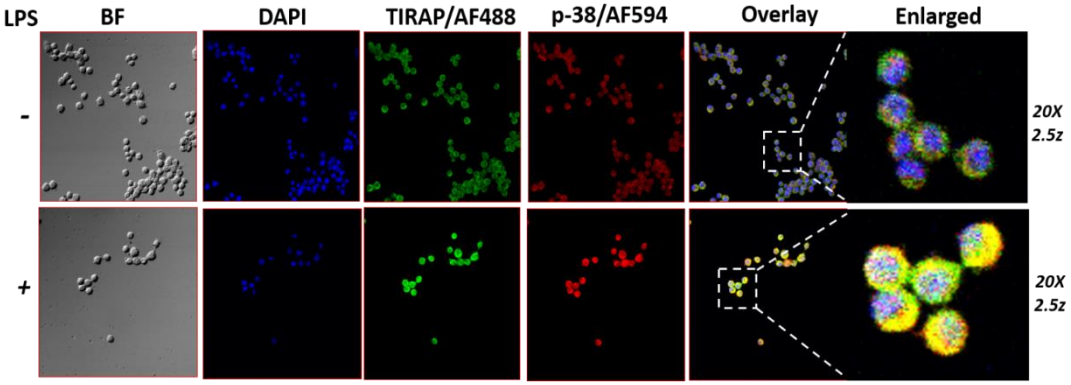

Supplementary Figure S4.1: Representation of immunofluorescence staining of TIRAP and p38 MAPK for their cellular co-localization in RAW264.7 murine macrophages through confocal microscopy. The RAW264.7 cells were treated with 250ng/ml of lipopolysaccharide (LPS) for 1h and immune-stained with mouse-raised anti-TIRAP and rabbit-raised anti-p38 MAPK antibody and probed with secondary antibody anti-mouse conjugated with Alexa Fluor 488 and anti-rabbit conjugated with Alexa Fluor 594. The images shown are captured in a confocal laser scanning microscope at 20X 2.5z magnification. The cellular colocalization of TIRAP and p38 MAPK in the number of cells is observed in the cytoplasm in LPS-treated cells in the overlay image as compared to control cells. BF- Bright field; DAPI- 4′,6-diamidino-2-phenylindole.

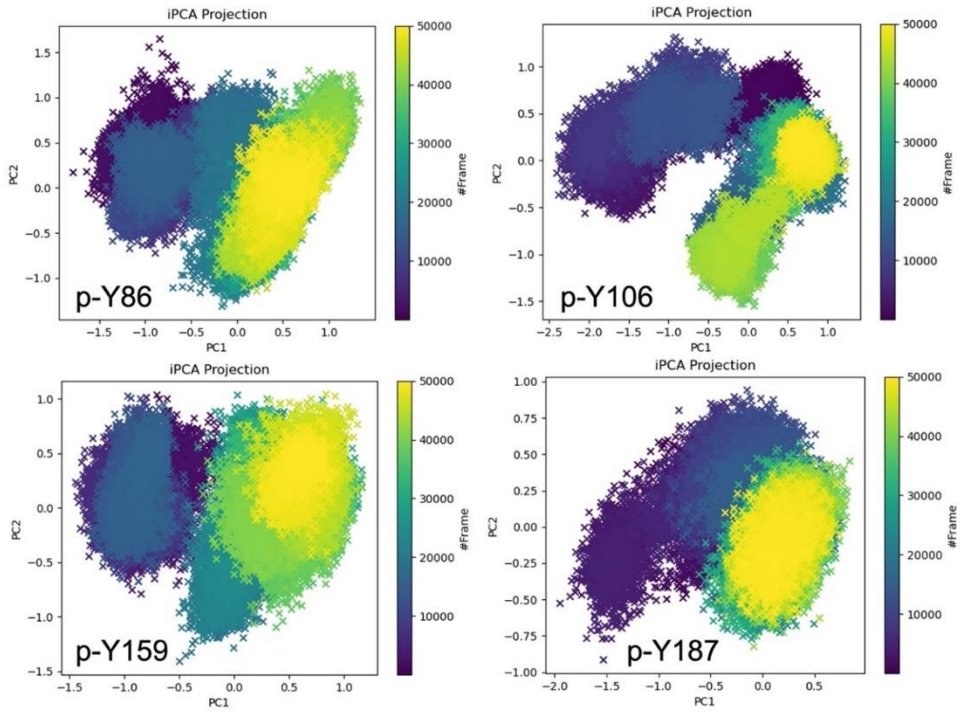

Supplementary Figure S4.2: Principal component analysis to study the effect of tyrosine phosphorylation on TIRAP structure within the TIRAP p38 MAPK protein-protein complex.

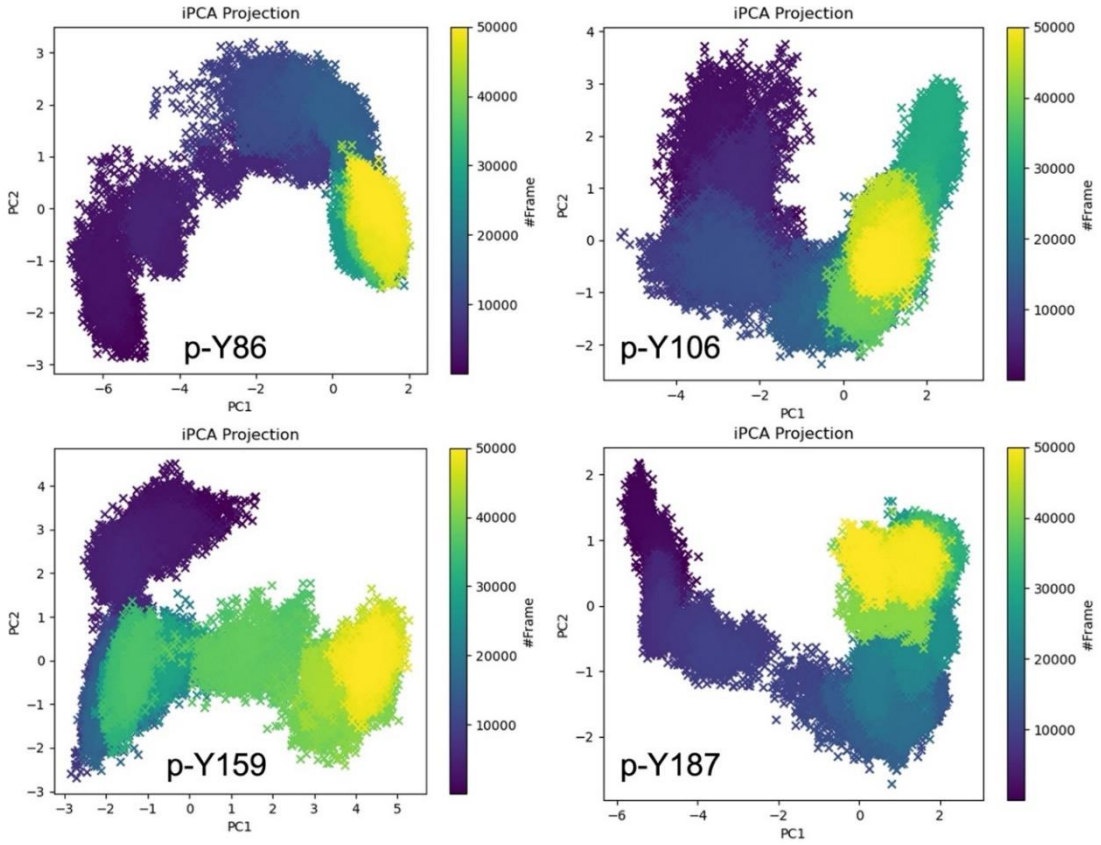

Supplementary Figure S4.3: Principal component analysis to study the effect of TIRAP tyrosine phosphorylation on p38 MAPK structure within the TIRAP p38 MAPK protein-protein complex.

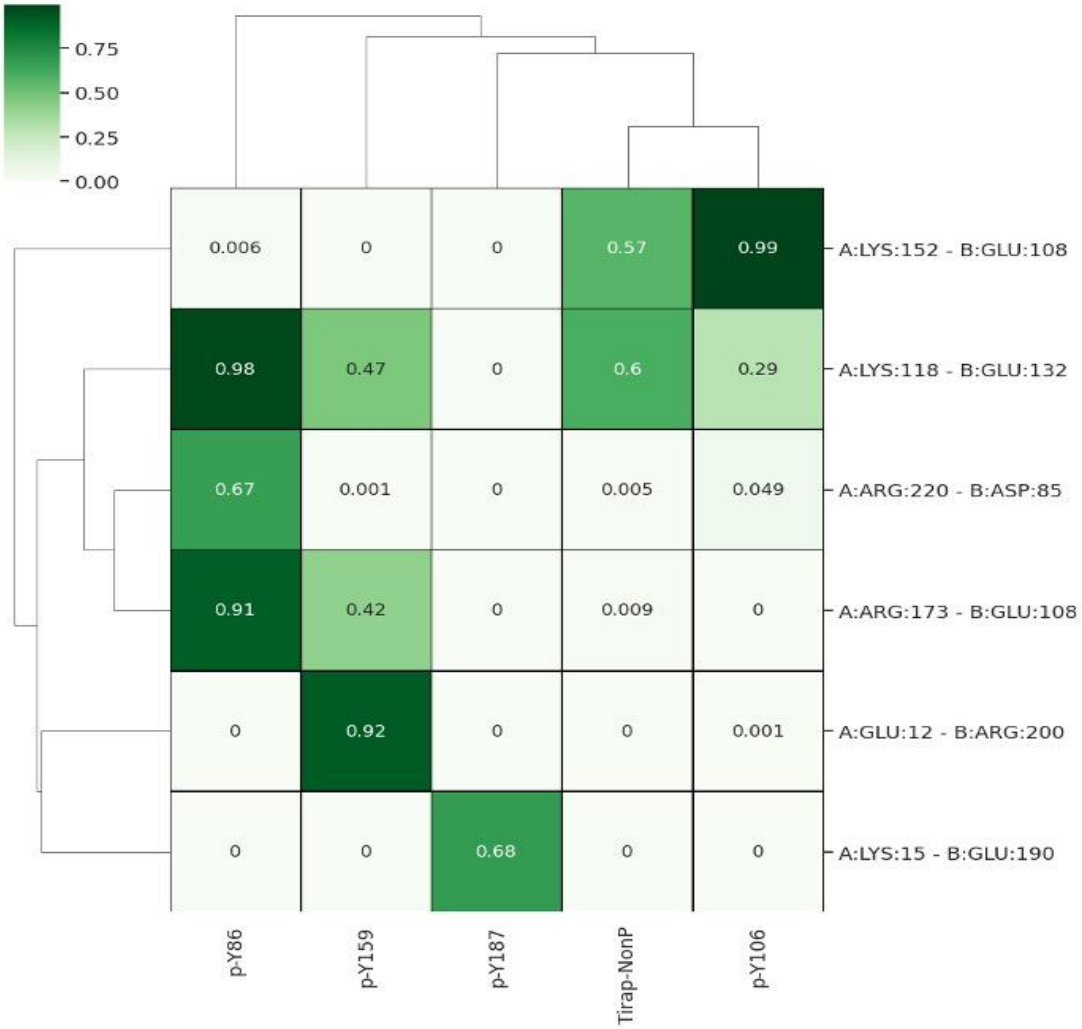

Supplementary Figure S4.4: A heatmap showing the frequency of salt bridges between TIRAP and p38 MAPK calculated throughout the 500 ns MD trajectory. Contacts with more than 60% occurrence frequency (frequency value = 0.6) for either of the complexes are shown.

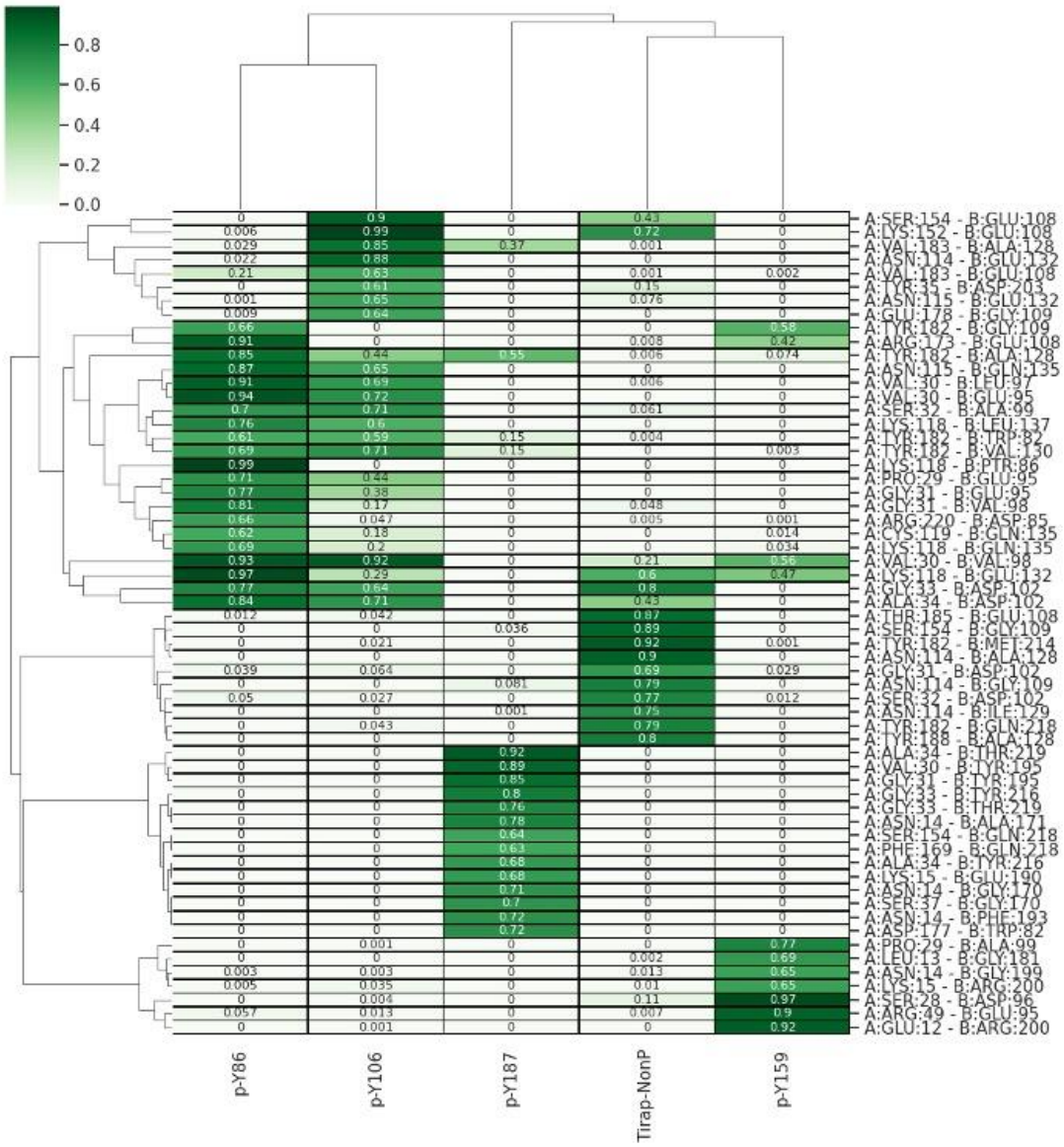

Supplementary Figure S4.5: A heatmap showing the frequency of van der Waals contacts between TIRAP and p38 MAPK calculated throughout the 500 ns MD trajectory. Contacts with more than 60% occurrence frequency (frequency value = 0.6) for either of the complexes are shown.

3. Supplementary Figures from Chapter 5: Identification of novel inhibitors targeting TIRAP interactions with BTK and PKCδ in inflammation through an in silico approach

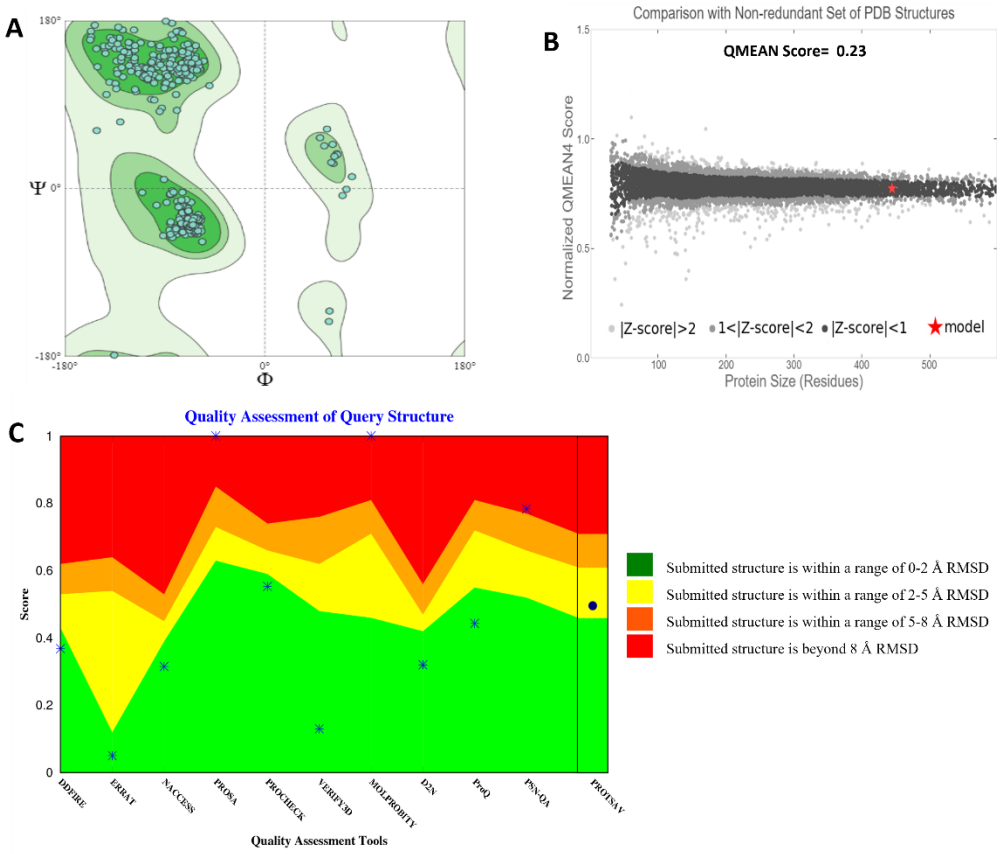

Supplementary Figure S5.1. Stereochemical analysis and structural validation of BTK model_2. (A) The Ramachandran plot with a 98.2% score for the model with no outlier residues in the unfavoured region, (B) QMEAN (Qualitative Model Energy ANalysis) quality factor normalized score with total protein size and its Z-score value, and (C) Overall structure assessment and validation by ProTSAV tools results in model structure quality score in the range of 2-3Å RMSD.

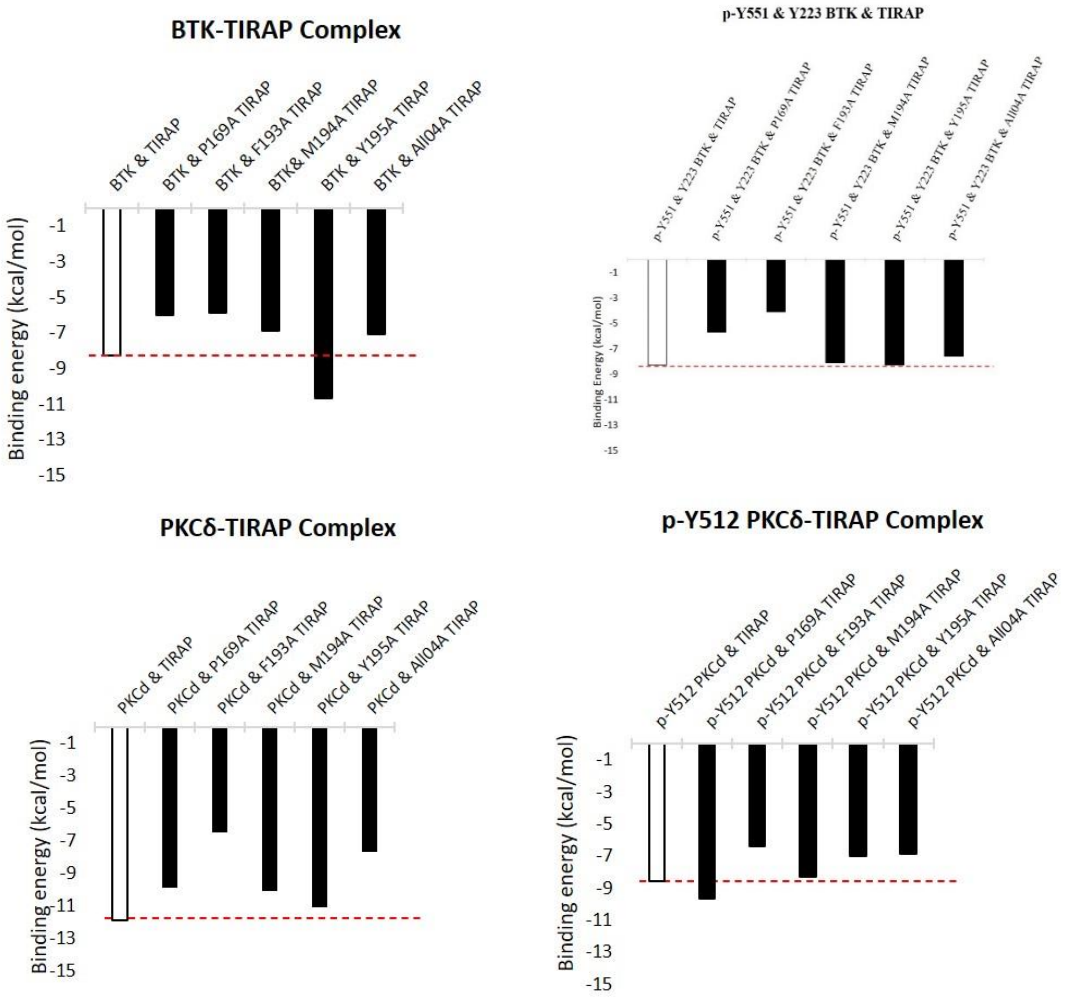

Supplementary Figure S5.2: Protein-protein docking of wild-type and mutated TIRAP (wtTIRAP & muTIRAP) with non-phosphorylated and phosphorylated state of BTK and PKCδ in HADDOCK 2.4 tool. (A) and (B) Docking result of wtTIRAP and muTIRAP with non-phosphorylated and phosphorylated Y551 and Y223 BTK structure. (C) and (D) Docking result of wtTIRAP and muTIRAP with non-phosphorylated and phosphorylated Y512 PKCδ structure. The binding energy (in kcal/mol) is found to be reduced in most of the muTIRAP docking with BTK and PKCδ signifies the importance of TIRAP residues P169, F193, M194, and Y195 at the interface site in the complex.

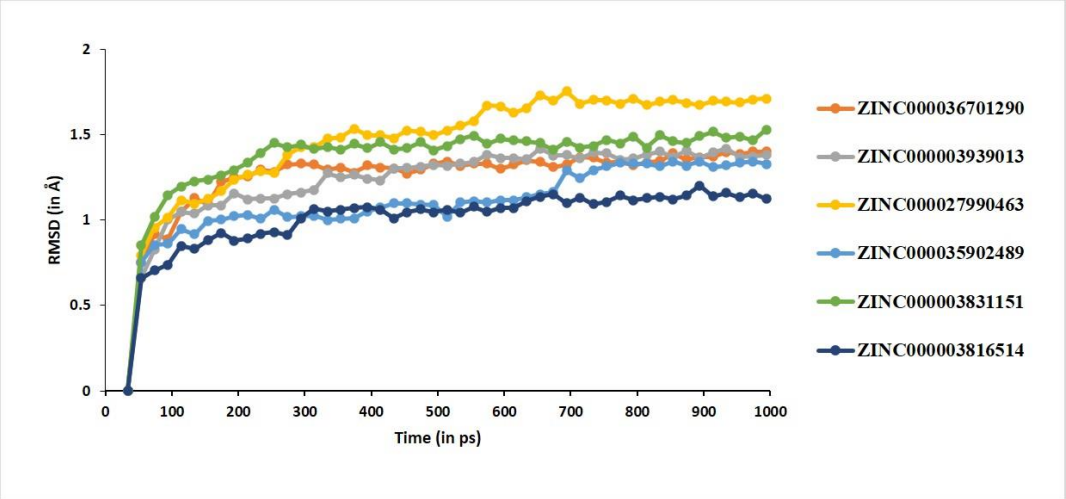

Supplementary Figure S5.3. Short duration Molecular Dynamic (MD) simulation of TIRAP and six drugs complex in Discovery Studio tool. The complex of six screened drugs with TIRAP was used as the initial system for MD simulation to determine their stability. A total simulation of 1000ps was performed in Discovery Studio using the default parameter and all the complexes represent a stable complex conformation as represented in the plot of RMSD values against total simulation time. The value of RMSD was calculated for 50 conformations with a time interval of 20 ps. The average RMSD for all six drugs were 1.25, 1.23, 1.47, 1.1, 1.37, and 1.01Å for ZINC000036701290 (Ponatinib), ZINC000003939013 (Fosaprepitant), ZINC000027990463 (Lomitapide), ZINC000035902489 (Crizotinib), ZINC000003831151 (Monteleukast), and ZINC000003816514 (Rolapitant) respectively.

Appendix B: Supplementary Tables

1. Supplementary Tables from Chapter 3: Dorzolamide (DZD) suppresses PKCδ-TIRAP-p38 MAPK signalling axis to dampen the inflammatory response

Sr.no.	Gene	Primer sequence (5' – 3')	
1	GAPDH	GCACAGTCAAGGCCGAGAAT	Forward
		GCCTTCTCCATGGTGGTGAA	Reverse
2	IL-12	AGTAGTTATGGCTAAGGACATGA	Forward
		AGGGATTCCAGATTTTCTTTGCA	Reverse
3	IL-23	CAAGGACTCAGGGACAACAG	Forward
		GCTCCCCTGTGAAAATATCC	Reverse
4	IL-1B	TGCCACCTTTTGACAGTGATG	Forward
		AAGGTCCACGGGAAAGACAC	Reverse
5	TNF- α	AGGCACTCCCCCAAAAGATG	Forward
		CCACTTGGTGGTTTGTGAGTG	Reverse
6	IL-6	GCCTTCTTGGGACTGATGCT	Forward
		TGCCATTGCACAACTCTTTTC	Reverse

Supplementary Table S3.1: Primer sequences of GAPDH and cytokines used for real-time polymerase chain reaction (RT-PCR).

2. Supplementary Tables from Chapter 4: TIRAP-mediated activation of p38 MAPK in inflammatory signalling

Sr No.	TIRAP & p38 MAPK Complex	BE (kcal/mol)	Interacting and Interface Residues Position Within 3Å		Number of interface Residues
1.	TIRAP-p38 MAPK	-10	TIRAP	D85, Y86, E94, E95, D96, L97, A100, Q101, E108, G109, S131, E132, L133, Q135, L179, S180, G181, Y187, D198, G199, R200, and D203	22
			p38	E12, N14, K15, N26, S28, P29, S32, R49, M109, G110, D112, N114, N115, K118, C119, Q120, K152, S153, A184, and R220	20
2.	p-Y86 & p38 MAPK	-15	TIRAP	D85, pY86, E95, V98, Q101, Y106, E108, G109, A128, I129, E132, Q135, L137, S138, P149, G181, L182, Y187, D198, G199, R200, G201, D203, G204, and F206	25
			p38	N14, T16, S28, S32, G33, A34, G36, R49, S56, M109, G110, D112, K118, C119, K152, S154, T180, Y182, V183, T185, R220, and T221	21
3.	p-Y106 & p38 MAPK	-10.9	TIRAP	D85, Y86, E94, E95, Q101, V104, S105, pY106, E108, G109, A128, I129, S131, E132, Q135, S138, P149, S180, G181, L182, Y187, D198, G199, R200, D203, G204, F206, R207	28
			p38	N14, S28, P29, G31, S32, G33, A34, G36, S37, R49, S56, M109, A111, D112, N114, K118, C119, K152, S154, N155, L156, A172, E178, T180, Y182, V183, A184, T185, and R220	29
4.	p-Y159 & p38 MAPK	-11.7	TIRAP	D85, Y86, EE94, E95, L97, A100, Q101, V104, S105, E108, G109, E132, L133, Q135, L137, S138, P149, G150, L179, S180, G181, D198, G199, R200, D203, and F206	26
			p38	N14, K15, N26, S28, P29, S32, A34, R49, G110, N115, K118, C119, Q120, K121, K152, S154, F169, A184, and R220	19
5.	p-Y187 &p38 MAPK	-12	TIRAP	R81, S105, Y106, G109, A128, G170, A171, E172, R184, R192, F193, Y195, Y196, V197, D198, G199, R200, G201, G205, R207, Q208, K210, E211, R215, Q218, T219, and S221	29
			p38	Y9, Q11, E12, N14, Q25, N26, S28, P29, S32, A34, A40, R49, A51, L108, M109, G110, N114, N115, C119, K152, S154, N155, E160, D177, and A184	25
6.	p-all04 & p38 MAPK	-20.5	TIRAP	pY86, H92, E94, E95, A99, Q101, D102, S105, E108, G109, A128, I129, E132, L133, C134, Q135, A136, P149, L179, S180, G181, pY187, G199, R200, D203, G204, G205, F206	28
			p38	N14, S28, P29, V30, G31, S32, G33, A34, R49, M109, G110, N114, N115, K118, C119, K152, F169, L171, D177, Y182, A184, T185, R220, and T221	24

7.	dpY86, pYall03 &p38 MAPK	-7.1	TIRAP	K84, D85, S93, E94, E95, Q135, L137, S138, S139, S140, R143, P149, G150, D154, P155, W156, C157, pY159, Q160, Q163, T166, E167, A168, E172, and G173	25
			p38	Q11, L13, N14, K15, T16, N26, L27, S28, P29, V30, S32, G33, A34, S37, R49, G110, A111, N114, N115, K118, C119, Q120, and L171	21
8.	dpY106, pYall03 &p38 MAPK	-16.2	TIRAP	R81, D85, pY86, E94, E95, D96, V98, Q101, S105, E108, G109, A128, I129, E132, L133, Q135, L137, S138, S180, G181, L182, pY187, R200, D203, and F206	25
			p38	E12, N14, K15, S28, P29, G31, S32, A34, R49, M109, G110, N114, K118, C119, K121, K152, S154, Y182, A184, W187, R220	21
9.	dpY159, pYall03 &p38 MAPK	-9.6	TIRAP	S79, S83, K84, D85, S93, E94, E95, Q135, A136, L137, H141, R143, G150, Q153, P155, W156, Y159, Q160, Q163, L165, T166, E167, A171, E172, and Y216	25
			p38	Q11, E12, N14, K15, N26, L27, P29, V30, S32, G33, S37, A40, R49, M109, N114, K118, C119, Q120, and L171	19
10.	dpY187, pYall03 &p38 MAPK	-15.5	TIRAP	S79, S83, K84, D85, E94, R143, P149, G150, F151, Q153, D154, P155, W156, C157, pY159, Q160, Q163, A164, T166, E167, and E172	21
			p38	Q11, E12, L13, N14, K15, N26, L27, P29, V30, S32, G33, S37, G110, A111, N114, N115, K118, C119, K152, N155, G170, L171, and A172	23

Supplementary Table S4.1: The interacting residues of non-phosphorylated and tyrosine phosphorylated (pY) TIRAP and p38 MAPK complexes from HADDOCK 2.4. The top poses were selected and interacting residues and binding energy ($\Delta G_{bind,}$ kcal/mol) were identified using the UCSF Chimera and PDBePISA tool within the 3Å region.

A

##	p38 MAPK	Dist. [Å]	pY86 TIRAP
1	A:ASN 14[HD22]	2.47	B:ASP 198[OD1]
2	A:SER 32[N]	3.85	B:ASP 102[OD1]
3	A:GLY 36[N]	3.30	B:ASP 203[OD1]
4	A:ARG 49[HH11]	1.53	B:GLU 95[OE1]
5	A:ARG 49[HH22]	1.55	B:GLU 95[OE2]
6	A:ASP 112[N]	2.96	B:GLN 101[OE1]
7	A:LYS 118[HZ1]	1.57	B:PTR 86[O1P]
8	A:LYS 118[HZ3]	2.32	B:GLU 132[OE1]
9	A:LYS 118[HZ2]	1.75	B:GLU 132[OE2]
10	A:CYS 119[HG]	2.32	B:GLN 135[OE1]
11	A:LYS 152[HZ2]	2.34	B:GLU 108[OE2]
12	A:LYS 152[HZ3]	2.06	B:GLY 109[O]
13	A:ARG 220[HH12]	1.64	B:PTR 86[O3P]
14	A:ARG 220[HH11]	2.29	B:ASP 85[OD1]
15	A:ARG 220[HH21]	1.50	B:ASP 85[OD1]
16	A:THR 221[N]	2.89	B:PTR 86[O2P]
17	A:GLY 110[O]	3.19	B:VAL 98[N]
18	A:GLY 110[O]	1.82	B:GLN 101[HE22]
19	A:THR 180[O]	2.85	B:ALA 128[N]
20	A:TYR 182[O]	3.01	B:VAL 130[N]
21	A:ASN 14[OD1]	3.55	B:GLY 181[N]
22	A:ASN 14[OD1]	3.57	B:LEU 182[N]
23	A:ASN 14[O]	3.22	B:GLY 201[N]

B

##	p38 MAPK	Dist. [Å]	pY106 TIRAP
1	A:ARG 220[HH11]	1.82	B:ASP 85[OD2]
2	A:ARG 220[HH21]	1.70	B:ASP 85[OD2]
3	A:ARG 49[HH11]	1.59	B:GLU 95[OE2]
4	A:ARG 49[HH22]	2.25	B:GLU 95[OE2]
5	A:ASP 112[N]	2.87	B:GLN 101[OE1]
6	A:ASN 155[HD22]	1.95	B:SER 105[OG]
7	A:LYS 152[HZ2]	1.65	B:GLU 108[OE2]
8	A:ALA 172[N]	3.07	B:GLY 109[O]
9	A:LEU 171[N]	3.49	B:GLY 109[O]
10	A:ALA 184[N]	3.31	B:ILE 129[O]
11	A:ASN 114[HD22]	2.47	B:SER 131[O]
12	A:LYS 118[HZ3]	1.64	B:GLU 132[OE1]
13	A:LYS 118[HZ2]	2.37	B:GLU 132[OE2]
14	A:GLY 36[N]	2.85	B:ASP 203[OD1]
15	A:SER 154[O]	3.85	B:SER 105[OG]
16	A:THR 180[O]	2.82	B:ALA 128[N]
17	A:TYR 182[O]	3.58	B:VAL 130[N]
18	A:PRO 29[O]	2.96	B:GLY 181[N]
19	A:ASN 14[OD1]	3.38	B:LEU 182[N]

C

##	p38 MAPK	Dist. [Å]	pY159 TIRAP
1	A:ASN 14[HD21]	2.41	B:ASP 198[OD1]
2	A:ASN 14[HD22]	2.15	B:LEU 179[O]
3	A:SER 32[N]	3.88	B:GLY 204[O]
4	A:ALA 34[N]	2.65	B:ASP 203[OD1]
5	A:ARG 49[HH11]	1.89	B:GLU 94[OE2]
6	A:ARG 49[HH22]	1.77	B:GLU 94[OE2]
7	A:ARG 49[HH21]	2.44	B:GLU 94[O]
8	A:GLY 110[N]	3.54	B:GLN 101[OE1]
9	A:LYS 118[HZ3]	1.60	B:ASP 85[OD1]
10	A:CYS 119[HG]	1.65	B:GLU 132[OE2]
11	A:GLN 120[HE22]	1.84	B:GLN 135[OE1]
12	A:LYS 152[HZ2]	1.64	B:GLY 109[O]
13	A:ALA 184[N]	2.89	B:GLU 108[O]
14	A:ARG 220[HH11]	1.62	B:ASP 85[OD2]
15	A:ARG 220[HH21]	1.68	B:ASP 85[OD1]
16	A:ASN 14[OD1]	2.70	B:GLY 181[N]
17	A:ASN 14[OD1]	3.75	B:SER 180[OG]
18	A:ASN 115[O]	3.17	B:LEU 133[N]
19	A:LYS 118[O]	2.45	B:TYR 86[HH]

D

##	p38 MAPK	Dist. [Å]	pY187 TIRAP
1	A:CYS 119[HG]	1.77	B:SER 105[O]
2	A:GLN 11[HE21]	1.85	B:ARG 192[O]
3	A:ASN 14[N]	3.44	B:PHE 193[O]
4	A:ASN 26[HD21]	1.75	B:TYR 196[OH]
5	A:ARG 49[HH22]	1.98	B:ASP 198[O]
6	A:ARG 49[HH11]	2.28	B:GLY 199[O]
7	A:ARG 49[HH12]	2.42	B:ARG 200[O]
8	A:ARG 49[HH21]	1.77	B:GLN 208[OE1]
9	A:ARG 49[HE]	2.20	B:GLN 208[OE1]
10	A:MET 109[N]	3.00	B:GLU 211[OE1]
11	A:GLY 110[N]	2.65	B:GLU 211[OE2]
12	A:ASN 155[HD22]	1.99	B:GLN 218[OE1]
13	A:ASN 114[OD1]	3.71	B:ILE 129[N]
14	A:GLN 25[OE1]	2.13	B:ARG 192[HH21]
15	A:GLU 160[OE1]	1.53	B:ARG 207[HH22]
16	A:GLY 110[O]	3.87	B:GLU 211[N]

E

##	p38 MAPK	Dist. [Å]	pYall04 TIRAP
1	A:ASN 14[HD21]	2.19	B:GLY 199[O]
2	A:GLY 33[N]	3.80	B:ASP 203[O]
3	A:ARG 49[HH12]	1.98	B:GLU 95[OE2]
4	A:ARG 49[HH22]	1.63	B:GLU 95[OE2]
5	A:ALA 111[N]	3.45	B:GLU 94[OE2]
6	A:GLY 170[N]	3.66	B:ASP 102[OD1]
7	A:LEU 171[N]	2.77	B:ASP 102[OD1]
8	A:ALA 184[N]	2.68	B:GLU 108[OE2]
9	A:THR 185[N]	2.98	B:GLU 108[OE1]
10	A:THR 185[OG1]	3.16	B:GLU 108[OE1]
11	A:ARG 220[HH11]	1.64	B:PTR 86[O3P]
12	A:THR 221[N]	3.39	B:PTR 86[O2P]
13	A:THR 221[N]	3.76	B:PTR 86[O3P]
14	A:MET 109[SD]	2.29	B:GLN 101[HE22]
15	A:TYR 182[O]	3.50	B:ILE 129[N]
16	A:ASN 114[OD1]	2.98	B:LEU 133[N]
17	A:LYS 118[O]	3.38	B:ALA 136[N]
18	A:CYS 119[SG]	3.41	B:ALA 136[N]
19	A:ASN 14[OD1]	3.08	B:GLY 181[N]

Supplementary Table S4.2: Analysis of hydrogen bonding with the bond distance between the interacting interface residues in tyrosine phosphorylated TIRAP and p38 MAPK docking complexes (A) pY86 TIRAP & p38 MAPK, (B) pY106 TIRAP & p38 MAPK, (C) pY159 TIRAP & p38 MAPK, (D) pY187 TIRAP & p38 MAPK, and (E) pYall04 TIRAP & p38 MAPK, respectively obtained from PDBePISA tool (https://www.ebi.ac.uk/pdbe/).

3. Supplementary Tables from Chapter 5: Identification of novel inhibitors targeting TIRAP interactions with BTK and PKCδ in inflammation through an in-silico approach

No supplementary table.